UNIMORE
UNIVERSITÀ DEGLI STUDI DI
MODENA E REGGIO EMILIA

UNIVERSITÀ DEGLI STUDI
DI MODENA E REGGIO EMILIA

Dottorato di ricerca in
"Ingegneria Industriale e del Territorio"

Ciclo XXXVII

Thorough Validation of a CFD Modelling Approach for Hydrogen Mixing in RANS/LES and Synthetic Fuels Chemical Kinetics Calculations for Internal Combustion Engines

Candidato: Luca Dalseno

Relatore: Prof. Stefano Fontanesi, PhD

Correlatore: Prof. Fabio Berni, PhD

Coordinatore del Corso di Dottorato: Prof. Alberto Muscio, PhD

Index

Nomenclature

Abbreviations:

AI *– Artificial Intelligence*
AKI *– Anti-Knock Index*
AMR *– Adaptive Mesh Refinement*
AMST *– American Society for Testing and Materials*
BDC *– Bottom Dead Center*
BEV *– Battery Electric Vehicle*
BMEP *– Brake Mean Effective Pressure*
bTDC *– Before Top Dead Center*
CAD *– Crank Angle Degree*
CCV *– Cycle to Cycle Variation*
CD *– Central Difference*
CFR *– Courant-Friedrichs-Lewy*
CFD *– Computational Fluid Dynamics*
CHRR *– Chemical Heat Release Rate*
COV *– Coefficient Of Variation*
COP *– Conference of the Parties*
CR *– Compression Ratio*
DI *– Direct Injection*
DME *– Di-Methyl Ether*
DNS *– Direct Numerical Simulation*
EGR *– Exhaust Gas Recirculation*
ECFM-3Z *– Extended Coherent Flame Model – Three Zones*
ECN *– Engine Combustion Network*
eFuels *– Electronic fuels*
EGR *– Exhaust Gas Recirculation*
EXP *– Experimental*
EPIONA *– EthanolPIONA*
ETBE *– Ethyl tert-butyl ether*
ETRF *– Ethanol Toluene Reference Fuel*
EV *– Electric Vehicles*
fTDC *– Firing Top Dead Center*
GDI *– Gasoline Direct Injection*
H2ICE *– Hydrogen Internal Combustion Engine*
HPC *– High Power Computing*
HT *– High Tumble*
ICE *– Internal Combustion Engine*
IDT *– Ignition Delay Time*
IMEP *– Indicated Mean Effective Pressure*
IQ *– Index Quality*
ISSIM *– Imposed Stretch Spark Ignition Model*
IVC *– Intake Valve Closing*
KT *– Kinetic Theory*
KLCR *– Knock Limit Compression Ratio*
LCA *– Life Cycle Assessment*
LCH *– Low Carbon Hydrogen*
LES *– Large-Eddy Simulation*
LFS *– Laminar Flame Speed*
LHV *– Lower Heating Value*
LT *– Low Tumble*
MFB *– Mass Fraction Burnt*
MON *– Motor Octane Number*
MtG *– Methanol to Gasoline*
MtO *– Methanol to Olefins*
MUSCL *– Monotonic Upstream-centered Scheme for Conservation Laws*
MTBE *– Methyl tert-butyl ether*
NIST *– National Institute of Standards and Technology*
NOC *– (non presente — forse volevi NOx?)*
NZE *– Net-Zero Emission*
NTC *– Negative Temperature Coefficient*
OEM *– Original Equipment Manufacturer*
ON *– Octane Number*
OP *– Operative Point*
OxPIONA *– OxygenatesPIONA*
PFI *– Port Fuel Injection*
PIONA *– Paraffins/Iso-paraffins/Olefins/Naphthenes/Aromatics*
PISO *– Predictive-Implicit Splitting of Operators*
PIV *– Particle Image Velocimetry*
PLIF *– Planar-Laser Induced Fluorescence*
POSYN *– Porsche Synthetic Fuels*
PWI *– Port Water Injection*
PRF *– Primary Reference Fuel*
PRR *– Pressure Rise Rate*
RCM *– Rapid Compression Machine*
RCM *– Rapid Compression Machine*
RNG *– Renormalised-Group*
RON *– Research Octane Number*
RSGW *– Reverse Water-Gas Shift*
RVP *– Reid Vapor Pressure*
SAF *– Sustainable Aviation Fuel*
Sc *– Molecular Schmidt Number*
Sct *– Turbulent Schmidt Number*
SctVar *– Variable Turbulent Schmidt Number*
SGS *– Subgrid Scale*
SI *– Spark Ignition*
TAME *– Tert-Amyl Methyl Ether*
TJI *– Turbulent Jet Ignition*
TPRF *– Toluene Primary Reference Fuel*
URANS *– Unsteady Reynolds Navier-Stokes*
VVR *– Variable Volume Reactor*
WALE *– Wall-Adapting Local Eddy-viscosity*

Abstract (english version)

The recent increase in carbon dioxide (CO_2) emissions has propelled the automotive sector to continuously evolve technologies related to internal combustion engines (ICEs). In particular, given the strict timelines and the complexity of current scenarios, it is clear that no single "silver bullet" technology can address the continuous rise in CO_2 emissions. For this reason, multiple complementary solutions must be considered. In recent years, several strategies have demonstrated benefits in CO_2 reduction, especially concerning the energy carriers used to power ICEs. Among these developments, hydrogen direct injection engines (H_2ICEs) have shown significant promise as a carbon-neutral fuel option capable of eliminating CO_2 emissions without major changes to existing ICE technology. In parallel, and consistently with governmental strategies, e-fuels have emerged as another effective technology able to reduce CO_2 emissions immediately, as they can be used in both existing and next-generation ICEs. Computational Fluid Dynamics (CFD), central to this work, has demonstrated substantial advancements, enabling the study and development of new technologies in a timely and efficient manner. However, enhanced computational capabilities available to universities and companies are ineffective without proper modelling solutions, an issue that still persists and continues to evolve with advances in HPC and CFD modelling frameworks. This further highlights the necessity of approaches suitable for industrial application in ICE development, supported by a detailed and rigorous evaluation of the CFD setup. This work begins with a fundamental evaluation of the current feasibility of using hydrogen as an efficient and suitable fuel for ICEs. In this context, and aligned with automotive industry needs and available resources, GDI and PFI gasoline Spark Ignition (SI) engines retrofitted for hydrogen operation have been analysed. The study demonstrates the feasibility and the impact on emissions, while also providing a detailed overview of the risks, drawbacks, limitations, and correct operational and combustion-management practices required when converting a gasoline ICE to hydrogen. After assessing retrofitting strategies, combustion behavior, and abnormal combustion risks associated with hydrogen, emphasis is placed on mixture formation as the precursor of proper distribution, stratification, and mixing up to the firing top dead centre (fTDC). This specific investigation on hydrogen mixing was carried out on the SOpHy research engine, an optically accessible hydrogen-fueled ICE. The work involved developing a meticulous setup and a clearly defined methodology for modelling direct injection H_2ICEs, with the aim of providing additional insights beyond previously published modelling frameworks in this field. In this regard, new CFD modelling approaches, both chemical and physical, have been developed within frameworks applicable to industrial scenarios, considering computational power and time to solution constraints, approaching an original "engineering LES" approach. The work includes two different modelling frameworks: Unsteady Reynolds Averaged Navier–Stokes (URANS) simulations and, for the first time on the SOpHy engine in a high tumble (HT) configuration, a consecutive multi-cycle Large Eddy Simulation (LES) analysis. This comprehensive effort aims to provide a clear overview of limitations, well-established practices, and emerging aspects and a focus on the turbulent Schmidt Number, and an original approach proposed with a variable law at the wall, opening to future investigation scenarios. Furthermore, the increasing need to diversify both technology and modelling underscores the importance of detailed chemistry as a foundation for advanced simulation studies. Given the limited availability of literature and the still poor real-world applications, the second major topic of this thesis primarily addresses modelling aspects related to e-fuels, with particular attention

to their numerical representation and potential applicability in advanced engine concepts. This contribution aims to establish a methodological foundation for future simulation studies and to support the broader transition toward sustainable combustion technologies. Therefore, an original methodology for calculating laminar flame speed (LFS) and ignition delay time (IDT) for different fuels is developed and applied to compare two e-fuels with a conventional RON 98 gasoline using 0D/1D detailed chemical kinetics simulations. This methodology is based on a published work by the author, OxPIONA, which structured a six-component surrogate fuel composition. It involves selecting appropriate chemical kinetic mechanisms from the literature, ensuring that the application and feasibility are properly aligned. It is then used to calculate IDTs and LFSs across a wide range of engine-relevant conditions, enabling comprehensive fuel behavior comparisons and paving the way for future 1D and 3D CFD studies. Results show that the free aromatics gasoline presents a 3–6% higher laminar flame speed under engine-like conditions, while IDTs, consistent with RON/MON similarities, display overall comparable trends and a characteristic NTC behavior in the presence of MTBE. Finally, engine test-bench experiments performed with both e-fuels and conventional gasoline confirm, once again, that synthetic fuels represent a promising opportunity. They are capable of reducing harmful emissions and lowering CO_2 output in life cycle assessment (LCA) analyses, while maintaining the same engine layout, fueling systems, and performance. The latter has also been investigated through 0D/1D/3D-CFD modelling, achieving results that are well aligned with the experimental test-bench data by using the calculated LFS following previous methodology and an internally well-established methodology for engine simulation. The output from the methodology and calculations of the fuel combustion properties is then applied to four-stroke and two-stroke engines for different applications, reaching a good match with the combustion indicators. Combined with the approaches developed for hydrogen-mixing modelling, the detailed chemistry-based methodology for combustion prediction, and the suitable capabilities enabling direct industrial application, the validation and results of this work aim to give a contribution to accelerating the development of new fuels and next-generation ICEs, supporting a cleaner and more sustainable future.

Abstract (versione italiana)

Il recente aumento delle emissioni di anidride carbonica (CO_2) ha spinto il settore automotive a un'evoluzione continua delle tecnologie legate ai motori a combustione interna (ICE). In particolare, considerando le tempistiche stringenti e la complessità degli scenari attuali, è evidente che nessuna singola tecnologia "risolutiva" può affrontare da sola il costante incremento delle emissioni di CO_2. Per questo motivo, è necessario considerare soluzioni complementari e integrate. Negli ultimi anni, diverse strategie hanno mostrato benefici nella riduzione della CO_2, in particolare per quanto riguarda i vettori energetici utilizzati per alimentare gli ICE. Tra questi sviluppi, i motori a idrogeno con iniezione diretta (DI-H_2ICE) hanno mostrato un notevole potenziale come opzione di carburante carbon-neutral, capace di eliminare le emissioni di CO_2 senza richiedere modifiche sostanziali alla tecnologia ICE esistente. Parallelamente, e in linea con le strategie governative, gli e-fuels sono emersi come un'altra tecnologia efficace, in grado di ridurre immediatamente le emissioni di CO_2, poiché utilizzabili sia negli ICE esistenti sia nelle generazioni future. La Fluidodinamica Computazionale (CFD), centrale in questo lavoro, ha dimostrato avanzamenti significativi, consentendo lo studio e lo sviluppo di nuove tecnologie in modo rapido ed efficiente. Tuttavia, capacità computazionali avanzate, oggi disponibili sia in ambito universitario sia industriale, risultano inefficaci senza adeguate soluzioni di modellazione, un limite che persiste e continua a evolversi con i progressi nell'HPC e nei framework CFD. Ciò evidenzia ulteriormente la necessità di approcci adatti alle applicazioni industriali nello sviluppo degli ICE, supportati da una valutazione dettagliata e rigorosa del setup numerico. Questo lavoro prende avvio da una valutazione fondamentale dell'attuale fattibilità dell'utilizzo dell'idrogeno come combustibile efficiente e idoneo per gli ICE. In questo contesto, coerentemente con le esigenze dell'industria automotive e con le risorse disponibili, sono stati analizzati motori GDI e PFI convertiti all'alimentazione a idrogeno tramite iniezione diretta e indiretta. Lo studio dimostra la fattibilità e l'impatto sulle emissioni, fornendo al contempo una panoramica dettagliata dei rischi, delle criticità, dei limiti e delle corrette pratiche operative e di gestione della combustione necessarie durante la conversione di un ICE a benzina a un ICE a idrogeno. Dopo aver valutato le strategie di retrofitting, il comportamento della combustione e i rischi di combustione anomala associati all'idrogeno, l'attenzione è posta sulla formazione della miscela, intesa come precursore della corretta distribuzione, stratificazione e miscelazione fino al momento di innesco della combustione al punto morto superiore. Questa analisi specifica sulla miscelazione dell'idrogeno è stata condotta sul motore di ricerca SOpHy, un ICE alimentato a idrogeno con accesso ottico. Il lavoro ha richiesto lo sviluppo di un setup meticoloso e di una metodologia chiaramente definita per la modellazione dei motori H_2ICE a iniezione diretta, con l'obiettivo di fornire approfondimenti aggiuntivi rispetto ai framework di modellazione precedentemente pubblicati. In questa direzione, sono stati sviluppati nuovi approcci CFD, sia chimici sia fisici, all'interno di framework applicabili agli scenari industriali, considerando la potenza computazionale disponibile e le limitazioni in termini di tempo-soluzione con riferimento diretto all'ambito aziendale. Questi approcci includono simulazioni: URANS (Unsteady Reynolds-Averaged Navier–Stokes) e, per la prima volta sul motore SOpHy in configurazione ad elevato tumble (HT), un'analisi multi-ciclo consecutiva in Large Eddy Simulation (LES). Questo ampio lavoro mira a fornire una panoramica chiara delle limitazioni, delle pratiche consolidate e degli aspetti emergenti inerenti la tecnologia di idrogeno come combustibile per motori a combustione interna. Nello specifico, viene trattato il numero di Schmidt turbolento, determinante la diffusione dell'idrogeno in applicazioni CFD,

proponendo un approccio variabile a parete e aprendo così nuovi scenari di investigazione futura. Inoltre, la crescente necessità di diversificare sia le tecnologie sia gli approcci modellistici, come anticipato ed evidente nello scenario attuale, sottolinea l'importanza di diversificazione tecnologica e dell'impatto della chimica dettagliata come fondamento per studi di simulazione avanzata. Data la limitata disponibilità di letteratura e la scarsa diffusione di applicazioni reali, il secondo tema principale di questa tesi è prevalentemente dedicato agli aspetti di modellazione degli e-fuels, con particolare attenzione alla loro rappresentazione numerica e alla potenziale applicabilità in *layout* motore avanzati. Questa tesi si propone di stabilire una base metodologica per lo studio, simulazione e di supporto verso la più ampia transizione a tecnologie di combustione sostenibili. Pertanto, nel dettaglio, viene sviluppata e applicata una metodologia originale per il calcolo della velocità di fiamma laminare (*Laminar Flame Speed*, LFS) e del tempo di ritardo all'accensione (*Ignition Delay Time*, IDT) per diversi combustibili, al fine di confrontare due e-fuels con una benzina convenzionale RON 98, utilizzando simulazioni 0D/1D basate su cinetica chimica. Tale metodologia si fonda su un combustibile surrogato, strutturato a sei componenti di tipo OxPIONA, pubblicato dall'autore, e prevede la selezione di adeguati meccanismi cinetici chimici, in relazione all'applicazione, garantendone la fattibilità, affidabilità e predittività coerentemente allineate agli obiettivi dello studio. Dai risultati, nello specifico, si evidenzia che la benzina priva di idrocarburi aromatici presenta una velocità di fiamma laminare superiore del 3–6% in condizioni motoristiche, mentre gli IDT, in accordo con le similitudini RON/MON, mostrano tendenze complessive analoghe e un comportamento NTC caratteristico in presenza di MTBE. Infine, le prove al banco motore effettuate sia con e-fuels sia con benzina convenzionale confermano, ancora una volta, che i carburanti sintetici rappresentano un'opportunità promettente. Essi sono in grado di ridurre le emissioni dannose e diminuire il contributo di CO_2 nelle analisi LCA (Life Cycle Assessment), mantenendo invariati il layout del motore, il sistema di alimentazione e le prestazioni. Questi combustibili sono stati inoltre analizzati mediante modellazione 0D/1D/3D-CFD, ottenendo risultati ben allineati ai dati sperimentali grazie all'utilizzo della LFS calcolata secondo le metodologie precedenti e a un *framework* di simulazione del motore consolidato. Definita la metodologia e i calcoli delle proprietà di combustione delle benzine analizzate, i database sono stati applicati a motori di produzione, per differenti applicazioni sia a quattro sia a due tempi e i risultati validati su base sperimentale. Il confronto ha mostrato un'ottima correlazione relativamente al set di dati sperimentale considerato. In combinazione con gli approcci sviluppati per la modellazione della miscelazione dell'idrogeno, con la metodologia basata sulla chimica dettagliata per la predizione della combustione e con le capacità adeguate per l'applicazione diretta in ambito industriale, la validazione e i risultati di questo lavoro mirano a contribuire all'accelerazione dello sviluppo di nuovi combustibili e di motori a combustione interna di nuova generazione, supportando un futuro più pulito e sostenibile.

1 Fuels and Energy Carrier – Scenario, Carbon-neutral Fuels, Engines

1.1 Current Scenario of CO_2 and Environment (2025)

There are currently roughly 1.47 billion cars around the world [1], mostly spread out from Asia, Europe, and North America, accounting for almost 90% of the vehicle fleet in the world, of which nearly 19% are in the US. It is noteworthy that most vehicles are powered by internal combustion engines (ICEs) (about 99.8%) which 95% are propelled by liquid fuels from petroleum [2]. From the actual literature and projected scenario, we will still have a huge amount of ICE vehicles in the following decades. Reporting some of the data about overall vehicles sold during 2023 [3], nearly 18% were electric cars against the rest, which concerns non-electric vehicles. Following the aforementioned data, the analyst's predictions reported in [4] estimate a more than half of the vehicles in the world will still be powered with ICEs by 2050. Of course, these are data against the well-known targets set by the Paris Agreement adopted on 12 December 2015 at the COP21 [5] and revised in Glasgow at the COP26 [6], where the pursuit of 2 [°C] in temperature increment was reduced to the limit of 1.5 [°C] above pre-industrial levels. Furthermore, this scenario moves far from the European Green Deal and the related plan introduced by the "Fit for 55" [7], aiming for the achievement of carbon neutrality of the EU by 2050. Nevertheless, the large amount of ICE-equipped vehicles should also be critically reviewed since such technology is still quite flexible. Some ways to improve the efficiency of ICEs are still being developed by car companies, manufacturers of cars, and OEMs, as well as extensive support from the academic and scientific community. Recently, the proposal of Europe to set a ban on vehicles equipped with ICEs in 2035 has "called to the floor" the scientific community and experts in this sector. On the 27 of March 2023, Italy, Poland, Finland, and Germany revealed their position against the ban for different reasons. In particular, Italy claimed the ban should strongly impact the economy and pose risks for lots of people employed in the automotive sector, as Italy is the cradle of luxury and sports car manufacturing. Nevertheless, it also supported the electrification of light vehicles but highlighted its preferences for other solutions. Germany was also opposed to that legislation but reached a deal to continue developing carbon-neutral synthetic fuels (the so-called E-Fuel) to run ICE-equipped vehicles after 2035 [8]. According to the great literature from [9, 10, 11], the future of ICEs could be cleaner than expected from "non-sector operators". Of course, the World is continuously facing new issues, that of course are linked to economic development and geopolitical issues. Russia's invasion of Ukraine in February 2022 led to a global energy crisis. Prices rose and the economic and political scenarios tightened. However, from the invasion and up to now, the global scenario of fossil fuel feedstock started changing as never been happened in the last decades. In fact, a cleaner alternative to the dependence of gas from Russia or crude oil from the rest of the World, starting to change toward a new fuels scenario and, targeting power plants, different technologies such as electric vehicles and heat pumps. So, the biggest legacy of the energy crisis exploded in recent years and, at the time of the author writing, still fighting on the Ukraine floor. This scenario, according to some predictions, which of course can also be strongly influenced by political or economic standpoint, as Goldman Sachs reports [12], could lead to the peak of demand for oil, gas and coal set within the decade [13]. In a global scenario, the energy demand is currently accelerating, moving from a 1.3% of a decade to 2013-2023 and then to 2024 in which the increment was set to 2.2%. Renewable energy demand is at the top among the sources, considering in order of request, Natural Gas, Coal, Oil and Nuclear [14]. From the perspective of global stock markets, a similar pattern is reflected in the increasing demand for electricity, driven by the rapid expansion of emerging economies and the growth of industries that lead renewable-energy production, such as Siemens Energy AG through its subsidiary Siemens Gamesa and wind turbine

technology and products and more. China's energy demand growth of 3% in 2024, before India, which is the second-largest rise in energy demand. This is also confirmed by the development of new frontiers of technology, it can be attributed to the artificial intelligence (AI) in which the Chinese car markets of electric cars is currently leading in electric car sales in the 2024, reaching numbers around 11 million cars sold. On the contrary, the EU reached a stagnation point with around 2.2 million due

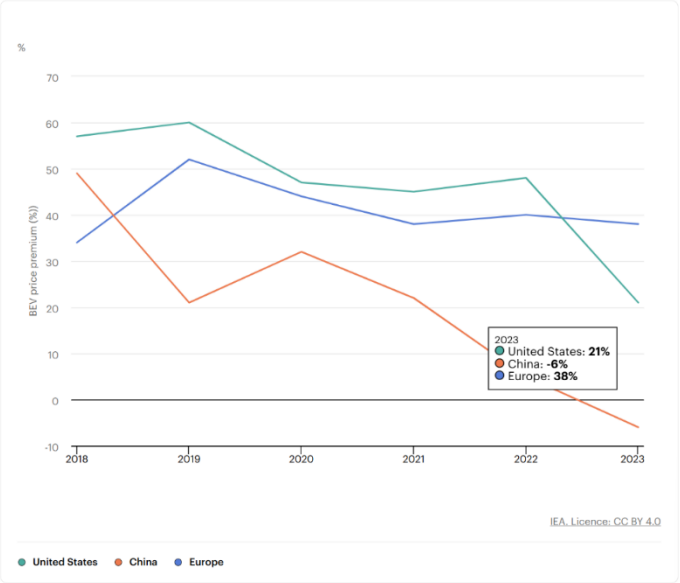

Figure 1 Battery electric vehicles prices along the years [IEA]

to the phase out of subsidies, referring to the highest market for EVs which is Germany, and followed to the US with around 1.2 million of BEVs. [15]. Of course, Europe, guided by Germany in EV production, risk to fall into a longer stagnation of the EV market if prices still registered to be higher than the rest of the world in the years to come. The plot shows, in fact, how the prices of EVs are varying over the years, with not so easy and good perspective for the upcoming years [16]. The latter, with the recent great increment in the stock market, showed a massive impact of AI and new

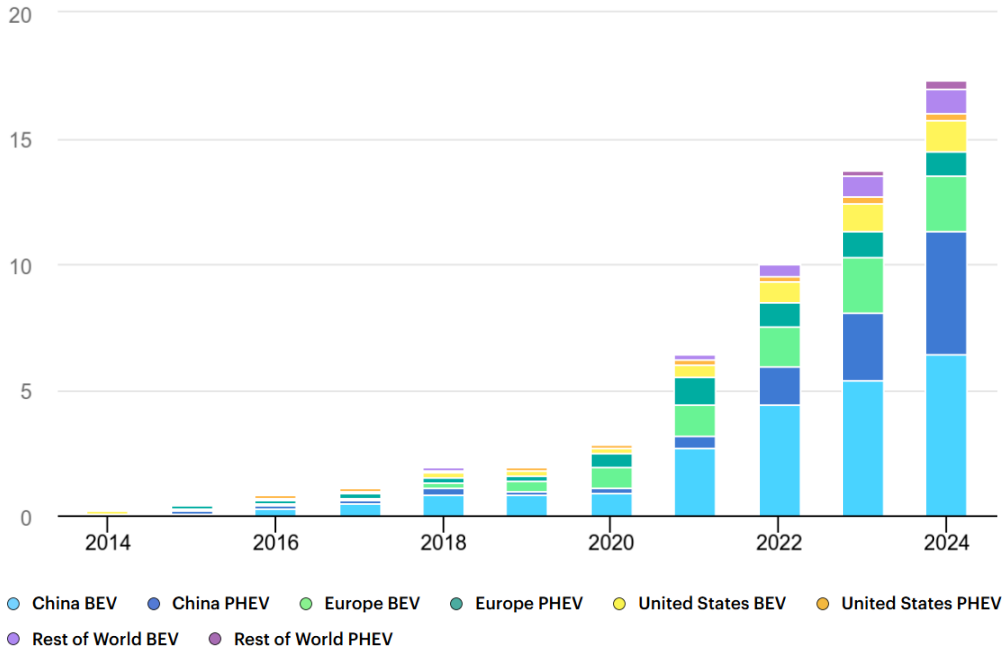

Figure 2 Technology based on battery electric vehicles (BEVs) has evolved over the years and varies by country and region around the world.

technologies in the field of computational field, digitalization, and data centers. It is the case of NVIDIA Corporation, where the plot reported in Figure 3 reports the recent increment in the share of the stock market. A huge amount of electricity has been devoted to these new techs, but also the more and more adoption of air conditioning and intensive manufacturing that guided the refreshing of air and technologies with specific appliances. It is very important today, to consider the cooling systems that showed recently the massive impact of energy consumption. The diversification of transportation through the state-of-the-art of the most recent technology developments seems to be the only way to reach a fast-to-wheel carbon impact reduction. The previously cited technology for fuel-propelled vehicles, such as synthetic fuels, could play a significant role in achieving net-zero CO_2 targets. Of course, the diversification plays today, in the opinion of the writer, a precious milestone. In a World that, or better, in a political World that pushes conditioning toward full electrification without considering the technologies that are currently available, as well as the infrastructure that is needed before transitioning with efficiency, it seems to be quite difficult to target the deadlines of CO_2 reduction and an efficient plan to reduce the CO_2 progressively in a fast scenario. Although EVs produce no direct tailpipe emissions, life-cycle assessment (LCA) clearly shows that CO_2 emissions remain associated with their manufacturing, electricity generation mix, and end-of-life phases. Again, currently, there is a strong lack of infrastructure, as mentioned, buildings that concern the recharging supplier for the EVs. To account for this point, challenges come to the floor, related especially to the costs, space, protocols, charging technologies, payment, and infrastructure network [17]. The question is: "How much time we need to make it possible, realistically?", and again, "It is better to invest in a single technology or it could be more efficient to spread the road transportation in more than one technology depending on specific needs?" The answer to this questions can be a single one, an reflect the possible scenario that the net-zero CO_2 emissions can be reached through several technologies and in specifically adapting these technologies along a timeline, preferring the ones that are realistically ready to be adopted in fast-to-wheel way compared to the ones that needs more time due to infrastructure based. In this scenario, in recent years, many technologies have seen an increase in their use, as well as several technologies developed, and today are ready to be spread on a wide scale. The scheme reports some of the currently major technologies that can help us to face in an efficient way and diversification without emphasizing the limits of some of them, but emphasizing the benefits through diversification. In this manuscript, the author wants to focus on zero-carbon and net-zero carbon footprint fuels. Specifically, the new frontier of unconventional fuels, the so-called "synthetic" or "electronic" fuels (e-fuels) and the energy carrier for the new engine frontiers,

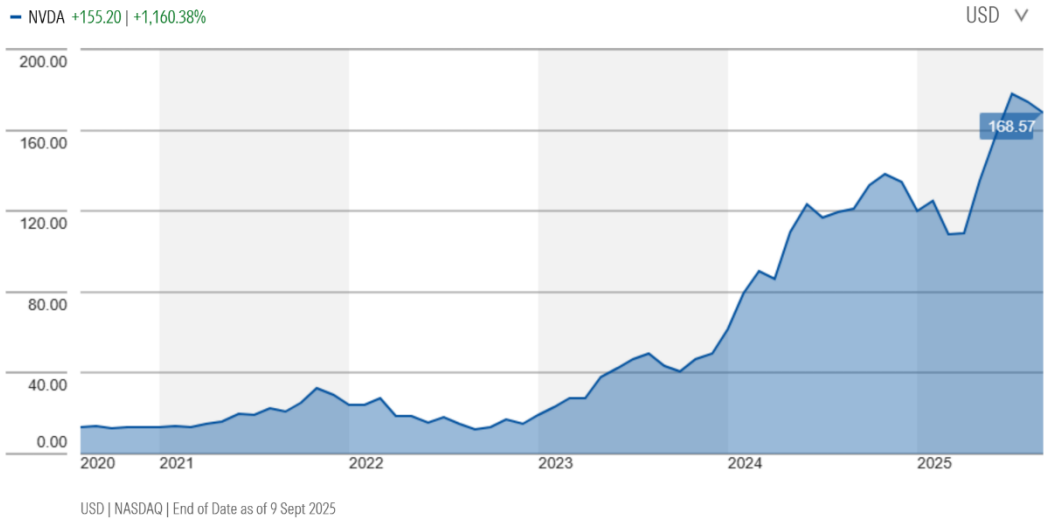

Figure 3 Growth of the NVIDIA Corporation in the last few years in the stock market (data from NASDAQ: NVDA) due to data-center infrastructure, GPUs, and AI accelerators

hydrogen. The first one that we consider starts from the conventional fuels concept, in which hydrocarbons are present together with specific oxygenates. Starting from an introductory of conventional fuels, despite new ones are already more efficient and with a lower impact on the environment, their compositions of the last years in the use of specific alcohol/ethers as oxygenated compounds for hydrocarbon fuels such as ethanol, butanol, ETBE instead of MTBE, TAME, in many countries have brought fuels always less climate effect [18-26]. Here, the racecar competition sector plays a big role in developing and testing the technology as well, especially thanks to cooperation with the fuel producers. Of course, Porsche was one of the first to invest in E-Fuel technology with its first integrated pilot plant in Haru Oni in co-operation with HIF [21] to produce this synthetic fuel in 2022 by investing more than 100 million USD in this sustainable technology. Racing competitions such as the "Porsche Mobil 1 Supercup", which is already using E-Fuel, as well as Formula 1 and Le Mans, will adopt 100% sustainable fuels to propel their high-performance engines from 2026, to reach a reduction of CO_2 emissions up to 65% [28-30]. Recently, e-fuels have been increasingly developed for use in internal combustion engines, particularly in applications where electrification is not feasible and ICEs remain indispensable. A recent application from EMAK S.p.A, published by the author of this manuscript and its co-authors, in collaboration with R&D CFD Srl, revealed some insights and potential in using this technology for gardening applications in also extremes conditions for 2-stroke ICEs [31]. Recent applications also reveal the potential of CFD simulations in the e-fuels scenario, in a 4-stroke engine in this specific application, for high-performance engines, developing a detailed methodology to simulate LFS and IDT of e-fuels and potentials in ICEs predictive applications by Dalseno et al [32]. In that work, the authors gave an extensive and detailed view of the modelling of e-fuels in ICEs, which constitute of a lack in the literature since the novelty of the innovative fuel technology. Here, numerical analyses based on detailed chemistry and Computational Fluid Dynamics (CFD) can play a significant role in reducing tests and costs related to performance, emissions and reliability assessment of the eFuel technology. To increase the reliability of numerical predictions, a cost-effective modelling approach, based on 0D/1D chemical kinetics, is proposed by the author in this work, laying the foundation for the development of eFuels-based engines via 1D and 3D-CFD simulations. In particular, a methodology able to predict the laminar flame speed (LFS) and the ignition delay time (IDT) of eFuels is developed and applied to assess the characteristics of two different *POSYN (POrsche SYNthetic)* eFuels, which are compared to a Standard *SUPER PLUS RON98* European Gasoline. Both LFS and IDT are fundamental inputs to characterize the sensitivity of flame propagation and knock tendency of ICEs through 1D and 3D-CFD simulations on the eFuel composition. The same scenario could also be faced with hydrogen, with specific applications on ICEs, where also in this case, the application does not force a change in engine frameworks, but can just be accounted for by changing the injector. Noticing the recent scenario of H_2 application for high-power specific engines from Toyota, Yamaha, and AVL, which developed H_2ICEs for race applications [33-36]. The latter reached the target of stoichiometric lambda according to PFI water injection strategies, or DI water injection as explored by the author in a high-performance engine application [37], which is a potential strategy to extend the knock limit in hydrogen-fuelled engines [38-41]. Some literature in recent years has also proposed by the authors researching and developing strategies to propel high-performance retrofitted engines from gasoline to hydrogen based on CFD/EXP comparison [42-45]. As mentioned, the above-cited applications are mostly supported by CFD tools to reach their targets. The numerical approach is an extensive and always more impactful approach in developing such new technologies in less time and cost, rather than only testbed ring applications. Some well-established papers have focused on CFD modelling of the major aspects of H_2ICE, including the mixture formations, adopting the techniques for Planar-Laser Induced Fluorescence (PLIF) discussed in [46], and applied to ICEs first from experiments of Salazar and Kaiser [47-49] and then numerically direct injection H_2ICE studies for engines which is reported an extensively literature reported and discussed in detail later in this work [50-66], injectors specific

with cap adoption [67,68] and combustion of hydrogen in endothermic engines [37,42,43,69-71]. The reported overview on H_2ICE for mobility and high-performance applications introduces the reader to the focus of this work in the hydrogen mixing modelling section. The author aims to give an extensive evaluation of the hydrogen direct injection by comparing the results achieved on the SOpHy engine, a research engine widely used in the last decades, since a large amount of data is available and largely discussed in many papers from experiments conducted by Salazar and Kaiser. Then the detailed exploration and modelling of e-fuels as a co-technology adoption in a future scenario for net-zero CO2 emission will be detailed with a specific real application in the ICE sector.

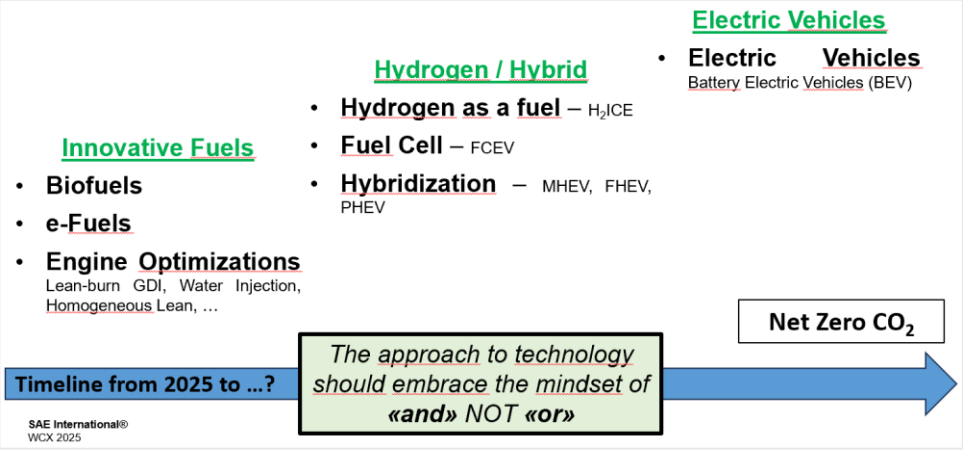

Figure 4 Extract from the author's presentation at the SAE WCX 2025 Congress in Detroit (MI), showing the thought behind technology diversification in a timeline

1.2 Hydrogen – An energy carrier

Hydrogen is the most abundant material on Earth, and contributes to almost 75% of the total mass of the universe. So, its availability is for sure not an issue, especially if it is to be used as an energy carrier. In fact, hydrogen can be adopted as a fuel, as recently (and in the past) adopted to fuel vehicles. Hydrogen has lots of properties that make it a precious element that can be used to fuel ICEs, or adopted for recently developed fuel cell technology. With this preface for hydrogen, some of the major properties are reported in the Table 1, following [72,73]:

Table 1 A comparison between properties of hydrogen and gasoline

Properties: **Hydrogen** compared to **Gasoline**		
Property	**Hydrogen**	**Gasoline**
Carbon content (mass %) / Formula	0 / H_2	84 / C_4-C_{12}
H/C ratio	0	1.7-1.9
Lower Heating Value [MJ/m^3]	119.7	44.8
Density [kg/m^3]	0.089	730-780
Dynamic Viscosity [mPa*s]	0.009	0.37-0.44
Volumetric energy content [MJ/m^3]	10.7	33 x 10^3
Molecular weight	2.016	~110
Boiling point [K]	20	298-488
Minimum ignition energy in air [mJ]	0.02	0.24
Stoichiometric air/fuel mass ratio	34.5	14.7
Stoichiometric volume fraction in air [%]	29.53	~2
Quenching distance [mm]	0.64	~2
Laminar Flame Speed in air [m/s]	1.85	0.37-0.43
Diffusion coefficient in air [m^2/s]	8.5 x 10^{-6}	-
Flammability limits in air [vol%]	4-76	1-7.6
Adiabatic flame temperature [K]	2480	2580
RON	130	95-100
Auto-ignition temperature [K]	845	529

1.2.1 Gross or Net-Zero CO_2 emissions

The new frontiers of technologies and regulation concern the differences between gross emissions, net emissions, net-zero, carbon neutral, etc. The target we should consider, in a realistic way, should be the stop of CO_2 emissions as soon as possible. The current scenario requires the NZE (Net-Zero Emission) target, which can be reached in different ways, or better, with different technologies. Of course, it must be differentiated between the gross and the net zero emissions that technologies can achieve. Furthermore, in the specific view of a transportation scenario, the target should be considered as an LCA (Life Cycle Assessment). In fact, the current push toward battery electric vehicles, the so-called green mobility or electric mobility that is seen as the only technology that allows reaching carbon neutrality, is still based on the energy supply. Many studies showed that the electrification of mobility and related emissions should be considered linked to the place that is linked to the technology through which the energy is produced. In fact, recent studies demonstrated the importance of the location of production, use, and impact on CO_2 emissions of EVs, despite the zero tailpipe amount of carbon dioxide of BEV. As for the leak of infrastructure, EVs can have a reduced benefit in terms of carbon footprint impact. In fact, in countries in which the coal-intensive electricity generation is largely adopted, the lifetime emissions of a BEV as well as an hybrid one can be of significative importance. Despite several data are available, also the methodology on studying this emission can lead to different results, nonetheless, the location at which some data analysis is performed. Related to the latter, a BEV such as the Nissan Leaf EV were measured to be about three times lower lifetime emissions per kilometer compared to a conventional car [74]. Nevertheless, the results obtained in the UK, and in similar studies conducted in countries with a comparable electricity mix, differ significantly when the same analysis is performed in other regions, particularly in India, China, and in all countries where most electricity is still generated from petroleum, coal, or other fossil fuels.

Table 2 An overview of the power generation materials around the world.

Country	Coal	Natural Gas	Oil	Renewables	Nuclear
India	73.4%	3.3%	0.2%	20.5%	2.6%
China	58.4%	3.2%	0.1%	33.9%	4.4%
U.S.	15.6%	42.6%	0.7%	23.3%	17.9%
EU	10.7%	15.6%	1.5%	48.7%	23.6%
Global	**34.5%**	**21.8%**	**2.4%**	**32.1%**	**9.1%**

In the UK, for example, the carbon footprint associated with electricity generation has already been reduced by around 38% in recent years, with projections indicating a potential reduction between 50% and 70% in the near term. This structural improvement strongly enhances the environmental benefits of electric vehicles. Similarly, in countries such as Norway or France, the carbon footprint of EV usage decreases drastically, thanks to Norway's almost fully renewable electricity infrastructure and France's substantial reliance on nuclear energy.

Conversely, in many regions of Europe and in the United States, comparisons between EVs and high-efficiency gasoline or diesel vehicles may lead to similar results, especially when the electricity mix still relies heavily on fossil fuels and when assessing vehicles with particularly optimized internal combustion engines.

Another crucial factor is the location of battery production. While this text does not address in detail the extraction impacts of raw materials, another important component of the LCA, the geographical origin of battery manufacturing plays a fundamental role. The carbon intensity of the electricity used in the manufacturing phase can dramatically affect the total emissions associated with the vehicle. In this regard, the Gigafactory located in Nevada currently represents one of the most efficient and low-emission facilities in the world for EV battery production [75], largely due to the state's low-carbon electricity mix. By contrast, as highlighted in Table 2 and supported by global energy data, China and India still rely predominantly on coal for their electricity generation. This leads to significantly higher emissions for batteries produced in these regions, given that nearly 50% of the total CO_2 footprint of a battery electric vehicle can be attributed solely to the electricity used during battery manufacturing. Therefore, the choice of production site becomes a determinant factor in shaping the overall environmental footprint of EVs and plays a central role in the sustainability of the entire manufacturing ecosystem and supply chain.

For these reasons, it becomes evident that differences in production and assembly sites substantially influence the overall emissions profile of a vehicle, reinforcing the need to consider manufacturing locality as a key element in any comprehensive LCA assessment.

1.2.2 Production

The hydrogen production is one of the crucial points of using this as an energy carrier to be used together with other technologies toward a cleaner scenario for the transportation sector. Hydrogen, as mentioned, is one of the most abundant materials on Earth, but to be used, it must be extracted using some of the most recent technology or most well-established procedures. Related to the procedure, the quality and type of hydrogen can be defined. Since a sort of rainbow scale of colors is currently established to characterize the production of hydrogen, in this section, just the most important ones will be cited: grey, blue and green. The grey hydrogen is the one that is obtained following the most common process through the steam methane reformation and removing impurities from hydrogen to obtain the pure substance [76]. The same process is used to produce the so-called blue hydrogen, which has the same process at the root but through the capturing and storage of the CO_2 trapped in specific tanks, this is known as a "low-carbon hydrogen" technology. Another fundamental process to obtain hydrogen is electrolysis by using electrolysers. The electrochemical reaction that splits molecules of water into both hydrogen and oxygen compounds emits CO_2 as a byproduct. Of course, this process needs energy, which, in the case of green hydrogen, comes from solar or wind power. The major drawback of this technology consists of many issues, the first one being cost. In fact, this kind of application needs power, as high as the quantity of hydrogen to be produced. Generally, the world places at which these technologies are based are far from the places at which this energy carrier will be adopted, making it difficult to transport, store and then use.

1.2.3 Storage

Hydrogen is considered an energy carrier, which means that its application can be widespread and meet different applications. Then, it is a gas and has a very high volatility, which, according to its very high flammability, makes it extremely important to be managed with care and safety conditions. Due to these considerations, when talking about hydrogen storage, the peculiarity of hydrogen makes the process a big challenge. Currently, the major procedure for storing hydrogen consists of different states of this substance. In fact, the first stage to be considered is the storage in compressed tanks. The most commonly used are the steel ones and then maintained compressed from 350-700 [bar] [77]. Then, temperature can play a role when liquid hydrogen is required for storage. The liquid hydrogen is reached at -251.95 [°C] at standard pressure conditions. The requirements for this kind of storage is that large tanks are needed due to the low density of the liquid hydrogen; for example, to transport 10000 [kg] of Kerosene (ρ=810 [kg/,m^3]) the volume should be around 12.3 [m^3] compared to the 143 [m^3] required for liquid hydrogen (ρ=70 [kg/,m^3]) [78]. The last chance to store hydrogen in a liquid state is demanded in a cryo-compressed way, through which the high pressure is considered together with cold temperatures to achieve high energy density [79]. Another way to store hydrogen concerns the chemical storage that allows making hydrogen molecules to be bonded to other specific compounds, generating a dense new compound. Then, through an exothermic reaction, the dehydrogenation process occurs, releasing hydrogen [80].

1.2.4 Strategies/Considerations of H_2ICE Management

1.2.4.1 Hydrogen Port Fuel Injection

The hydrogen fuel supply systems in hydrogen internal combustion engines (H_2ICEs) can be implemented using two different methods. The first method involves a *Port Fuel Injector* (PFI) framework. This approach introduces hydrogen into the intake port using a specialized injector system. While the injection of hydrogen into the port presents several challenges that can complicate various applications, this technique is known for its stability and reliability. It requires low injection pressure and provides sufficient time for the mixing of fuel and air (hydrogen and air, in this case). However, there are uncertainties regarding delivery efficiency and difficulties in controlling the amount of hydrogen entering the combustion chamber, which are among the initial issues with this application.

One of the significant drawbacks of this framework in internal combustion engines (ICEs) relates to hydrogen's characteristics. Due to its higher volume ratio, as reported in Table 1, compared to conventional liquid fuels like gasoline, this results in a lower intake volume mixture, leading to reduced torque and directly impacting engine performance [80]. Consequently, some studies have focused on finding solutions to ensure that power output remains consistent when retrofitting a gasoline direct injection (GDI) engine to an H_2ICE. For instance, Pandey et al. [81] adopted a methodology to control and adjust the compression ratio and equivalence ratio, aiming to increase power and torque compared to gasoline applications. This adjustment is crucial for enabling a hydrogen engine to operate safely, particularly by identifying the limits that prevent knock

occurrence. Detailed findings from this research are presented in the relevant section of this thesis, along with CFD analyses for engine design and development.

Additionally, when considering engine performance, combustion efficiency and emission scenarios must be evaluated. In hydrogen-fueled PFI engines, the lack of intake valve permeability can pose risks. Backfiring is one potential issue that could arise, leading to structural damage, power losses, and safety hazards related to manifold walls. Gao et al. [82] highlighted that backfiring occurs due to various adverse factors, including improper intake valve timing and injection strategies, high equivalence ratios, and excessive residual exhaust gas in the exhaust manifold, compounded by a slow combustion rate. Mechanical systems can help mitigate these negative outcomes, along with efforts to avoid most of these conditions. Moreover, a mechanism considered effective in preventing backfiring is a flame arrester, which consists of a wire mesh frame designed to capture flames while absorbing a significant amount of heat without disrupting the engine's normal operation.

1.2.4.2 Hydrogen Direct Injection

In recent years, to address safety issues and enhance engine efficiency while minimizing the drawbacks of the PFI strategy, *Direct Injection* (DI) of hydrogen has emerged as a promising alternative. This approach offers several advantages over PFI hydrogen systems. One key benefit is the improved control over the injection strategy; injection parameters can be tailored to match the power output required, leading to better engine efficiency through enhanced mixing and combustion.

Higher efficiency is one of the primary goals for modern engines, and the optimal injection strategy should aim to reduce the risks of backfiring, promote lean combustion, and improve the mixing process, all while minimizing NO_x emissions. Over the past few decades, various applications of H_2ICEs have been explored to enhance combustion efficiency and overall performance. As mentioned earlier in this work, numerous companies have successfully developed prototype engines powered by hydrogen, despite the associated challenges and considerations. The significance of this approach is supported by advancements in CFD, which can provide valuable insights and guidelines for improving the entire hydrogen injection process, mixing, and safe combustion conditions while avoiding unintended consequences.

A portion of this work focuses on this subject, detailing the method of direct hydrogen injection in an optically accessible internal combustion engine, utilizing both *Unsteady Reynolds-Averaged Navier-Stokes* (URANS) and *Large Eddy Simulation* (LES) frameworks in a high-tumble configuration, which is relevant for internal combustion engines.

1.2.4.3 Hydrogen Spark Timing Management

The ignition strategy of a H_2ICE needs to be carefully assessed, just like the other key characteristics associated with this fuel. It's important to note that the different polytropic index of hydrogen, compared to GDI engines that use fossil fuels, can also significantly impact this parameter. This will be deepened later on in this work. Salvi et at and Shi et al [83,84] studied the spark timing and combustion in a H_2ICE, concluding that by advancing the spark timing, at constant equivalence ratio and speed, the in-cylinder pressure rises greatly, also changing the relationship between in-cylinder pressure and volume, concluding that this leads directly to a reduction in BMEP and combustion duration. Of course, this is directly connected to possible further risks from abnormal combustion.

On the same results, the conclusion is also that, compared to fossil fueled counterpart, the use of hydrogen must be carefully evaluated in case of increment of equivalent ratio, where the spark timing must be delayed in order to avoid pressure rise and knock. The adoption of different strategies, such as the EGR, can be afforded to reduce the global lambda and reduce the chemistry activity, mitigating abnormal combustion events. Of course, the proper evaluation of the quantity of EGR must be considered; a recent study demonstrated that values up to 20% does not affect the IMEP significantly [85]. Then, another important consideration that must be carefully evaluated is the NO_x. As the CO_2 cannot be produced with an engine fueled with hydrogen (apart from the counterpart related to the oil burned), the NO_x play a role and must be carefully controlled. The temperature-related NO_x emissions can be mitigated by the EGR adoption but also by the water injection. Some studies have been performed over the years on the water injection topic, controlling temperature inside the engines as well as reducing the risk of auto-ignition of the mixture [86-88]. In the retrofitting section of this work, we explore strategies for converting a gasoline engine to run on hydrogen. This includes discussions on water injection, NO_x emissions, and the pressure rise rate (PRR) based on variations in spark timing. These strategies are critically analyzed within the context of a real engine geometry in the specific section dedicated to retrofitting gasoline engines for hydrogen fuel in this work.

1.2.4.4 Abnormal Combustion: Auto-ignition/Surface-ignition/Knock

According to abnormal combustion, the details from mixing and reliability in computational approaches have become more and more important as more predictivity can be afforded. During the introduction of this thesis work, a lot of works have been reported related to the SOpHy engine, an optical-accessible engine at the Sandia National Laboratory, which will be recalled later in this work. The fidelity of predicting mixing is without doubt an important challenge, especially at high-tumble operative points, which is one of the targets of this work to shed more light and effort on this topic. Of course, this is just a “piece” in the modelling of an ICE fuelled by hydrogen, it is the middle step

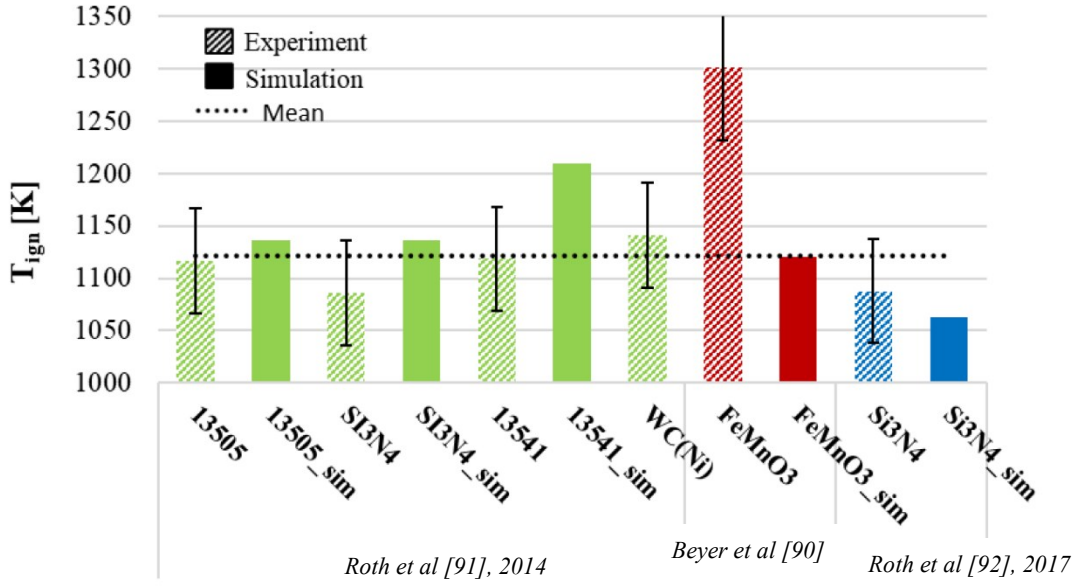

Figure 5 Surface ignition temperature is based on various literature. The average line shows the arithmetic average calculated by the author to highlight discrepancies between individual studies.

after the great way to match flow dynamics in the same architecture. Hence, the last step is represented by the combustion, or the most prominent and important drawback in hydrogen engines, such as abnormal combustion. The previous "pieces" of work developed to be feasible and well predictable in flow and mixing, leaving the floor of the surface ignition [89] and risk of auto-ignition, surface ignition plays a role in hydrogen engines. Of course, the focus on these temperatures mainly relates to the surfaces that are under very high temperature condition such as exhaust valves and spark plug. Some interesting experiments have been carried out over the years by Bayer and Roth [90-92], the latter evidenced and highlighted the importance of surface ignition in spheres of diameters of 800 [μm] as reported in their work. Here the concept of energy density as well as higher temperatures such as the reference ones for hydrogen [93] auto-ignition guided the work. The authors report relevant temperature for auto-ignite around 1100 [K] referring to the impact of surface, material and conditions. Furthermore, in second place, the concentration of hydrogen plays a secondary role in the self-ignition context. In the field of writing, we decided to report the experiments of both previously cited studies and through the survey, we reported a series of reference data, which put an average of the values reported in their literature, and collected in Figure 5.

The results reviewed clearly shows some differences referring to different works, majorly due to different approaches adopted by the authors during the experiments. In any case, avoiding this fact, it emerges that in all the cases the temperature is significantly higher than generally reference temperature of surface ignition for hydrogen [93,94], around 800 [K] and confirming that in an ICEs, as will be reported in this work, the temperature of surface ignition can be considered around 1050 [K], 250 [K] far from the standard data, and in agreement with the previous works. Furthermore, recent studies also enrich these results and statements, referring to the work of Xing et al [95], a catalytic surface is adopted confirming the impact of material surfaces, adsorption, and proving the role of chemistry at various lambda conditions, emphasizing the role of chemistry and local conditions as in ICEs. From these statements, it is also clear that local conditions are of significant importance when operating with hydrogen as a fuel in an ICE. In a work of Chi et al [96], another interesting point that linked directly to ICEs emerged through DNS simulations, where the authors emphasize the importance of a balance between chemical/diffusion as well as the presence of radicals which play a role during the ignition process. This means that, despite high temperatures, the auto-ignition could also not occur due to the presence of not enough radicals around the hotspot. The turbulence and local conditions can reduce the risk of surface ignition by affecting diffusion. This diffusion moves away from the radicals, which helps prevent the development of chemistry that might lead to auto-ignition. This study will emphasize that in conditions of high turbulence, such as those around the spark plug, surface ignition tends to be delayed compared to similar hotspot conditions in lower-turbulence areas, like the exhaust valve seat. This phenomenon is supported by the increased chemical activity observed in the spark plug, even though auto-ignition occurs later due to the turbulence.

1.2.4.5 Internal Temperature Management: EGR and Water Injection

The intake strategy plays a role in the evaluation of a good and efficient approach in hydrogen engines. Especially, the role of cooling management takes a significant role when approaching hydrogen as a fuel instead of a liquid one. The management of temperature is directly linked to the cooling systems as well as the adoption of water injection or EGR (cooled or not) to be premixed

with the intake air. Operatively, a fundamental attention should be taken when approaching hydrogen injection according to the specific limitations of the intake temperature that should not exceed the 80 [°C] to maintain a good response from combustion efficiency [85], low coefficient of variation (COV) and combustion duration. Furthermore, of significant importance the intake quantities of EGR, which according to recent literature, should never exceed the 23.5% to avoid any critical variation in pressure fluctuation and performance[97,98]. According to the evidence, in this thesis, will be performed a sweep of the EGR content up to the limits previously mentioned will be performed, pushing to the maximum value of EGR introduction in retrofitted gasoline engines up to 20%. In fact, it is clear that a further increase in EGR quantity directly leads to a significant reduction in power output. In our case, temperature is not evaluated, but only the variation of the EGR quantity. The EGR temperature variation can also be faced experimentally in PFI configuration in an SI engine performed by Wei et al [99]. Then, as performed by the author of this thesis, an evaluation of the impact of EGR on NO_x emission is also considered. Some literature also reported similar considerations and results that can be compared with CFD. From the experimental standpoint, Salvi et al [100] showed that NO_x emission reduction is optimal when facing 20% of EGR volume fraction, resulting in a reduction of 50% in NO_x, results that are also reported in this work from CFD predictive models. Of course, EGR is one of the strategies to mitigate the temperature and NO_x emissions which are directly related. Another significant solution could be the injection of water targeting the reduction of the overall temperature in the combustion chamber; this can be assessed both directly injected inside the engine as well as a *port water injection* (PWI). Generally speaking, the strategy can help firstly in reaching a temperature reduction up to 40 [K] in boosted H_2ICE with the most effective strategy and complexity reduction when adopting a PFI [101]. In this work, this strategy is targeted, despite not directly from PWI, to reduce the computationally expensive approach and since the application comes from a retrofitting approach, a premixed condition with the sweep in terms of water fraction content is performed. Furthermore, the approach through the temperature reduction can also improve to mitigate the knock occurrence [102], or if needed, to increase the dilution of the mixing, allowing for a reduction of pressure peak by increasing the combustion duration [103,104].

1.3 Synthetic Fuels

Recently, starting in 2016, AME started conducting its first studies to identify places in which the wind resources were majorly developed and where local potentials can be found. The idea was the implementation of Power-to-X technologies, in other words, research in finding how to use the wind to produce a sort of energy or fuel. The organism selects methanol to produce gasoline and fuels for transportation. In 2020, HIF (High Innovative Fuels) [21] was born in Santiago de Chile and developed its interest in e-fuels production. In 2022, the German government announced financial support for a plant that will find its location in Haru Oni through the adoption of the Siemens Energy wind Turbine. Some important companies, such as Porsche, EIG, AME, Baker Hughes and Gemstone, have started financing the project through funds. In 2023, Aramco assessed its pilot plant with the aim of producing 35 barrels per day of low-carbon, synthetic gasoline from renewable-based hydrogen and captured CO_2 systems. Of course, producers are currently increasing, but the production is still something related to a niche market, depending on the decision of the governments and the choices related to the endothermic engines up to 2035.

1.3.1 Innovation

The recent restrictions from the legislation led to pushing toward different technologies such as the electronic production of synthetic fuels. These fuels are basically similar to the conventional fuels, so, based on hydrocarbons and oxygenates and made up of thousands of components. Nevertheless, different from conventional ones, the process through which these fuels are obtained changes substantially. Especially, changing the process through which the composition is obtained also changes the production system, aiming to reduce the impact of these fuels in terms of CO_2 emissions compared to conventional ones. The production system, in fact, aims to capture CO_2 from the atmosphere to be used to form new molecules of methanol, the so-called e-methanol, a type of methanol obtained by combining hydrogen with carbon dioxide. This process allows for capturing CO_2 from the atmosphere, reducing its content, which will be reemitted into the atmosphere during the combustion process of this substance. It is simply a balance between what is absorbed from the environment and what is reemitted, with a perfect balance and net-zero CO_2 emission. Then, the details related to the production can follow different types of reactors, which will be discussed in the next section.

1.3.2 Production

As previously introduced, e-fuels or synthetic fuels are fuels obtained from renewable energy sources by using CO_2, captured from the atmosphere, coupled with hydrogen. This procedure, chemically based and known as synthesis, can be allowed through two pathways to obtain long-chain hydrocarbons: Fischer-Tropsch Synthesis or Methanation.

The Fischer-Tropsch Synthesis consists of a catalytic conversion of the Syngas (CO + hydrogen). As mentioned, the start of the process for producing e-fuels requires the capturing of CO_2, or its extraction from other sources (companies, industries, etc.) in order to remove any source of CO_2 production in the atmosphere. Then, with the same concept, the production of hydrogen requires a green process; in this way, the hydrogen will be called “green” hydrogen. Thus, no emission of CO_2 is permitted, but on the contrary, the process will consist of CO_2 consumption. However, the F-T process needs to be fed with CO and hydrogen, making it necessary to take a further step where carbon dioxide must be converted into carbon monoxide. This process or better, the reaction, takes the name of “Reverse Water-Gas Shift” (RWGS):

$$CO_2 + H_2 \rightarrow CO + H_2O \qquad \textit{Eq. 1}$$

The reaction is endothermic, and requires energy with the same concept explained before, without emitting other sources of carbon dioxide for producing energy. The temperature to obtain such reactions is between 170-220 [°C], around 1 to 10 [MPa]. Then, the CO is adopted by the next reactions in the Fischer-Tropsch reactor, which consist of a couple of fundamental reactions for the main hydrocarbons produced: *alkanes* and *alkenes*.

The equation that governs the formation of the first ones (alkanes → C_nH_{2n+2})

$$nCO + (2n+1)H_2 \rightarrow C_nH_{2n+2} + nH_2O \qquad \textit{Eq. 2}$$

Instead, the one related to the formation of alkenes → C_nH_{2n}:

$$nCO + 2nH_2 \rightarrow C_nH_{2n} + nH_2O \qquad Eq.\ 3$$

This process can also include different reactors, such as Cobalt for their highly catalytic properties and for the production of long-chain saturated hydrocarbons (for example, the *paraffins*). Furthermore, those reactions with the adoption of Cobalt allow reducing the quantity of CO_2 and water content. Iron can also be used, especially when Syngas is derived from biomass, where the content of CO_2 is higher compared to other sources. Then, depending on the catalyst, the products can also change, in this case, with the output of light hydrocarbons and *olefins*. Other catalytic materials can be selected, such as Magnesium oxide, thorium dioxide, etc., with consequent different properties related to the stability of the reactions that can be suitable in relation to the outcome. Of course, the process allows obtaining low-octane fuels that will be improved through specific addition of octane enhancers, oxygenates, or the specific process of catalytic reforming (isomerization of alkanes, dehydrogenation for *aromatics* production, etc.)

The second process that is described is the one that is mainly adopted in the e-fuels industry and it is based on the methanol synthesis. This requires the hydrogenation of the CO_2, which is captured from the environment. The hydrogenation consists of three reactions that occur in the reactor of the plant. The reactions are exothermic, and also in this case will require energy to allow the reaction to occur at a temperature around 250-300 [°C] and 5-10 [MPa], which are the more efficient ones [105-107]. The major reactions are reported:

$$CO_2 + 3H_2 \leftrightarrow CH_3OH + H_2O \qquad Eq.\ 4$$

$$CO_2 + H_2 \leftrightarrow CO + H_2O \qquad Eq.\ 5$$

$$CO + 2H_2 \leftrightarrow CH_3OH \qquad Eq.\ 6$$

As visible from the equations reported, the reactions led to the production of byproducts such as water (steam) and carbon monoxide, which are then reused. The major component obtained by the process is the methanol, which, following the green procedure and by reusing the CO_2 in the atmosphere, is an e-methanol. Most of the fuel suppliers that produce e-fuels also allow the use of e-methanol directly or then adopt the e-methanol in specific reactors that allow obtaining the final shape of the synthetic fuels such as e-gasoline, e-diesel, and e-LG.

1.3.3 Methanol to Olefin / Methanol to Gasoline

Focusing on the fuel production and characteristics of fuels for ICEs, the production of e-methanol can be considered the second product of this chain for fueling ICEs through next-step fuels for the future. The e-methanol, as previously described, is obtained from the synthesis process that uses carbon dioxide and hydrogen. Hydrogen, as discussed in the previous chapter, is an energy carrier that itself can fuel an ICE in an efficient way. Furthermore, if the production of this energy carrier is carried out with renewable sources, wind, geothermal, solar, or nuclear, it also allows for meeting the carbon-neutral perspective. Then, at the end of the Fischer-Tropsch or Methanol Synthesis, the use of hydrogen as a reaction species in the catalytic reaction allows the production of e-methanol, which is

a substance with different properties and characteristics of usage compared to hydrogen. So, here, before the next process that can occur in specific reactors, the early process for e-fuels led to the production of two early products: green hydrogen and e-methanol.

Making a comparison of these two products of the early reactions involved for the next reagents in methanol reactors, such as *Methanol-to-Olefins* (MtO) and *Methanol-to-Gasoline* (MtG), it is important to consider that two energy carriers are already available and ready for use. The use of these components "as it is", especially targeting the automotive and transportation sector, can be summarized as follows:

Table 3 Comparison of major properties between Hydrogen and e-Methanol

Property	**Hydrogen**	**e-Methanol**
Production	Electrolysis	Methanol Synthesis / F-T
Costs	3-6 $ / kg | 0.09-0.28 $/kWh	0.80-1.20 $/kg | 0.13-0.20 $ /kWh
Transport/Delivery	Expensive and complex pipelines or transportation | special/cryogenic tank	Fuel tank / existing infrastructures
Storage	High-pressure tank (250-700 bar) or cryogenic maintenance	Liquid at ambient temperature conditions and easy storage in a regular fuel tank
Ready technology	Limited / new refueling pipelines ang stations	Mature technology (widely adopted over years)
Carbon Footprint	Zero impact (green hydrogen)	Biogenic and CO2 capture technology – Net-zero impact
Use	Fuel cells / Industry / (recently developed) ICEs	ICEs (Marine and high-performance competitions and transportation) / Chemical feedstock
Safety	Highly flammable / invisible flame and highly volatile	Flammable / Easier to handle compared to gas fuels
Density	0.09 kg/m^3	792 kg/m^3
Laminar Burning Rate	250-300 [m/s]	40-50 [m/s]
Lower Heating Value	120 [MJ/kg]	20 [MJ/kg]
RON	~130	~109

Of course, these two energy carriers can be handled and adopted in different scenarios of industry and transportation, leading to the same outcome of reaching an important target: net-zero or zero CO_2 emissions today.

The next process that this part would like to consider is the use of reactors that utilize these two energy carriers, enabling the achievement of the same net-zero CO_2 emissions while offering numerous advantages for the transportation sector. The technology that we are considering for the automotive market has the same outcome: a balance of net-zero CO_2 emissions at the tailpipe of a passenger car or road transportation truck, along with reasonable performance and infrastructure. The characteristic of infrastructure-based technologies is one of the most important properties of a fuel that allows it to

be used on a large scale with a low impact on the deliverability and accessibility. The two most important reactors that allow the production of synthetic fuels are the Methanol-to-Olefin and Methanol-to-Gasoline. The first one is adopted, focusing on obtaining fuels for aviation, such as e-SAF (electronic - Sustainable Aviation Fuel). First applications were pursued by carbon-neutral SAF for Boeing 737 in February 2021 from Amsterdam to Madrid using 500 liters of e-kerosene mixed with regular aviation fuel [108]. The possibility of the e-SAF currently adopted is one of the most important strengths of this technology, which is extended for all kinds of e-fuels without requiring or forcing the use of different injection systems or dedicated tanks. The process to obtain these e-SAF depends on the specific technology adopted, patent-based in relation to the company that produces the e-fuel. Typically, the MtO consists of a reactor that starts with the usage of e-methanol, then follows a different process for different outputs for industry or the transportation sector. The e-methanol follows [109]:

- Low carbon chain hydrocarbons through the SAPO-34 zeolite to produce light olefins.
- Long chain hydrocarbons through oligomerization by combining short olefins into C8-C16 hydrocarbons. Typically, the SAF includes n-alkanes, isoalkanes and cycloalkanes from C8 to C18 [110].
- Hydrogenation and Fractionation (splitting the chain for specific use) transform saturated olefins into paraffins, which are compatible with Jet A/A-1.
- Hydrocracking also allows the production of e-diesel as another byproduct.

The process can be summarized as: CO2 + H2 → e-methanol → Olefins → Oligomers → Hydrogenated → e-SAF

The technology and major producers are Honeywell UOP, which adopts MtO + eFining^{TM} (based on oligomerization + hydrogenation) [111] and is currently adopted by ExxonMobil in their pilot plant for e-fuels production, being able to reach 88% of CO_2 reduction compared to regular SAF. The Methanol-to-Olefin or Methanol-to-Jet fuel allows producing highly efficient e-SAF converting methanol into jet-range hydrocarbons suitable for aviation transportation. Then, another technology developed by Honeywell, the FT Unicracking, is a refining process that upgrades the FT products in drop-in SAF, as previously explained, the fractionating process. This process is strongly important in order to allow the production to reach the targeted properties of eSAF with a high carbon efficiency and performance. Then, Janson-Matthey uses their own proprietary eMERALD technology [112] for capturing CO_2 and hydrogen production for synthesis and e-methanol production or from syngas (from biomass or waste gasification). This technology finds its base in the Haru Oni pilot plant in Chile, allowing the production of e-methanol from captured CO_2 and hydrogen. Then, the group developed the LCH (low carbon hydrogen) system that allows producing low carbon intensity hydrogen at scale and then integrates with the previously Honeywell technologies toward the decarbonization technology by JM's CLEANPACE to decarbonize synthesis (Syngas) gas plants in a more efficient way. Both are specialized in e-fuels, innovative and green fuels technology development and production, and recently have established their partnership with HIF, which leads toward the best collector of the most innovative and developing sector of this new technology scenario.

Then, the second important pathway regards the further usage in a fundamental conversion driven the next generation fuels for road transportation, such as e-Gasoline, e-Diesel and e-LG. The concept is the same as seen for MtO, but here e-methanol is pushed in reactors toward ICEs suitable fuels. The MtG technology began development in 1970 by Mobil. It has since evolved and is now utilized in various applications, including the Haru Oni plant. ExxonMobil [113,114] has adopted this technology, and more recently, Aramco implemented it in a new demonstration plant for e-fuel production in Saudi Arabia, focusing on next-generation, highly efficient, and low-carbon fuels. The technology is based on the starting point of usage of e-methanol that is guided in the MtG reactor through a specific process to reach a well-distilled fuel with mixed *paraffins*, *napthenes* and *aromatic* components. The process allows the production of DME (Di-Methyl Ether), which can be used similarly to e-methanol but with some more peculiar properties. Then the process follows the reported reactions:

- Methanol to Di-methyl Ester: $2\ CH_3OH \leftrightarrow CH_3OCH_3 + H_2O$
- $CH_3OH\ and\ CH_3OCH_3\ (DME) \rightarrow Light\ Olefins + H_2O$
- Light Olefins → $C_5 + Olefins$ | Oligomerization where light olefins form C_5 hydrocarbons and also longer olefins → Precursor of the gasoline-range molecules

  Toward Gasoline:

  1) Oligomerization: $C_5 + Olefins$ → From short-chain olefins to long-chain hydrocarbons:
     $$C_3H_6 + C_2H_4 \rightarrow C_5H_{10}\ \text{(example n-pentene)}$$
  2) Cyclization: $C_5 - C_6$ ring formation by producing *Naphtenes* (cycloalkanes):
     $$C_6H_{12} \rightarrow Cyclohexane$$
  3) Aromatization: *Olefins* and *Cycloalkanes* are converted into aromatic compounds by the catalyzed ZSM-5, which is able to promote the dehydrogenation and rearrangement into aromatic rings:
     $$Cyclohexane \rightarrow Benzene + 3H_2$$
  4) Alkylation of *Benzene*: this leads to toluene formation, which is present in most of the gasoline as an important knock enhancer, as will be considered later in the specific definition of fuel surrogates:
     $$Benzene + CH_3 \rightarrow Toluene$$
  5) Isomerization: important to obtain branched isomers from C_8 *alkanes*, such as n-octane (or n-pentane following the reactions and iso-pentane), without any knock resistance (almost RON = 0) and that needs to be rearranged through an acid-catalyzed (catalytic isomerization) process to obtain the Isooctane:
     $$n - Octane \rightarrow |catalytic\ Pt/Al_2O_3\ and\ \text{heat}| \rightarrow Isooctane$$

  The MtG concludes with the formation of a single fuel, an e-fuels that contains all the presented compounds/hydrocarbons with many more byproducts in reasonably negligible percentages. Then, since this process allows for chemical design of the fuels, further additives, the so-called *oxygenates*, can be added to reach more properties for specific usage in ICEs.

Table 4 Comparison of the major properties of Hydrogen, e-Methanol, and eGasoline as final product for the automotive sector

Property	**Hydrogen**	**e-Methanol**	**eFuels - eGasoline**
Production	Electrolysis	Methanol Synthesis / F-T	MtG (through FT/MeOH)
Costs	3-6 $ / kg | 0.09-0.28 $/kWh	0.80-1.20 $/kg | 0.13-0.20 $ /kWh	5 $ / kg → planned to reach 2 $ / kg
Transport/Delivery	Expensive and complex pipelines or transportation | special/cryogenic tank	Fuel tank / existing infrastructures	Fuel tank / existing infrastructures
Storage	High-pressure tank (250-700 bar) or cryogenic maintenance	Liquid at ambient temperature conditions and easy storage in a regular fuel tank	Liquid at ambient temperature conditions and easy storage in a regular fuel tank
Ready technology	Limited / new refueling pipelines ang stations	Mature technology (widely adopted over years)	Mature technology and improving currently
Carbon Footprint	Zero impact (green hydrogen)	Biogenic and CO_2 capture technology – Net-zero impact	Net-zero CO_2 emissions
Use	Fuel cells / Industry / (recently developed) ICEs	ICEs (Marine and high-performance competitions and transportation) / Chemical feedstock	ICEs road transportation / Trucks / Aviation
Safety	Highly flammable / invisible flame and highly volatile	Flammable / Easier to handle compared to gas fuels	Flammable – same as regular fuel
Density	0.09 kg/m^3	792 kg/m^3	~ 750 kg/m^3
Laminar Burning Rate (@20-25 [°C])	~ 280 [m/s]	~ 50 [m/s]	~ 40 [m/s]
Lower Heating Value	120 [MJ/kg]	20 [MJ/kg]	~ 45 [MJ/kg]
RON	~130	~109	~ 95/98 (E10 / SP)

It is possible to observe in Table 4, a comparison of the hydrogen, methanol and eGasoline, which represents an overview of the potential and drawbacks of the eGasoline (or e-fuels) compared to other energy carriers. As discussed earlier, the production chain of an e-fuel plant allows obtaining all these fuels, and they can all be used for different purposes. Of course, since this thesis focuses on ICEs and automotive applications, the focus in Table 4 is reported on the eGasoline, which presents the same performance as regular gasoline but with a drastic reduction of CO_2 footprint. Furthermore, it is compared to the other fuels that the F-T or Methanol Synthesis allows to obtain, highlighting that e-fuels are the most suitable for ICEs and the automotive sector, and can easily replace the current fuels for the transportation sector. Nevertheless, the lack of current plants and the requirement for specific locations or favorable locations for renewable energy sources represent points for future discussions.

The drawbacks, however, are not so big to avoid the development of these fuels; in fact, it seems more due to political and economic reasons. The benefits of these fuels can be achieved immediately, based on current infrastructure and pushing toward continuous development and widening the scope of production. Of course, the costs of these fuels are targeted to be reduced with the adoption. In fact, they are easy to deliver, transport and move from one location to another without issues related to their phase, which is liquid at ambient temperature. The transportation itself can be fed with methanol/hydrogen for marine transportation or eGasoline/eDiesel for road transport, such as trucks and other vehicles, as well as hydrogen for fuel cell trucks.

1.3.4 Oxygenates

Gasoline is a fossil fuel composed of a complex mixture of hydrocarbon species, often numbering in the hundreds, each contributing to the overall physical and chemical characteristics of the fuel. In addition to these hydrocarbons, gasoline also contains minor fractions of by-products and additives such as detergents, trace sulfur compounds, and other regulated species, that, although present in controlled and minimal amounts, may still influence the fuel behavior. Some components, when unnecessary or detrimental, can negatively affect combustion quality by promoting deposit formation on engine parts [115,116].

Within this heterogeneous composition, a relevant role is played by oxygenated additives, commonly known as oxygenates, which significantly contribute to the functional properties of gasoline. These compounds are primarily associated with improvements in anti-knock quality, as well as with reductions in soot and PAH emissions, thereby enhancing the environmental performance of the fuel. According to Sarathy, Farooq and Kalghatgi [11], oxygenates are increasingly relevant in the evolution of modern transportation fuels and in the transition toward cleaner, more efficient combustion systems.

Among the oxygenates used or investigated in gasoline formulations, the most important include ETBE (ethyl tert-butyl ether), MTBE (methyl tert-butyl ether), ethanol, TAME (tert-amyl methyl ether), DME (dimethyl ether), butanol isomers, pentanol isomers, alkyl-furans and furans, aromatic oxygenates, and esters derived from levulinic acid. These components have been widely discussed in the literature on future transportation fuels, both for their chemical versatility and their compatibility with modern high-efficiency engines.

In this work, specific attention is placed on ETBE, MTBE, and ethanol, as they represent the oxygenates most commonly adopted in practical ICE applications. As discussed in the dedicated section of this manuscript, these compounds are also considered when defining oxygenated surrogate fuels. Their selection is guided by the need to reproduce and control key combustion characteristics, such as knock resistance, stability during ignition and combustion, burning behavior, and overall fuel durability.

Recent applications in ICEs demonstrate that blending these oxygenates into gasoline can significantly enhance clean combustion free of injection deposits [117], combustion efficiency and power output, particularly at higher compression ratios, as reported by Di Iorio et al. [118]. In the present study, the availability of detailed fuel composition data, provided through collaborations with the automotive industry, enables a dual investigation approach: (i) a modelling analysis focused on

the chemical impact of oxygenated components in both conventional gasoline and e-fuels, and (ii) an experimental comparison of IMEP, power output, and combustion efficiency between conventional fuels and e-fuels, as published in [31,32].

A summary of the main properties of the adopted oxygenate compounds is reported in the table in section 5, together with a detailed comparison of the key physicochemical characteristics of ethers and alcohols.

Then, when discussing the properties of such substances, ETBE and MTBE, as ethers, some discrepancies are observed in terms of properties. Especially, it is quite misleading to specify the specific RON/MON that can describe these substances as well as some different properties. Nevertheless, the author wants to report such a table where the most indicative anti-knock properties are reported, giving an overall vision that MTBE and ETBE behave similarly. Some more information over the years has been completely treated with ethanol.

1.3.5 The Octane Index - OI

Referring to the anti-knock quality of a fuel, particularly gasoline, there is extensive literature describing the foundations of octane rating as well as the specific standardized procedures used for both RON (Research Octane Number) and MON (Motor Octane Number) tests. However, when examining these quantities more deeply, an additional analytical parameter becomes relevant, as also described by Kalghatgi [119]: the *Octane Index (OI).*

This parameter provides a more accurate representation of how prone or resistant a gasoline is to knock under real engine operating conditions.

$$OI = RON - KS \qquad Eq.\ 7$$

where S is the sensitivity of the fuel (S = RON – MON). Sensitivity is also considered in this work, especially in the CFD chemical-based simulations aimed at predicting laminar flame speed (LFS) and ignition delay time (IDT) of real gasolines through their surrogate mixtures. In practical terms, the OI represents the octane number of the PRF—or more generally the surrogate fuel—that matches the auto-ignition behavior of the real gasoline under non-standardized, engine-specific conditions.

It is important to highlight that S, which is typically around 10 for conventional gasolines, may differ significantly for new-technology fuels such as e-fuels. This difference can strongly affect the interpretation of RON/MON and the resulting OI. The methodology proposed by Kalghatgi is therefore crucial, because it emphasizes the need to consider not only PRFs but also more complex surrogate formulations in order to reproduce the real auto-ignition behavior of multi-component fuels.

In this framework, the parameter K is not only linked to the chemical composition of the fuel, but also to its behavior inside the engine under specific operating conditions. To determine K, a linear regression is performed based on engine-relevant auto-ignition indicators:

$$z = aRON - bMON + c \qquad \textit{Eq. 8}$$

$$OI = \frac{a}{a+b}RON - \frac{b}{a+b}MON \rightarrow z = c + (a+b)OI \qquad \textit{Eq. 9}$$

Finally,

$$K = \frac{b}{a+b} \qquad \textit{Eq. 10}$$

This formulation clarifies the physical meaning of the coefficients:

- if "*a*" is larger, the operating condition behaves more like a RON-driven regime,
- if "*b*" is larger, the behavior is more MON-driven, indicating higher severity (higher temperature/pressure) of the unburned gases.

This also confirms the initial statement: the real knock behavior of a fuel is governed by the engine operating conditions, not only by its RON and MON values. When two fuels have the same sensitivity S and K = 0, then OI = RON and a similar knock behavior would be expected.

2 CFD – The role of Computational Fluid Dynamics

2.1 Introduction

This entire thesis work is based on the importance of Computational Fluid Dynamics as a branch of fluid dynamics that, through its models, methods and their place in Science, allows for reaching "computational" results. Of course, from the title of this work, one term that is redundant and, in other cases, unfortunately not cited, is the validation. The CFD, in fact, to be reliable and useful, must be validated against experiments, with its basic concepts strictly adhering to the physical and chemical laws. Of course, despite the great degree of modelling that can be achieved in simulation frameworks, it must be kept in mind that the solution we obtain is affected by several factors, such as discretizations, numerics, approximation of space and time, and modelled quantities. So, CFD results or numerical results are always approximate according to Ferziger, Perić, Street [120]. Of course, looking back 1960s, when the first techniques from CFD were introduced into the design and manufacturing process for aircraft and engines, over almost 60 years, things have changed strongly. The current availability of previously unaffordable techniques is now radically improved, allowing us to move towards new perspectives of simulations. The current state and great improvements in HPC computers, new generation hardware, GPUs, and many more technological advancements have opened up many more frameworks and CFD techniques. In the automotive sector, as the field of this thesis, although some applications can be applied and adapted in other scenarios, the availability of an HPC opened the scenario for deepening evaluations in LES frameworks, while maintaining the targeting from the industrial perspective. In fact, despite the continuously developing hardware ruling the technology sector, the still very high computational costs for energy, cooling and simulation time still play a fundamental role in the CFD sector. This is why, as will be discussed in detail, when referring to the LES, we still refer to an affordable and feasible perspective, starting from the discretization of CFD, through an "Engineering" LES rather than a "Scientific" LES following Rutland [121], establishing and revamping the strong importance of the science in critically focusing on always updated problems in the industry field.

2.2 Navier-Stokes Equations

The computational approach is a faithful representation of the physical laws as well as the mathematical representation of them. The basics of CFD fall in the governing equations of fluids, as mentioned, a mathematical representation of the conservation laws of physics. The following discussion aims to give the fundamentals behind this fascinating world of physics through the complexity of the mathematical representation of mass conservation, the rate of change of momentum as the sum of the forces on a fluid particle, and the rate of change of energy through the heat and work on a fluid particle. The following dissertation aims to be synthetic as it is widely discussed in books and here reported as a basic introductory for Navier-Stokes equations, which are the fundamentals of the next models that are discussed in this work.

2.3 Mass Conservation

The first concept is based on the statement that the mass is conserved in a control volume or, generally speaking, in a fluid domain. This led to the following "continuity equation":

$$\frac{\partial \rho}{\partial t} + \nabla \cdot (\rho u) = 0 \qquad \textit{Eq. 11}$$

This equation (Eq. 11) is written in the compact vector notation and represents the unsteady, continuity equation in a three-dimensional domain for compressible fluids (note that in the case of incompressible ones the $\nabla \cdot u = 0$ since the constant value of density).

2.4 Momentum Equations

The following equations find their use as the momentum conservation laws related the properties of a fluid particle. Here, specifically, the approach meets the "Lagrangian" one, when refers to the particle itself. Thus, when referring to a fluid element, the approach will be called "Eulerian". So, the equations start being developed as the particle develops toward the secondary one, that is referred to the specifics of the simulation that is considered in a CFD domain.

Recalling the previous continuity equation, it can be reproposed as the generalization for a conserved property ϕ:

$$\frac{\partial \rho}{\partial t} + \nabla \cdot (\rho \phi u) = 0 \qquad \textit{Eq. 12}$$

As the interest in the rate of change of the property ϕ per unit volume for a fluid particle can be written as follows:

$$\rho \frac{D\phi}{Dt} = \rho \left(\frac{\partial \phi}{\partial t} + u \cdot \nabla \phi \right) \qquad \textit{Eq. 13}$$

By considering the time variation:

$$\frac{\partial (\rho \phi)}{\partial t} + \nabla \cdot (\rho \phi u) = \rho \left[\frac{\partial \phi}{\partial t} + u \cdot \nabla \phi \right] + \phi \left[\frac{\partial \rho}{\partial t} + \nabla \cdot (\rho u) \right] = \rho \frac{D\phi}{Dt} \qquad \textit{Eq. 14}$$

The equation (Eq. 14), highlighted in grey box, contains three major terms, starting from the left side:

- Rate of increase of ϕ of fluid element;
- Net rate of flow of ϕ out of fluid element;
- Rate of increase of ϕ for a fluid particle;

So, by considering Newton's second law, which states that the rate of change of momentum of a fluid particle equals the sum of the forces on the particle (F = m*a), in each of the directions (note the sign of the pressure is negative compared to the normal viscous stress due to the convention of tensile positive and compression negative):

$$\frac{\partial(-p+\ \tau_{xx})}{\partial x}+\frac{\partial \tau_{yx}}{\partial y}+\frac{\partial \tau_{zx}}{\partial z}+S_{M_x}=\ \rho\frac{Du}{Dt} \qquad \textit{Eq. 15}$$

$$\frac{\partial\left(-p+\ \tau_{yy}\right)}{\partial y}+\frac{\partial \tau_{xy}}{\partial x}+\frac{\partial \tau_{zy}}{\partial z}+S_{M_y}=\ \rho\frac{Dv}{Dt} \qquad \textit{Eq. 16}$$

$$\frac{\partial(-p+\ \tau_{zz})}{\partial z}+\frac{\partial \tau_{xz}}{\partial x}+\frac{\partial \tau_{yz}}{\partial y}+S_{M_z}=\ \rho\frac{Dw}{Dt} \qquad \textit{Eq. 17}$$

By considering the first law of Thermodynamics, the rate of increase of energy of a fluid particle is equal to the sum of the counterpart of the net rate of heat plus the net rate of work done on the fluid particle. Calling the following term as the rate of increase of energy as $\rho\frac{DE}{Dt}$, one can state that the energy equation in the following compact form:

$$\rho\frac{DE}{Dt}=\ \dot{w}+\dot{q} \qquad \textit{Eq. 18}$$

Going more into detail in each single major term $\dot{w}$, one can develop the term as related to the surface force as equal to the product of the force and velocity component in the direction of the force. Initially, splitting the terms for each direction from the momentum equations, recalling the momentum ones:

$$\left[\frac{\partial(u(-p+\ \tau_{xx})}{\partial x}+\frac{\partial\left(u\tau_{yx}\right)}{\partial y}+\frac{\partial(u\tau_{zx})}{\partial z}\right]\delta_x\ \delta_y\delta_z \qquad \textit{Eq. 19}$$

$$\left[\frac{\partial\left(v\left(-p+\ \tau_{yy}\right)\right)}{\partial y}+\frac{\partial\left(v\tau_{yx}\right)}{\partial x}+\frac{\partial\left(v\tau_{zy}\right)}{\partial z}\right]\delta_x\ \delta_y\delta_z \qquad \textit{Eq. 20}$$

$$\left[\frac{\partial(w(-p+\ \tau_{zz})}{\partial z}+\frac{\partial\left(w\tau_{yz}\right)}{\partial y}+\frac{\partial(w\tau_{xz})}{\partial x}\right]\delta_x\ \delta_y\delta_z \qquad \textit{Eq. 21}$$

From previous equations, the total rate of work done per unit volume is the sum of each term and by dividing by the volume $\delta_x\ \delta_y\delta_z$. The compact for is reported and will be adopted later on:

$$-\frac{\partial(up)}{\partial x}-\frac{\partial(vp)}{\partial y}+\frac{\partial(wp)}{\partial z}=-\nabla\cdot(\mathrm{pu}) \qquad \textit{Eq. 22}$$

So, the total rate of work done on the fluid particle by surface stresses:

$$-\nabla \cdot (\mathrm{pu}) + [\frac{\partial(u\tau_{xx})}{\partial x} + \frac{\partial(u\tau_{yx})}{\partial y} + \frac{\partial(u\tau_{zx})}{\partial z} + \frac{\partial(v\tau_{xx})}{\partial x} + \frac{\partial(v\tau_{yx})}{\partial y} + \frac{\partial(v\tau_{zx})}{\partial z} + \frac{\partial(w\tau_{xx})}{\partial x} + \frac{\partial(w\tau_{yx})}{\partial y} + \frac{w(u\tau_{zx})}{\partial z}] \quad \textit{Eq. 23}$$

Then, the net rate of heat transfer to the fluid particle due to the flow in the direction along x-axis, as reported hereafter for clarity, is given by:

$$[(q_x - \frac{\partial q_x}{\partial x}\frac{1}{2}\,\delta_x) - (q_x + \frac{\partial q_x}{\partial x}\frac{1}{2}\,\delta_x)]\,\delta_y\delta_z = -\frac{\partial q_x}{\partial x}\,\delta_x\delta_y\delta_z \quad \textit{Eq. 24}$$

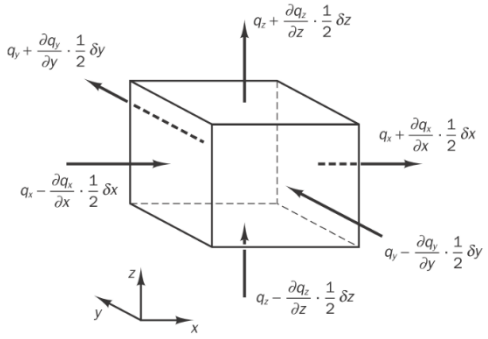

Of course, the same states for all the directions, and finally gives:

$$-\frac{\partial q_x}{\partial x} - \frac{\partial q_y}{\partial y} - \frac{\partial q_z}{\partial z} = -\nabla \cdot \mathrm{q} \quad \textit{Eq. 25}$$

Then, following Fourier's law of heat conduction relates the heat flux to the local temperature gradient and is expressed by:

$$q_x = -k\,\frac{\partial T}{\partial x};\; q_y = -k\,\frac{\partial T}{\partial y};\; q_z = -k\,\frac{\partial T}{\partial z} \quad \textit{Eq. 26, Eq. 27, Eq. 28}$$

By combining the latter two equations, we obtain that the rate of heat addition to the fluid particle due to heat conduction across the element boundary is:

$$-\nabla \cdot \mathrm{q} = \nabla \cdot (\mathrm{k}\,\nabla \mathrm{T}) \quad \textit{Eq. 29}$$

The conservation of energy equation is written as follows, by considering the previous terms acting on the fluid particle. Since the base of this work is developed for mechanical engineering applications, the energy can be represented as the kinetic energy, which yields the final formulation:

$$\rho\frac{DE}{Dt} = -\nabla \cdot (\mathrm{pu}) + [\frac{\partial(u\tau_{xx})}{\partial x} + \frac{\partial(u\tau_{yx})}{\partial y} + \frac{\partial(u\tau_{zx})}{\partial z} + \frac{\partial(v\tau_{xx})}{\partial x} + \frac{\partial(v\tau_{yx})}{\partial y} + \frac{\partial(v\tau_{zx})}{\partial z} + \frac{\partial(w\tau_{xx})}{\partial x} + \frac{\partial(w\tau_{yx})}{\partial y} + \frac{\partial(w\tau_{zx})}{\partial z}] + \nabla \cdot (\mathrm{k}\,\nabla \mathrm{T}) + S_E \quad \textit{Eq. 30}$$

Briefly summarized each term as follows:

$\rho \frac{DE}{Dt}$ → Rate of change of kinetic energy for the unit volume

$-\mathrm{u} \cdot \nabla \mathrm{p}$ → Work done by pressure on the fluid element; note the sign (-)

$u\left(\frac{\partial(\tau_{xx})}{\partial x}+\frac{\partial(\tau_{yx})}{\partial y}+\frac{\partial(\tau_{zx})}{\partial z}\right) \mid also\ for\ v,w$ → Viscous dissipation and energy exchange due to the shear stress; since (τ_{ij}) is the viscous stress tensor

$\mathrm{u} \cdot \mathrm{S_M}$ → External sources (ex. Gravity, etc.)

2.5 Navier-Stokes Equations (for Newtonian fluid)

Collecting information explained from conservation laws, the conservation equations contain a viscous stress tensor that requires a model such as reported in the form τ_{ij}, introduced in the previous discussion on the energy equation. So, since the three-dimensional model is what we are interested in, we can directly move to three-dimensional flow characteristics, in which the viscous stresses can be expressed by the composition of linear deformation and volumetric deformation. As reported by Schlitching [125], the second viscosity, which relates to volumetric deformation, can be represented synthetically by $\lambda = -\frac{2}{3}\mu$, and μ stay on representing linear deformation in flows.

Again, following Schlichting, the three elongating deformation components represent the rate of deformation by the following components:

$$S_{xx} = \frac{\partial u}{\partial x}; S_{yy} = \frac{\partial v}{\partial y}; S_{zz} = \frac{\partial w}{\partial z} \qquad \textit{Eq. 31, Eq. 32, Eq. 33}$$

The six shearing linear deformation components are:

$$S_{xy} = S_{yx} = \frac{1}{2}\left(\frac{\partial u}{\partial y}+\frac{\partial v}{\partial x}\right); \qquad \textit{Eq. 34}$$

$$S_{xz} = S_{zx} = \frac{1}{2}\left(\frac{\partial u}{\partial z}+\frac{\partial w}{\partial x}\right); \qquad \textit{Eq. 35}$$

$$S_{yz} = S_{zy} = \frac{1}{2}\left(\frac{\partial v}{\partial z}+\frac{\partial w}{\partial y}\right) \qquad \textit{Eq. 36}$$

Since in the Newtonian fluid there is the proportionality of the viscous stress and the rates of deformation, the nine viscous stress components are reported by considering the volumetric deformation:

$$\frac{\partial u}{\partial x}+\frac{\partial u}{\partial x}+\frac{\partial u}{\partial x} = \nabla \cdot \mathrm{u} \qquad \textit{Eq. 37}$$

Recalling the momentum equation and by substituting the viscous stress tensors with the following statements that link the second viscosity to the first one:

$$\tau_{xx} = 2\mu\frac{\partial u}{\partial x} + \lambda\nabla\cdot \mathrm{u}; \quad \textit{Eq. 38}$$

$$\tau_{yy} = 2\mu\frac{\partial v}{\partial y} + \lambda\nabla\cdot \mathrm{u}; \quad \textit{Eq. 39}$$

$$\tau_{zz} = 2\mu\frac{\partial w}{\partial z} + \lambda\nabla\cdot \mathrm{u} \quad \textit{Eq. 40}$$

Finally,

$$\tau_{xy} = \tau_{yx} = \mu\left(\frac{\partial u}{\partial y} + \frac{\partial v}{\partial x}\right) \quad \textit{Eq. 41}$$

$$\tau_{xy} = \tau_{yx} = \mu\left(\frac{\partial u}{\partial y} + \frac{\partial v}{\partial x}\right) \quad \textit{Eq. 42}$$

$$\tau_{xy} = \tau_{yx} = \mu\left(\frac{\partial u}{\partial y} + \frac{\partial v}{\partial x}\right) \quad \textit{Eq. 43}$$

Finally, we obtain the Navier-Stokes equations:

$$\rho\frac{Du}{Dt} = -\frac{\partial p}{\partial x} + \frac{\partial}{\partial x}\left[2\mu\frac{\partial u}{\partial x} + \lambda\nabla\cdot \mathrm{u}\right] + \frac{\partial}{\partial y}\left[\mu\left(\frac{\partial u}{\partial y} + \frac{\partial v}{\partial x}\right)\right] + \frac{\partial}{\partial z}\left[\mu\left(\frac{\partial u}{\partial z} + \frac{\partial w}{\partial x}\right)\right] + S_{M_x} \quad \textit{Eq. 44}$$

$$\rho\frac{Dv}{Dt} = -\frac{\partial p}{\partial y} + \frac{\partial}{\partial x}\left[\mu\left(\frac{\partial u}{\partial y} + \frac{\partial v}{\partial x}\right)\right] + \frac{\partial}{\partial y}\left[2\mu\frac{\partial v}{\partial y} + \lambda\nabla\cdot \mathrm{u}\right] + \frac{\partial}{\partial z}\left[\mu\left(\frac{\partial v}{\partial z} + \frac{\partial w}{\partial y}\right)\right] + S_{M_y} \quad \textit{Eq. 45}$$

$$\rho\frac{Dw}{Dt} = -\frac{\partial p}{\partial x} + \frac{\partial}{\partial x}\left[\mu\left(\frac{\partial u}{\partial z} + \frac{\partial w}{\partial x}\right)\right] + \frac{\partial}{\partial y}\left[\mu\left(\frac{\partial v}{\partial z} + \frac{\partial w}{\partial y}\right)\right] + \frac{\partial}{\partial z}\left[2\mu\frac{\partial w}{\partial z} + \lambda\nabla\cdot \mathrm{u}\right] + S_{M_z} \quad \textit{Eq. 46}$$

Which can be written in their most useful form for the finite volume method:

$$\rho\frac{Du}{Dt} = -\frac{\partial p}{\partial x} + \nabla\cdot(\mu\nabla \mathrm{u}) + S_{M_x} \quad \textit{Eq. 47}$$

$$\rho\frac{Dv}{Dt} = -\frac{\partial p}{\partial y} + \nabla\cdot(\mu\nabla \mathrm{u}) + S_{M_y} \quad \textit{Eq. 48}$$

$$\rho\frac{Dw}{Dt} = -\frac{\partial p}{\partial z} + \nabla\cdot(\mu\nabla \mathrm{u}) + S_{M_z} \quad \textit{Eq. 49}$$

And its final arrangement here, as the adoption of the Newtonian model for viscous stress in the internal energy equation:

$$\rho\frac{Di}{Dt} = -p\nabla\cdot \mathrm{u} + \nabla\cdot(\mathrm{k}\nabla \mathrm{T}) + \Phi + \mathrm{S_i} \quad \textit{Eq. 50}$$

2.6 Frameworks: RANS/URANS

It is well known that, from an engineering standpoint, the final outcome is not an "exact", although quite aleatory term, but an approximation of reality. Through this first thought, it is necessary to choose the most appropriate approach to find a solution for a specific problem, in this case, fluid dynamics. As earlier introduced, the constant increase of CPU power and calculation resources has pushed toward the possibility of enhancing the standard of CFD simulation effort. First, we're going to talk about one of the two approaches adopted in this work, based on RANS simulation with the *RNG k-eps model*. The second approach, as the more detailed of the two, will be related to the *Large Eddy Simulation* with the *SGS Wale Model*.

The RANS framework and approach for turbulence modelling consist basically of an averaging process for quantities involved in the physics of the problem. Generally, the quantities are averaged in time, despite the fact that in the first approach of Osborne Reynolds, the so-called RANS equations were averaged over a spatial volume. By considering the averaging in time, two scenarios are possible to be described. The first one, by considering the average along with the entire time of the simulation, we will call them steady RANS equations. On the other hand, averaging over a time that is long compared to the time scales of turbulence, we're referring to an unsteady approach for the resolving equations, the so-called URANS simulations.

Referring to the main equations of the RANS approach and aiming at the major differences in modelling and turbulence details to be highlighted between RANS and LES, as the comparison carried out in the H_2ICE application presented in this work.

By considering a statistically steady flow, generally speaking, each of the variables considered can be written as the sum of a time-averaged $\bar{\phi}$ value and the fluctuation about the value ϕ':

$$\phi\,(x_i,t) = \bar{\phi}(x_i) + \phi\,(x_i,t) \qquad \textit{Eq. 51}$$

By mean time averaging: $\bar{\phi}\,(x_i) = \lim_{\mathrm{T}\to\infty} \frac{1}{T}\int_0^T \bar{\phi}(x_i,t)\,dt$ *Eq. 52*

Then, considering the ensemble averaging (for unsteady simulations for example, internal combustion engines, etc.):

$$\bar{\phi}\,(x,t) = \lim_{\mathrm{N}\to\infty} \frac{1}{T}\sum_{n=1}^{N} \phi(x_i,t), \qquad \textit{Eq. 53}$$

where N must be large enough to eliminate the effects of turbulent random fluctuation.

$$\overline{u_i\phi} = \overline{(\bar{u}_i + u_i')(\bar{\phi} + \phi')} = \bar{u}_i\bar{\phi} + \overline{u_i'\phi'} \qquad \textit{Eq. 54}$$

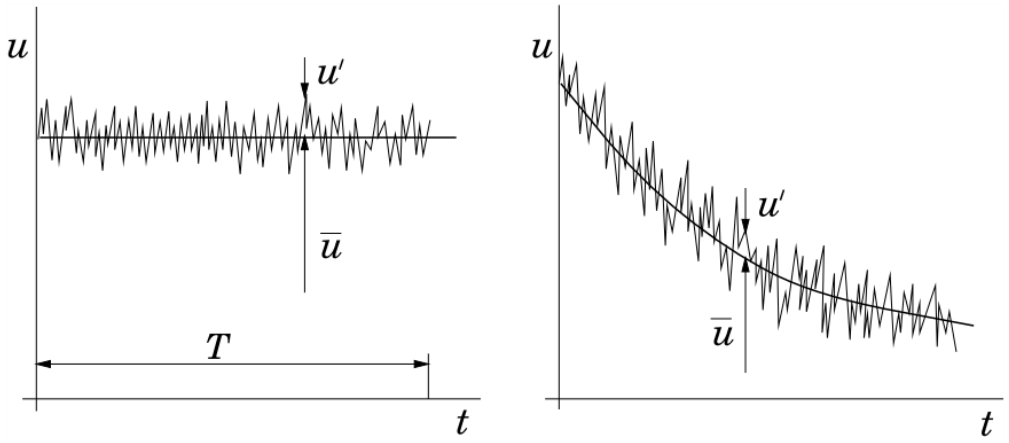

By referring to previously described formulation for Mass, Momentum, and Scalar quantities for incompressible flows:

$$\text{MASS: } \frac{\partial(\rho\bar{u}_i)}{\partial x_i} = 0 \qquad \textit{Eq. 55}$$

$$\text{MOMENTUM: } \frac{\partial(\rho\bar{u}_i)}{\partial t} + \frac{\partial}{\partial x_j}\left(\rho\bar{u}_i\bar{u}_j + \overline{\rho u_i'u_j'}\right) = -\frac{\partial\bar{p}}{\partial x_i} + \frac{\partial\bar{\tau}_{ij}}{\partial x_j} \qquad \textit{Eq. 56}$$

$$\text{SCALAR: } \frac{\partial(\rho\bar{\phi})}{\partial t} + \frac{\partial}{\partial x_j}\left(\rho\bar{u}_j\bar{\phi} + \overline{\rho u_j'\phi'}\right) = \frac{\partial}{\partial x_j}\left(\Gamma\frac{\partial\bar{\phi}}{\partial x_j}\right) \qquad \textit{Eq. 57}$$

So, the mean viscous stress is represented by:

$$\bar{\tau}_{ij} = \mu\left(\frac{\partial\bar{u}_i}{\partial x_j} + \frac{\partial\bar{u}_j}{\partial x_i}\right) \qquad \textit{Eq. 58}$$

Thus, from the momentum equations, it is possible to remark the new unknowns.

Reynolds stresses, such as the symmetric tensor with 6 unknowns and by recalling the above highlighted in grey term (by considering the 3 momentum equations):

$$\tau_{ij}^t = -\overline{\rho u_i'u_j'} \qquad \textit{Eq. 59}$$

And the turbulent scalar flux is such a vector with 3 unknowns:

$$q_j^t = -\overline{\rho u_j'\phi'} \qquad \textit{Eq. 60}$$

Finally, 4 averaged equations, with 4 variables and 6 averaged products of fluctuations, lead to the famous “closure problem” in turbulence modelling. The approximations are needed.

By considering the only flow away (for the moment) from the wall, and considering the fact that the energy dissipation, momentum, energy normal to the streamlines and transport of mass are quantities mediated by the viscosity in laminar flow, the turbulence can be considered as represented by the increment of viscosity. This point will be recalled in the specific topic of H_2ICEs simulations with the approach of the variable Turbulent Schmidt number. Anyway, by considering the eddy-viscosity model for the Reynolds stress, we can report:

$$-\rho\overline{u_i'u_j'} = \mu_t\left(\frac{\partial\bar{u}_i}{\partial x_j}+\frac{\partial\bar{u}_j}{\partial x_i}\right)-\frac{2}{3}\rho\delta_{ij}k, \qquad \textit{Eq. 61}$$

and the eddy-diffusions:

$$-\rho\overline{u_j'\phi'} = \Gamma_t\frac{\partial\bar{\phi}}{\partial x_j} \qquad \textit{Eq. 62}$$

The equations are still not closed, but the unknown quantities reduce to the two only quantities μ_t and Γ_t. The turbulent kinetic energy is described hereafter:

$$k = \frac{1}{2}\overline{u_i'u_j'} \qquad \textit{Eq. 63}$$

The quantities of eddy viscosity and diffusivity are not fluid properties and can vary in space and depend on the solution. The viscosity is proportional to the product of velocity scale q and a length scale L:

$$\mu_t = C_\mu\rho qL \qquad \textit{Eq. 64}$$

The two unknown terms are represented by q and L. The modelling of the quantities can find a solution by supporting the next calculation with the k-ε turbulence model.

2.7 Framework: Unsteady RANS

2.7.1 URANS Turbulence Modelling: The k-ε Turbulence Model

The complete equation for turbulent kinetic energy is:

$$\frac{\partial(\rho k)}{\partial t}+\frac{\partial(\rho\bar{u}_j k)}{\partial x_j}=\frac{\partial}{\partial x_j}\left(\mu\frac{\partial k}{\partial x_j}\right)-\frac{\partial}{\partial x_j}\left(\frac{\rho}{2}\overline{u_j'u_i'u_i'}+\overline{p'u_j'}\right)-\rho\overline{u_i'u_j'}\frac{\partial\bar{u}_i}{\partial x_j}-\mu\overline{\frac{\partial u_i'}{\partial x_k}\frac{\partial u_i'}{\partial x_k}} \qquad \textit{Eq. 65}$$

Remarked grey zones contain terms that are calculated exactly, instead of the modelled ones from the light grey term. The first of the latter ones is the turbulent diffusion of kinetic energy. The second one represents the rate of production of the turbulent kinetic energy by the mean flow. Finally, the latter one is the one from which the ε is represented as:

$$\varepsilon = \nu\frac{\partial u_i'}{\partial x_k}\frac{\partial u_j'}{\partial x_k} \cong \frac{k^{\frac{3}{2}}}{L} \qquad \textit{Eq. 66}$$

This term represents the rate at which the turbulent energy is irreversibly converted into internal energy (heat).

$$\mu_t = C_\mu \rho \frac{K^2}{\varepsilon} \qquad \textit{Eq. 67}$$

Recalling that for the eddy-viscosity model for turbulence modelling, the quantity that will be adopted will be the *effective viscosity* calculated as the sum of *molecular* and *turbulent viscosity*.

$$\mu_{eff} = \mu + \mu_t \qquad \textit{Eq. 68}$$

2.7.2 URANS Turbulence Modelling: Renormalisation Group (RNG) k-ε Turbulence Model

The current description relates to the turbulence model adopted by the author in all the cases and simulations performed in RANS frameworks. The choice of this approach is widely described in the literature, although it is not the only one that is used. The approach of statistical mechanisms, such as in this case, has led to new mathematical formalisms according to the limitation of assuming the small-scale turbulence. Then, due to the high complexity behind the procedure and mathematical description from Yakhot and Orszag from Princeton University [122], which led to the development of the RNG approach, we only stated the final set of equations, the major constants adopted in the specific Software and the concept behind the RNG. The RNG devised by Yakhot and Orszag represents the effects of the small-scale turbulence by means of a random forcing function in the Navier-Stokes equation. Conceptually, the procedure of renormalization consists of systematically removing the small-scale motion from the governing equations by expressing their effects in terms of larger-scale motions and a resulting modified viscosity. In other words, the RNG theory accommodates the fact that the turbulent eddies contribute to the turbulence, avoiding the specificity of the scales and considering the single turbulence scale, in fact, renormalized.

$$\frac{\partial(\rho k)}{\partial t} + \nabla \cdot (\rho \mathrm{k} \bar{V}) = \nabla \cdot \left[\left(\mu + \frac{\mu_t}{\sigma_k}\right) \nabla \mathrm{k}\right] + P_k - \rho(\varepsilon - \varepsilon_0) + S_k \qquad \textit{Eq. 69}$$

$$\frac{\partial(\rho\varepsilon)}{\partial t} + \nabla \cdot (\rho \varepsilon \bar{V}) = \nabla \cdot \left[\left(\mu + \frac{\mu_t}{\sigma_\varepsilon}\right) \nabla \varepsilon\right] + \frac{1}{T_e} C_{\varepsilon 1} P_\varepsilon - C_{\varepsilon 2} \rho \left(\frac{\varepsilon}{T_e} - \frac{\varepsilon_0}{T_0}\right) + C_{\varepsilon 4} \rho \varepsilon \nabla \cdot \bar{V} + S_{RNG} + S_\varepsilon$$

Eq. 70

With:

$$P_k = G_k + G_{nl} + G_b - \Upsilon_M \qquad \textit{Eq. 71}$$

$$P_\varepsilon = G_k + G_{nl} + G_{\varepsilon 3} G_b \qquad \textit{Eq. 72}$$

Where:

$$G_k: turbulent\ production$$

$$G_b: buoyancy\ production$$

$$G_{nl}: \text{non-linear}\ production$$

$$\Upsilon_M: compressibility\ modification$$

$$G_{\varepsilon 3} = \tanh \frac{|V_b|}{|u_b|}, itational\ vector\ g$$

where **V** and **u** are respectively the parallel and perpendicular velocity components to the gravitational vector **g**.

The model coefficients are reported below:

C_M (Sarkar)	C_t	C_T	$C_{\varepsilon 1}$	$C_{\varepsilon 2}$	$C_{\varepsilon 4}$	C_μ	β	σ_ε	σ_k	η_0
2	1	0.6	1.42	1.68	0.387	0.085	0.012	0.719	0.719	4.38

2.8 Framework: Large-Eddy Simulation

In 1922, Lewis Fry Richardson gave a poetic description of the so-called "turbulent energy cascade". The poetic description of this phenomenon through Richardson's words is reported:

"Big whirls have little whirls

that feed on their velocity,

and little whirls have lesser whirls

and so on to viscosity [...]"

The definition of the transition and transformation of the energy from large scales to small scales is clear, leading to a wide variety of turbulent eddies in a wide variety of length scales. Characteristic length scale, hence characterizes the vortex stretching and distorts the rotational turbulent eddies during the energy dissipation. According to the theory of turbulence, the characteristic velocity θ and the characteristic length scale ℓ of the larger eddies acquire the same order of velocity scale U and the length scale L constituting the "large eddy" Reynolds number $Re_\ell = \frac{\theta \ell}{\nu}$,which is the same as considering the magnitude of UL/ν. According to the latest statements, it is clear that large eddies are mainly dominated by inertia effects, and viscous effects are negligible. Of course, this is the only beginning of the energy cascade introduced earlier. In the 1940s, in fact, the Russian scientist Kolmogorov postulated, through mathematical form, the previously cited words of Richardson. Running directly to the very little scales, the lowest energy content is now governed by viscous effects, suggesting that inertia and viscous forces reach a time at which their ratio is equal to one. In other words, mathematically, we can report that $Re_\eta = \frac{\upsilon \eta}{\nu} = 1$. This means that the Reynolds number

of the smallest eddies based on their characteristic velocity υ and length scale η reaches the equality between inertia and viscous effects. This process ends by reaching the dissipative range, up to the dissipation through heat by viscous friction.

In the mean stage of the energy cascade, it is possible to mention the linear dissipation angle through which the energy moves from the integral range up to the Kolmogorov length scale in the dissipative range. The inertia range, the energy assumes the proportional value postulated by Kolmogorov [123] E~$E \sim k^{-\frac{5}{3}}$ then confirmed over the years from experimental evidence. Finally, resuming the most important formulations from turbulent flows and turbulence theory, we can just report the order of magnitude estimations of the ratio of the small length, time and velocity scales:

$$\eta/\ell \approx Re_{\ell}^{-\frac{3}{4}} \text{ – Length scale ratio;} \qquad \textit{Eq. 73}$$

$$\tau/T \approx Re_{\ell}^{-\frac{1}{2}} \text{ – Time-scale ratio;} \qquad \textit{Eq. 74}$$

$$\upsilon/\theta \approx Re_{\ell}^{-\frac{1}{4}} \text{- Velocity-scale ratio;} \qquad \textit{Eq. 75}$$

From the nature of turbulent flows, the wide range of eddies, and so, the length scales lead to a transport of energy from large to small ones; of course, this transport consists of the transport of conservative properties. In computational fluid dynamics, over the years, the more and more interesting and complex problems from fluid dynamics required more and more accuracy to better predict results in most physical and engineering applications. The RANS approach, and also the URANS, have been widely adopted in the last decades, but promising techniques such as LES (Large-Eddy Simulation) and DNS (Direct numerical Simulation), despite being more expensive, have found a place in the computational field. Thus, in more recent years, the higher computational resources and the advanced technology in the field of CPUs allowed a more detailed approach for computational calculations. Since in this work only LES and RANS/URANS frameworks are adopted, we will avoid a detailed description of the DNS, focusing more on the frameworks adopted here. In the core of this PhD thesis, relevant aspects of LES are considered together with the state of the art of some modelling approaches and specific evaluations and comparisons related to benefits and the full setup approach of LES instead of URANS. Nonetheless, the scope is not to prefer or impose a frame modelling but rather to give a wide evaluation of current applications of LES from an engineering standpoint. Far from a strictly “Scientific” approach, the author wants to focus and finalize the application to the usage of this modelling technique in a daily routing from a company's view, where time is usually poor and a good trade-off on modelling is the key to reach good results in a reasonable time. Talking about LES, compared to DNS, in which, in the latter, all the turbulence is resolved, and on the opposite, in URANS all the turbulence is modelled, in LES a selection of the turbulence to be resolved or modelled is considered. So, treating the large eddies, which contain more energy compared to the smallest one, to be resolved by extracting more information rather than modelling them, makes sense. The most sensible problem here is the selection of the length scale to be calculated rather than modelled. By using the LES, in fact, we placed in the middle of URANS and DNS, where the cut-off between what is considered large eddies (or larger than a filter) is resolved, instead of eddies considered small (or smaller than the cut-off filter) are modelled.

The notation between RANS and LES for velocity can be written in the same way, as follow:

$$u_i = \tilde{u}_i + u_i'' \qquad \textit{Eq. 76}$$

This consists of a separation of the velocity components into two parts, such as the term $\tilde{u}_i$ as the main velocity, formally the filtered velocity in LES. In both, this value represents an averaging process which is just conceptual from the operative standpoint. In LES, this stands for the filtered velocity can be identified in that term, as well as the mean velocity in RANS. The second term in right side of the equation stands for subgrid velocity in LES and for fluctuating velocity in RANS. From an overall standpoint, the impact on modelling in LES is directly affected by the filter size Δ, as the greater the reduction of filter dimension the lower the modelling.

Recalling the formulation that represents the velocity decomposition, one can write as follows:

$$\frac{\partial \bar{\rho}\tilde{u}_i}{\partial t} + \frac{\partial \bar{\rho}\tilde{u}_i\tilde{u}_j}{\partial x_j} = -\frac{\partial \bar{p}}{\partial x_i} + \frac{\partial \Gamma_{ij}}{\partial x_j} - \frac{\partial \bar{\rho}\tau_{ij}}{\partial x_j} \qquad \textit{Eq. 77}$$

By using the same expression for both RANS and LES, the term at the end of the right side of the equation τ_{ij} stands for the subgrid stresses in LES or the Reynolds stresses in RANS. Instead, the Γ_{ij} represents the viscous stress tensor.

Up to this point, it is possible to state that RANS and LES have the same equations, and by using the Boussinesq model, that state the turbulent stress behaves as the molecular viscous stress one proportional to the velocity gradient. Following the equation below, the Smagorinsky model [124] can be reported as:

$$\tau_{ij}^r = -2\nu_t \tilde{S}_{ij} \qquad \textit{Eq. 78}$$

$$\text{Where, } \tilde{S}_{ij} = \frac{1}{2}\left(\frac{\partial \tilde{u}_i}{\partial x_j} + \frac{\partial \tilde{u}_j}{\partial x_i}\right) \qquad \textit{Eq. 79}$$

It is clear that the major differences that RANS and LES approaches have by comparing themselves consistently fall into the ν_t calculation. The RANS equation has been widely discussed before discussing the way and the modelling behind the turbulent viscosity. Related to the specific modelling of LES, different models have been developed over the years, just the major and adapted models in our simulations will be mentioned. The calculations of ν_t which represents the subgrid-scale eddy viscosity is:

$$\nu_t = C_S^2 \Delta^2 |\bar{S}|, \qquad \textit{Eq. 80}$$

where C_s is a model parameter to be determined, Δ is the filter length scale and,

$$|\bar{S}| = \left(\bar{S}_{ij}\bar{S}_{ij}\right)^{\frac{1}{2}}. \qquad \textit{Eq. 81}$$

Recognizing that the Smagorinsky model has no additional transport equations, all the Smagorinsky-type models are zero-equation models.

2.9 The boundary wall layer in URANS/LES

As the interest in turbulence regimes, given their dominant role in internal combustion engines (ICEs), the predictivity and feasibility of CFD simulations under such high-Reynolds-number operating conditions become critically important. In ICEs, the interaction between the flow and the walls plays an essential role. In fact, the ability to accurately model these phenomena is fundamental to capturing the correct momentum exchange mechanisms and understanding the redistribution of flow variables induced by turbulence.

Turbulence continuously transfers momentum between fast-moving core-flow structures and slower-moving regions near the wall. As the wall is approached, the Reynolds number based on the local velocity scale decreases significantly, and viscous forces progressively dominate, eventually overwhelming turbulent stresses. For this reason, a turbulence model must correctly reproduce the velocity gradient from the fully turbulent core to the near-wall region, capturing the transition from turbulent to laminar-dominated behavior at the wall.

In turbulent boundary layers, the flow can be treated as fully turbulent over the majority of the thickness. However, the layer is classically subdivided into distinct regions, each governed by different physical mechanisms. Generally, two main macro-zones are identified: an *outer region*, dominated entirely by turbulent transport, and an *inner region*, which includes a near-wall viscous zone where molecular stresses exceed turbulent ones. The inner region is typically described using non-dimensional quantities that allow a universal formulation of velocity, wall distance, and shear stress.

$$u^+ = \frac{\bar{u}}{u_\tau};\ y^+ = \frac{u_\tau y}{\nu} \qquad \textit{Eq. 82,Eq. 83}$$

Of course, both the parameters are linked/based on the friction velocity, u^+ which is related to the term u_τ such as the wall shear stress:

$$\tau_w = \rho * u_\tau^2 \qquad \textit{Eq. 84}$$

The region closest to the wall, where u'= 0, is known as the *viscous sublayer*, where $y^+ < 5$, the mean velocity profile follows the linear law $u^+ = y^+$, and molecular viscosity dominates the momentum transfer. Moving outward, the flow enters the *buffer layer*, a transitional zone in which both viscous and turbulent mechanisms coexist and neither scaling law holds perfectly. Finally, the

outermost portion of the inner boundary layer is the *logarithmic layer*, where turbulent stresses dominate and the mean velocity profile follows the classical von Kármán formulation:

$$u^+ = \frac{1}{k}\ln(y^+) + B, \text{ with the } y^+ > 30. \qquad \textit{Eq. 85}$$

Referring to URANS simulations, the contribution of the turbulent fluctuations is related and connected to the closure models in models such as the previously mentioned k-ε (RNG), which is able to calculate the turbulent viscosity. Nevertheless, at the wall, wall functions must be triggered to allow for the different regimes of the flow against the wall. Of course, typically, in URANS the node of the computational grid must be inside the zone of $y^+ \approx 30$, falling inside the formulation of the logarithmic values. To be closer to the experiments, the value of y^+ which corresponds the limit for the logarithmic law is set to 11.6 and B is around 5.0 [125]. To be noted that, according to recent studies, the "B" constant follows different values depending on the Reynolds regime and the condition close to the wall [120].

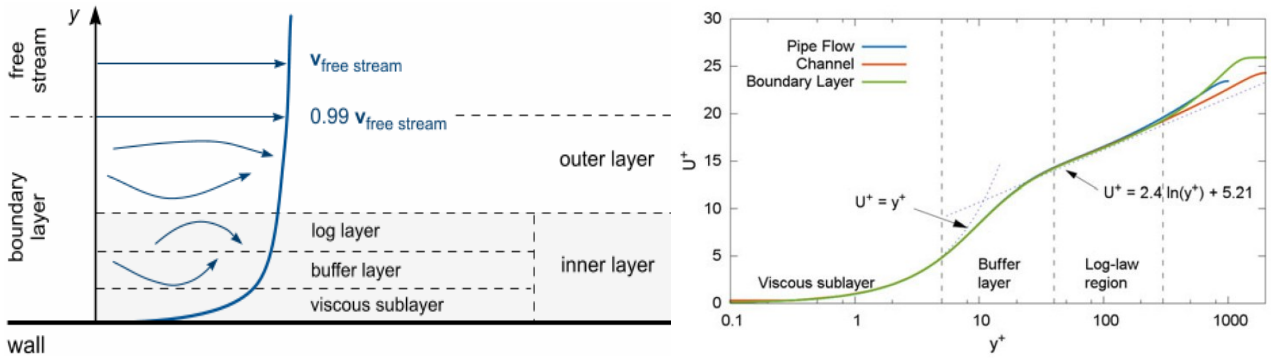

Figure 6 Boundary layer structure (left) and velocity profile in wall-bounded flows (right) [120]

Then, in this work, an improved modelling approach for turbulence in the LES framework is adopted and derived from Nicoud and Doucros. Given the importance of the wall boundary layer flow behavior in turbulent flow, and with the specific dissertation of this thesis related to internal combustion engine simulations, a detailed evaluation of the wall is reported. Especially, the importance of the local turbulent diffusion, which can impact the results in terms of mixing, if a well-resolved approach for turbulence is adopted in a multi-cycle LES framework. The major aspects of this framework are given by the accuracy with which the model is able to account for turbulence implications, particularly local behavior near the wall during flow development (or as will be seen later in this work, gas such as hydrogen) on the wall. The modelling here is not negligible, and due to the lack of Smagorinsky in reaching a very predictive approach in terms of viscosity, the approach from Nicoud and Ducros is used in this work, through the WALE (Wall-Adaptive Large Eddy Viscosity Model) model [126]. From the classical Smagorinsky, at the wall, the damping function from Van Driest function [127]:

$$1 - \exp\left(-\frac{y^+}{A^+}\right) with\ A^+ = 25 \qquad \textit{Eq. 86}$$

is adopted in the Software but is far from our target of wall-fidelity. This is why we selected the WALE model that has an adaptive term that allows natural reach zero viscosity, neither with damping nor with a dynamic procedure to reproduce the no-slip condition with the operator: $S_{ij}^{d}S_{ij}^{d}$.

When LES is run with the Low-y^+ wall treatment, the near-wall cell is placed at y+≈1. Under these conditions, the wall is fully resolved and the velocity profile in the viscous sublayer is directly computed from the Navier–Stokes equations. No wall-function is required, and the friction velocity $u^+ = \bar{u}/u_\tau$ is obtained explicitly from the resolved tangential velocity using the low Reynolds formulation implemented in Simcenter STAR-CCM+.

Conversely, when the All-y^+ wall treatment is used, as in the case of this work, the mesh is not required to resolve the viscous sublayer. In this case, the simulation does not use the velocity at the first cell next to the wall; instead, Simcenter STAR-CCM+ uses the second cell away from the wall as the reference location. At this point, the dimensionless velocity $u_\tau = u^*$ is evaluated and employed in the log-law wall function, which iteratively computes the friction velocity. This iterative procedure ensures consistency between the predicted velocity and the logarithmic wall-law, following Reichardt [128], and allowing the model to correctly estimate the wall shear stress even when the mesh is too coarse to resolve the viscous sublayer.

Finally, linking to the previously mentioned methods, in reference to URANS, the calculation of u^+ falls within the logarithmic law and is computed according to the previously mentioned formulation.

3 CFD – Retrofitting and Feasibility from Gasoline to H_2ICEs

3.1 Introduction

From an overall standpoint, transitioning from an internal combustion engine (ICE) fueled by fossil fuels appears to be relatively straightforward in terms of combustion feasibility. However, the adoption of hydrogen introduces more uncertainties. In the introduction of this document, various pieces of information and current applications have been drawn from the most authoritative literature and recent successful implementations. This manuscript is guided by considerations of the computational and numerical impact, as well as the feasibility and accuracy of the modelling. Before exploring perspectives and modelling approaches aimed at achieving high-fidelity accuracy, we first examine the feasibility of retrofitting a production gasoline direct injection (GDI) engine. This analysis is particularly relevant to the geographical context of this PhD Thesis, which is conducted in Modena, where high specific power output is a key focus as the extraction of this engine. Not for minus importance, the retrofitting is guided by the target in reaching a reduction of CO_2 emissions, a reduction in NO_x and harmful emissions from the tailpipe.

The author and their colleagues have conducted several studies exploring retrofitting possibilities to adapt existing engines or layouts for hydrogen fuel. The first study focused on retrofitting a pre-existing high-performance Gasoline Direct Injection (GDI) Spark Ignition (SI) engine. This exploration was primarily guided by the lambda target to ensure safe and effective operating conditions. In this context, several evaluations were conducted regarding the lambda target, port water injection, and Exhaust Gas Recirculation (EGR) strategies to mitigate overloaded conditions. Then, a brief exploration of NO_x output is considered, showing the beneficial application of hydrogen as a replacement for a conventional fuel. The detailed results have also been published in [37].

The second study represents an evolution in both detail and scope, examining an existing engine layout and realistic dimensions in collaboration with another partner, as referenced in a related publication [44]. This work explored a PFI application of hydrogen, emphasizing a chemistry-based approach, primarily focusing on phenomena such as auto-ignition and surface ignition in irregular combustion scenarios. Additionally, computational guidelines were developed, which can be applied in realistic projects and scenarios for high-performance engines, as well as for passenger car applications.

3.2 Engine and numerical validations of the modelling approaches

During the entire daily routine that guided my PhD, since from an industrial extraction, it is never missed the production and strict relation with the automotive sector on production engines. So, the engine here reported is an existing and production high-performance gasoline engine, for which the main parameters are reported in the figure 7. Then, it can be observed that the geometry and engine layout are constituted by a Spark Ignition engine with the spark plug located in the middle of the engine head, whereas the injector is placed on the bridge located between the intake valves.

Table 5 Engine data and operative conditions

Bore	86.5	mm
Stroke	80.8	mm
Number of cylinders	8	
Displacement	3797	cc
Compression ratio	9.6	
Connecting rod length	141.25	mm
Engine speed	7000	rpm
Pin offset	0	mm
EVO	141.27	CA
EVC	372.54	CA
IVO	364.43	CA
IVC	620.45	CA
Spark Time	707.8	CA

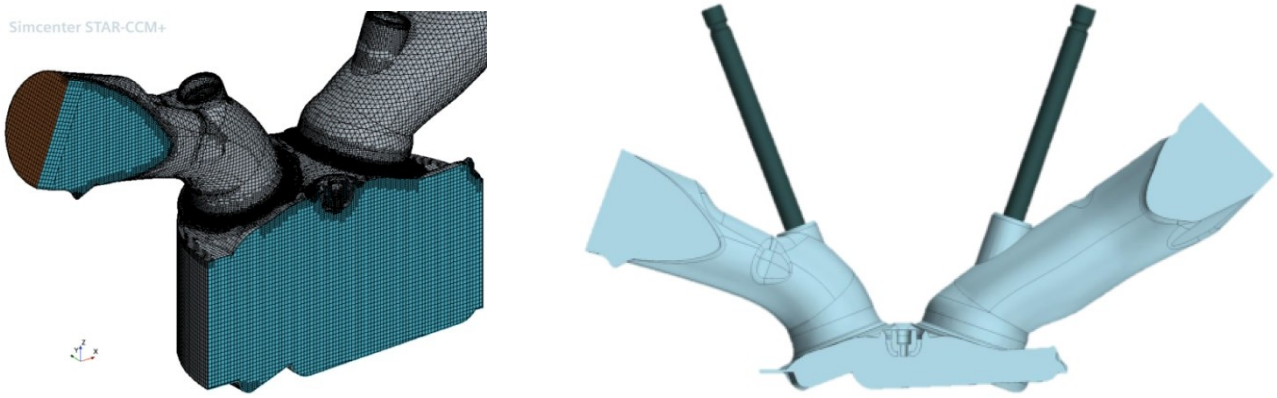

Figure 7 Engine geometry and overview of the mesh in symmetry model layout

To move from a GDI engine to a hydrogen-fuelled internal combustion engine, the first scenario that has been compared relates to the strategy through which hydrogen is introduced into an engine. The first application considers the DI of hydrogen as the target of the first study aimed at mimicking the direct injection as for the GDI configuration. This approach will be detailed in the core of this manuscript, where the direct injection hydrogen strategy is considered in detail, focusing on the mixing outputs. Specifically, also in this case, as will be discussed later, a specific temporally and spatial refinement is performed during the simulation to account for a better fidelity of the gas

injection modelling according to a specific and detailed setup that consistently helps on reaching the high-fidelity output desired from a CFD simulation.

A first consideration was related to the target of reaching the same energy released from a high-performance GDI engine under the conditions related to the table and reported in figure 8, showing the fidelity and the CFD/EXP accordance.

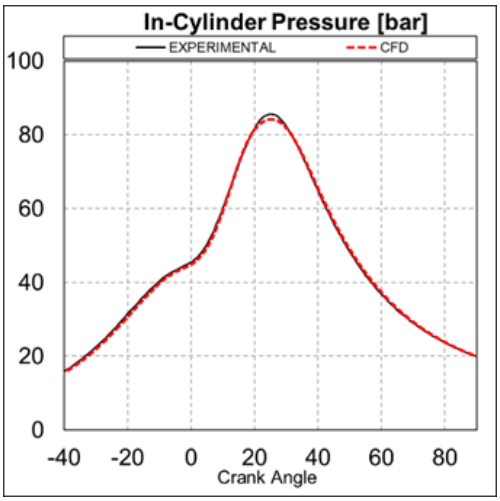

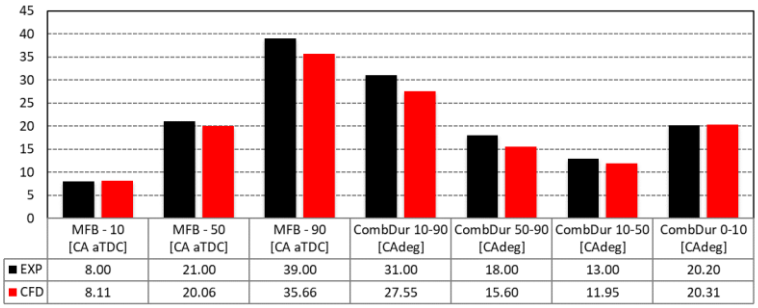

	MFB - 10 [CA aTDC]	MFB - 50 [CA aTDC]	MFB - 90 [CA aTDC]	CombDur 10-90 [CAdeg]	CombDur 50-90 [CAdeg]	CombDur 10-50 [CAdeg]	CombDur 0-10 [CAdeg]
EXP	8.00	21.00	39.00	31.00	18.00	13.00	20.20
CFD	8.11	20.06	35.66	27.55	15.60	11.95	20.31

Figure 8 Comparison between in-cylinder pressure and combustion phasing/durations

As mentioned above, the layout of the engine is reviewed to allow the injection of the hydrogen through a direct injection strategy. The strategy consists of a modified head to host an outward-opening pintle gas injector, with an ad-hoc approach for mesh and injection strategy. The mesh has been described in its approach and concept in paragraph 4 of this work, and then recalled and further developed with a detailed approach for a hydrogen injector reported in this manuscript. Briefly resumed in the following description, the mesh strategy is based on local mesh refinements introduced with the aim of better modelling the very high speed of the gaseous jet and its mixing with the surrounding air. Furthermore, the interaction that is generated during the injection event is well-captured by the full cone and the further three levels of refinements present during the injection event. Hence, the simulation of hydrogen becomes stable in this way as well, enhancing the final output.

In this study, it was found that injecting hydrogen under closed-valve conditions resulted in higher pressure within the engine. This underscores the importance of a proper hydrogen injection strategy to ensure adequate cooling, preventing overpressure and reducing the risk of abnormal operating conditions.

Numerical observations indicated that the pressures achieved were 30.59 [bar] and 42.35 [bar] for gasoline and hydrogen, respectively, while the temperatures reached were 729 [K] and 885 [K]. This shows that hydrogen leads to approximately 40% higher pressure and 20% higher temperature, which can contribute to more adverse combustion conditions.

In fact, targeting a lambda value of around 1.8 is the only scenario that reasonably aligns with the same laminar flame speed (LFS). Therefore, for a fair comparison in the following sensitivity analyses, we will assume a lambda of 1.8.

To adequately assess the impact of nitrogen oxides (NO_x) output while considering the presence of water, a port fuel injection (PFI) strategy will be adopted.

3.3 Premixed cases: spark sweep & water concentration

As will be discussed in the next section, the exploration of hydrogen-fueled engines requires a thorough evaluation of possible improvements to address existing criticisms. One of the most important considerations is the timing of the spark, which can vary under different conditions. This study presents evidence that can be initially reviewed and later detailed in a subsequent analysis. In this comparison, we simplify the impact of spark sweep and water concentration through PFI simulation after the initial assessment of the DI strategy. This approach helps avoid stratification and makes the comparison more relevant by focusing solely on the changes being examined. However, this comparison isolates the different behaviors of spark sweep and water concentration, providing insights into how each variable affects combustion output. It is important to note that knock is intentionally excluded from the modelling framework in this initial analysis. Nevertheless, as observed in the details of the pressure rise rate (PRR), knock and abnormal conditions may likely occur. This topic will be explored in greater depth in a forthcoming publication by the author and co-authors, which will concentrate on abnormal combustion.

Furthermore, as will be reported later, the same study highlights the impact of using hydrogen and the differences in the polytropic index. This suggests that strategies for achieving top dead center (TDC) firing should be re-evaluated. As previously mentioned, there is an increase in pressure and temperature when transitioning from gasoline to hydrogen. This is primarily due to the direct injection (DI) of hydrogen and the effects of its polytropic coefficient, which further influence the conditions needed to reach TDC firing.

Some results are reported here, showing significant pressure increases under nominal conditions. Conversely, the effect of spark timing variations can lead to a reduction in pressure of up to 10 degrees crank angle (CAD) when adjusted accordingly. It is important to note that these results were obtained while maintaining the same engine geometry and operational conditions as those of a spark ignition (SI) engine, using hydrogen at a lambda value of around 1.8.

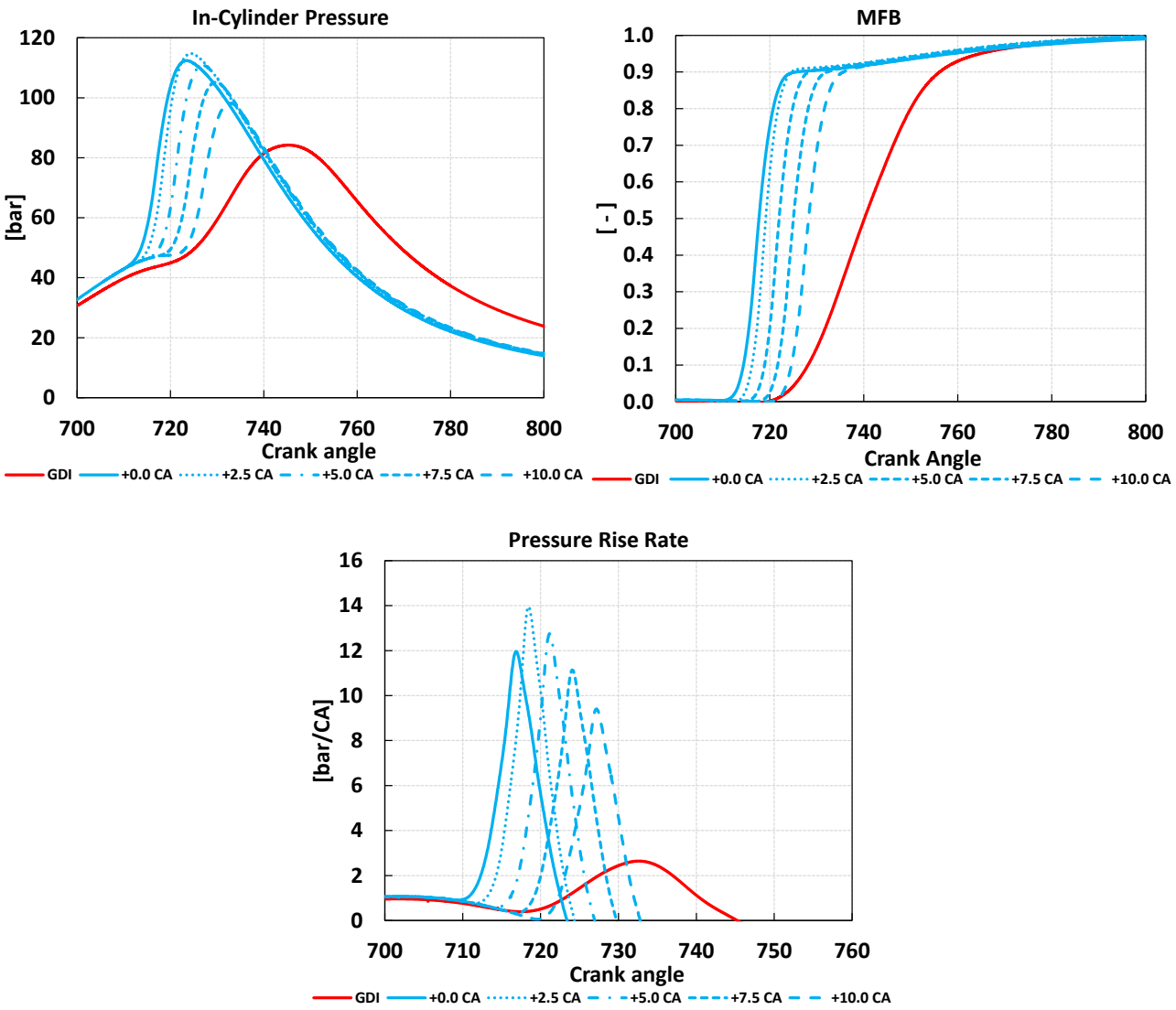

Figure 9 The impact of the spark sweep on in-cylinder pressure and combustion development is shown at the top. The bottom image details the pressure rise rate, highlighting the significant increase in pressure achieved during hydrogen combustion.

3.3.1 Spark Sweep

The spark sweep analysis has been performed, starting from the default condition for the spark timing properly adopted for the gasoline engine layout. The spark ignition for the SI operative point is 707.8 [CAD] and the sweep consists of delaying the spark time of 2.5 [CAD] for each combustion test. In figure 9 (top), the results are reported, showing clearly that retarding the spark time, the pressure peak is always higher compared to the gasoline reference case. So, in light of the same operative condition, but considering the impact of different pressures at the spark timing as well as the temperature, the same pressure peak cannot be reached up to 10 [CAD] of delay. Furthermore, the figure also reports the PRR, which leads to the direct conclusion that not only is the pressure not aligned reasonably with the gasoline counterpart, but also the rise in pressure seems to be significantly dramatic for the engine structural resistance. This led the author to consider properly studying the abnormal combustion with the hydrogen engine to deepen this topic in detail.

Table 6 Analytical combustion results and comparison (spark sweep): Gasoline Vs Hydrogen

Case	GDI	H_2 +0.0 CA	H_2 +2.5 CA	H_2 +5.0 CA	H_2 +7.5 CA	H_2+10.0 CA
Combustion indicators						
MFB50 [CA_aTDC]	20.06	-2.35	-0.87	1.98	5.03	8.25
Comb._Dur. 10-90 [CA]	27.55	11.28	8.40	9.38	10.53	11.05
Thermodynamic Outputs						
Theor. Heat [J]	3720.7	1543.6	1543.6	1543.6	1543.6	1543.6
IMEP [bar]	22.4	14.6	14.1	14.9	14.8	14.6
Maximum Pressure [bar]	84	112	115	111	105	98
Maximum Temperature [K]	2419	2438	2520	2499	2473	2444

It is evident that the engine output shows durations that are less than one-third of those of the gasoline-fueled counterpart. Additionally, there is a critical concern regarding the rapid rise in peak pressure. The same observation applies to the gross Indicated Mean Effective Pressure (IMEP) presented in the table, where a partial recovery is observed with very delayed spark timings. However, this recovery is insufficient to prevent abnormal combustion and potential damage to the engine. To address these issues, further leaning of the mixture may be necessary, but this could result in additional performance losses. To reduce the overall mixture within the combustion chamber, two strategies can be considered: Exhaust Gas Recirculation (EGR) and port water injection (PWI). The latter will be selected and explored in the following section.

3.3.2 Water injection

This section aims to provide an overview of the impact of water concentration in a hydrogen mixture combustion chamber. To achieve this, we will use the same simplification of premixed conditions evaluated earlier. This approach allows us to isolate the specific effects of water concentration on combustion.

The primary focus of this comparison is to assess the direct effects of a port water injection (PWI) strategy on combustion in terms of combustion pressure peak and development mitigation, making hydrogen a viable fuel in this configuration. The variation in concentration, specifically the dilution of the mixture, is accomplished in a simplified way, as mentioned, just by adding premixed water to the mixture, maintaining consistent thermodynamic conditions at the end of the compression phase.

The simulation begins from predetermined conditions, with only the initialization of the concentration composition being considered. In a fully operational scenario, factors such as temperature reduction, pressure changes, and the effects of motion during the PWI event should be taken into account.

However, to isolate the effects of water concentration, these factors are not considered in this analysis.

The simulation starts with early conditions, and the spark timing is set at 712.8 [CAD], identified as the most promising case for achieving the highest Indicated Mean Effective Pressure (IMEP) for high-performance engine output. The results, as illustrated in the accompanying figure 10, clearly demonstrate the impact of water concentration, highlighting its effectiveness in reducing the pressure peak and significantly mitigating the Pressure Rise Rate (PRR). Reasonable results from a feasibility standpoint are reached from 10 – 20 % of water concentration. The table 7 illustrates the sum up of the results showing the compromise can be achieved, reducing the power output but reaching the PRR for a safety application.

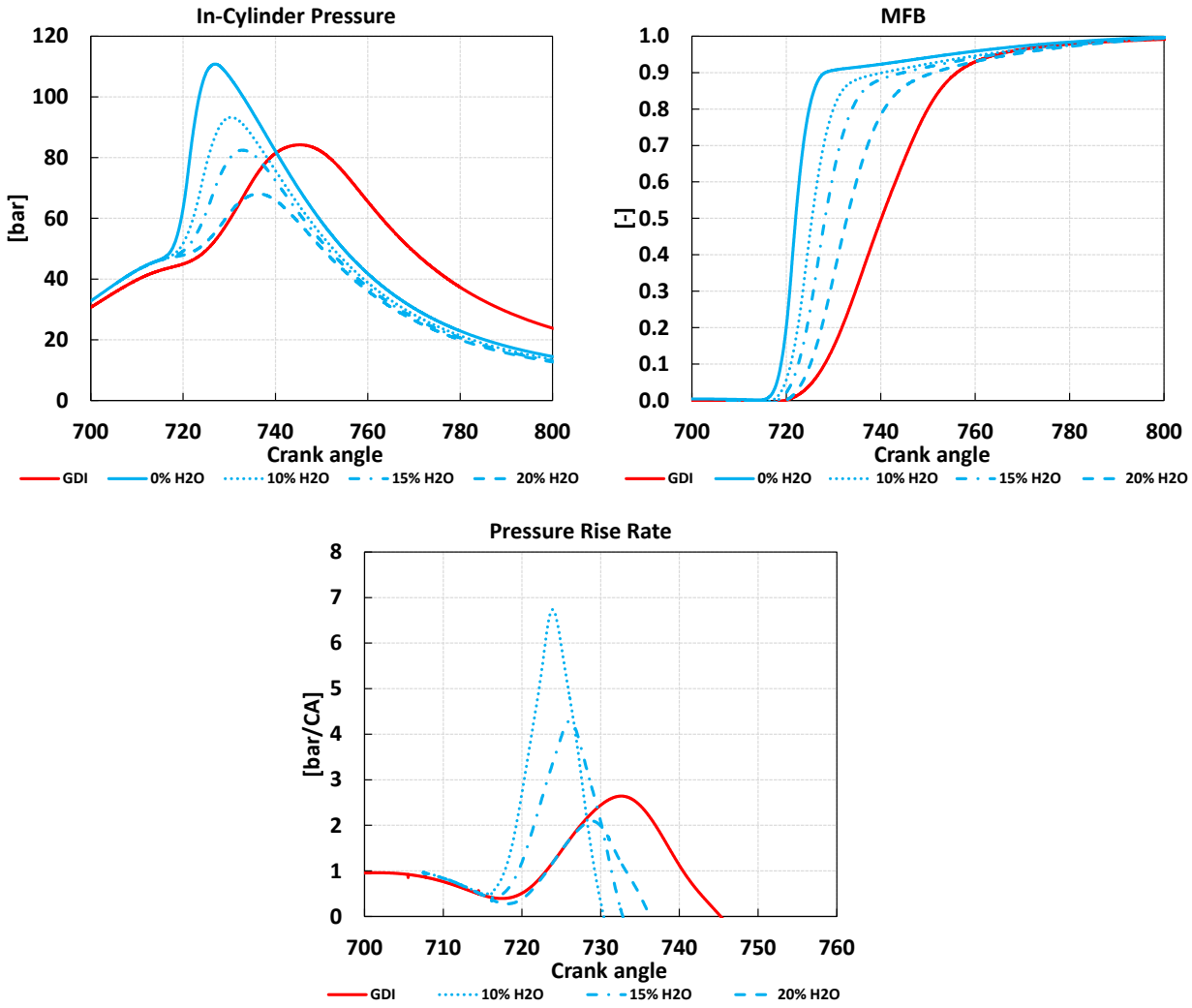

Figure 10 Impact of the water injection in pressure and combustion development: Gasoline Vs Hydrogen

Table 7 Analytical combustion results and comparison (water injection): Gasoline Vs Hydrogen

Case	GDI	0% H2O	10% H2O	15% H2O	20% H2O
Combustion indicators					
MFB50 [CA_aTDC]	20.06	1.98	5.43	8.20	12.83
Comb._Dur. 10-90 [CA]	27.55	9.38	19.48	22.23	26.10
Thermodynamic Outputs					
Theor. Heat [J]	3720.7	1543.6	1355.0	1260.2	1168.2
IMEP [bar]	22.4	14.9	16.8	15.9	14.9
Maximum Pressure [bar]	84	112	93	82	68
Maximum Temperature [K]	2419	2438	2208	2055	1868

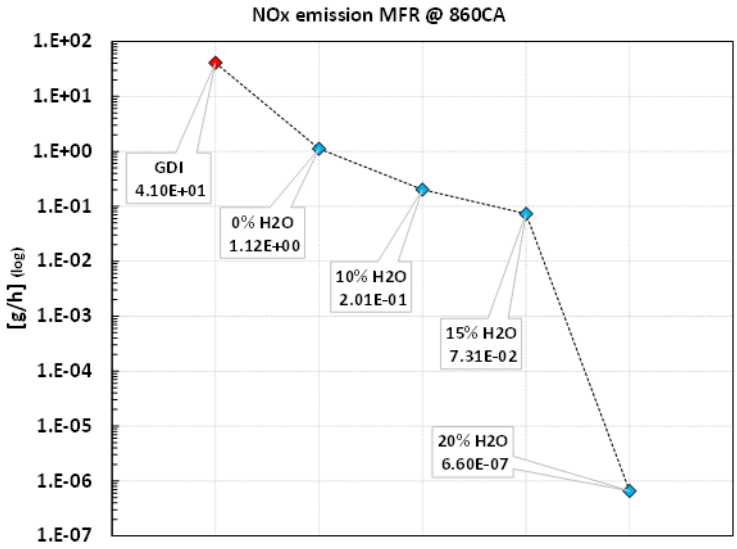

Figure 11 NO_x emission at the end of the combustion process at different values of water mass fraction

A brief overview of NO_x emissions is provided, noting that validation is not possible in this particular study. However, the results align well with expectations, especially considering the outcomes achieved through the introduction of water. Although these results cannot currently be compared with experimental evidence, they can serve as a reference point for future studies. The results indicate a significant reduction in NO_x emissions when operating with hydrogen mixtures. Additionally, increasing the water content further reduces overall NO_x emissions, reaching the minimum in the analyzed trend up to 20% H_2O. Numerically, the software allows the use of the NORA, according to the modelling from literature [129,130]. From the results and final outcomes, these confirm that hydrogen, when combined with an appropriate strategy, can be a valuable solution toward achieving the targets set in the regulatory framework for internal combustion engines (ICEs).

3.4 Abnormal Combustion with a PFI Hydrogen Engine

3.4.1 Introduction – H_2ICE

Recent developments in chemistry detail applications for ICEs, prompting the author to pursue research in this area for ICEs as the new and most promising side of CFD. Specifically, this field of complex chemistry, despite several developments and literature along the years, has been as interesting as in the last decade. In fact, as discussed in the introductory area, the availability of more CPU power and recent HPC allowed Companies and research groups from Universities to achieve new standards for computational computing. Hence, following the previous chapter, and collecting also information from chemical kinetics from the last topic of this PhD, the next chapter will be focused on abnormal combustion when retrofitting from simil-GDI engine, here simplified as a PFI with premixed condition engine to H_2ICE.

The engine, which is considered in the following description, comes from a high-performance architecture from a real engine, despite some components being designed for the specific application and to be more simply managed for the CR variation and modelling.

Table 8 Engine data

Displacement [cm^3]	435
Bore [mm]	92
Stroke [mm]	65.5
Connecting Rod Length [mm]	115
Engine Speed [rpm]	10000

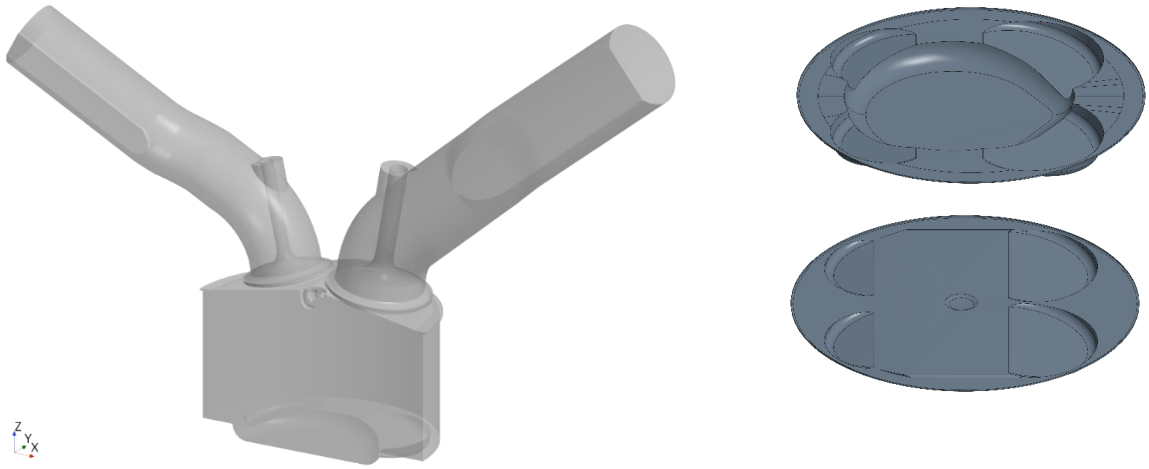

Figure 12 Engine geometry and two configurations of the piston crown (top: low CR; bottom: high CR)

3.4.2 0D – Chemistry evaluation

As the first step of the analysis of the feasibility of an H_2ICE framework, the first approach finds its basis on the full chemical considerations and comparison between hydrogen and petroleum-based fuels. This comparison falls into a wider coverage, which consists of a proper evaluation of the RON/MON connection with the auto-ignition or the ability of a fuel to be more or less knock-prone.

Specifically, in this case, the reference is strictly focused on hydrogen, which is, over the years, less considered in engine applications with respect to the counterpart from fossil fuel.

Table 9 Chemical kinetic mechanism for gasoline surrogates

Chemical Mechanism	Number of species	Number of reactions
Ren et al. [131]	178	758
Mehl et al. [132]	323	1488

Table 10 Chemical kinetic mechanism for hydrogen

Chemical Mechanism	Number of species	Number of reactions
Ó Conaire et al. [133]	10	21
Ranzi et al. [134-136]	21	62
Konnov [137]	15	74

An evaluation of the ignition delay time for various fuels has been conducted to enhance our understanding of the auto-ignition resistance of both current and innovative fuels from a chemical kinetics perspective. This study, which is a key milestone in this PhD, includes a detailed analysis, the methodology developed, the selection of a suitable chemical kinetic mechanism and simulations to compare a new generation of fuels with conventional ones. These findings are basically adopted for the selection of the Ren et al chemical mechanism reported in summary in table 9, thoroughly discussed and published in detail [32].

In this section, the focus will be on the iso-octane, gasoline and hydrogen, where a comparison with available data, as well as, hydrogen, is reported and discussed.

Calculations of IDTs at different conditions are performed against the experimental data available from the literature. Nevertheless, as one of the biggest lacks in this operative and specific field of engineering, the data from experiments is still far from the real engine-like operative points (OPs). So, the validation and check of the results against experimental evidence led directly to a good output that guides the choice of the best chemical kinetic mechanism for both gasoline/hydrocarbon fuels and hydrogen as well. The Ren et al. [131] and Ó Connaire [133] chemical mechanisms, respectively from gasoline/hydrocarbon fuels and hydrogen, have been selected both from a high-fidelity standpoint and computational effort as well.

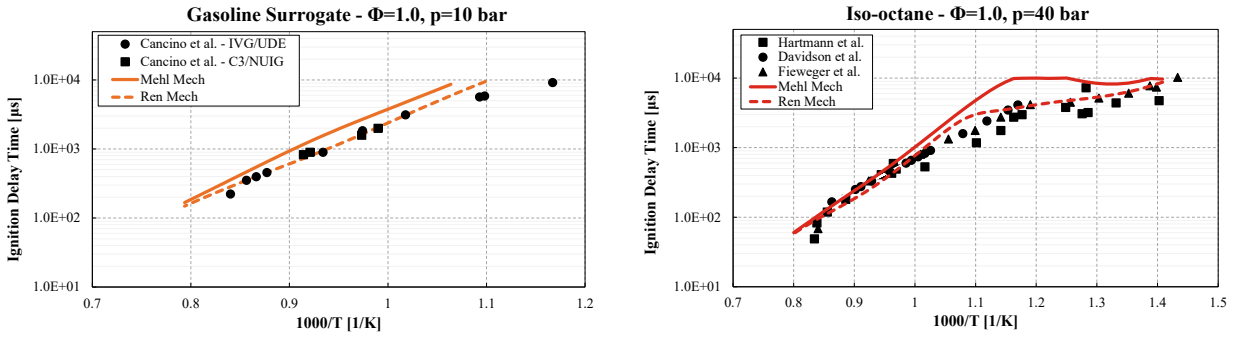

Figure 13 Ignition delay time calculations of both gasoline surrogate and iso-octane at reasonably low/high pressure conditions: CFD Vs experiments

In the summary, figures 13, show the Iso-octane and gasoline IDTs calculation, where the surrogate comes from literature as well as its adoption in the experiments by Cancino et al [138], for relative low pressure on gasoline, where the composition comes from the same literature from Cancino et al

for coherence, and Fieweger [139,140], Davidson [141] and Hartman [142], for relative high pressure on iso-octane with good results compared to experiments. The better trend of the Ren et al mechanism leads to the better choice of using this chemical mechanism the reference one for the gasoline approach.

The next comparison, far from hydrocarbon-based fuels, focuses on hydrogen ignition delay times, with reference results from literature for the experiments of Laster et al [143] and Petersen et al [144]. Here, three chemical kinetic mechanisms are considered: Ó Connaire, Konnov, and Ranzi. The final output, also according to the time-to-solution, which is strongly dependent on the number of reactions and the pathways through which the chemistry develops (despite hydrogen, the impact is lower compared to fossil fuels), leads to the final choice of the Ó Connaire mechanism. Despite the quite similar behavior, as expected from these recently widely adopted mechanisms for hydrogen chemistry-based combustion, the chemical mechanism selected allows for slightly better prediction approaching lower temperatures as well as good stability and overall runtime.

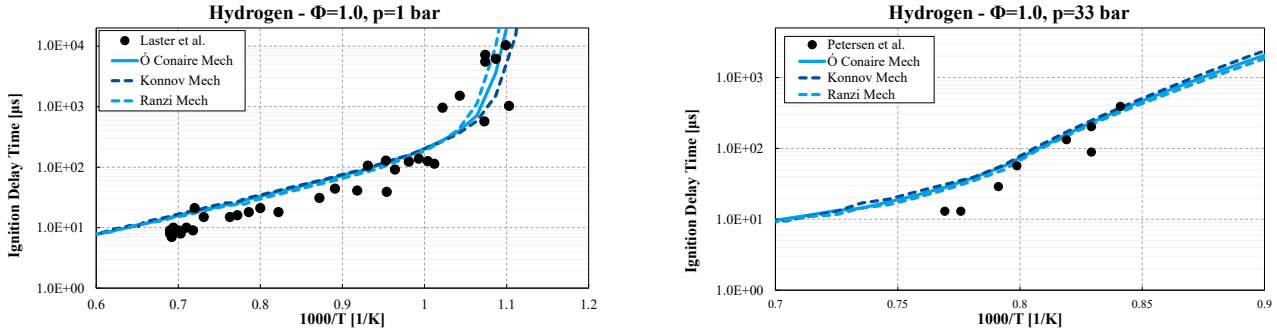

Figure 15 Ignition delay time calculations of hydrogen at reasonably low/high pressure conditions: CFD Vs experiments

Finally, a comparison of the fuels and the hydrogen ignition delay times is reported in the same plot, giving the information required for 0D analysis. The endpoint, which is reported in figure 15, highlights the fact that hydrogen is more knock-resistant than fossil fuels considered. Reasonably, both iso-octane and hydrogen IDTs decrease with increasing pressure, despite the pressure rise rate of the fossil counterpart being higher. Giving some numbers to close the circle, at 1000 [K], 40 [bar] hydrogen IDT is almost four times higher than isooctane, meaning that 173 [CAD] and 46 [CAD] is required to auto-ignite the mixture at the OP. Then, this gap widens at 1000 [K], 80 [bar] with 118 [CAD] and 25 [CAD] for hydrogen and fossil fuel, respectively. In conclusion, this comparison highlights how hydrogen is less knock-prone compared to iso-octane or gasoline as well.

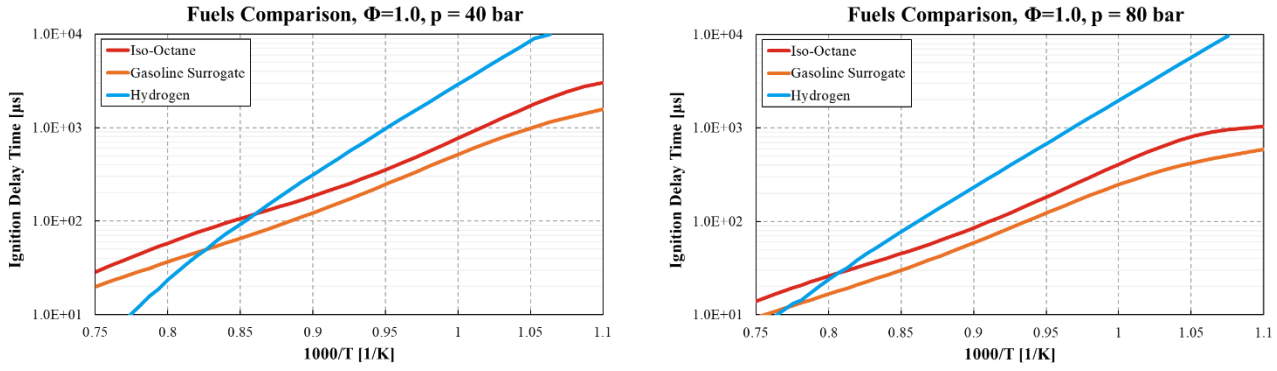

Figure 14 Ignition delay time calculations and comparison between gasoline surrogate, iso-octane ad hydrogen at engine-like pressure conditions

3.4.3 0-D Variable Volume Reactor

As mentioned in the previous study, the assessment of Gasoline Direct Injection (GDI) in relation to Hydrogen Internal Combustion Engines (H_2ICE) showed an interesting relationship between hydrogen injection and pressure development. This observation could be significant for advancing the adoption of hydrogen as a fuel, and from the combustion insights here evaluated with premixed conditions.

However, the focus of the study was primarily on the individual effects of combustion duration and pressure output. This meant that the conditions prior to the spark event were somewhat unfavorable. The introduction of hydrogen resulted in an increase in pressure during the injection phase, which further elevated the pressure at the firing point.

Despite this, there was a second, noteworthy consideration that was not addressed. While hydrogen injection under closed valve conditions does lead to an increase in pressure, this is not the only factor to consider. The operational fluid, whether it involves fuel injection or hydrogen injection through the intake port, as in PFI layout, results in different overall mixtures after fuel evaporation. In fully gaseous conditions, the resulting relation is useful to be adopted with the p_0 and T_0 conditions (IVC) of the current engine with specific CR= 18 by the following equation:

$$\boldsymbol{T \cdot p^{\frac{1-k}{k}} = constant} \qquad \textit{Eq. 87}$$

Evaluating the equation (Eq. 86), it is clear that the *k* parameter, or better, the physical parameter, plays a fundamental role in the formulation. The *k* value, the *value of specific heat*, or adiabatic index, of hydrogen, is different compared to its counterpart, iso-octane/gasoline, providing different results for different mixtures. According to the National Institute of Standards and Technology (NIST) and literature [145], the comparison has been evaluated in a mixture (mass-weighted) of O_2, N_2, H_2O, and H_2 or iso-octane, referring to the specific mixture. Averaging the ranges of *k* along with the variation of temperature low-high, the final output is 1.375 for the hydrogen mixture and 1.3 for the fossil-based mixture, figure 16 (right).

The figure 16 (left), reports the analytical comparison by running the full compression stroke without combustion in a Variable Volume Reactor (VVR) of the case under discussion, reaching the related differences in the pressure and temperature development between the two different mixtures. The final understanding point shows how different behavior is reached, emphasizing the reduction of the knock resistance of hydrogen if the same compression ratio is adopted in the engine cycle.

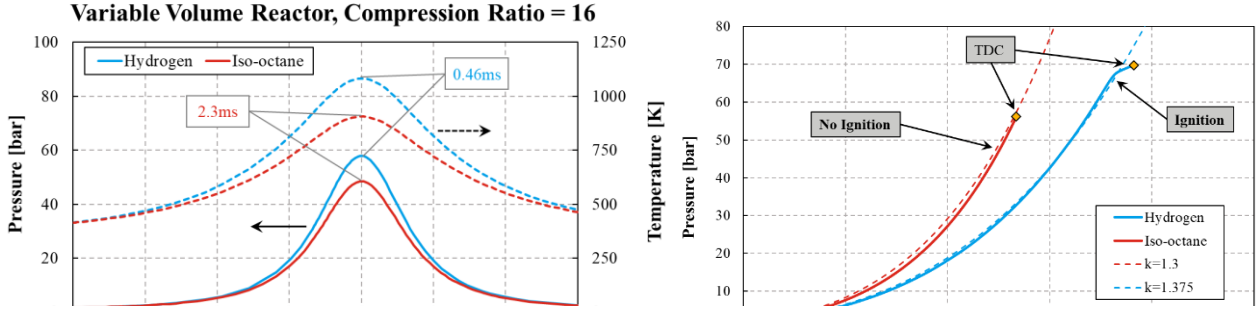

Figure 16 Variable volume reactor clearly shows the impact of using fossil gasoline and hydrogen due to the different ratio of specific heats k. The impact of k is evident in (b) where the focus on pressure over temperature is reported.

Finally, evaluating the previous equation (Eq. 86), with the VVR compared to the analytical one, the results are almost the same. All things considered, it is evident that by adopting hydrogen as a fuel, a stronger impact can be expected by increasing the compression ratio on the ignition delay time and, of course, a significant reduction in knock/auto-ignition resistance as reported in figure 17.

Finally, to evaluate the influence of the compression ratio on the operating conditions of hydrogen and iso-octane, the Livengood–Wu integral [146] is employed to quantify the onset of knock. According to the literature, knock is considered to occur when the value of the integral reaches unity, and this criterion is therefore used to define the knock-limited compression ratio in the present analysis. Based on the 0D-CFD simulations carried out and discussed in detail in [44], the resulting trend highlights the strong correlation between in-cylinder pressure evolution and knock propensity.

The final outcome of this modelling activity is summarized in figure 18, which reports the CR at which hydrogen, at each considered compression ratio, exceeds the knock threshold earlier than iso-octane. The results confirm that iso-octane can sustain significantly higher compression ratios before reaching the knock limit, whereas hydrogen becomes knock-prone at lower CRs due to its intrinsically shorter ignition delay and higher reactivity.

It is important to note that knock behavior does not depend solely on pressure rise, but also on the residence time at critical thermodynamic conditions and on the temperature profile within the combustion chamber throughout the combustion process. For this reason, additional analyses based on the Wiebe function used to reproduce different combustion phasing and heat-release developments are performed and presented in the next section of this work.

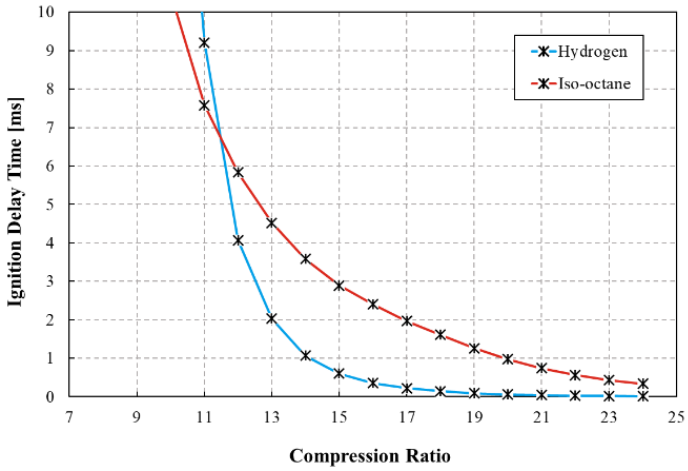

Figure 17 Variation of the ignition delay time at the corresponding compression ratio for both iso-octane and hydrogen

3.4.4 0D – Spark Ignition Impact on Auto-Ignition

Still in the modelling from 0D, spark ignition is evaluated, since the residence time of the mixture can affect the *knock limit compression ratio* (KLCR). To perform these simulations, a Wiebe function is applied to represent the combustion of both the fuels considered. The model, in fact, is a 0 dimension approaching the combustion without multi-dimensional, at the time, phenomena. Referring to iso-octane, a Wiebe function is chosen considering the MFB10 to MFB90 around 25 [CAD]. Then, according to the reference maximized torque OP, the MFB is fixed between 10 and 15 [CAD aTDC].

It can be seen that, adding to the simulation the combustion effects, the KLCR tends to reduce for both fuels, enhancing the probability of knock. As reported in figure 18 (left), it is possible to observe that the hydrogen case reaches knock at a lower compression ratio than iso-octane. Numerically, hydrogen needs a 4.1-point lower compression ratio compared to the counterpart with iso-octane. This can be explained by the higher pressure-temperature development in the hydrogen combustion. Nevertheless, the residence time during which the end-gas stays during the combustion process must be evaluated carefully.

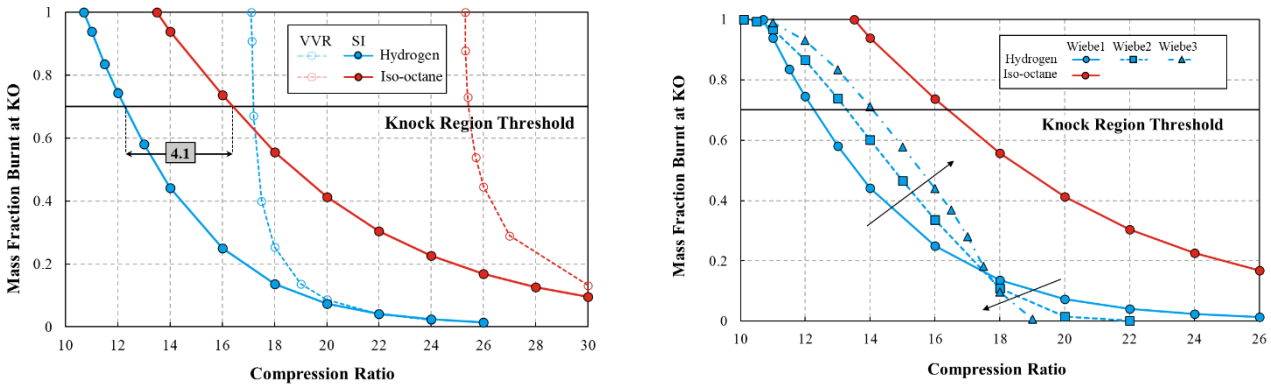

Figure 18 Comparison between only the VVR approach and spark ignition modelling triggering the combustion effects (left). On the right, three Wiebe considered to evaluate the knock onset, highlighting the MFB 20 as the inflection point (right).

An inflection point is present around MFB20, reported in figure 18 (right), when the other two Wiebe functions are considered. In fact, it must be considered that hydrogen combustion is, basically, faster than the conventional combustion with iso-octane. Hence, "Wiebe function 1" with MFB10-90 equal to 25 [CAD] is parallelized to "Wiebe function 2" with 15 [CAD] and "Wiebe function 3" with 9 [CAD]. This leads directly to the point previously introduced, through which the inflection point to MFB20 can be generally analyzed as:

- Below this value, the increment in pressure and temperature toward fTDC leads to KLCR reduction. Here, the pressure and temperature play their fundamental role in knock occurrence.
- Beyond this value, the reduction of resident time thanks to the faster combustion leads to an increase in KLCR. Here, chemistry is dominant and the chemical reactions cannot develop despite the worst thermodynamic conditions.

3.4.5 3D-CFD – Hotspot evaluations

The final section of the abnormal combustion overview discussed in these paragraphs focuses on a 3D approach to the application, considering the entire in-cylinder simulation. The results presented here pertain to the simulation of hydrogen and iso-octane internal combustion engines (ICE) using the 3D-CFD tool, Simcenter STAR-CCM+ DISW licensed Software. The Simcenter STAR-CCM+ In-Cylinder Solution allows for comprehensive full 3D-CFD simulations with the following overall setup:

Table 11 Computational setup for 3D-CFD simulations from modelling and operational temperatures.

Detailed Setup – Physical/Chemical/Models & Temperatures	
Discretization Domain	*Cylinder mesh size: 1 [mm]* *Spark plug refinements: up to 0.25 [mm]* *Valve zones refinements cell size: up to 0.25 [mm]*
Numerics (Flow/Species/Enthalpy)	*Second Order Numerical Scheme (Convection Hybrid Scheme MARS / CD)*
Turbulence	*RNG k-ε*
Wall Treatment	*Two-Layer All y+*
Combustion Model	*CC-TFC (complex chemistry)*
Gas Model Reference	*Real Gas (Soave-Redlich-Kwong)* *Kinetic Theory Of Gases (Thermal Conductivity/Molecular Diffusivity)* *Dynamic Viscosity with Sutherland's Law (Coeff. from literature for H2/N2)*
Algorithm for Pressure Correction	*PISO* *(Predictive-Implicit Splitting of Operators)*
Temperature	Gradient temperature for spark plug / constant for the rest of the engine parts
Piston	550 [K]
Liner	450 [K]
Head	480 [K]
Intake/Exhaust Valve	500/800 [K]
Spark plug	Variable – gradient: from 500 up to 900 [K]
Time steps	Valve opening/closing events – Minimum 0.005 [CAD]; Overlap far from closing/opening seats – 0.05 [CAD] Otherwise: 0.1 [CAD]

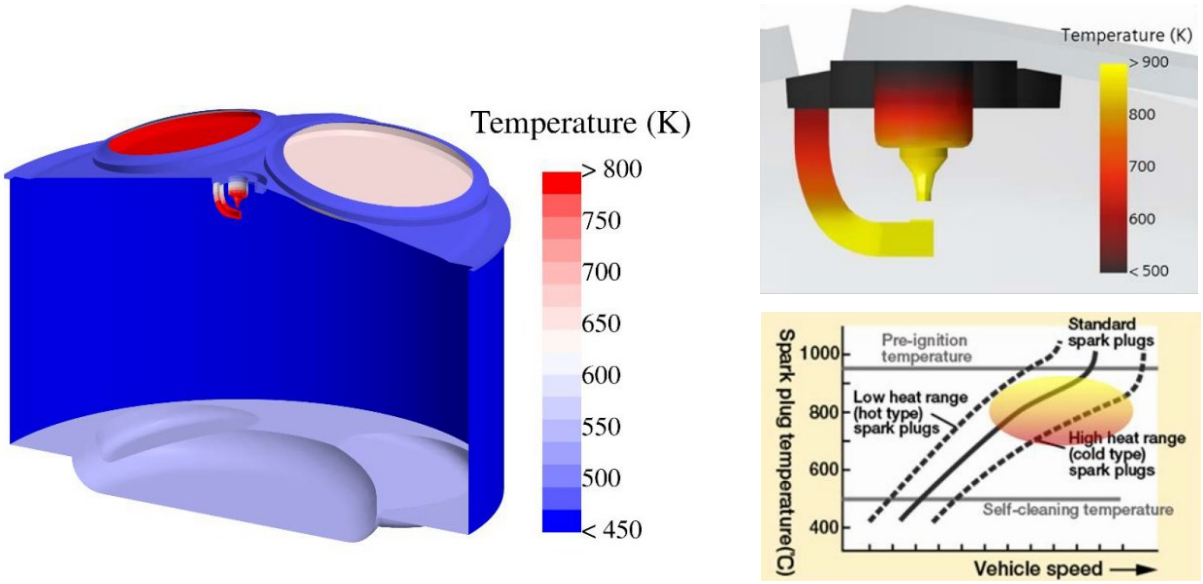

Figure 19 Engine temperature at each surfaces (left). The details of the gradient for realistic conditions is performed for the spark plug (right) according to Denso [147]

To simplify the overall approach for 3D-CFD simulations, fully premixed conditions are utilized, which refers to specific modelling of hydrogen direct injection (H_2 DI) engines. A minor discrepancy in volumetric efficiency and theoretical heat/energy within the engine can be quantified as follows: 0.95 for iso-octane compared to 0.65 for hydrogen, and 869.8 [J] (iso-octane) versus 674.9 [J] (hydrogen) after Intake Valve Closure (IVC). This discrepancy leads to lower power output expectations for hydrogen; however, it is significantly offset by the previously discussed gap in the polytropic coefficient, which continues to enhance pressure development in hydrogen-fueled engines. In fact, the temperature in the hydrogen case is measured to be 110 [K] higher than that of iso-octane, along with an overpressure of nearly 5 [bar], visible in figure 20, and is compared to the petroleum-based engine, which aligns with the 0D simulations.

In light of the previous engine conditions and the growing interest in abnormal combustion from a 3D-CFD perspective, a more in-depth analysis related to surface ignition can be conducted. In fact, based on the nature of the simulation, one of the parameters that can be varied is the wall temperature. Additionally, the simulations remain chemically relevant, so the same chemical mechanisms utilized earlier will be revisited and specifically addressed in this context.

Referring to the tendency for auto-ignition, it is well recognized that two of the most sensitive components in an ICE that can lead to self-ignition of the mixture due to surface ignition are the exhaust valve and the spark plug. Recently, an innovative layout for high-performance engines has been developed through Turbulent Jet Ignition (TJI) technology. This technology can be significantly affected by high temperatures. In both petroleum- and hydrogen-fueled engines, managing the temperature, thermal dynamics, and the risks associated with the pre-chamber are of utmost importance. Nevertheless, this application is not considered specifically in these studies.

In this specific application, the ignition onset is first analyzed by examining the time derivative of the temperature of the mixture measured inside the combustion chamber, in line with a zero-dimensional (0D) approach. Additionally, we monitor a second output: the maximum chemical heat release rate (CHRR). Auto-ignition is considered to occur when this rate exceeds a reasonable threshold value.

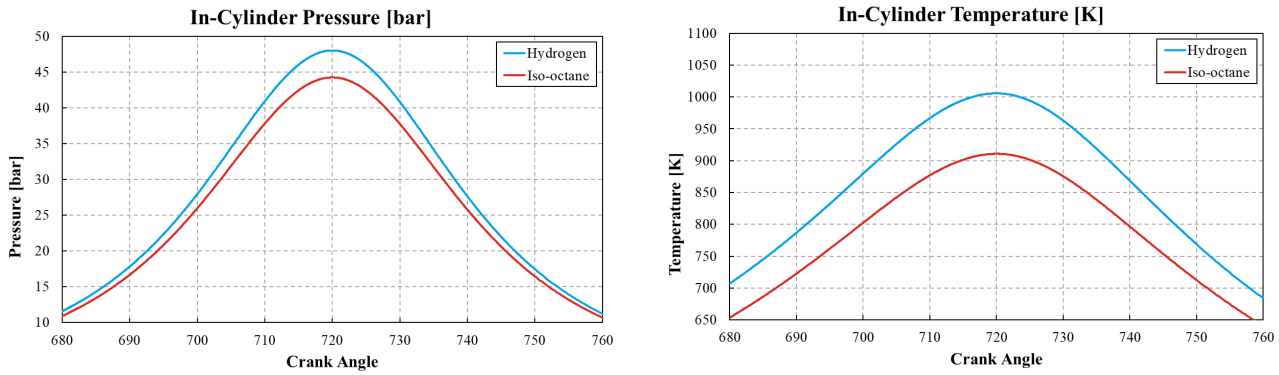

Figure 20 Pressure and temperature evolution in 3D-CFD simulations with the plots centered at the fTDC (no combustion IS triggered here)

3.4.6 Auto-ignition – Overview and Results

The dynamic condition shown in figure 20 clearly highlights the differences in pressure and temperature evolution between the two simulations. However, before addressing the hotspot-analysis case, which, as will be shown, concerns only the hydrogen configuration, a brief verification of the chemical-kinetics results within the 3D-CFD simulations is considered. These outcomes are in good agreement with the ignition delay times (IDTs) obtained from the 0D analysis. In fact, as illustrated in figure 21 (a, right), the IDT computation is reported and compared under reference ICE-relevant conditions reproduced in a constant-pressure reactor. For iso-octane, increasing the hotspot temperature has almost no effect on the simulated IDTs. This observation confirms that, under engine-like conditions, iso-octane remains intrinsically safe with respect to surface-induced autoignition up to a maximum surface temperature of 1200 [K]. Conversely, as reported in figure 21(a, left), hydrogen is significantly affected by hotspot-surface temperature. This requires further investigation when such temperatures are reached locally inside the combustion chamber. As shown in figure 21 (b,c,d), only the hydrogen-fuelled configuration is considered at different temperature conditions for the specific surfaces. Specifically, in figure 21 (b), the nominal operating points for both fuels remain safely below self-ignition limits, indicating that the default conditions do not trigger abnormal combustion. For this reason, a dedicated sweep of exhaust-valve and spark-plug surface temperatures was carried out to identify thermal-boundary conditions capable of inducing mixture ignition, potentially posing risks associated with knock-prone behavior.

3.4.7 Chemistry Heat Release at different locations

The first analysis, according to the temperature sweep, relates to the figure 21 (c and d), which clearly shows that higher chemical activity is observed when increasing the temperature of the valves rather than that of the spark plug. This phenomenon leads to poorer expected behavior regarding self-ignition, particularly related to the exhaust valve and exhaust conditions. A possible reason for this behavior can be attributed to the different turbulence conditions surrounding the spark plug compared to those at the exhaust valve location.

When higher turbulence is present, as is typical around the spark plug location, the conditions of high turbulence and intense motion make ignition release more challenging. This observation is supported by the study conducted by Chi et al. [148], which investigated the effects of turbulence on ignition delay and onset probability through direct numerical simulation (DNS) at varying turbulence intensities. The results of that study demonstrated the relationship between turbulence levels and ignition delay times, indicating that an increase in turbulence intensity corresponds to an increase in ignition delay time. This occurs due to enhanced mixing, heat diffusion, and their combined impact on cooling the hotspot faster than the chemical reaction can sustain ignition. This phenomenon becomes even more pronounced at relatively high temperatures.

3.4.8 Auto-ignition analysis

In this study, it has been observed that ignition occurs in all cases where temperatures exceed 1050 [K]. Notably, the most critical incidents happen at the crevice location of the exhaust valve, specifically between the valve and its seating. This underscores the importance of carefully managing the retrofitting process of a GDI engine to prevent stagnation areas, improve mixing quality, and control high temperatures effectively. These findings further reinforce that the direct injection of hydrogen, when properly calibrated for high tumble conditions, can be the optimal approach for designing an H_2ICE. Additionally, selecting the right type of spark plug is crucial for enhancing thermal heat rejection resistance; therefore, a “cold type” spark plug is preferred over standard types. Consequently, the subsequent analysis will focus on the design, specifically, the modelling of a high-tumble, hydrogen direct injection engine. This will include detailed outputs, considerations, and methodologies for high-fidelity modelling of an optically accessible H_2ICE.

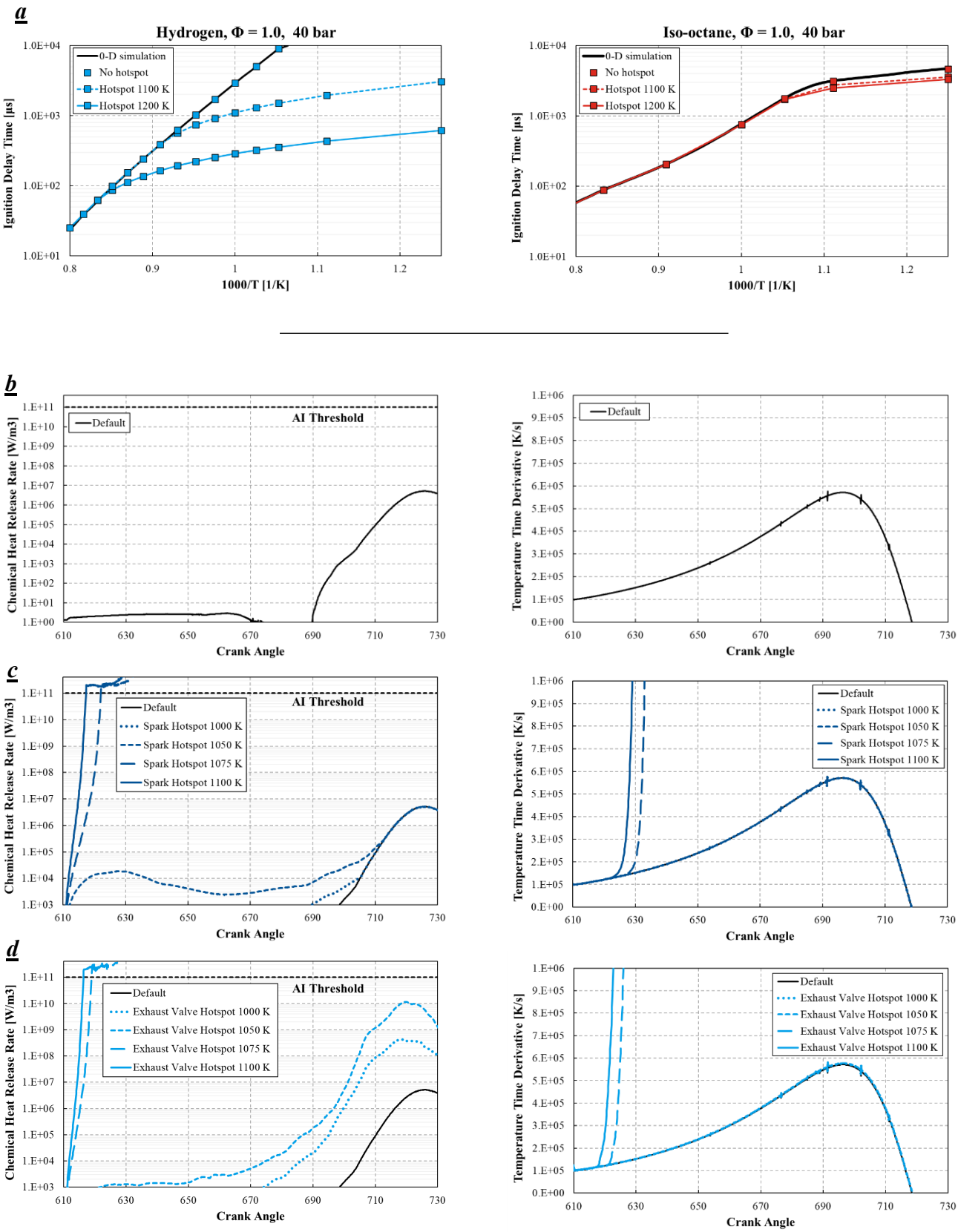

Figure 21 Auto-ignition occurrence in combustion simulations with different temperatures of exhaust valve and spark plug: a) IDT at the reference at engine-like pressure conditions in a static vessel, b) ICE simulation with reference temperatures reported in table 11, c) spark plug temperature sweep and d) exhaust valve temperature sweep

3.5 Sum up: Retrofitting from GDI to PFI/DI H_2 ICEs

Retrofitting an ICE originally fuelled by gasoline with a direct-injection and port fuel injection strategy to a DI or PFI (premixed simplified in this approach) H_2ICE is evaluated in detail, focusing first on several operational aspects and providing insights into engine-management considerations. Then, a more detailed perspective on combustion behavior, auto-ignition, and surface-ignition criticalities is presented for the PFI H_2ICE, using a geometry derived, again, from a real production engine. The major outcomes from these two applications are reported hereafter, also providing relevance to the preliminary assessment of the modelling framework.

Retrofitting GDI/PFI gasoline-fueled engine to DI/PFI H_2ICE for ICE management:

1) **Real-engine configuration and CFD modelling reliability**: the engine originates from a real high-performance production ICE, enabling the author to establish a detailed CFD modelling setup that confirms the high reliability of the modelling framework and the close agreement of Software predictions with expected engine behavior.

2) **Lambda target for comparable combustion characteristics**: a first assessment of the transition from GDI to hydrogen DI highlights a target λ of approximately 1.8, allowing the hydrogen flame development to reasonably match the LFS behavior of gasoline without dramatically altering the engine's overall energy content.

3) **Spark sweep to mitigate pressure-rise-rate spikes**: a spark-timing sweep is carried out to reduce pressure peaks due to hydrogen combustion, quantified through the pressure rise rate. A reasonable spark time is set to +5 [CAD] from GDI to H_2ICE.

4) **Premixed strategy preliminary assessment**: the premixed strategy with water is evaluated, cooling and diluting mixtures through EGR, significantly reducing peak temperatures and the risk of abnormal combustion. The reference value, which balances performance and feasibility, is 10% H_2O.

5) **NO_x emissions reduction**: NO_x emissions respond positively, showing an overall reduction when introducing approximately 10% water into the mixture, maintaining the performance output.

Retrofitting PFI to H_2ICE for abnormal-combustion evaluations:

1) **IDT behavior from chemistry-based 0D simulations**: hydrogen simulations carried out using chemistry-based 0D tools yielded higher IDTs for hydrogen compared to iso-octane/gasoline.

2) **Thermodynamic discrepancy in compressed-gas conditions**: comparison of the two fuels revealed a significant discrepancy due to differences in specific heat ratios. When hydrogen is adopted as a replacement for gasoline at a compression ratio of 18, compressed-gas temperatures and pressures differ by more than 200 [K] and 10 [bar], respectively.

3) **Maximum compression ratio for knock-safe operation**: the maximum compression ratio is estimated to be more than two points lower for hydrogen engines compared to gasoline engines to avoid knock while keeping the operation within safe limits. Knock onset is identified when end-gas auto-ignition is experienced below MFB70, limiting the compression ratio for safety applications.

4) **Surface-ignition sensitivity**: analyses show that hydrogen auto-ignition is promoted in stagnation regions, particularly near the exhaust valve, while the more turbulent spark-plug region exhibits a mitigating effect. The enhanced transport of species and heat removal due to turbulence mitigate auto-ignition in spark-plug zone. The use of cold-type spark plugs is recommended for H_2ICEs. Iso-octane remains safety from auto-ignition up to surface temperatures of about 1200 [K].

4 CFD – Mixing in an Optically-Accessible H_2ICE

4.1 Long history of the SOpHy engine studies

The following rows aim to provide a clear and complete vision of the studies and the major outcomes that have shaped the last decades in the study and development of hydrogen direct injection in an optically accessible ICE. So, first results calls from a couple of decades ago, before reaching the first results of SOpHy, a previous study on the acetone PLIF technology was performed by Herold and Ghandi [46], who conducted an in-depth evaluation of the averaging process and data normalization schemes to address noise sources in the mixture stratification of PLIF [149]. In 2009, the optimization of PLIF was first assessed on the same engine by Salazar, Kaiser and Halter [47] through a thorough evaluation of tracer selection and optimization techniques using acetone PLIF. This aimed to provide insights into the average processes and data processing for visualizing hydrogen injection. This assessment focused on evaluating the mixing of acetone using PLIF and included a Particle Image Velocimetry (PIV) experimental campaign related to the research of the SOpHy engine. In their work, the first evaluation of a PLIF on a light-duty engine was performed with several injection strategies and single/multi-hole injectors. In between 2009 and 2010, the first experiments of Salazar and Kaiser were officially delivered [48,49], providing new insights into hydrogen direct injection in optically accessible ICEs and establishing the foundation for further studies. In 2010, a year later, Scarcelli, Wallner, Salazar, and Kaiser [51] conducted the first numerical simulation modelling of an engine equipped with a single-hole injector, focusing on the impact of the numerical grid. The software used in their study was Fluent. The authors emphasized the importance of the computational domain, utilizing grids ranging from 200,000 to 1,000,000 cells at 140 [CAD bTDC]. The same authors also performed CFD analyses, assessing the effects of different grid sizes and turbulence modelling approaches, ranging from RNG k-ε to Realizable k-ε [52]. In particular, they examined how reducing the turbulent Schmidt number (Sct) affected results when applying the Realizable k-ε model. This study was the first to evaluate and compare the CFD modelling of the SOpHy engine in relation to the potential influence of the operating conditions on the engine's configuration in a low tumble (LT) scenario. Ultimately, the findings indicated that a reduced Sct enhances the accuracy of hydrogen diffusion results. The study, in the same year, was followed by the work of Lucchini et al [53] to predict the hydrogen mixing in SOpHy by using another software, OpenFOAM, and highlighting the impact of different turbulence models as well as the impact of the mesh discretization approach again on the low-tumble configuration. In 2015, from the Convergent Science headquarter, with the Software Converge, J. Le Moine et al [54] performed the first URANS simulation of the SOpHy engine in high-tumble (HT) configuration with the AMR approach, showing its potential in better predicting the fuel and velocity outcomes when a detailed refinement strategy and meshing approach are adopted, reaching very good agreement between CFD and EXP. The higher cell size moved from 4 [mm] up to 0.25 [mm] with specific refinements of 0.125 [mm] locally at the injector tip location and a mesh orthogonal structure was triggered by the software, showing an improvement in mixture formation. In 2019, Li et al. [55] conducted a study related to H_2ICE using the AMR and an orthogonal mesh approach characteristic of their software modelling. Due to the unavailability of test rig results, the authors utilized SOpHy with a low-tumble configuration to validate their method. They also provided details on the Sct, which was set to 0.3 in their study. In the following year, from the University of Modena and Reggio Emilia, Barbato and Cantore [56], released a work performed on

the SOpHy engine in STAR-CCM+ software through the Simcenter STAR-CCM+ In-Cylinder Tool that reached great results in URANS by using a trimmed mesh approach with a specific temporally and spatial mesh refinement approach during the injection event, the Realizable k-ε turbulence model and a second order Monotone Advection and Reconstruction Scheme (MARS) for numeric coupled to a Two-Layer All-y^+ near wall approach. In this case, the high-tumble approach was the target of the study, considering expanding the comparison to the second operative comparison. A year later, Addepalli et al. [57] performed a detailed study on the SOpHy engine, in both the configuration low- and high-tumble. They conducted their study focusing on mesh cell orientation in the near-wall locations to predict gas jet penetration. An inlaid orientation of mesh was demonstrated that impacts the shear stress and velocities near the wall, leading to better prediction of H_2 jets. Then, a further comparison on the nature of the software, mesh-structured impact was released by Potenza et al. [58], evaluating the results achieved with AVL-Fire and Ansys Fluent. In 2023, Anaclerio et al [59] analyzed the impact of the Reynolds Stress Model in spite of the RNG or Realizable k-ε, with positive results in line with the previous one achieved in recent years. Later, the work of Ramognino et al [60] showed the impact of another approach for turbulence modelling in a light-duty H_2ICE, such as the k-ω SST, which was able to better match the hydrogen at the wall. According to both, it can also be concluded that the turbulence modelling, as seen in the previous work, has an impact, but to be considered linked to the modelling approaches, such as numerical and, in particular, the near-wall modelling of turbulence and local quantities. Then, the authors highlighted the fact that, although a positive impact of different modelling (k-ω SST) as in this case, this is not the crucial point if compared to the ability of the modelling and numerical to reach better agreement in jet-wall and wall guiding of hydrogen against walls. In 2023, Wu, Torelli, and Pei [61] published a comprehensive study detailing their modelling approach using the Converge Software on the SOpHy engine. They investigated the sensitivity of Sct in low-tumble (LT) configurations, noting that a higher number of numerical iterations was required to achieve better accuracy in alignment compared to experiments that set Sct to 0.5. The authors selected the RNG k-ε turbulence model, utilizing adaptive mesh refinement (AMR) and second-order numerical methods for the momentum equations, while employing a first-order approach for the other equations. In 2025, the same authors conducted an LES analysis of the SOpHy engine in low-tumble configuration [62]. This analysis employed a parallelization strategy that encompassed 20 consecutive flow-only cycles, with a restart implemented at each interval prior to hydrogen injection. While it does not strictly adhere to a multi-cycle approach, this technique effectively achieves outcomes comparable to multi-cycle LES while significantly reducing computational runtime. They later averaged these results to obtain the LES average to compare with the experiments. Utilizing the same software and modelling settings of their previous work, with the exception of the turbulence model, they brilliantly demonstrated the capability of LES to achieve a high level of detail in hydrogen mixing within H_2ICE and highlighted the feasibility of this approach in contemporary research. In 2024, a study focused on heavy-duty direct injection H_2ICE presented an interesting application of CFD modelling, incorporating some new aspects compared to previous works. The research established by Akar and Özener [63], then, laid the foundation for modelling settings and validation migrated to a heavy-duty engine, starting from an evaluation on the SOpHy engine. A notable consideration in this setup was the Sct, which was set to 0.78 from the default of the software, and then adjusted by the authors to the value of 0.58 and adopted in the analysis of the heavy-duty engine. The study performed with their approach showed that a reduced Sct allows for improving the results of mixing in the SOpHy engine, but again, a different value compared to the previous study has been considered for the Sct. This confirms the significant

role of Sct in turbulent diffusivity, a topic that is still under discussion, as highlighted in the historical review reported within this work. Additionally, the authors presented relevant insights from the kinetic theory of gases (KT), successfully applying the real gas equation of state to H_2ICE using the Soave-Redlich-Kwong equation of state (SRK) introduced in 1972 by Soave G. [150] and implemented and used in CFD codes. This approach follows a previous study that, while not strictly focused on ICEs, explored the hydrogen injection strategy of the SOpHy engine, paying particular attention to supersonic hydrogen jets. In that research, Kaczmarczyk, Liu, Turner, and colleagues [64] demonstrated the impact of the real gas approach utilizing the SRK equation of state, combined with a variety of numerical schemes. They noted that at least second-order accuracy is necessary and enough to reach a high fidelity of the results. The findings led to several recommendations: the RNG k-ε or k-ω SST turbulence models do not significantly influence the solution when applied to adaptive mesh refinement (AMR), and a central differencing (CD) scheme is sufficient for capturing macroscale features in unsteady Reynolds-Averaged Navier-Stokes (URANS) simulations. Finally, if the goal is to achieve greater detail in simulations, the MUSCL (Monotonic Upstream-centered Scheme for Conservation Laws) reconstructed central differencing method with a minmod limiter is recommended, although it entails greater numerical and computational costs.

4.2 The original application of an LES industry-oriented

The focus of this work aims at developing and evaluating the fidelity in mixture outputs in a time-oriented modelling approach consistent with industrial constraints, such as a milestone in this PhD. Then, a deliberate shift from purely academic high-fidelity methodologies toward solutions that provide robust and reasonably timely accessible results for automotive applications.

In this context, an "engineering LES" approach is adopted as a fundamental concept. This approach refers to a Large Eddy Simulation (LES) framework designed to achieve a balance between predictive capability and computational efficiency, rather than focusing on fully resolving turbulence. Convergence needs, minimum cycle for consistency, resolving the multi-cycle LES is highlighted and compared with the adoption and assessment of the impact of the turbulent Schmidt number.

For the first time in the literature, the present LES fully multi-cycle analysis has been applied to the high-tumble configuration of the optically-accessible SOpHy engine, aiming to be representative of modern engines for passenger cars, with the same mesh adopted in URANS, achieving an original application of an “engineering LES” approach. This choice aims to bridge the current gap in high-fidelity predictivity for realistic automotive configurations, where tumble motion is both dominant and consistent with hydrogen direct injection (H_2DI) architectures. Particular emphasis is therefore placed on wall-guided injection strategies and the associated modelling features required to accurately capture hydrogen transport and mixing output within the combustion chamber using a detailed CFD modelling and settings approach.

Another innovative aspect of this work is the treatment of the turbulent Schmidt number (Sct) coupled to the “engineering LES” concept. Here, in agreement with the nature of the non-constant Sct, which was widely demonstrated in several works, but currently not in engine applications, supported by DNS, an implementation of a variable-Sct law within the engineering-LES framework demonstrated a noteworthy impact on hydrogen stratification and mixture formation in H_2ICE.

These results establish a set of physical foundations for future investigations, showing that meaningful improvements in predictive capability can be achieved by acting on scalar diffusivity, adopting an LES-informed approach. This has also been adopted for a coherent comparison moving from constant to the variable Sct strategy, highlighting both similarities and discrepancies in the resulting mixture formation and stratification trends.

Finally, the outcomes establish potentials for a future detailed methodology for linking Sct to non-dimensional quantities such as Reynolds number or, more generally, to ratios involving molecular and turbulent viscosity. Using this approach, the high-fidelity LES behaves as an informative approach for the proper evaluation of the proper Sct based on the same quantity that can be found in URANS, extending the detailed diffusivity prediction to both frameworks.

4.3 Engine and test-bench

This summary provides an overview of the engine layout and test bench for the SOpHy engine from Sandia National Laboratory. Although extensive technical descriptions are available in the literature from Salazar and Kaiser, this brief account aims to maintain completeness. The engine is a four-stroke figure 22 (top), single-cylinder research engine specifically adapted to operate with hydrogen and features an injection pressure of 100 [bar].

There are two configurations available: one with low tumble and the other with high tumble. Given the focus of this manuscript on engine characteristics, particularly the high-tumble configuration, only the high-tumble setup will be discussed. The engine design includes large transparent segments that enhance optical accessibility, allowing for a detailed examination of the hydrogen-fueled operating conditions, mixing, and results obtained from tumble and velocity PLIF (Planar Laser-Induced Fluorescence) processing.

The engine features a four-valve head with a pent-roof combustion chamber. The intake system consists of two intake ports that form a 40° angle with respect to the fire deck on the horizontal plane. The engine's revving speed is set at 1500 [rpm] without combustion being triggered, as the injector system replaces the traditional spark plug. This hydrogen injector operates at an injection pressure of 100 bar and introduces fuel directly into the combustion chamber via a solenoid injector from Westport Inc.

The injector's nozzle angle has been the subject of discussion over the years and is defined to be 50° with respect to the cylinder axis, as depicted in figure 22 (bottom-left). The orifice diameter is set at 1.46 [mm]. The injector operation is illustrated in figure 22 (bottom-right) and table 12, controlled by a thermal mass flow meter provided by Brooks SLA5860. The goal for the injector system is to achieve a global lambda of 4.0, which corresponds to an equivalence ratio of 0.25 and a hydrogen mole fraction of 0.095, injected for 17.5 [CAD].

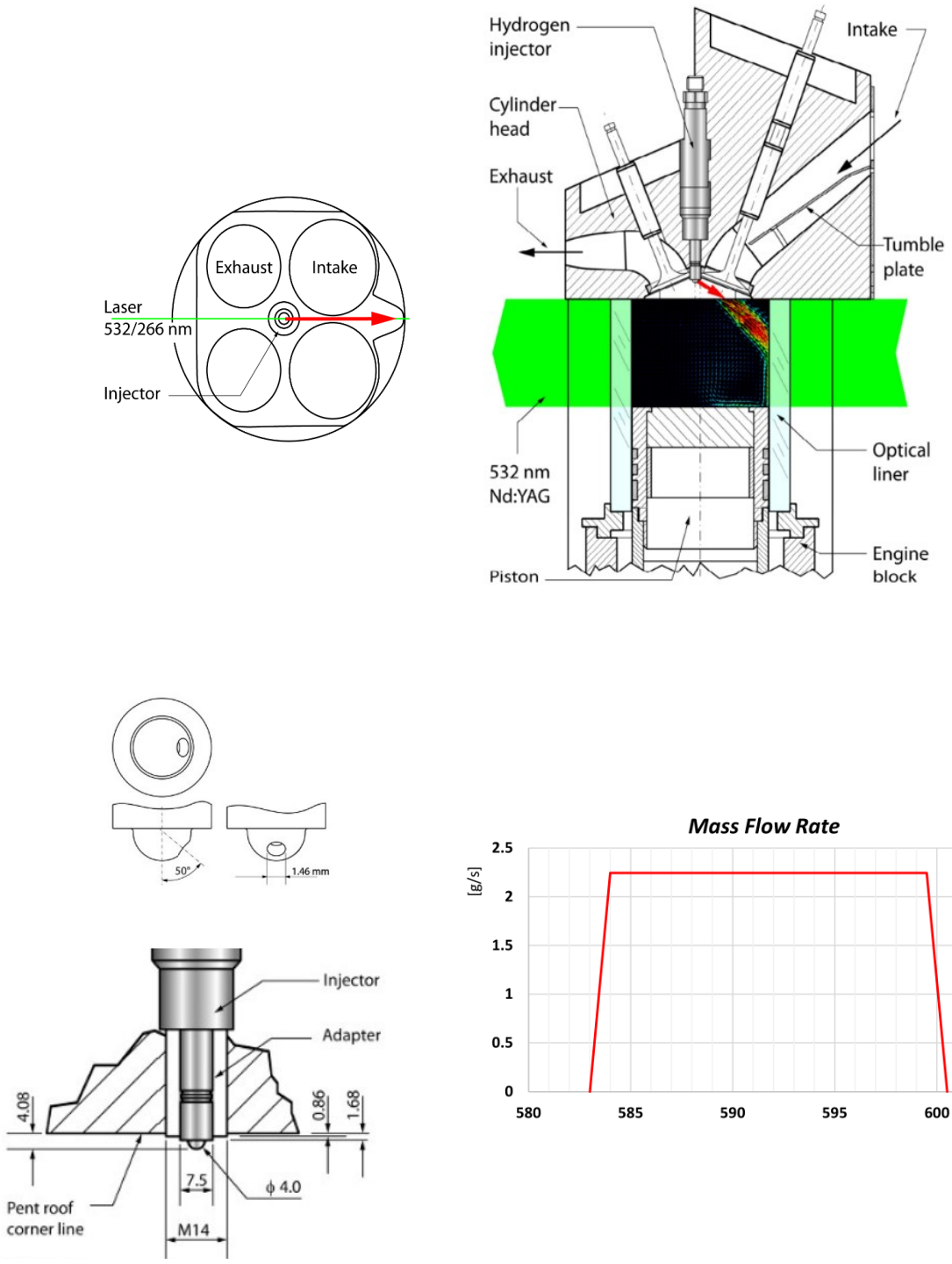

Figure 22 Engine layout of the optical-accessible SOpHy engine at Sandia National Laboratories (top). Injector geometry and layout (bottom-left). Mass flow rate over CAD applied to the engine simulations (as in the experiments) (bottom-right).

Table 12 Engine data and operative conditions

Specific	***Data***
Overall DATA	
Equivalence ratio	0.25
Fuel	H2
Flow/Bulk gas	N2
Injection pressure	100 [bar]
Fuel temperature	309.15 [K]
MFR - static	2.245 [g/s]
Injection ramp up/down	1 [CAD]
SOI	583.0 [CAD]
DOI	17.5 [CAD]
Configuration – plates	High Tumble configuration with plates
ENGINE DATA	
BORE/STROKE/DISPLACEMENT	92 [mm] / 85 [mm] / 565 [cm^3]
Compression ratio	10.96
Connecting rod length	166.67 [mm]
Revving speed	1500 [rpm]

The Planar Laser-Induced Fluorescence (PLIF) technique is utilized to accurately measure the development of mole fractions inside the engine. Gaseous acetone is used as a fuel tracer to obtain quantitative images that will serve as references for the subsequent Computational Fluid Dynamics (CFD) matching. This procedure involves introducing gaseous acetone into the hydrogen fuel using a high-pressure bubbler.

For completeness, some data related to the procedures will be reported, including the extrapolation of mole fraction mixing evolutions and the velocity of the flow inside the cylinder, as obtained through PLIF and Particle Image Velocimetry (PIV), respectively.

4.4 PLIF – Mole fraction processing

Optical measurements of the hydrogen fraction inside the engine are conducted using an Nd:YAG laser at 266 nm with a pulse energy of approximately 100 mJ per pulse. A 1500 mm focal-length lens is used to create a thin laser sheet. The induced visible fluorescence is captured through a 50 mm, f/1.2 lens, combined with a 500 mm achromatic close-up lens, and recorded using a back-illuminated, non-intensified CCD camera. As noted in the extensively referenced literature, the rejection of elastically scattered UV light along the optical path is sufficiently high to eliminate the need for long-pass filters, as reported by Salazar and Kaiser.

To ensure the quality of the results, quantitative accuracy is achieved through standard background subtraction and flat-field corrections. Temperature field inhomogeneities and tracer mixing

uncertainties are addressed using known spectroscopic calibrations and the assumption of adiabatic mixing between the hot residual gases and the cold, induced hydrogen injection. The overall uncertainties in the ensemble-mean equivalence ratio field have been estimated by Salazar and Kaiser to be around 25%. Approximately 90 images are captured per crank angle to construct the phase-locked fields of hydrogen mole fraction, which are then used for comparison with Computational Fluid Dynamics (CFD) analyses.

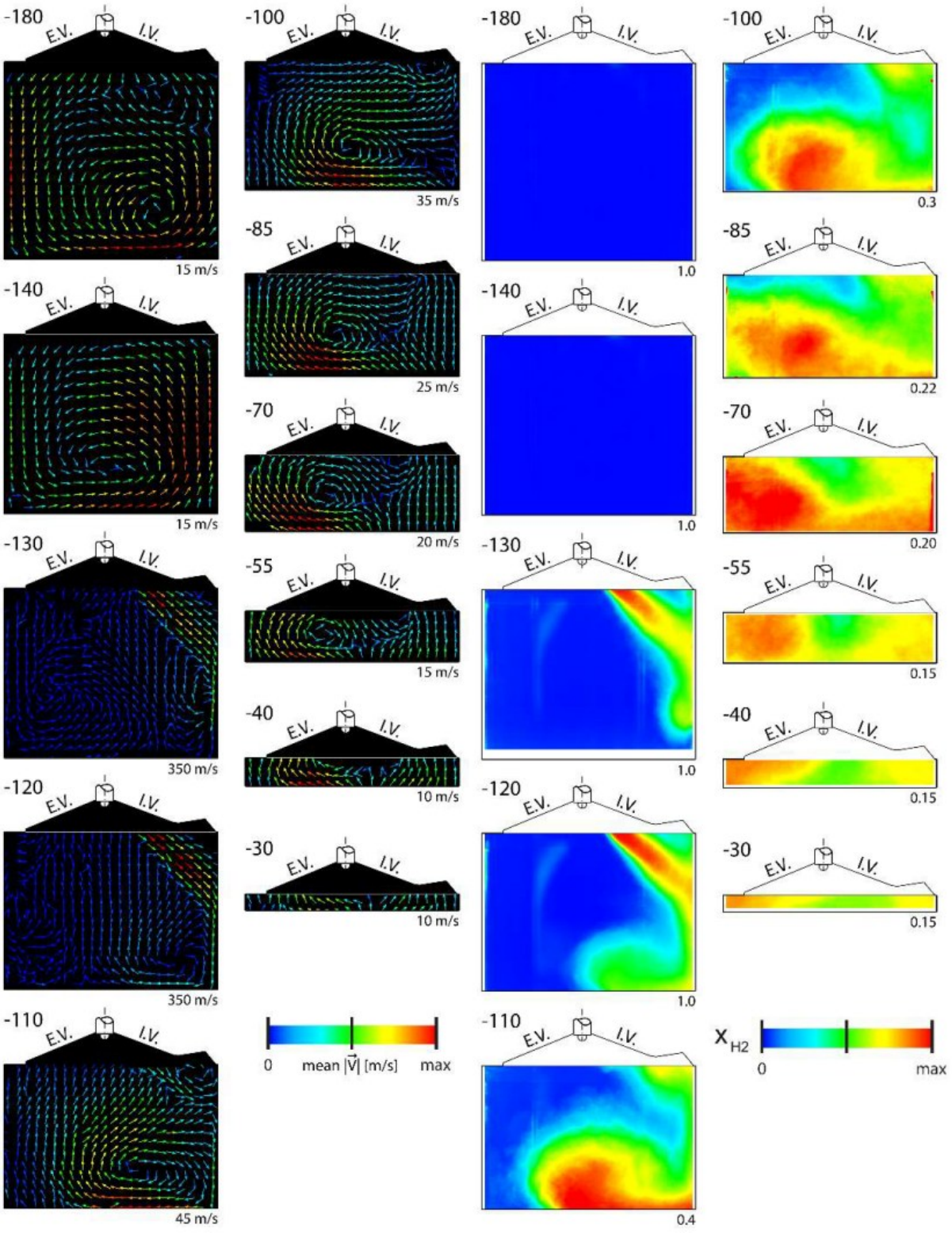

Figure 23 Experimental results from Sandia National Laboratories (ECN Website)

4.5 PIV – Velocity magnitude processing

This application utilizes seeded tracer particles introduced into the intake flow to directly measure the velocity of the flow inside the engine. A dual-pulse laser sheet illuminates the 2D measurement plane inside the cylinder. It is important to note that when reporting results from computational fluid dynamics (CFD), the same planar measurements have been considered. High-resolution imaging is performed with synchronized cameras to capture two successive frames of particle positions. From these frames, instantaneous velocity vectors and relevant turbulence implications are computed and stored. The same resolution achieved in the experimental setup is also maintained in the CFD analysis, ensuring reasonable similarities in grid configurations to make the comparisons with the experiments valid and fair. However, as shown in the overall results from the experiments, a limitation in the experimental assessment can be observed in the particle image velocimetry (PIV). The velocity at which hydrogen is injected, which exceeds sonic conditions, exhibits clipping around the maximum value of 350 [m/s]. Later, CFD results will demonstrate the ability to reach higher velocities. The discrepancies arise because the injection of the seed tracer inside the intake port causes the particles to struggle to reach the core of the hydrogen injection. Additionally, limitations in the acquisition technique tend to underestimate the velocity near the injector tip. This will be taken into account when comparisons are made.

4.6 The bridge from LES to URANS setup

In light of the notable examples of CFD modelling, the author of this manuscript has dedicated the last couple of years to these topics, alongside decades of work on relevant aspects of ICEs by the native group of ICEs from the University of Modena and Reggio Emilia and R&D CFD Srl company, where this PhD was spent. Drawing from the experiences and authoritative references mentioned above in the introductory review, and based on the feasible and reasonably high computational resources available to the author for the various cases presented in this manuscript, a summary of the knowledge gained over the years in modelling H_2ICE using 3D-CFD software is reported. The work aims to provide a detailed modelling structure and setup that serves as a valuable guideline for simulating H_2ICEs using a LES multicycle approach, but also evaluating the same settings in URANS. Here, LES can be extensively useful for validating the unsteady Reynolds-averaged Navier-Stokes (URANS) simulations proposed by the author, but it has broader applications as well. The idea presented is that LES can be beneficial for companies modelling these types of engines with a feasible runtime, provided that all orbital considerations and modelling settings are properly accounted for. This manuscript includes a comprehensive evaluation of the LES framework with the “Engineering LES” approach, emphasizing that achieving a high-fidelity numerical setting must be combined with a thorough chemical-physical approach without the need for super-fine mesh. However, this can only be feasible if the discretization domain is carefully configured to achieve a balanced and harmonious model. This balance is essential for reaching the high-fidelity targets within a reasonable time-to-solution for the company's needs, as mentioned before, a milestone of this work. The author defines a suitable mesh strategy, involving integrating temporal and spatial discretization into the mesh while eliminating unnecessary refinements during the compression phase, which helps prevent excessive computational time when it is not required. The limitations and benefits of this application are reviewed in detail, highlighting that an engineering LES is consistent in reaching more detailed motion structures with respect to the URANS. The approach is tailored to the user based on the specifics of each case, but it is essential that the LES follow the Rutland statement [121], as

mentioned, "Engineering LES". Since the author has academic and professional backgrounds and experience, as well as direct connections with industry prompted to find a balance between computational requirements, numerical accuracy, and CPU needs for these applications. This framework effectively balances simulation time with a high-fidelity discretization method and a robust chemical-physical approach. Details regarding the settings and model selections will be provided in a dedicated section presented later in the manuscript. It is important to note that all contributions are considered and evaluated to create a comprehensive setting that leverages insights from previous studies while integrating the author's own experience in this field. As previously mentioned, this study relates to the LES multicycle approach, where turbulence is modeled using the Wall-Adapting Local Eddy-viscosity (WALE) subgrid viscosity model proposed by Nicoud and Ducros [126]. This model is well-suited to address the challenges associated with jet-wall "impingement", enabling high fidelity at the wall and avoiding issues related to the filtering that is common with other subgrid-scale models. Additionally, the author adopts a real gas approach utilizing the SRK equation of state, coupled with a specific second-order MARS, a method that the author and GruMo (Gruppo Motori from the University of Modena and Reggio Emilia) have extensive experience with, ensuring high fidelity in internal combustion engine (ICE) modelling. Significant work has also been conducted to determine accurate values for the dynamic viscosity of both hydrogen and nitrogen, ensuring precision in the modelling process. The modelling accuracy is further enhanced through a novel Two-Layer All-y^+ wall treatment, firstly suggested by Rodi [151] and then implemented in the STAR-CCM+ software with a Two-Layer All-y^+ wall treatment recently introduced in the latest software releases to be used together with RNG k-ε [122], which accommodates varying working conditions while considering the high variability of wall conditions in the SOpHy engine and similar ICEs. One noted shortcoming in correlating SOpHy engine performance with experimental results is the Sct, which reflects the turbulent diffusivity of hydrogen. The author references various studies and DNS-based validations conducted over the years in the field of jets and similar applications [152-157], despite not being linked to ICEs. The aim of this study is to analyze the impact of using a constant versus a variable Sct approach to isolate the effects of the wall and its relationship to the diffusivity of the flow, specifically focusing on the diffusivity effects related to the core. By comparing these two approaches, we expect to gain a better understanding of the advantages and limitations of transitioning from a constant to a variable Sct. Then, based on results, placing the basis for the future potential approaches that could link this value to physical and flow-related targets, opening the view of a more detailed, physically-related diffusivity in engine applications. This also addresses the low-Reynolds modelling proposed in earlier works as a potential means to provide further insights into turbulence within the boundary layer. Through the Two-Layer All-y^+ approach, a balance between time-to-solution and modelling fidelity is achieved, especially when coupled with the WALE subgrid scale model. Again, the effectiveness of the results when transitioning to highly different values of Sct at the wall, it is suggested that a detailed approach, and a variable Sct as presented in this work and also mentioned in others, can be trained and adapted in the best suitable way in LES and URANS, as will also be evaluated for future analysis. So, the preservation of the overall URANS mesh setup is properly executed, confirming the reliability and the higher grade of fidelity in both flow fields and mole fraction consistency, avoiding the adoption of a highly effort fine mesh, in LES. In addition to LES, as mentioned, the author has also conducted URANS simulations to underscore the significant potential inherent in URANS modelling. This has been performed using a similar modelling approach, differing primarily in turbulence modelling, where the RNG k-ε model is applied. The benefits of employing different Sct values are

comprehensively evaluated in both frameworks, offering insights and advantages related to the simulation approach in URANS for modelling hydrogen and, by extension, gas-fueled internal combustion engines. The study also utilizes the Simcenter STAR-CCM+ In-Cylinder Solution (release: 18.06.006-R8), licensed by Siemens, as an add-on for simulating ICE alongside Simcenter STAR-CCM+. This software offers a unique perspective, and based on its latest versions and customizable features, the author has performed specific reviews and developed tailored approaches. This represents the first application of this software for this purpose using the LES framework, running the cycle-by-cycle progressively with hydrogen injection events. Despite the wide numerical approaches carried out in H_2 mixture predictions, all the proposed studies are performed with the URANS approach. To propose a modelling review of the following great previous works from the above-cited authors, the present work aims to reinforce the modelling predictivity through an extensive study in an LES framework of the SOpHy engine. In this way, a comparison of LES framework results will be made with the setup provided by the author, aiming to compare the CFD framework results together and finally highlight the predictivity of both assessments to the experimental results. Nonetheless, the author aim to present a sensitivity and the first application of a Variable Turbulent Schmidt Number (SctVar) approach conducted in a multi-cycle LES Framework with the SOpHy engine in high-tumble (HT) configuration, which is one of the inputs that affects the H_2 diffusivity and affects the mixing evolution in the mostly adopted ICEs.

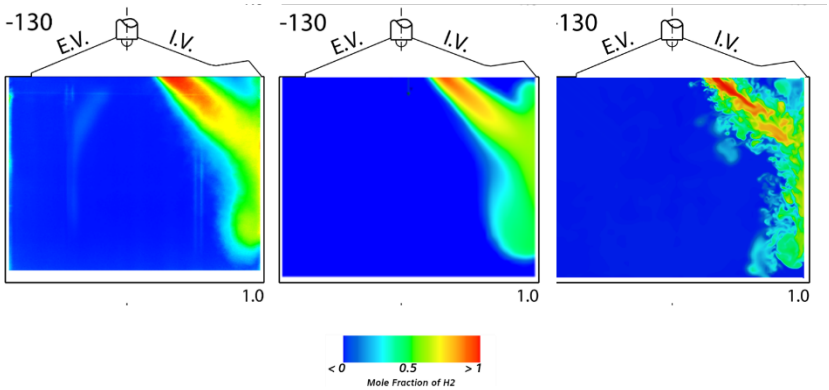

Figure 24 From the experiments to CFD URANS (middle) to LES (right)

4.7 CFD – SETUP

In this section, the author provides an overview of the modelling framework and numerical settings adopted for the CFD simulations of the engine. For completeness, additional details concerning the engine configuration and the layout of the optically accessible test-bench setup are also included. These specifications, which are well documented in the literature and publicly available through the SANDIA website [94], are reported here to support clarity and reproducibility of the analyses.

Table 13 CFD setup concerning chemical and physical models

Detailed Setup – Physical/Chemical/Models	
Discretization Domain	*«Engineering LES» Mesh with spatially/temporally cone mesh refinements*
Numerics (Flow/Species/Enthalpy)	*Second Order Numerical Scheme (Convection Hybrid Scheme MARS / CD)*
Turbulence	*RNG k-ε (RANS) / WALE (LES)*
Wall Treatment	*Two-Layer All y+*
Gas Model Reference	*Real Gas (Soave-Redlich-Kwong)* *Kinetic Theory Of Gases (Thermal Conductivity/Molecular Diffusivity)* *Dynamic Viscosity with Sutherland's Law (Coeff. from literature for H_2/N_2)*
Algorithm for Pressure Correction	*PISO* *(Predictive-Implicit Splitting of Operators)*
Turbulent Schmidt Number	*Constant/Variable Approach for Turbulent Schmidt Number – A Sensitivity*

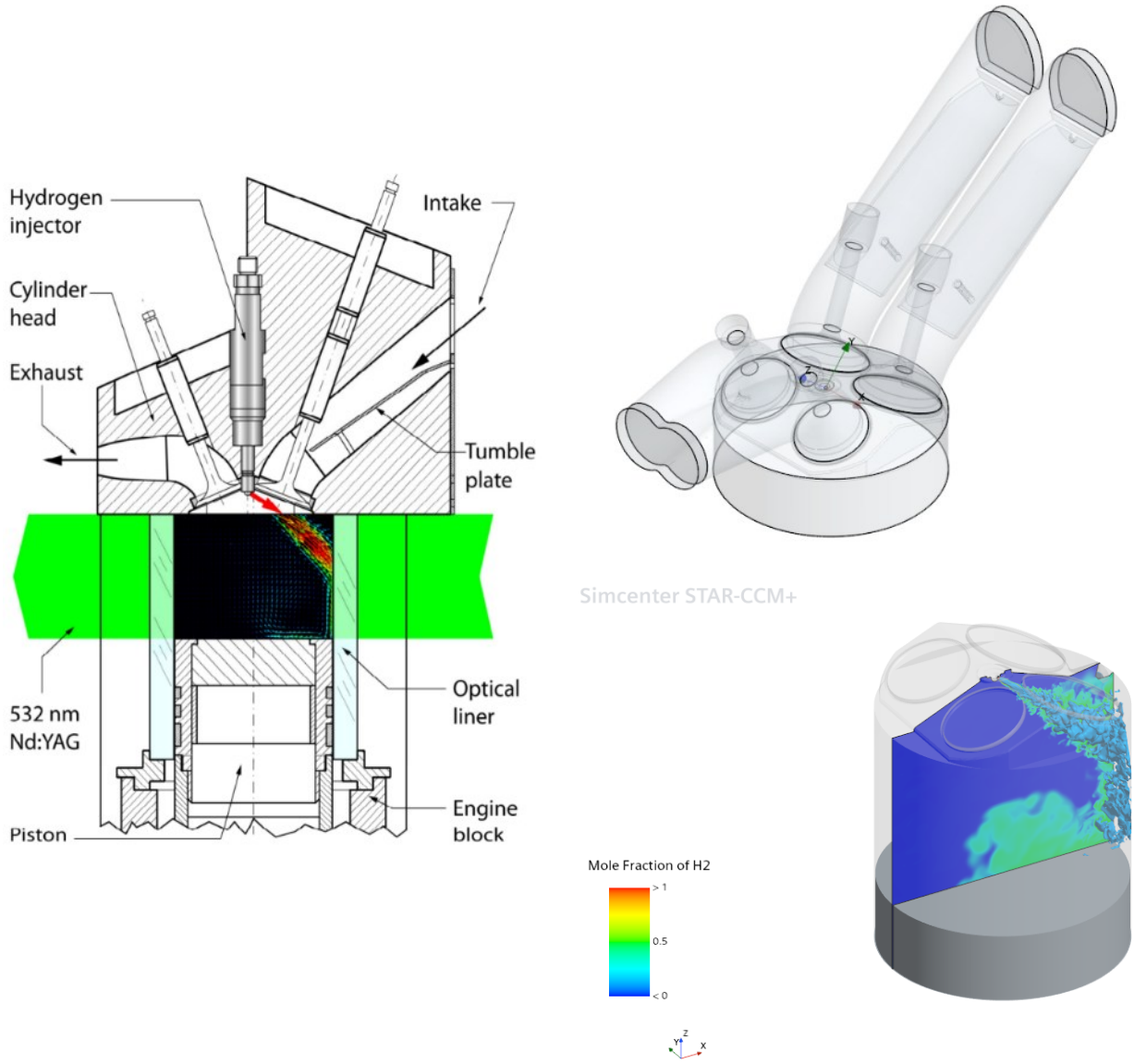

Figure 25 Engine layout and model overview

4.7.1 Discretization Domain – URANS and the "Engineering LES" Approach

Scale-resolving simulations (SRSs), as reported by Hasse [149], have recently improved the study and the understanding of the phenomena affecting the ICE operation. The increase in high-performance computing (HPC) resources and the availability of well-performing and user-friendly software tools make the use of SRS, and in particular LES, attractive not only for academic researchers and research laboratories, but also for R&D engineers and the automotive industry. According to Rutland [121], it is possible to define two different kinds of Large Eddy Simulations: "scientific LES" and "engineering LES". The latter is adopted by the author in this work: the discretization domain is reported in figure 26 where the same planar section as the PLIF is shown. The core of the mesh is set to 1 [mm], with specific in-house developed spatial refinements appearing and disappearing through the simulation process. Such a choice is adopted to balance accuracy and computational effort. In particular, a multi-conical refinement appears before the injection and disappears towards the TDC. This mesh strategy allows for saving time while retaining a high degree

of fidelity for the hydrogen flow development and its mixing with the trapped air, reaching reasonably low CFR (Courant-Friedrichs-Lewy) values up to the injector tip. The minimum mesh cell size is reached at the injector nozzle exit with a value of 0.03125 [mm]. The remaining cones bridge progressively, such as a very fine mesh up to 0.5 [mm] while covering the volume of the combustion chamber covered by the high-speed/low-momentum hydrogen jet. The refinements disappear well after EOI, to speed up the simulation without significantly affecting the quality of the solution and its stability. A more detailed description of the mesh strategy and the maximum number of cells at the injection and BDC timing is reported in table 14.

Table 14 Mesh settings related to the core, refinements and specifics for the near-wall prism layers

Engine Mesh Settings	
Mesh Size (CORE)	*1 [mm]*
Cone Refinement (injection)	*0.25 [mm] / 0.125 [mm] / 0.03125 [mm]*
Boundary Layer / N. of Prism Layers	*0.03125 [mm] x 4 layers; 0.5 [mm] x 2 layers*
Total number of Cells (INJECTION/ BDC)	*1.27 Million cells @bTDC* *7.0 Million cells @Injection*

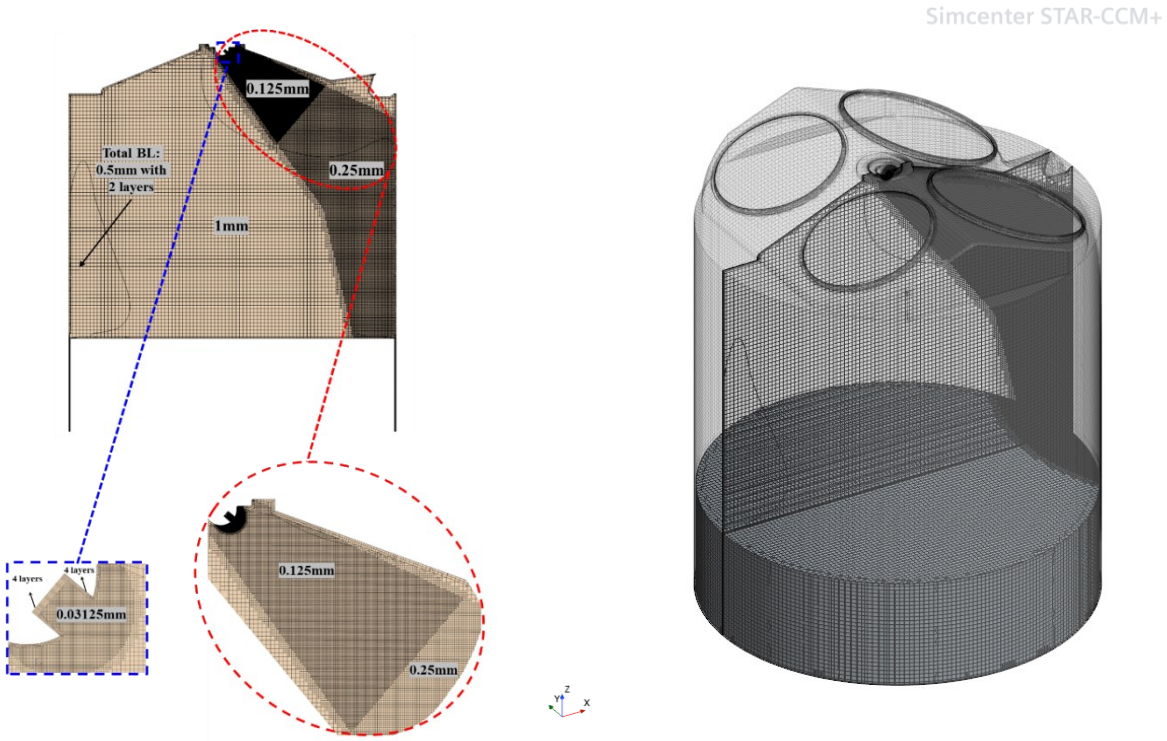

Figure 26 Discretized domain with details. On the left, the section linked to the PLIF according to the experiments. On the right, the cylinder core with the related specific cone refinement.

4.7.2 Physical Modelling

In line with the observations in [64], the author adopt the Soave Redlich Kwong real gas equation of state. Particular care is devoted to the definition of the dynamic viscosity of hydrogen [158,159] and its diffusivity, which is modelled using the Kinetic Theory of gases following the formulation from Soave G. [150], reported here for clarity:

$$p = \frac{RT}{\nu - b} - \frac{a\,\alpha\,T_r}{\nu(\nu + b)} \qquad \textit{Eq. 88}$$

where: $\alpha(T_r) = [1 + (0.48 + 1.574\omega - 0.176\omega^2)(1 - \mathrm{T_r^{0.5}})]^2$ *Eq. 89*

$$a = \frac{0.42748\ R^2 T_c^2}{p_c} \qquad \textit{Eq. 90}$$

$$b = \frac{0.08664\ RT_c}{p_c} \qquad \textit{Eq. 91}$$

, being ν the kinematic viscosity.

In CFD, especially when talking about these detailed settings, both in URANS and LES, there are a couple of quantities that relate to the diffusion of substances, depending also on the nature of the transportation of heat or mass. Following the latter of the two considerations, as more interesting in this study, the diffusivity of the mass (especially related to hydrogen) plays a relevant role in SOpHy engine modelling, as well as, more widely, in hydrogen engines. Furthermore, it can also be split into the diffusivity of the substance related to the regime at which the simulation is performed, in relation to the local values of Re: laminar or turbulent. This aims to emphasize the role of jet-wall impingement and the modelling details introduced in the setup described here, utilizing the WALE model, the KT of gases, and a variable approach for the Sct. In relation to the molecular KT of gases, molecular viscosity and thermal conductivity are calculated based on that formulation. The relevant parameters for this modelling can be found in the Lennard-Jones characteristic length and Lennard-Jones energy, which, for the sake of completeness, are reported:

$$L - J\ Ch.Length:\ H2\text{: } 2.92\ [\text{Å}];\ N2\text{: } 3.621[\text{Å}] \qquad \textit{Eq. 92}$$

$$L - J\ Energy:\ H2\text{: } 38\ [K]\ ;\ N2\text{: } 97.53\ [K] \qquad \textit{Eq. 93}$$

These conditions lead to good fidelity between chemical statements and the approach that has been selected to calculate turbulence with the WALE, which details the near-wall through an active approach and adaptive filtering of the eddy viscosity coupled with the kinetic theory mentioned above. This condition aligns with a potential variation of the Sct to fit and optimize the local insights during boundary layer transition. The Thermal Conductivity and Molecular Diffusivity according to the theory of Chapman and Enskog on intermolecular forces are followed here [160-162]. Finally, related to the dynamic viscosity for each of the substances adopted for the SOpHy engine, Sutherland's Law, with a proper selection of the coefficients, table 15 and the plot in figure 27 represent both calculations through the Sutherland coefficients from [158] and the NIST database. The Hirschfelder coefficients from [160] are adopted in this case as well, representative of the hydrogen experimental data from NIST and thermal values.

Table 15 Material properties settings for hydrogen and nitrogen

	Reference Value [Pa*s]	Sutherland Constant [K]	Reference Temperature [K]
Hydrogen	8.411 e-6	97.0	273.15
Nitrogen	1.716e-5	111.0	273.15

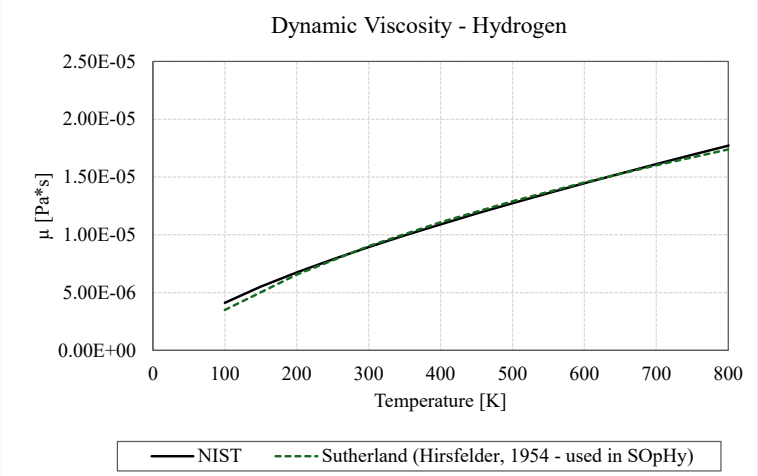

Figure 27 Dynamic viscosity of hydrogen comparison between the NIST and Sutherland's one adopted in the simulation setup

4.7.3 LES Modelling Approach – Convergence

The LES multicycle simulation has been performed with consecutive cycles targeting the stability of the solution through an evaluation of the average and standard deviation of the velocity magnitude. The procedure of averaging concerns the values collected in the PLIF section from experiments and generated in CFD. The velocity magnitude is the reference quantity that is considered representative of the flow motion, while the mole fraction is representative of the mixing. The data extrapolated from the CFD software is then elaborated toward an average procedure for the LES multicycle performed. Figure 28 reports the comparison between consecutive averaged cycles at stepping of 2, starting from the 3rd one, bearing in mind that the first two LES cycles are used as initialization and not considered in the computational CCV evaluation. It is possible to see that the standard deviation reaches acceptable and reasonable values by 10 consecutive engine cycles. The authors retain an overall of 12 cycles to be considered an acceptable result of multicycle LES for engineering applications. This is in line with a very high-level setup following chemical-physical approaches, as well as a detailed and coherent numerical approach behind these solutions.

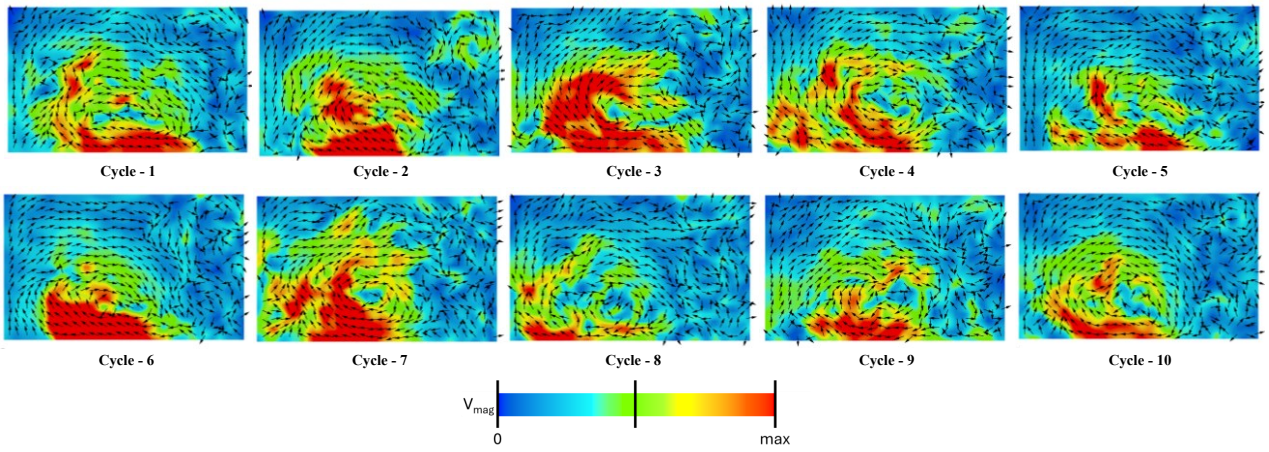

Figure 28 CFD cycle-to-cycle velocity magnitude and vectors at the PLIF for the 10 LES cycles (avoided the first 2 for initialization). Data extrapolated and remapped on the reference grid iso-EXP.

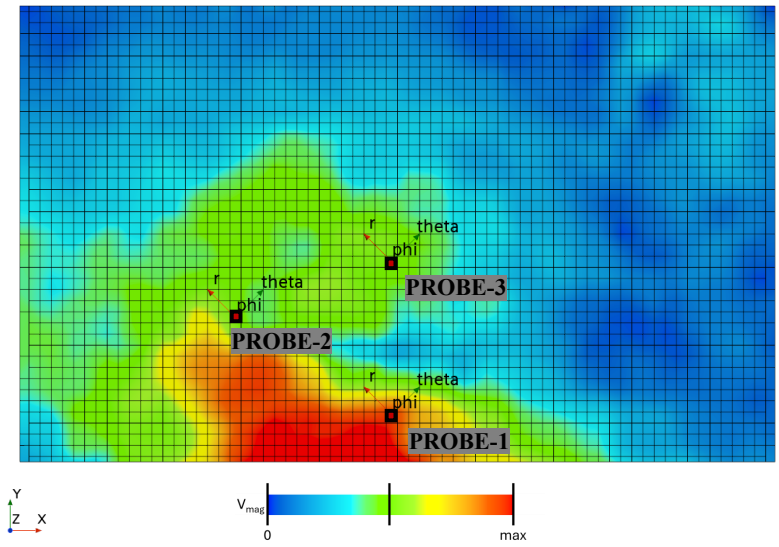

Figure 29 Overview of the computational reference grid iso-EXP and locations of the three probes adopted for the detailed post-processing investigation

The CCV can be seen, again, in figure 30, in which each cycle is reported with the field of the velocity magnitude, together with the vectors from the PLIF/PIV section. Instead, if the reader looks at figure 31, the average process allows for reaching a very close standard deviation, as the multicycle LES simulation is reported. Furthermore, to deepen and quantify the comparison and accordance of the CFD to EXP, three points are considered as probes in the CFD SOpHy engine to extrapolate the velocity magnitude. To clarify this consideration, in figure 29, the three probes are placed in the section to get the values of the velocity in the specific locations. Here, the author investigated the monotonically characteristic of the average process if in agreement with a sufficiently high number of consecutive cycles and, at the same time, extrapolated values to be compared with the experiments. More specifically, as the experimental dataset is provided as a planar section (2D), the probes are representative of a cell at which the experimental data are remapped in the CFD engine. The same has been performed for the experimental data, which are placed, instead of a 2D grid, in a 3D single cell thickness, but maintaining the same resolution as the 2D one. The same approach for the comparison is maintained and adopted for the pure 3D-CFD, in which, due to the nature of the 3D-

CFD framework, the data are extrapolated in a grid with the same discretization adopted for the experimental post-processing from the works of Salazar and Kaiser. Then, to be fair with the experiments, the author remapped the data from the 3D-CFD grid and imported the data through a remapping process that allows for a fair comparison with respect to the experimental exported results. This procedure, despite a longer effort to be spent in each of the comparisons performed in this work, allows the benefit of removing errors or discrepancies between experiments and CFD comparison, especially in the extrapolation of 3D-CFD results, where the resolution of the very fine mesh is not the same as the experimental one. This is the reason behind this choice, as more time for post-processing, as stated, allows for being as fair as possible, with comparison of the experimental side.

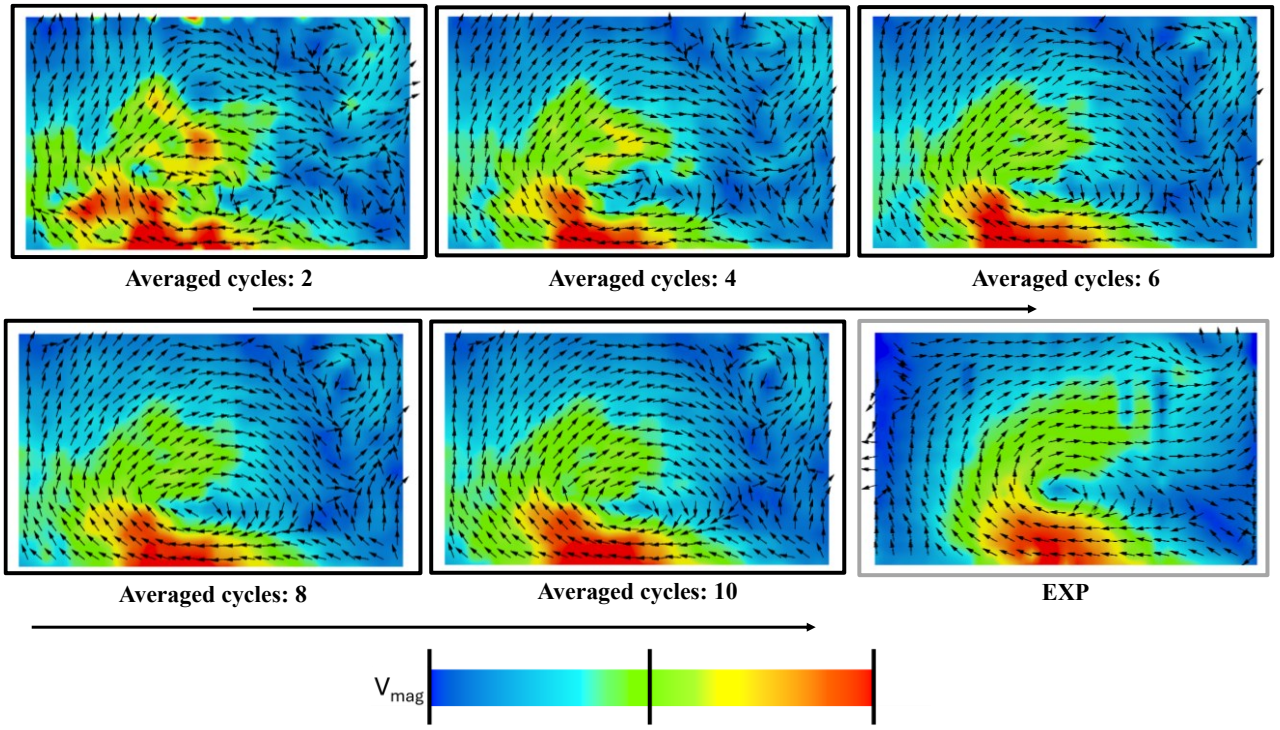

Figure 30 CFD cycle by cycle averaging (2 cycles) to highlight the averaging process up to the convergence reached in 10 consecutive LES cycles

Defined the computational domain, the same as the EXP, the data is remapped in the single cell thickness along the Z direction (cutting plane XY), and the data of mole fractions and velocity magnitude are used for the post-processing. Thus, convergence consideration and evaluation are reported in the analytical plot in figure 33, where a progressive averaging every 2 full cycles has been performed. More specifically, a comparison between each case and specific settings will be evaluated later in the dedicated section. The crank angle at which the standard deviation is calculated is 100 [CAD bTDC] and the average is performed in the planar section for both the CFD and EXP, and PIV average fields are reported in figure 30. Furthermore, an interesting visualization analysis is able to show the average of the 10 LES cycles compared to the experimental one. In figure 30, in fact, the experimental PIV reported with the same color band of the CFD as well as the vectors of the remapped data on the same grid appear very similar to each other, concluding that CFD is very close to the EXP. So, the latter comparison confirms how the LES averaging leads to the convergence, reaching the experimental average value in 10 LES cycles, leading to reasonable simulation convergence.

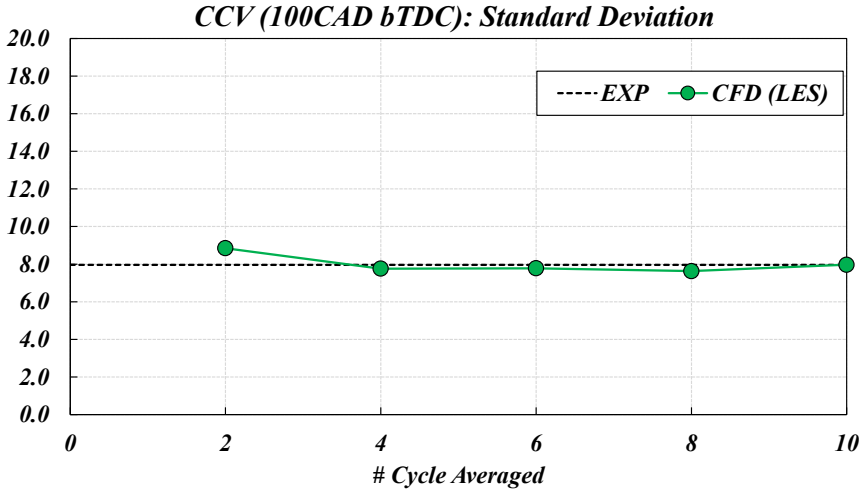

Figure 31 Standard deviation calculated in the longitudinal section plane of the engine cylinder at 100 [CAD bTDC]. The comparison is performed between experiments and CFD (LES)

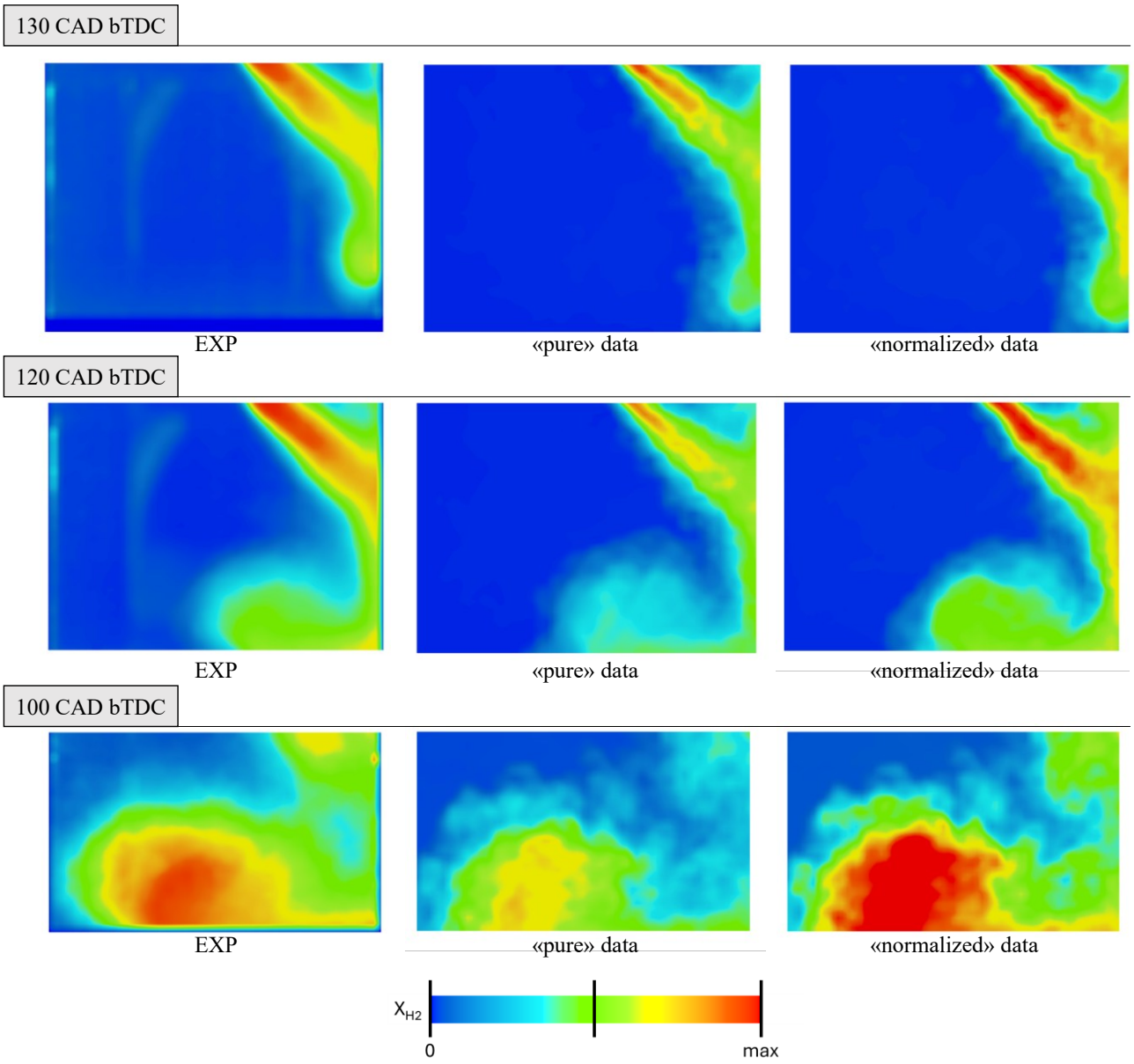

Figure 32 Pure, Normalized and experimental imaging on the PLIF of the mole fraction of hydrogen

As mentioned, a normalized view of the results is considered, as the optically accessible engine apparatus and the light interaction with the gas could be affected by uncertainties during cycle-by-cycle acquisition. To account for these uncertainties, the author will report both the visualizations (such as "pure" and "normalized"), as mentioned previously, for further comparison between CFD and EXP outcomes. This is a reliable and reasonable way to approach a far comparison through the normalization of the mole fraction according to the same process followed by the acquisition and post-processing from experiments, as also treated by Herold and Gandhy [46]. Going deeper into the figure 32 reports the same comparison seen before, but scaled through the following formulation:

$$CFD_{LES} = R * CFD_{LES_\theta} \qquad \textit{Eq. 94}$$

$$R = \frac{\int_{VOL} EXP}{\int_{VOL} CFD_{LES}} \qquad \textit{Eq. 95}$$

4.7.4 LES Modelling Approach – Results (Analytical)

4.7.4.1 Cycle-to-cycle Variability

The results of the LES simulations are reported in this section, focusing on the mole fraction and velocity magnitude achieved with the best settings and compared to the experiments. However, before analyzing the previously mentioned outcomes, the author wants to review and check the results from a "motorist" standpoint, including the tumble and the equivalence ratio (ER) by comparing CFD to experiments. The results obtained from the reference configuration allow for a detailed analysis of the CVV in LES. Specifically, the results are reported at 100 [CAD bTDC], where previously identified probes provide data necessary to understand the convergence of the simulations in achieving the experimental target. This evidence demonstrates a clear consistency in the accuracy of simulation averaging in the multi-cycle LES, highlighting the need for at least 12 cycles in the LES analysis following an "Engineering LES" approach (figure 33). Cycle-to-cycle averaging is performed every two consecutive cycles. Starting from the calculation of tumble, the formulation (Eq. 96) is reported, which is the one that the software adopts internally. This approach allows directly calculate the tumble by remapping the results on the same grid both for experiments and CFD. The major steps to describe the velocity fields are reported and analyzed according to the tumble ratio reached at specific CAD and analytical results reported in figure 33 and 34.

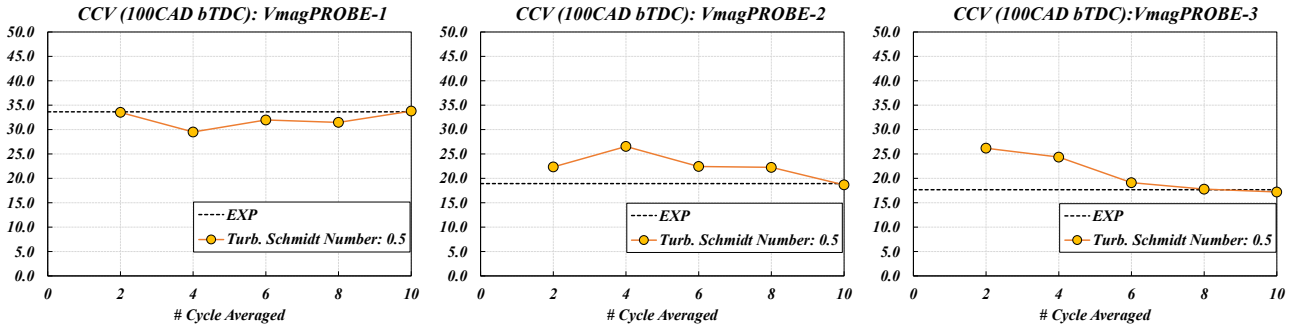

Figure 34 Cycle-to-cycle variability and convergence behavior by averaging results every two consecutive cycles

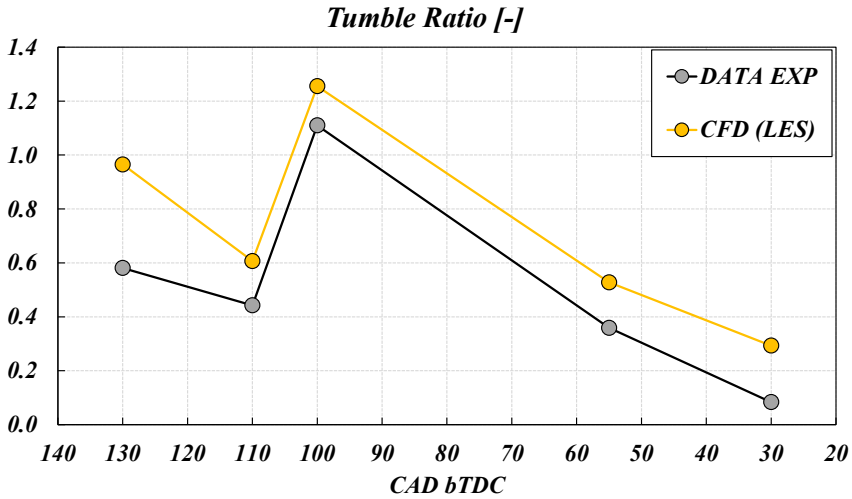

Figure 33 Tumble ratio of CFD and EXP compared for significant crank angle times

$$Tumble_y = \frac{M_y}{w_c I_c} = \frac{\sum_{cells} \rho_i V_i [(Z_i - Z_m) u_i - (X_i - X_m) w_i]}{w_c \sum_{cells} \rho_i V_i [(X_i - X_m)^2 + (Z_i - Z_m)^2]} \quad \text{Eq. 96}$$

By comparing the results achieved with CFD to the ones from EXP, it can be noticed that differences can be observed mainly before the SOI and reach their minimum around 100 [CAD bTDC]. The reason for these differences could be given by the results that are extrapolated on the planar section, since the EXP results come from a single planar section (PLIF/PIV) and it is the only data that can be used for the comparison. It should be noted that some other motions, such as slightly swirling or deflating flux during the intake phase in the high-tumble (HT) configuration, may happen. This could lead to the differences noticed in the tumble motion, generally overestimated as visible in the plot, despite quite similar behavior and, of course, aligned to previous studies, despite most being with the low-tumble (LT) configuration. To reinforce the quality of the results and to fulfill the comparison between multicycle LES and EXP, as reported later in the manuscript, the evolution of the velocity magnitude with vectorial representation is reported. The results show that the overall velocity

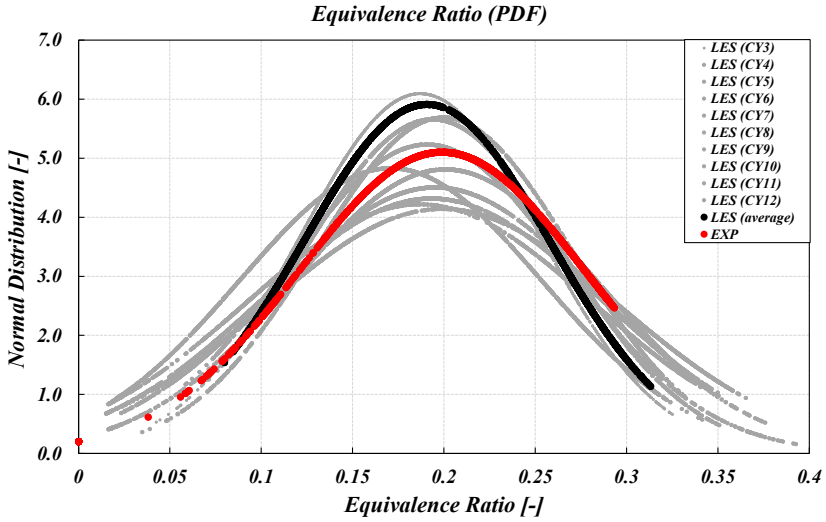

Figure 35 Equivalence ratio probability density function for each LES cycle, the average LES one and the EXP

magnitude is achieved, according to the center of the rotation/tumble inside the engine. The maximum velocity is matched with a good degree of approximation, with a slight overestimation of the absolute velocity at the 130 [CAD bTDC] and 30 [CAD bTDC] where slightly misalignment could occur in terms of motion and experimental apparatus/average process. Nevertheless, it can be supposed that the CFD compared to EXP is quite well aligned, leading to the conclusion that for LES simulations, the chance to reach a great detail of results by capturing detailed vortices and motions can be satisfied. This allows to compare the results from experiments and CFD in the same way and allows the avoidance of the discrepancy due to the use of an absolute scale that could occur when comparing LES multicycle to the experiments. Some details related to the well-aligned results can also be checked through the velocity magnitude and vector analysis reported. Also in this case, as reported in previous works, the first averaged data from experiments highlighted a maximum velocity that never exceeded 350 [m/s]. As in an effective and realistic application, as well as achieved with the CFD, this limit is significantly overcome. The limit of the experimental apparatus governs the reason for this misalignment between CFD and EXP. Nevertheless, according to the experiments, the maximum of the velocity scalar field of CFD is reached in the coherent zones despite the absolute

values at the tip, where the instrumental apparatus is limited to 350 [m/s]. Far from this zone, the velocity aligns reasonably between the numerical solution and the experiments.

Nonetheless, an overview of the ER, still from an analytical standpoint, is pertinent in this section. According to the ER reached in LES simulations, and reported in figure 35, the average value of the ER is slightly lower compared to the experiments. This is the major reason why, in the direct comparison, and targeting imaging is the more reliable way to compare the two results for CFD Vs EXP. Generally speaking, lower mole fraction intensity is achieved in CFD compared to EXP. To be said that, these differences could be the cause of this little discrepancy in ER, despite the same law of injection as reported from the experiments being adopted. The first consideration concerns the Westport injector, in which, over the years, some uncertainties have arisen, including slight uncertainties related to the tip shape, inclination, and some issues during the injection process. Another consideration could be related to the injection law, with little uncertainties related to SOI/EOI that could affect the injection cycle-by-cycle and the H_2 trapped. Looking at the next reported images (figure 39), right side, it is possible to appreciate that the maximum value reached in the CFD mole fraction is slightly lower compared to the one from EXP. The values tend to align, reaching the TDC, confirming that considerations could be explored behind this. It is possible that deviation of the fluxes due to crossing motions could slightly deviate the hydrogen mole fraction inside the engine, leaving H_2 from the planar view, which considerations are the same as those related to the discrepancy in the ER plot. So, as previously mentioned, considerations, and due to no information regarding the mole fraction of the hydrogen in more than one section, a method is introduced to compare the results following the maximum of the example fraction gained in CFD and normalized. The reasonable consideration behind this procedure pushed the author to perform and report an alignment between the EXP dataset and CFD through the above-cited CFD scaling factor. Figure 32 shows in detail the comparison between “pure” and the “normalized” results representation from CFD and EXP.

In the analysis of the normalized results, the author conducted a detailed and fair comparison between two approaches for the turbulent Schmidt number to confirm their negligible impact on turbulent diffusivity, which could affect the LES. A third approach, which uses a variable law up to the wall, is also mentioned, and its results are compared to the two constant values.

From an analytical standpoint, it is noted that the approach with the constant turbulent Schmidt number Sct set to 0.5 shows the highest difference when compared to the Sct 0.9, and similar when compared to the variable one, despite some closer details being achieved with the variable one. This observation confirms that the deviation in the Sct approach plays a role during the evolution of motion and mixing, specifically, inside the cylinder.

4.7.5 LES Modelling Approach – Results (velocity and mole fraction – PIV/PLIF)

The next comparison focuses on the evolution of mixing in terms of mole fraction in the LES framework and modelling approach. As previously mentioned, the CFD–EXP comparison must account for slight spatial or temporal misalignments arising from luminescence-based measurements and their associated post-processing. The next comparison reported, in figures 39-40, includes both qualitative and quantitative comparisons, but is normalized by the integral of the CFD field over the corresponding experimental field. This normalization provides a more coherent basis for comparison, effectively reducing the impact of possible CFD–EXP misalignments. Based on these normalized results, which offer a clearer and more balanced visualization, the author conducted a detailed and fair comparison among the three turbulent Schmidt number values and approaches. The analysis confirms that the choice of turbulent Schmidt number model has a non-negligible, albeit limited at

this stage, influence on the turbulent diffusivity, and therefore has a contribution to the LES solution under the investigated conditions in the "engineering LES" framework. The three configurations of the turbulent Schmidt numbers are collected and refer to Sct= 0.9, Sct= 0.5 and a hybrid or variable approach SctVar (figure 36).

Furthermore, although the WALE subgrid-scale model is formally derived from the Smagorinsky formulation within the software implementation, with the key exception of its treatment near the wall, originally introduced by Nicoud and Ducros, a more detailed degree of fidelity is expected at the near wall from the standpoint of eddy-viscosity prediction. This statement holds under the assumption that the dominant portion of the turbulence is directly resolved, leaving the SGS viscosity active only at the unresolved scales. In regions where the turbulence intensity is very low, the model naturally transitions toward the regime where molecular viscosity dominates, further minimizing the influence of the subgrid formulation. Nevertheless, as from the concept adopted in an "engineering" field, the turbulent Schmidt number still plays a role in identifying the correct approach for a better diffusivity prediction. This conclusion is consistent with the theoretical expectations of the adopted SGS formulation. When the majority of turbulent scales are resolved, the contribution of the subgrid terms, and consequently the dependence on the modeled turbulent viscosity, naturally becomes negligible. Under these conditions, the turbulent Schmidt number loses its role as a controlling input parameter and can instead be interpreted as an output quantity of the resolved turbulence dynamics, particularly in the context of dynamic or non–eddy-viscosity-based SGS approaches [174].

At the same time, the detailed treatment of turbulence–scalar interaction from both a physical and chemical standpoint enables a reliable representation of near-wall behavior, including gas–wall interactions that are critical for hydrogen mixture formation. This reinforces the suitability of the proposed framework not only for bulk mixing predictions but also for capturing wall-dominated transport mechanisms.

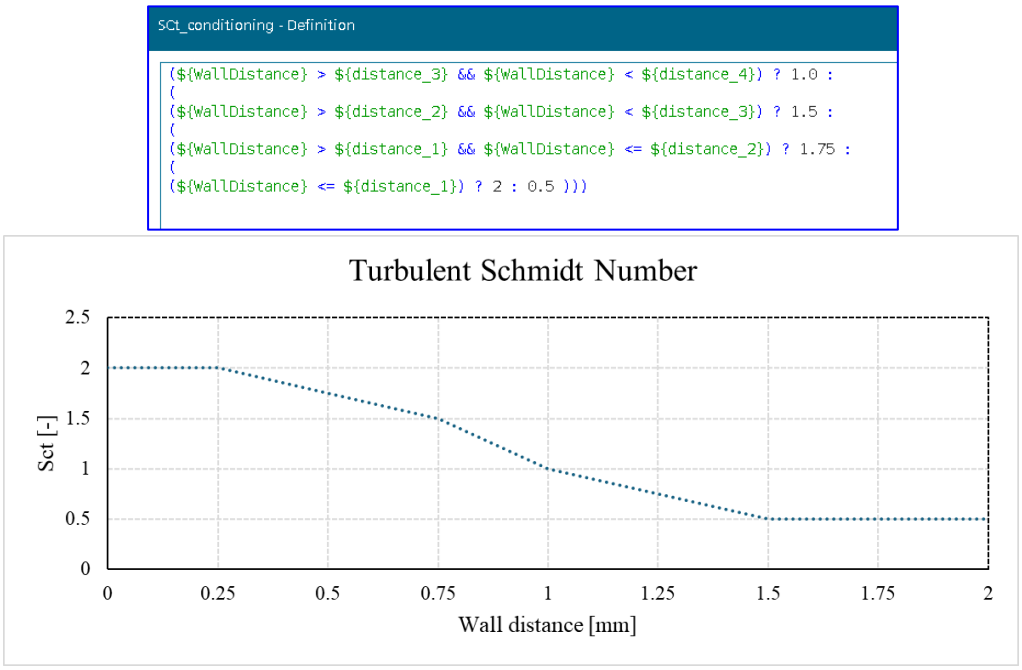

Figure 36 Implementation of the "field function" for the Software and turbulent Schmidt number plot over the wall distance from the wall

The explicit linkage between the turbulent Schmidt number and local flow properties will be further investigated in future studies. In this regard, existing literature consistently indicates that the turbulent Schmidt number should not be treated as a universal constant, but rather as a quantity dependent on the local turbulence state and molecular transport properties. Its variability has been shown to correlate with parameters such as molecular and turbulent viscosity, Reynolds number, Péclet number, and other non-dimensional quantities rooted in turbulent flow theory, supporting the rationale for the variable Sct (SctVar) formulation adopted in this work.

Despite a small mismatch in the comparison of the mole-fraction fields, such differences can reasonably be attributed to the engineering-level LES resolution used in this study. In fact, since the adopted SGS models are viscosity-based, the turbulent Schmidt number remains an input parameter rather than a dynamically computed one. For instance, in the case of the WALE model, the SGS viscosity is computed through the classical Nicoud–Ducros formulation:

$$\nu_{SGS}^{WALE} = (C_w \Delta)^2 \frac{\left(S_{ij}^d S_{ij}^d\right)^{3/2}}{\left(S_{ij}S_{ij}\right)^{5/2} + \left(S_{ij}^d S_{ij}^d\right)^{5/4}} \qquad \textit{Eq. 97}$$

$$S_{c_T}^{SGS} = \frac{\nu_{SGS}^{WALE}}{D_T^{SGS}} \qquad \textit{Eq. 98}$$

where Δ is the filter width, C_w the model constant, S_{ij} the resolved strain-rate tensor, and S_{ij}^d the traceless symmetric part of the square of the velocity-gradient tensor. Since this formulation is still fundamentally tied to the local viscosity field, any insufficient mesh resolution in the core-flow region may lead to slight deviations, such as those observed in the mole-fraction comparison, because the SGS viscosity and the imposed turbulent Schmidt number are still partly responsible for the unresolved mixing dynamics.

These differences, however, remain limited and do not compromise the excellent agreement achieved between LES and experimental data, both in terms of the internal flow structures and the scalar-field evolution. This reinforces the conclusion that, for the present configuration, the selected modelling strategy represents a robust and computationally efficient solution. Its effectiveness is not strictly dependent on the specific LES formulation adopted; rather, it is further supported by URANS-based evidence indicating that a turbulent Schmidt number of Sct=0.5 is, at this stage, an appropriate choice for capturing the dominant mixing mechanisms, but the variability of the Sct further link with the DNS evidences which confirm that a constant value of the turbulent Schmidt number is not accepted generally. In fact, as will be reported, differences are also visible in URANS when the turbulent Schmidt number switches from constant to variable, although the closer results are not enough to show significant differences during compression.

Following this line of reasoning, adopting models capable of directly calculating Sct, or frameworks in which Sct emerges naturally from the resolved flow physics, could ultimately allow this quantity to serve as a physically meaningful input for URANS or hybrid URANS/LES approaches. This would represent a significant step forward compared to the current practice, where Sct is treated as a global, reduced parameter applied uniformly in both URANS and LES. A future transition toward physics-driven turbulent Schmidt-number closure has the potential to enhance the predictive

capability of engineering-grade simulations, especially in highly diffusive mixtures such as hydrogen-air systems.

In addition, considering that the grid resolution in the engine core is comparable to that of a URANS-level mesh, a future investigation could involve a “scientific LES” approach based on a substantially refined grid capable of resolving a larger portion of the turbulent energy spectrum. Such a study would help assess the extent to which increased mesh resolution improves the agreement in velocity structures and mole fraction evolution, particularly for configurations involving highly diffusive fuels such as hydrogen.

However, the results obtained with the present “engineering LES” approach already show a satisfactory level of agreement with experimental data. This observation supports the choice of avoiding, at this stage, a fully “scientific LES” strategy, while still achieving reliable predictions through a computationally affordable setup. In this context, the correct evaluation of the turbulent Schmidt number value and approach plays a key role, enabling accurate results to be achieved at significantly reduced time-to-solution.

Moreover, the increased grid resolution associated with “scientific LES” would reduce the dependence on SGS viscosity modelling and consequently diminish the sensitivity of the results to Sct, albeit at the cost of a dramatic increase in computational expense. Therefore, the methodology presented in this work deliberately seeks to balance accuracy and efficiency, maintaining a level of fidelity higher than URANS while defining appropriate modelling strategies, parameter values and settings for both LES and URANS CFD frameworks when applied to hydrogen engine simulations.

Finally, the LES mesh quality index, which will be introduced later, will provide further quantitative insight into the fraction of turbulence that is actually resolved and, accordingly, into the expected reliability of the SGS contributions.

4.7.5.1 Impact of Turbulent Schmidt Number: Variation and Results

The turbulent Schmidt number (Sct) modelling approaches adopted in this work are essentially two. The first approach consists of a parametric sweep of constant Sct values applied over the entire engine domain. This methodology represents the most common practice found in the literature, both for URANS and LES simulations, as discussed in the preface section.

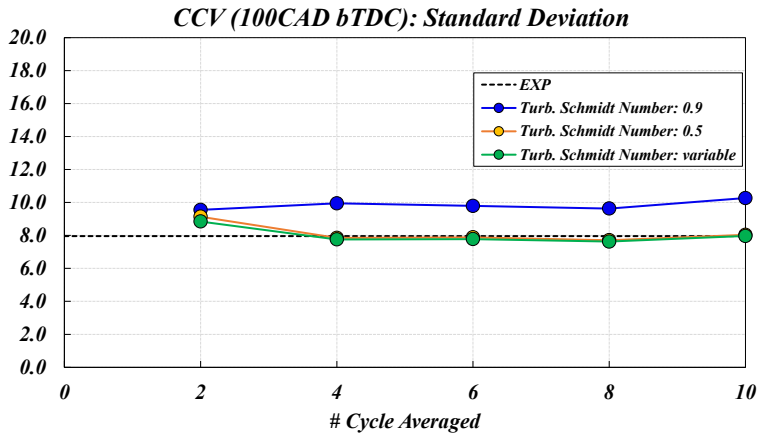

Figure 37 Standard deviation of the LES simulation averaged by using different turbulent Schmidt numbers.

Nevertheless, in most studies, the optimal constant value is selected on a case-by-case basis, closely by comparing numerical outputs with experimental data. A clear trend emerging from the literature is the reduction of the assumed Sct when hydrogen is used as a fuel in internal combustion engines. In the present study, a comparison based on constant Sct values is first reported. Subsequently, an original modelling approach is introduced, in which the turbulent Schmidt number varies as a function of the wall distance. As shown in figure 37, adopting a constant turbulent Schmidt number of 0.5 leads to improved results, particularly in terms of standard deviation, showing closer agreement with experimental measurements. In addition, results are reported for the velocity magnitude extrapolated from probe locations, which directly correlate with the trends observed in the standard deviation analysis.

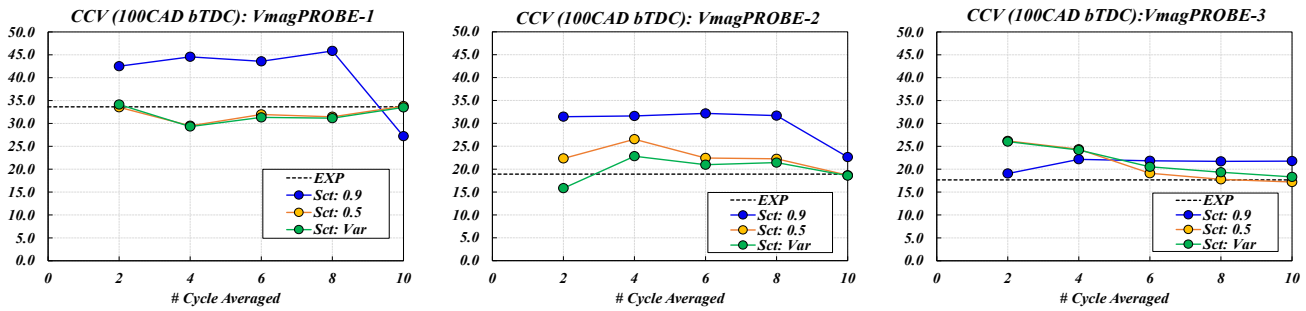

Figure 38 Analytical evaluation of the cyclic convergence of the LES simulations with different values of the turbulent Schmidt number setting. Results are related to the velocity extrapolated at each probe location.

The cycle-to-cycle evaluation at the probe locations, in figure 38, highlights a remarkable improvement when moving from a constant Sct value of 0.9 to 0.5, further reducing the discrepancy with experimental data. The next step, carried out by the author, consists of increasing the turbulent Schmidt number in the near-wall region, up to 2, while maintaining the same minimum value of Sct = 0.5 in the core region. The purpose of this approach, which constitutes one of the main objectives of the study, is to isolate and assess the influence of wall effects on hydrogen mixing, as well as to

evaluate the resulting impact on the overall flow field, mixing processes, and velocity distribution. As will be clearly shown in the following figures (39,40,41), figure 38 clearly demonstrates a significant improvement in the velocity magnitude predicted at the probe locations when the variable Sct approach is employed. Compared to the constant-Sct formulations, the space-dependent Schmidt number model yields results that better match the experimental observations.

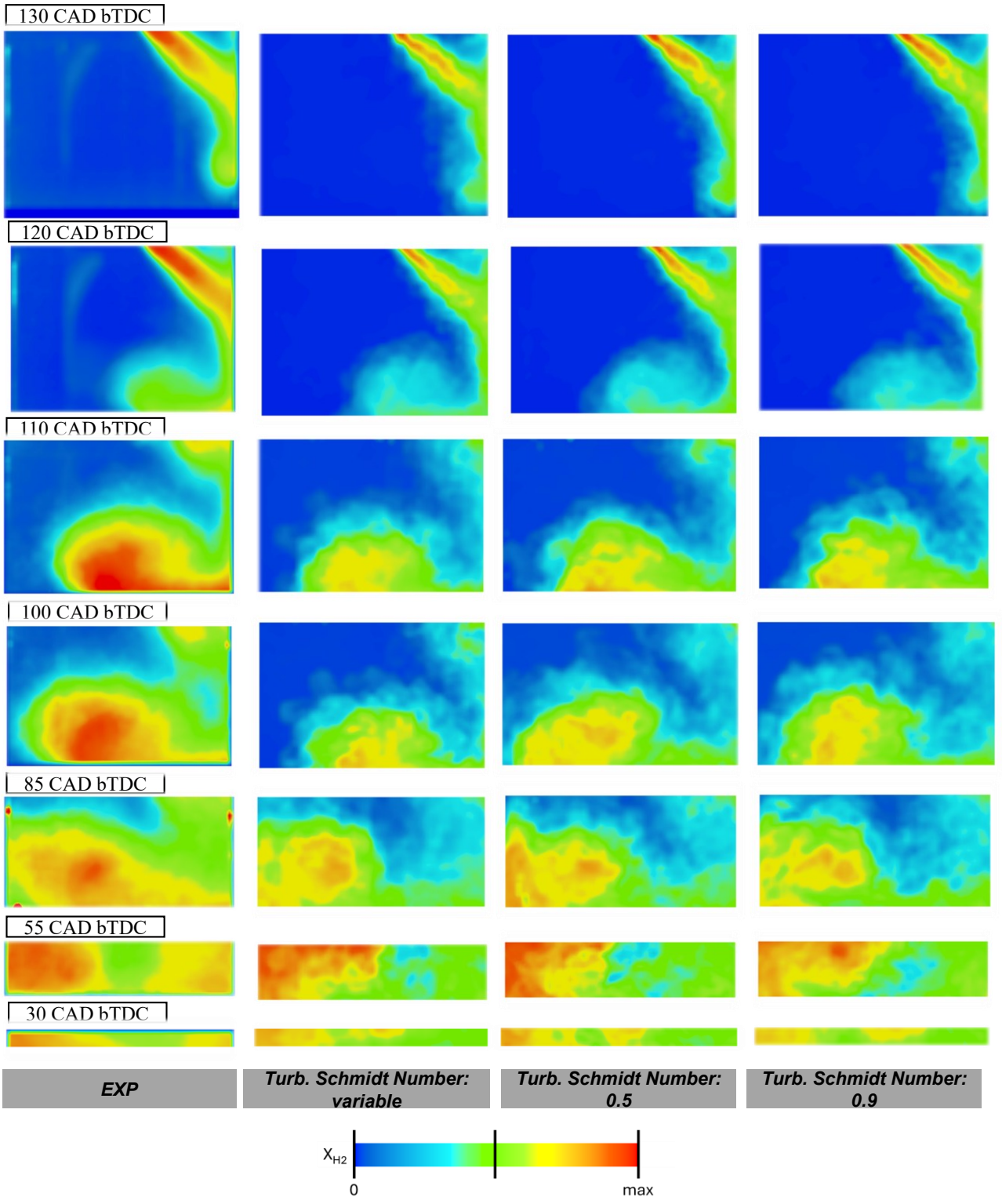

Figure 39 Hydrogen mole fraction comparison between different approaches of the turbulent Schmidt number in LES framework (all are averaged by 10 consecutive cycles, pure data).

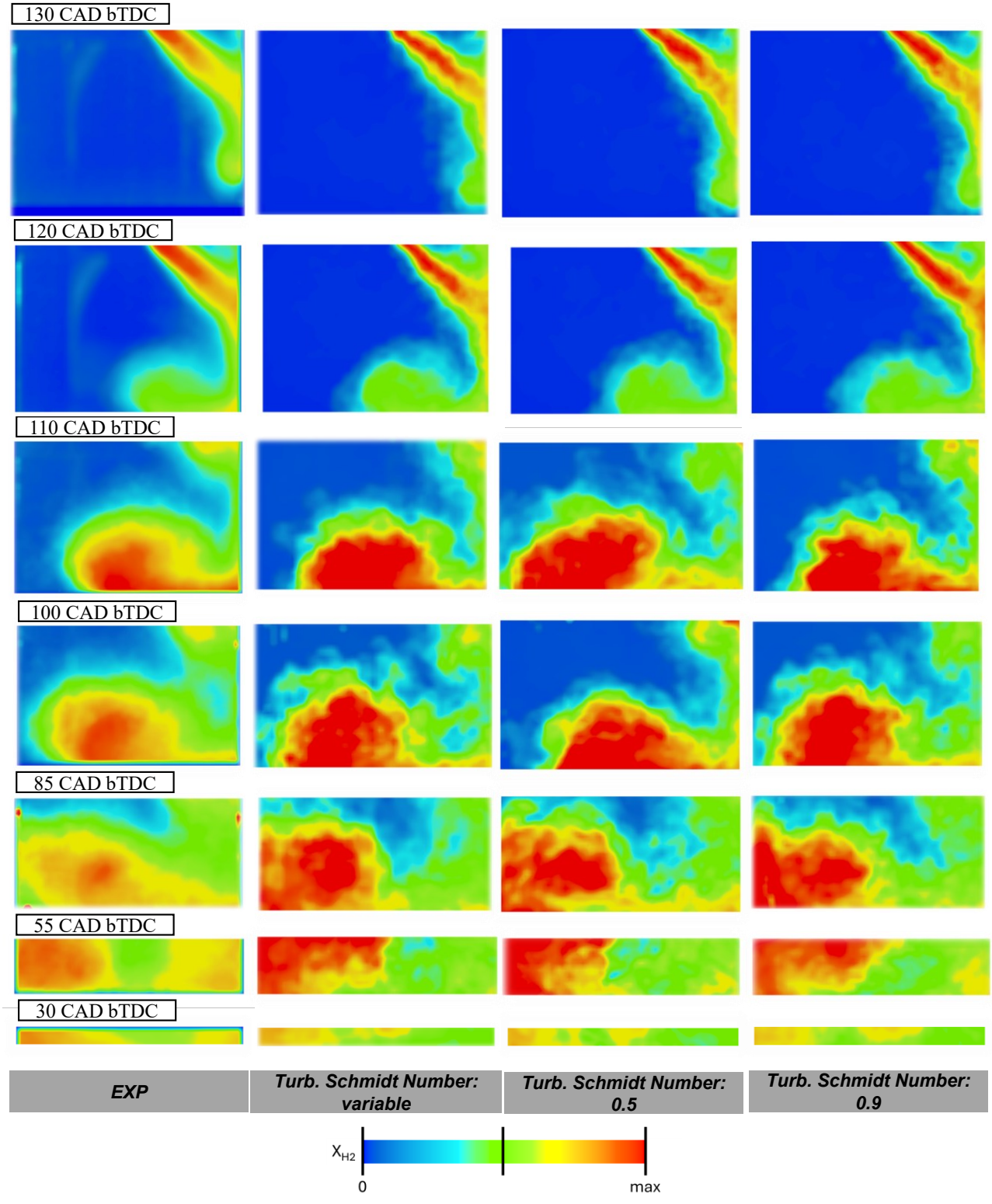

Figure 40 Hydrogen mole fraction comparison between different approaches of the turbulent Schmidt number in LES framework (all are averaged by 10 consecutive cycles, normalized data).

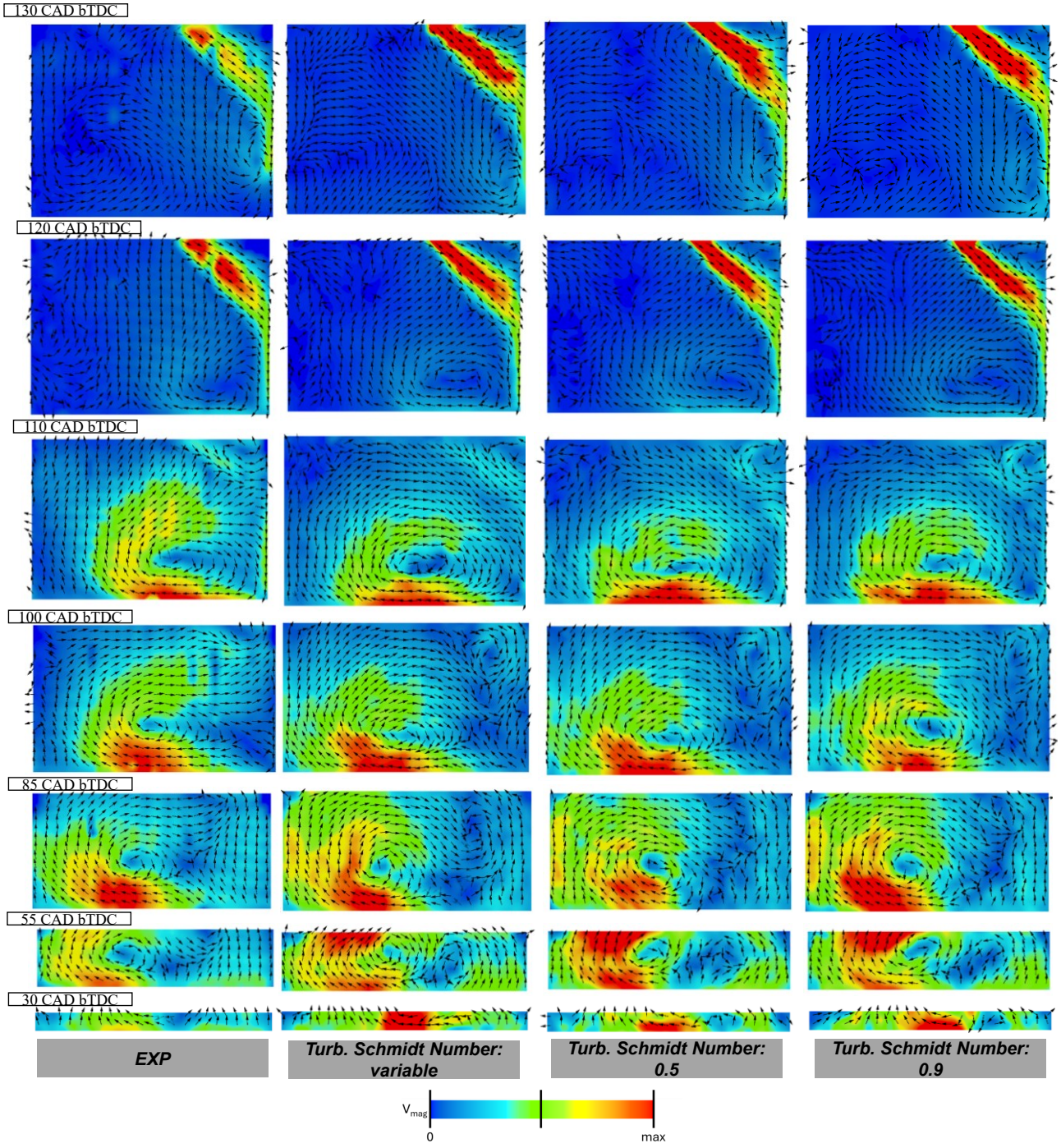

Figure 41 Velocity magnitude and vector comparison between different approaches of the turbulent Schmidt number in LES framework (all are averaged by 10 consecutive cycles).

4.7.5.2 LES – Quality Index

As well known, the SGS frameworks constitute a class of numerical approaches able to resolve the most turbulent scales. Nevertheless, related to the percentage of the resolved turbulent scales, different approaches are depicted. From URANS, where all of the turbulent scales are modeled, up to the DNS approach, where small scales are resolved. In the middle of the previous, it is possible to describe the LES. The latter targets focus on reaching at least 80% of the resolved scales according to Pope [163]. From the above statement, some criteria have been defined and applied in the last decades to describe the degree and limitations of accuracy of a multicycle LES numerical domain [164-166]. Despite more than one methodology to evaluate the IQ_{LES}, Di Mare et. al [167] describe some difficulties related to this investigation by applying several approaches to evaluate the LES quality. A year later, that work, some further considerations are reported by Baumann et. al [168] on the same Darmstadt engine and focusing on the fidelity of the result and proving that the M(x,t) reached reasonable values (> 80%) to guarantee the simulation fidelity. Similar to this study, in this work setup, the second-order scheme MARS and PISO were adopted, proving that it is a well-suited approach for this particular variant of the TDV scheme linked to LES frameworks, despite [168] and [167] adopting the classical Smagorinsky model. In light of the several approaches that can be used, the author decided to include the quality index or estimators for the LES on the average of the realization performed based on *viscosity*, as the major of the outcomes following the latter physical quantity. Following the Celik et al [165] approach, to rearrange the modelling to the software-implemented SGS model (WALE), the method is based on a quite sophisticated approach, able to give the adequacy of the grid resolution of the subgrid modelling. The target here is to give an overview of the quality of the mesh-grid size during the injection of hydrogen, hence the reference averaged timing fits the development of the hydrogen injection event at 120 [CAD bTDC], addressing the application of “engineering LES”.

The reported images, figures 42a and 42b, help clarify an important point that must be addressed and later discussed in the final analysis. It becomes evident that using the same mesh strategy adopted for the URANS simulations leads to several noteworthy observations. The IQ-viscosity index clearly shows that the mesh is able to resolve turbulence only in those regions where the grid spacing is sufficiently refined, particularly around the injector tip, in areas with limited turbulent activity, and in zones where the velocity gradients are not excessively strong.

As the mesh gradually increases in cell size, following the internal refinement strategy used for the conical region, the viscosity-quality index also increases. This indicates that the LES becomes progressively under-resolved, with a growing contribution from the SGS viscosity. Of course, there are localized areas where the LES achieves a satisfactory level of resolution, and considering that a single section is reported, the overall picture reveals that, when evaluating the injection event, the mixing process, and the resulting scalar fields, this setup operates firmly within the domain of an engineering-grade LES.

Such an approach is fully consistent with the intended modelling objective; however, it also highlights its inherent limitations. While the global flow motion, velocity magnitudes, and large-scale structures can be reproduced accurately and compared successfully with experimental measurements, the mesh resolution is low to capture the finer details of the mixing process. Nevertheless, this may not be necessary from an internal combustion engine engineering standpoint, where the degree of resolution and result must always be in accordance with the time-to-solution response of the industry field. As a result, while there is good agreement regarding the main flow structures, this “engineering LES” framework enables reaching an adequate degree of fidelity, especially showing the ability to catch the structures and values in detail compared to experiments. Furthermore, the cycle-to-cycle

variability is also possible, enabling and extending the reliability of the approach for next ICE combustion simulations in which the mixing is of mandatory importance for predicting the mixture field and conditions before park ignition. This approach, here presented, allows balancing the motion accuracy with the mole fraction and mixing overall outcomes, significantly closer to the experiments compared to the URANS counterpart, without dramatically increasing the time-to-solution.

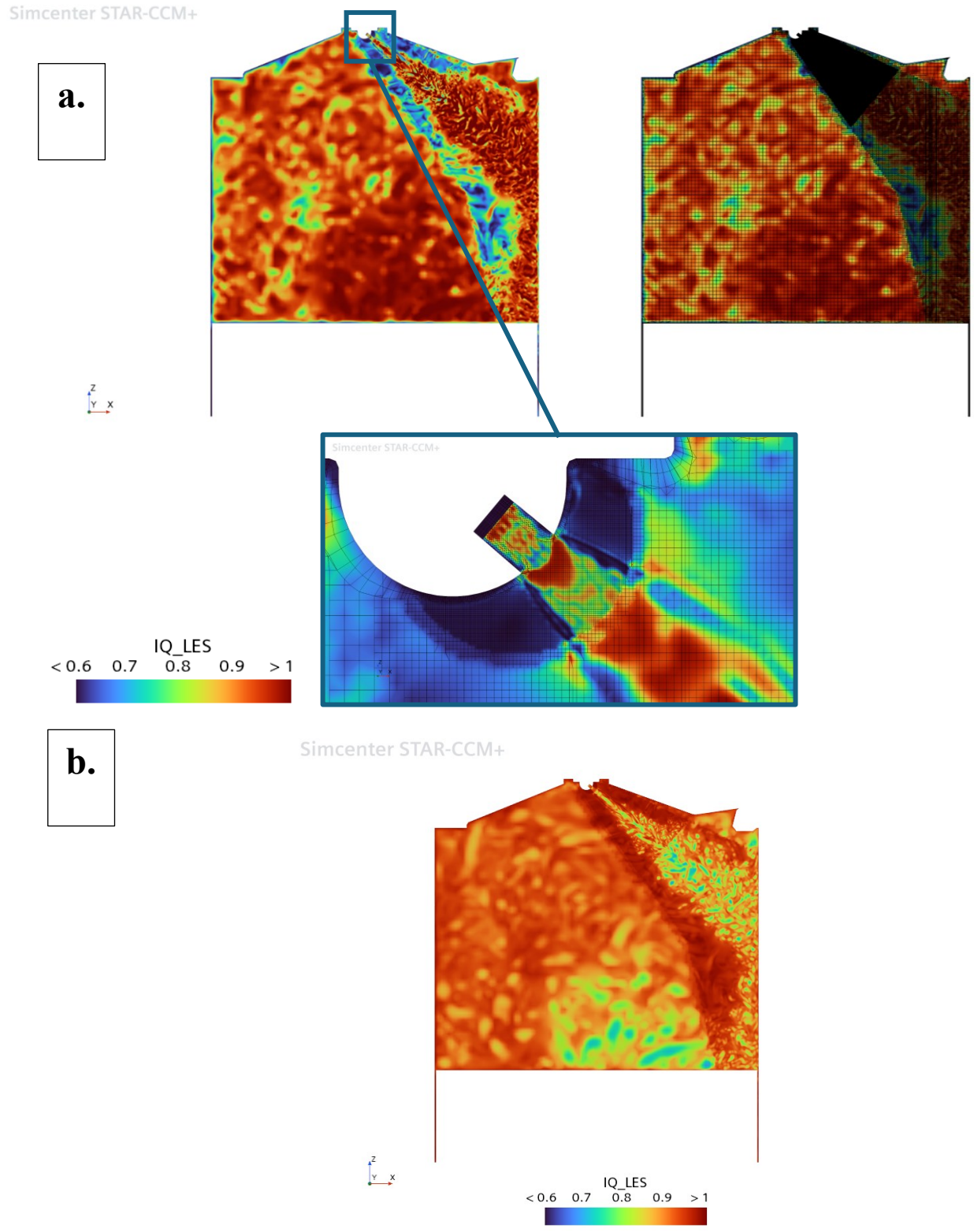

Figure 42 Quality index based on turbulent viscosity, detailing its correlation for a single cycle and mesh quality of results (a). The quality index averaged over 10 cycles is presented in (b).

4.8 URANS and LES – A comparison and outcomes

As previously stated, this manuscript aims to give a full description of the CFD setup with a dedicated focus on the innovative approach for the turbulent Schmidt number applied to different CFD frameworks, opening the way for future applications for better predicting diffusivity at several operative conditions, as here reported, for high-tumble ICEs. The reason behind this approach and the aims of the author are a comprehensive and computationally expensive activity to give a robust validation of the CFD modelling settings from a chemical and physical standpoint. The approach of the variable law of the turbulent Schmidt number (SctVar) is something not available in literature for this kind of application, and the author aims to delve deeper into this kind of approach. In this work, a first application has been considered to evaluate the active variable Sct feasibility in the software as well as the future application linking this value to physical operative and dynamic conditions. So, in this section, some detailed comparisons to understand the impact of this approach and the differences that arise when modelling through the URANS and LES frameworks is considered, both considering constant and variable values of the Sct. Nonetheless, the better results are discussed and compared between the two frameworks, aiming at giving a clear and comprehensive view of the potentials and limitations intrinsic to settings and modelling approach. As already described, the variable approach of the Sct is particularly useful when the hydrogen enters the engine at high velocity, high Reynolds, high gradients as well as when it impacts the wall and, as a consequence, the wall guides the gas throughout the entire phase of the injection and later on phases of the engine cycle, affecting the mixing development, during and after the injection event. Moving to the flow, dynamic conditions around the injection event, and the CFD point, it is of particularly relevant importance when the simulation is able to catch the local turbulence and the details of the motion, while reducing the fidelity of the wall guidance when simulating with low-order numerical, raw models and not specific chemical and physical approaches.

In these cases, the setup was deepened and the same models are adopted with different frameworks, URANS and LES. This idea allows the manuscript to give fidelity information related to the impact of different modelling environments, while maintaining the same models and comparing different values for the turbulent Schmidt number in a fair way. In the following comparison, the focus will be especially related to the different values of the Sct, exploring from the constant value with the default of the software 0.9, to the reduced constant value of 0.5 as reported in recent literature and the SctVar introduced in this work. Finally, a comprehensive comparison of velocity magnitude and mole fraction across the isosurfaces at different levels will be presented to highlight the major and minor differences in mixing development at several times. As for the multi-cycle approach and the different setup, the LES multicycle framework is performed with 10 cycles each. The starting point is always the same, with the end of the second injected cycle, the next 10 cycles are considered (overall 12 cycles). The following cycle is averaged, and the starting point considers different turbulent Schmidt number settings.

It can be seen that great differences between the software default turbulent Schmidt number 0.9 and the constant 0.5 and variable ones are not negligible. Nevertheless, by comparing the case with a turbulent Schmidt number fixed at 0.5 compared to the variable one, the results are quite close, despite the approach affecting details in both flow fields and hydrogen diffusion. On one hand, the constant value fixed at 0.5 is the current value that can possibly be found with this kind of application and is

coherent with the fact that hydrogen typically has a value of Sct that can be significantly lower than 1. Some sensitivity can be found in previously cited literature [52,61] in which, by lowering the Sct, the diffusivity tends to increase according to high diffusion of hydrogen. On the other hand, the similarities in the standard deviation calculated on the entire section are similar to the ones obtained with the variable approach for the Sct, due to the fact that both reach the core with the same value of 0.5. The SctVar approach, as previously described, triggers the value of 0.5 at the core, reaching higher values just near the wall. This statement led directly to the thought that when averaging on the entire section, little differences are not achievable and the two cases seem to be quite similar despite not being properly true if details are considered.

To deepen the behavior of considering these three approaches for Sct, the point values are also reported for the CCV, as shown in figure 37. The same probes are considered in figure 38, where some details are caught in the velocity magnitude by maintaining the 100 [CAD bTDC] as representative for the comparison. According to the previous evidence, closer results can be observed from the first averaged cycles, leading to reduced variability from cycle to cycle when the VarSct is adopted compared to the constant one. For the sake of truth, the major differences are visible only for Sct set to 0.9, whereas minor differences are noticed with the reduced value of Sct and a more diffuse hydrogen configuration. Nevertheless, looking at the shape of the mole fraction in SctVar, compared to the other approaches, especially Sct 0.5, a closer harmonious shape can be appreciated, similar to the one in Sct 0.9. This further enhances the concept through which the wall guidance and treatment of the wall, numerically, fit with the physics of the flow-gas-motion interaction inside the ICE. This further aligns with the literature, which supports the valuable approach for Sct approaching the near-wall layer is consistent and higher Sct are proven from DNS [152-157]. To conclude the comparison, this section provides a detailed overview of the imaging results for both velocity magnitude and mole fraction, followed by a comprehensive evaluation of the isosurfaces. For completeness, a dedicated comparison between URANS and LES is presented, highlighting their differences in tumble motion predictions. This is clearly illustrated in figure 43a, which shows the coherence of the tumble ratio aligned with experimental results when using LES. In contrast, although URANS demonstrates reasonable agreement with the experiments, it exhibits a greater reduction in the tumble ratio. To further clarify the similarity, figure 43b shows an offset of the tumble ratio, which clearly shows the great response of the behavior with the “engineering LES” approach in predicting tumble (SctVar data adopted).

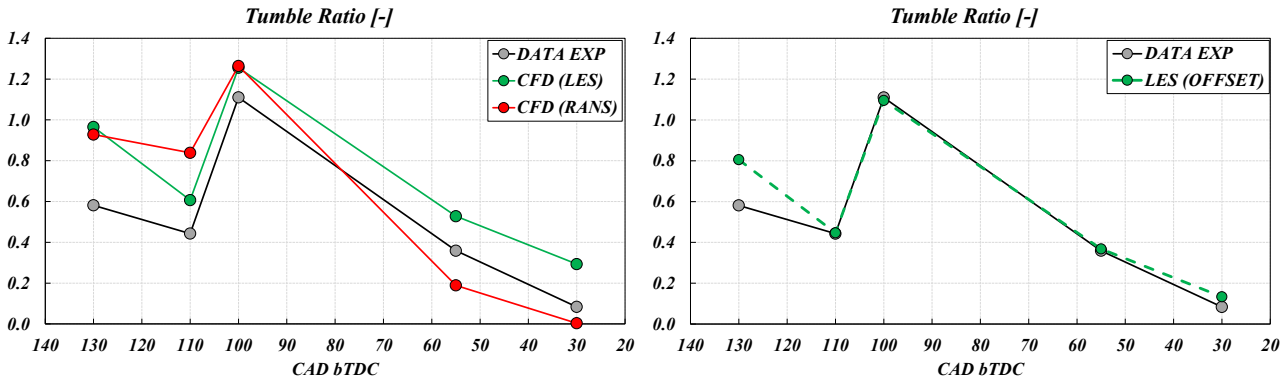

Figure 43 Tumble ratios of CFD (LES), CFD (URANS), and experimental data (EXP) compared at various crank angles. (a) Displays the tumble values for the CFD configurations with VarSct. (b) Illustrates the offset of the LES values, highlighting the method's significant accuracy and fidelity compared to the experimental results.

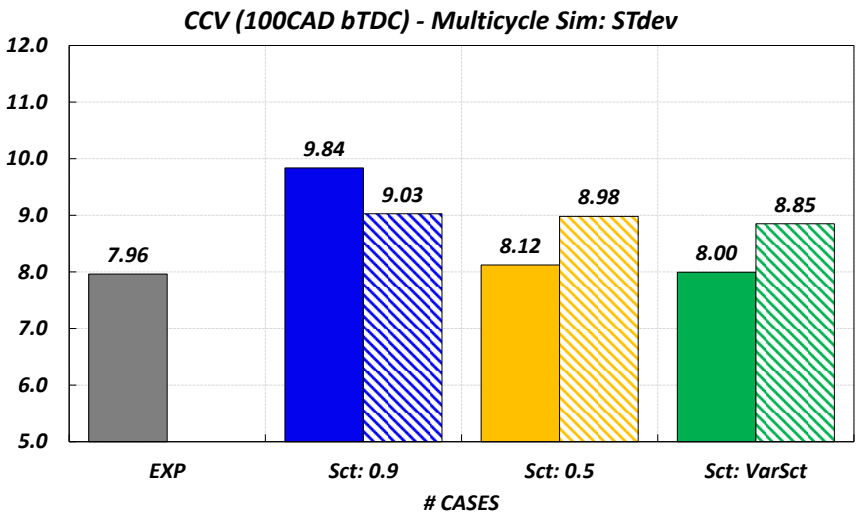

Figure 44 Analytical evaluation of the standard deviation in both LES and URANS environment "solid" is URANS, and "cross background" is the LES

The detailed comparison of figures 39, 40, 41 offers a clear evaluation of the development of both velocity and mole fraction, highlighting great results with high fidelity in similarities between CFD and EXP.

The velocity magnitude reaches a maximum in the same position of the experiments with a greater closeness to the experiments with the SctVar configuration in CFD. Very good shape and reasonable values of the mole fraction comparison lead to the same outcome that a specific and detailed approach for Sct helps reach the mixing of the experiments. Furthermore, figure 44 reports the standard deviation obtained when transitioning from a constant to a variable turbulent Schmidt number formulation within both modelling frameworks. The observed trend, in agreement with the previously discussed analyses, further confirms that the LES approach is significantly more effective in capturing the velocity structures of the flow. Once again, the comparison between constant Sct and the variable Sct (SctVar) formulation highlights a progressive reduction of the standard deviation, bringing the numerical predictions closer to the experimental data. This behavior is consistently observed across both configurations, reinforcing the robustness of the trend. Overall, these results strongly support the hypothesis that a variable turbulent Schmidt number formulation can substantially enhance the predictability of both the flow motion and the hydrogen molar fraction distribution. The consistent improvement observed in multiple metrics and modelling frameworks further emphasizes the relevance of accurately modelling turbulent mass diffusion, particularly in hydrogen-fueled engine applications.

Further details on results are then reported for the unsteady RANS simulations in which local turbulence cannot be achieved due to the nature of the modelling linked to the framework. The figures 46 and 47, report the details of the related simulations considering both velocity and mole fraction. Here, the turbulent Schmidt number is again compared for each configuration, as well as the impact that it has on the velocity and mole fraction. It is interesting to note here again the major differences reached when moving from Sct 0.9 to 0.5, detecting a negligible impact of the results compared to the variable approach. This is why, in a "detailed simulations" setting, a detailed chemical and physical accordance between CFD and EXP real conditions leads to better prediction compared to a simplified Sct constant value. The author emphasizes that while there may be negligible differences in URANS due to the modelling approach, this does not justify a uniform method or simplification for the Sct. Instead, the author wants to highlight that effective modelling in CFD should be approached with a variable approach for the Sct since the minimal computational cost of implementing a law to the wall and also respecting physical and phenomenological principles

validated in a high-fidelity LES environment, showing to be both physical and reliable. Furthermore, future studies in which the Sct is linked to the local non dimensional or viscosity ratio of specific cases will be adopted and transitioned from LES to URANS applications to get the same proper evaluations on hydrogen turbulence diffusivity in both frameworks. A detailed comparison of simulation results and experimental data is presented in Figure 45. This comparison focuses on the behavior of velocity and mole fraction approaching the TDC. In ICEs, specifically H_2ICE in this case, the TDC represents the pre-spark or pre-ignition conditions, which are critical for ensuring the correct combustion process. In this study, the detailed modelling settings for the SOpHy engine aim to enhance the mixing modelling to produce results that closely align with the experimental data, even

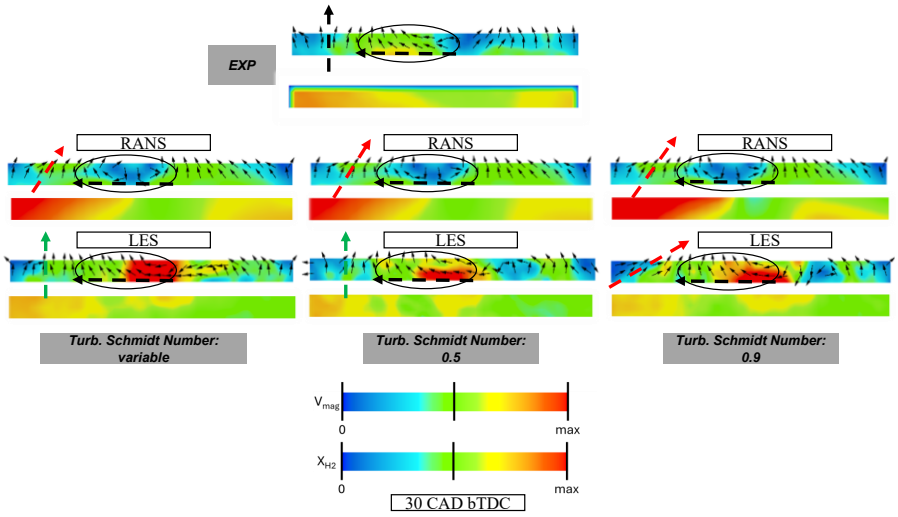

Figure 45 Comparison of velocity and mole fraction of both LES and URANS results approaching the TDC.

though combustion is not occurring. While the author needs to achieve consistent mixing of hydrogen and flow motions throughout the entire engine cycle, the focus here is particularly on the TDC conditions from a planar perspective, since experimental imaging near the spark plug is lacking. The advancements proposed in this manuscript related to the hydrogen modelling can also be appreciated here, especially concerning the variable approach for the Sct and its impact moving from the wall to the core, reaching different flow structures and velocity intensities and mole fraction. This further enhances the importance of wall values for diffusivity reaching the TDC. Here, faster velocity can promote the hydrogen and tumble motion close to the TDC up to its destruction, producing the mole fraction agreement with the EXP. The results are presented for both the modelling framework and all Sct configurations. The vectors shown in the planar section summarize the outcomes, indicating that while the URANS shows good agreement in terms of velocity magnitude, it falls short in capturing the same flow motion. Notably, when comparing the vectors and velocity magnitudes moving from Sct 0.9 to constant 0.5 and SctVar, negligible differences are observed. When comparing these results with those obtained from LES, the vector directions are relatively different from those from URANS. Differences between unsteady RANS and LES are evident across all Sct configurations. Moreover, distinctions become apparent when transitioning from Sct 0.9 to 0.5 and then to VarSt in cases performed with LES. Thus, differences between URANS and LES are largely due to LES's general ability to capture local turbulence, which yields meaningful outcomes compared to unsteady RANS. Furthermore, the value of the velocity in an absolute sense shows more fidelity in LES (higher velocity) compared to the counterpart in URANS (lower velocity), close to the local agreement from high-fidelity simulations and EXP. To be considered that, the velocity here is relatively low, and the scale significantly emphasizes the differences between CFD and EXP (velocity scale: 0-10 [m/s]). However, the importance here is the localized higher velocity visible in the centre of the chamber in EXP, which is also achieved in LES.

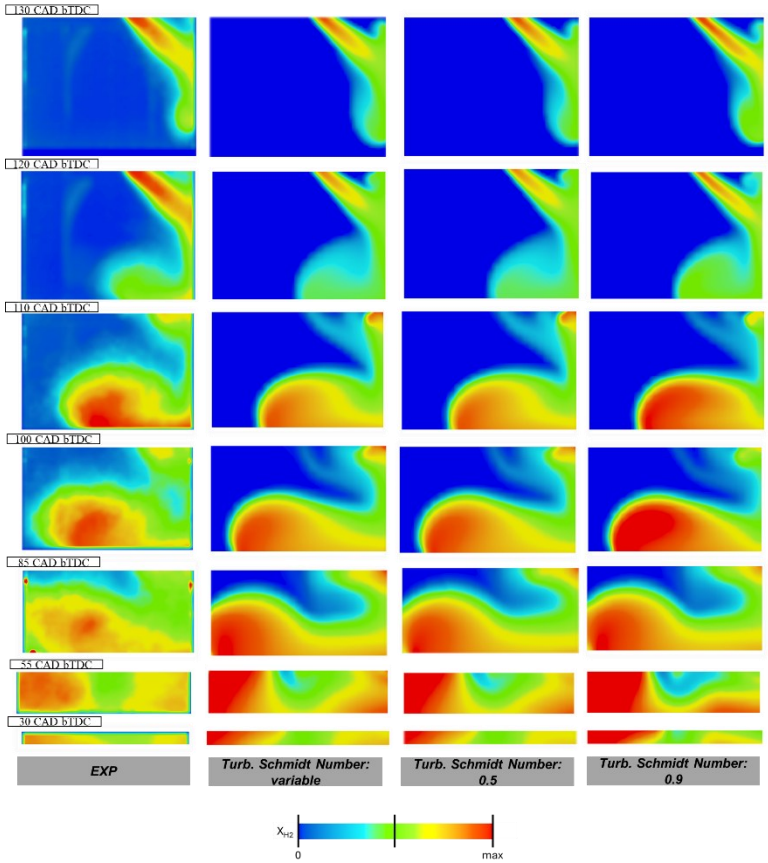

Figure 46 Mole fraction and vector comparison between different approaches of the turbulent Schmidt number in URANS framework.

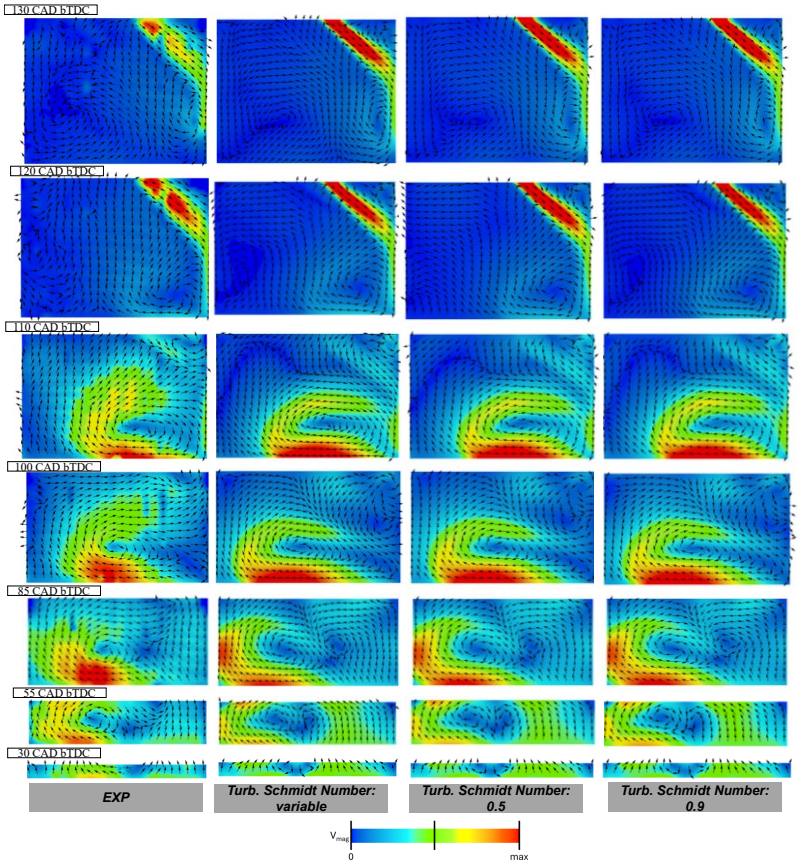

Figure 47 Velocity magnitude and vector comparison between different approaches of the turbulent Schmidt number in URANS framework.

This latter comparison is based solely on the planar results, and the mole fraction displays some variations attributed to secondary motions or enhanced motions due to the faster downward movement of hydrogen, which isn't apparent in the experimental data. The absence of imaging post-processing and comparisons near the spark plug poses a limitation in establishing concordance between CFD and experimental results in all studies conducted on this engine.

Future research could also be carried out considering more sections of accessible ICEs when available from experimental campaigns, which are known for their complexity in testing setups. Nevertheless, the findings presented are of significant interest for internal combustion engine research and can greatly aid in modelling H_2ICEs.

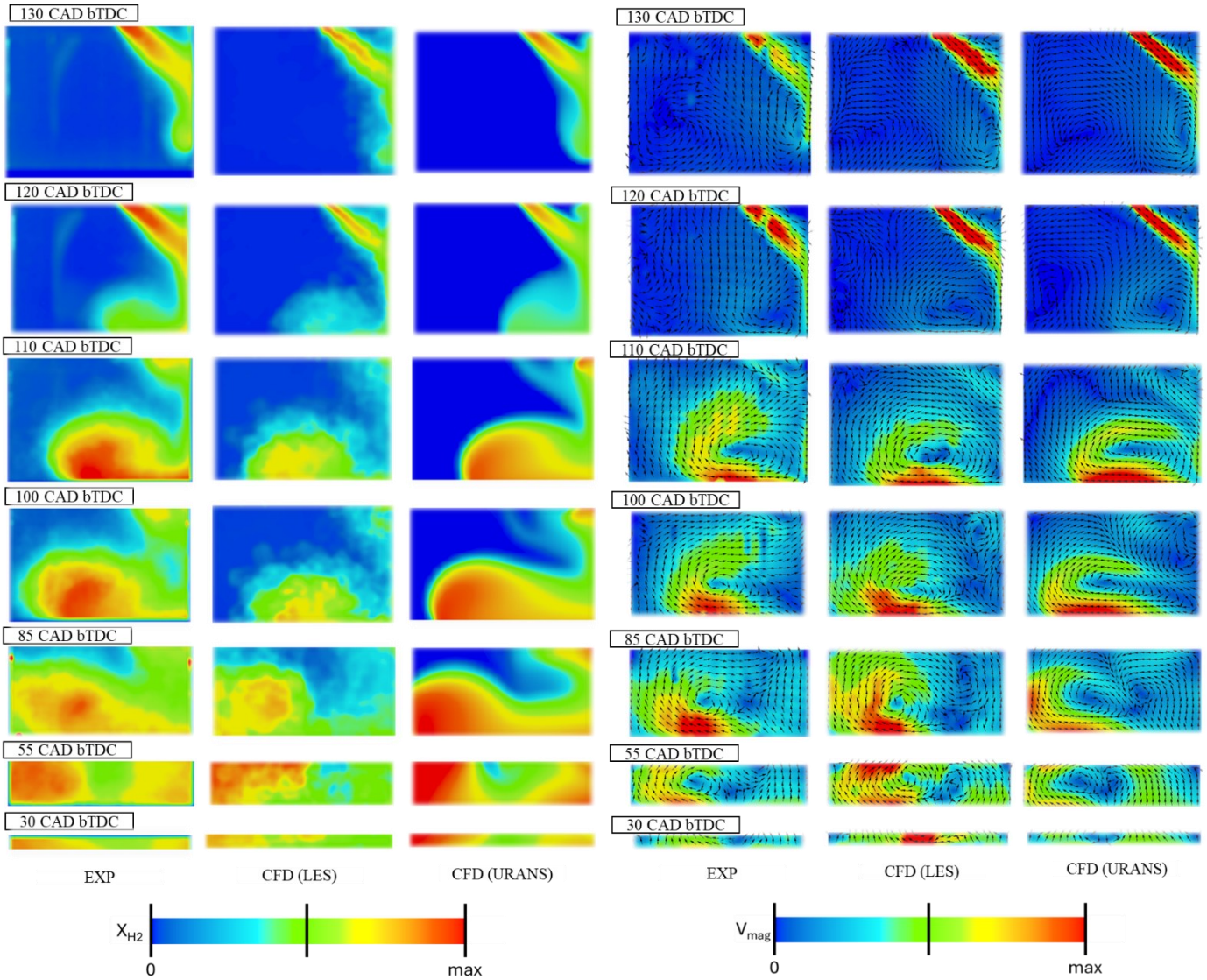

Figure 48 Mole fraction and vector comparison between the different modelling approaches with the variable approach of the Sct .

4.8.1 The iso-surface and details

Deepening the study on the mole fraction, figure 49 represents the isosurfaces at several CADs. Here, some insights related to the sensitivity of the models to catch turbulence and secondary motions to the mole fraction evolution, as well as the differences achieved according to the framework selected, are reported in detail. The images report the pure PLIF from the experiments that were post-processed in the past to colored images and published on the Engine Combustion Network (ECN) Website [169]. In this image, the pure data from the dataset available only are then proposed and the isosurfaces that consider the threshold or the extremes of the hydrogen mole fraction at different values are reported for a deeper comparison. This visualization allows catching more details between each configuration of the Sct as well as the more details that LES, coupled with the author's proposed modelling approach, is able to reach compared to the URANS. The isosurfaces relate to normalized mole fraction post-processing from both LES and URANS simulations.

As stated in the previous section of this manuscript, the author performed a normalization of the mole fraction of hydrogen that is particularly useful to compare experiments and CFD with LES-averaged cycles. Here are presented normalized mole fractions with specified isosurfaces for each CAD to better and clearly compare both RANS, LES and the different approaches for the Sct impact on results. Following the isosurfaces, the results are not exactly the same, especially when varying the Sct up to 0.9 (the software default). Here, differences are highlighted, leading to local differences in hydrogen mixing as is pretty clearly visible at 130, 110, 30 [CAD bTDC]. Again, this confirms that the reduced value of the Sct is the correct way to better model hydrogen toward a higher fidelity approach. Of course, the transition to the variable approach and the constant 0.5 leads to significant differences just when moving from Sct 0.9 to 0.5. To the latter consideration, the LES is reported with the results aside from the URANS ones.

It can be noticed differences between LES and unsteady RANS starting from the first approach of the hydrogen jet against the wall at 130 [CAD bTDC]. The height of the gas against the wall is in better agreement in LES compared to the RANS, as well as a better shape of the isosurfaces moving to 120 and 110 [CAD bTDC]. The same can be stated also for the 100 [CAD bTDC]. Reaching the near TDC, the latter angle considered at 30 [CAD bTDC] shows a detailed agreement with the experiments, with the URANS framework with Sct 0.5/SctVar reaching the closest shape of the EXP, which is better compared to the more corrugated Sct equal to 0.5 or the variable approach and the default one.

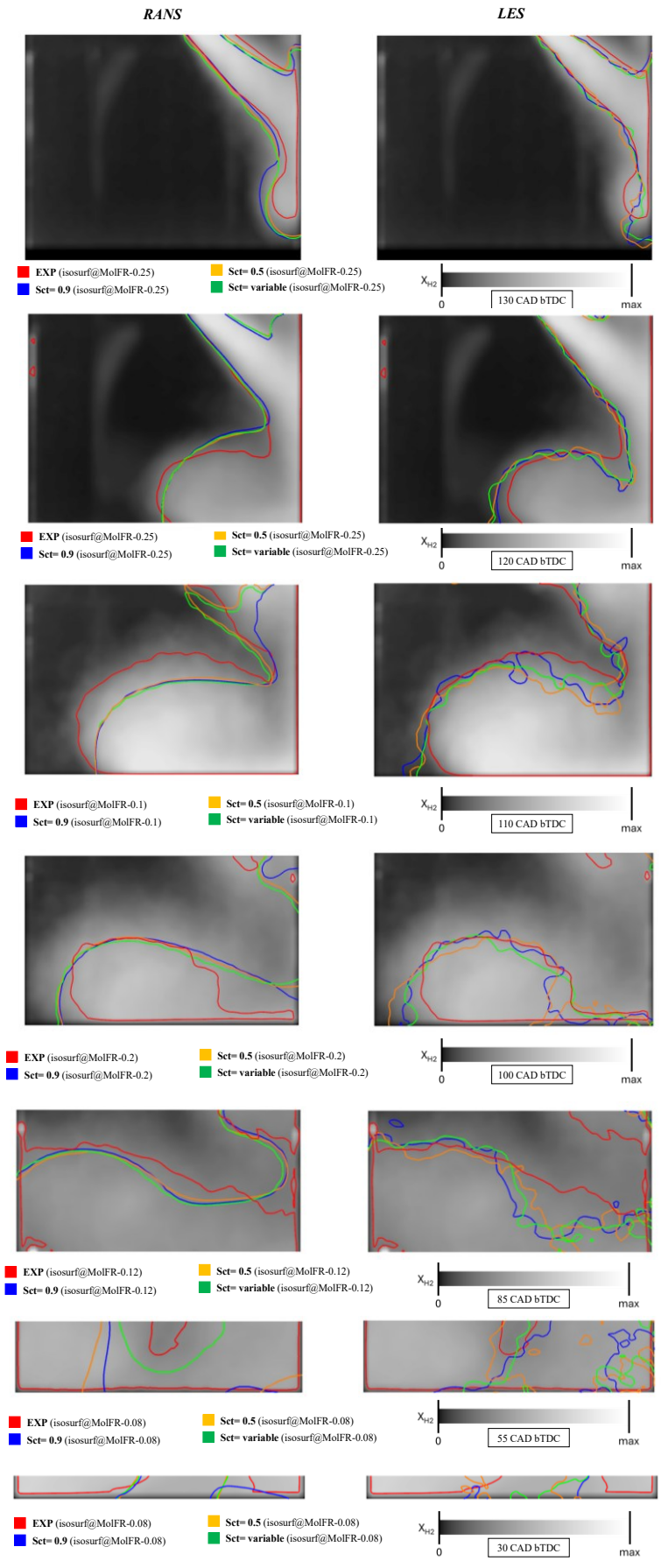

Figure 49 Iso-surfaces comparison for each computational case and setup (experimental PLIF from source data – ECN)

4.9 URANS – Cycle to Cycle

The previous results demonstrated that reducing the turbulent Schmidt number improves predictions of both the mole-fraction evolution and the overall mixing characteristics. This outcome justifies selecting the case with Sct = 0.5 (constant) as the reference for the following comparisons. The intent is to evaluate whether a single-cycle RANS injection event is sufficient to provide a reliable description of the mixing process, thereby avoiding any effects associated with the so-called cycle-to-cycle variability.

Naturally, such variability cannot be captured by URANS, as confirmed by the results, and as expected from the fundamentally time-filtered nature of the method. LES, on the other hand, is inherently more capable of representing the impact of local flow variations and the differences that arise from one engine cycle to the next. For this reason, LES becomes the more appropriate framework when the objective is to quantify cyclic variability or the detailed evolution of scalar mixing.

It is also important to note that each simulation is initialized using a motored run of four cycles. Previous studies had already shown that two cycles were sufficient to reach a periodic and stable flow field, with no meaningful differences observed when additional cycles were included. Nonetheless, the choice of four cycles provides a conservative initialization strategy, ensuring a fully developed flow field before fuel injection begins.

An analytical view of the velocity does not show a unique trend but it is clear that the results are quite aligned with the experimental output. The reasonable delta through which the cycle-to-cycle output is evinced leads to the conclusion that a single cycle with injection is enough to well-predict the experimental results. Furthermore, it must be bear in mind that before the start of injection, four cycles are performed, leaving doubts or uncertainties due to the initialization of the simulation.

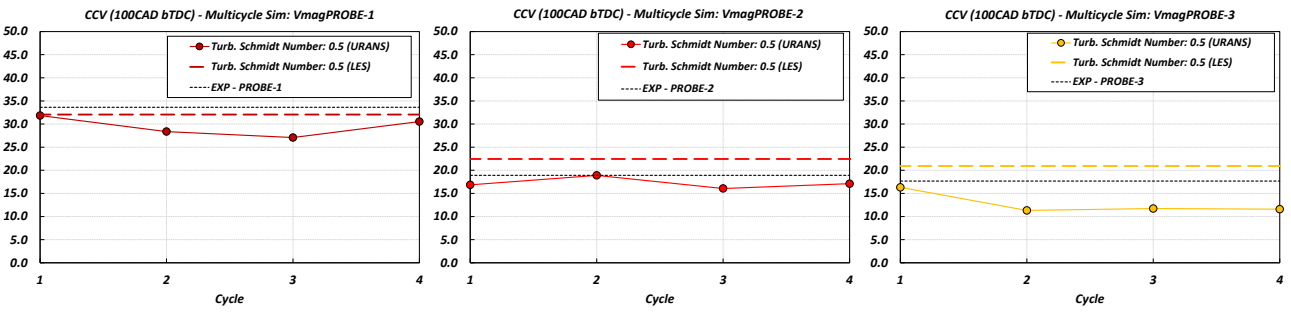

Figure 50 Results of multi-cycle probe acquisitions compared to experimental data. CFD data is exported as the average of LES and for each URANS cycle, both with Sct = 0.5.

Going deeper also from the mixing and overall velocity and motion structures inside the engine, the figure 51, represents the results achieved in particular timing of the simulation. Since the relevance of the reported angles and the close similarities between the results, the outcomes are considered for just four of the entire set of simulation outputs analyzed in the other selected cases around this work.

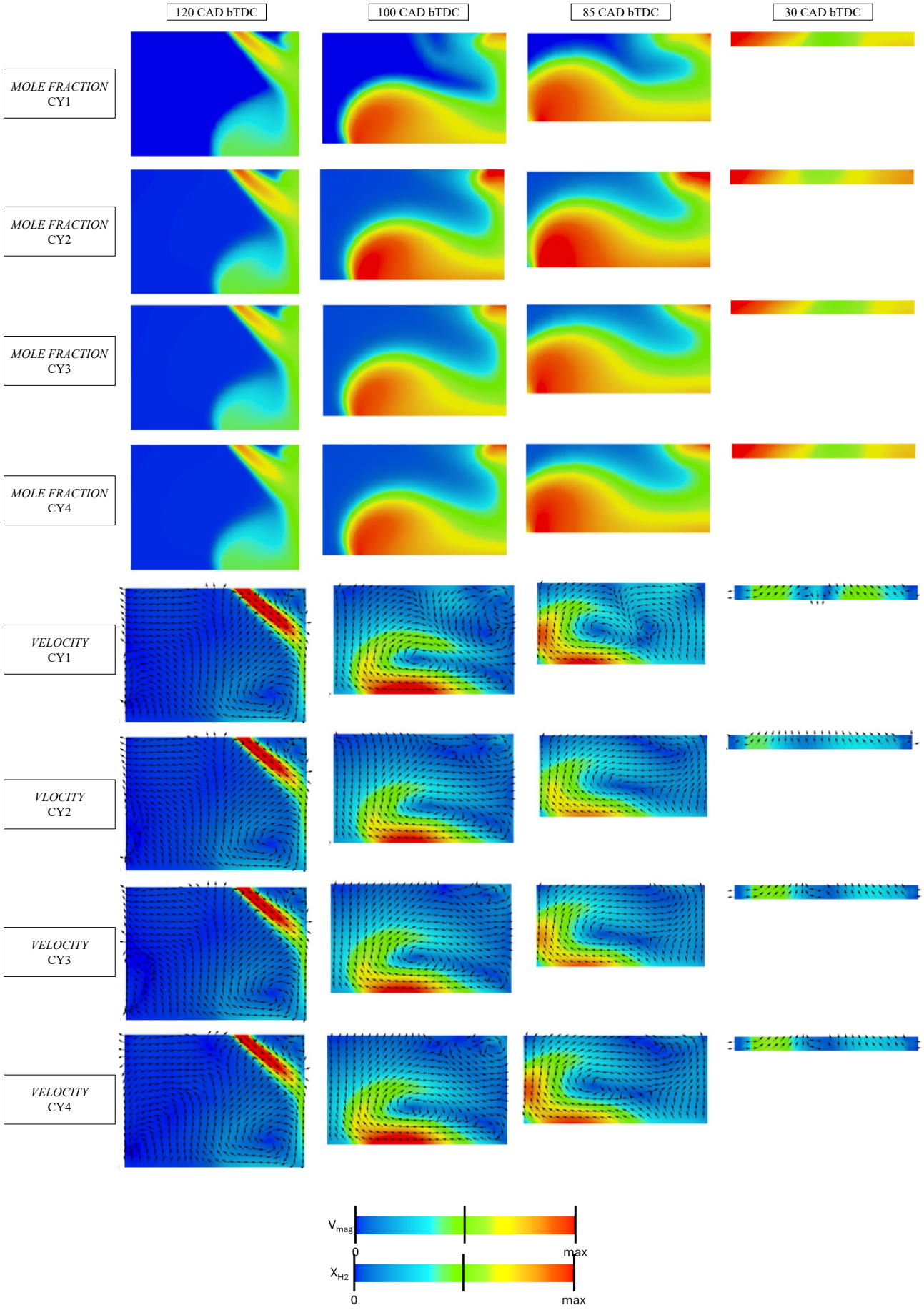

Figure 51 Representative angles for comparing the URANS simulations across multiple cycles with the turbulent Schmidt number set to 0.5.

As for the previously analyzed results, the final outcome also confirms the use of a single injection event, preventing the previously between 2 up to 4 consecutive URANS cycles from the motored operative point is enough to be well predictable and achieve robust and reliable results from CFD.

4.10 Time-to-solution (CFD modelling effort)

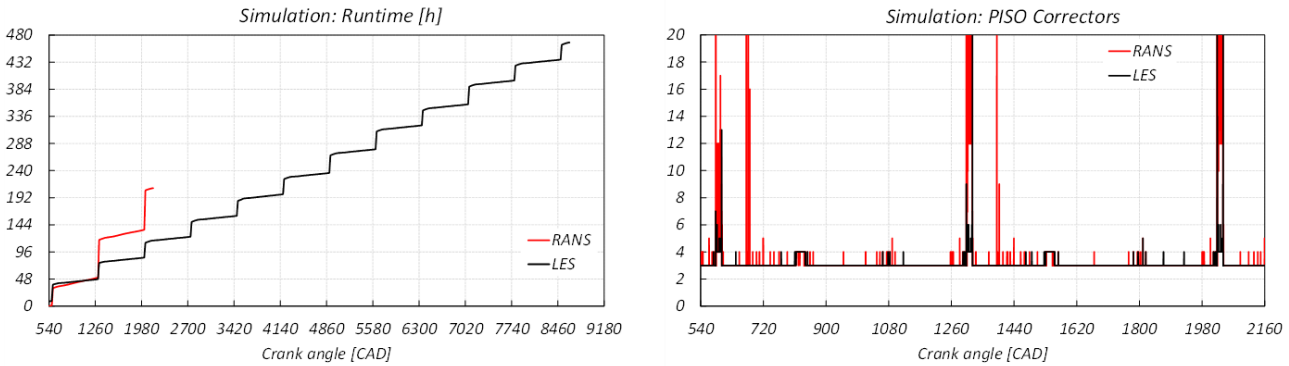

Figure 52 Simulation runtime and PISO correctors to give an overall view of the simulation setup on the performance and stability of the solution in both frameworks. Cluster architecture is formed by two nodes of 52 cores for a total of 104 CPUs.

The time-to-solution metrics were assessed to ensure computational efficiency throughout the modelling process. The time-to-solution achieved by the LES with the proposed setup based on CFD is illustrated in figure 52. It should be noted that the LES requires averaging over multiple simulation cycles; in this study, simulations were conducted cycle-by-cycle, excluding the first two cycles used for initialization purposes. The total time-to-solution for executing 12 LES cycles is approximately 467 hours (or about 20 days). Conversely, for URANS simulations, the time required for a single cycle is around 90 hours (approximately 4 days). It is important to observe that the simulation runtime for URANS tends to increase as the hydrogen mass in the system rises from the first to the second cycle. Overall, URANS simulations are more sensitive to numerical factors, as the convergence challenges associated with high gradients during hydrogen injection lead to extended CPU time for solution attainment. In fact, as evidenced by the corresponding plot, the PISO correctors enhance runtime significantly, even within a narrow CAD window. In contrast, while the LES demonstrated a faster runtime for each cycle, it is considerably influenced by the requirement for averaging across multiple cycles to achieve the final solution.

4.11 Sum up: H_2ICE Mixing Modelling with URANS/LES

The recent increase in carbon dioxide (CO_2) emissions has propelled the automotive sector to continuously evolve technologies related to internal combustion engines (ICEs). Over the years, various strategies have demonstrated benefits in CO_2 reduction, particularly regarding energy carriers used to power ICEs. Among these advancements, the hydrogen direct injection H_2ICEs have shown significant promise. Computational Fluid Dynamics (CFD), which is central to the author's investigation, has indicated notable improvements, especially in computational performance. However, enhanced computational capabilities, accessible both to universities and companies, are ineffective without a proper modelling solution. This work emphasizes the necessity of approaches suitable for corporate application in the ICE development, presenting a detailed and thorough evaluation of the CFD setup. The work has been conducted on the research engine SOpHy, an optically-accessible hydrogen-fueled ICE. The effort involved devising a meticulous setup and clearly defined methodology for modelling direct-injection H_2ICE, aiming to contribute additional insights to previously published setups in this domain. In this context, the innovative approaches in CFD modelling, particularly from a chemical and physical perspective, within frameworks applicable to corporate scenarios, considering both computational power and time-to-solution, are faced and developed. These frameworks include Unsteady Reynolds-Averaged Navier-Stokes (URANS) and, for the first time for the SOpHy engine in High-Tumble configuration, the consecutive multi-cycle detailed approach in Large Eddy Simulation (LES). Here, as a milestone for this application, addressing the relevance of the application in the industry field, the “engineering LES” approach is applied. Then, a further original application of this work, considered modelling turbulent diffusivity adopting a variable approach for the turbulent Schmidt number, laying the base for next diffuses in which this value links directly physical and numerical quantities to improve results and physics compared to experiments. Lastly, the same is applied also in URANS, again, finalizing the evaluations for future approaches also in URANS. This has been comprehensively carried out with the aim of providing a full and clear vision of possible limitations and well-established approaches, as well as some points that will be evaluated in the future in this field of research, but, of course, more relevant than ever, according to prior reviews and focusing on the LES original and first approach for the HT configuration of this engine in the literature. This part of this PhD opens with an advanced modelling approach for H_2ICE, which is fundamental to this study and leads to the following considerations:

1. An **"Engineering LES" framework** is utilized because it effectively captures the dynamics relevant to modelling hydrogen internal combustion engines (H_2ICEs), as long as the setup aligns with the specific details of this application. The mesh is developed through spatial and temporal refinements that optimize both the time-to-solution and the accuracy of the results. Moreover, the "Engineering LES" approach has demonstrated significant importance in the simulation outcomes related to motion and tumble predictiveness. The achieved agreement with experimental data confirms that an **engineering-LES approach** is sufficient to ensure reliable predictions without resorting to a **fully resolved scientific LES**.

2. The **LES results indicate that a reasonable convergence of LES can be achieved, evaluating the Cycle to Cycle Variation (CCV), with an overall of 12 cycles,** discarding the first two for initialization purposes. While additional cycles could enhance result fidelity, the author targeted sufficient precision to correlate with experimental data, thus enabling the application of LES in the automotive sector, in a **reasonable time-to-solution**, focused on hydrogen-fueled ICEs.

3. The **overall modelling setup** is based on a detailed review and defines a solid and robust approach for H_2ICE presented in this work in both URANS and LES, which can also be extended for firing applications. **Wall-Adapting Large-Eddy Viscosity (WALE) Subgrid Scale Model** is utilized for LES simulations, "replacing" the RNG k-ε model in URANS. This is supplemented by a **Monotone Advection and Reconstruction Scheme** (MARS) as an advanced numerical method, coupled with a **Two-Layer All-y+ near-wall treatment**. This approach is advantageous for its predictive capabilities and stability characteristics inherent to the WALE model, further refined by incorporating a **real gas with SKR EOS, kinetic theory, and the turbulent Schmidt number customization**. The latter represents the lack of the modelling approach in which, as for the models present in the Software, possible further explorations could be carried out through detailed models with a dynamic approach or free-viscosity, as well as avoiding the adoption of the pre-defined Sct. Specifically, the approach selected considers the viscosity-based models, then opens to the application of a variable approach of the Sct to be explored, especially with the target of linking the **Sct to physical quantities at different local conditions**, such as the linked quantities of Reynolds numbers, velocity gradients and turbulence. The **variable approach for Sct** is implemented in this work.

4. **In terms of results and comparison, the "engineering LES" approach developed in this study is a valuable approach to better match the flow fields and details of internal motions** (showed also in standard deviation and tumble) **compared to URANS**. High-quality results are achieved without dramatically affect the feasibility and the industry requirements, avoiding a "scientific LES" approach, guided by the fidelity of the target analytical outputs from EXP. Great fidelity in both flow field and mole fraction depicted this full approach concerning the "engineering LES", model and physical settings and the turbulent Schmidt number approach to fully collect the setup that describes in a well-established method and computationally consistent results for industry-oriented applications.

5. The **URANS methodology has shown very good results from multiple perspectives**, demonstrating a strong alignment in both motion and mole fraction predictions. Additionally, the results analyzed using a **multi-cycle URANS approach confirm that adopting a single cycle with injection (previous motored ones for initialization, at least two) is always representative of the fidelity and coherence of URANS** compared to experimental data.

6. **A comprehensive evaluation of the turbulent Schmidt number** has been carried out, leading to the development of a variable formulation tailored to the behavior of hydrogen within the engine. The approach initially considered the possible interactions between near-wall effects and the high-velocity hydrogen injection, accounting for the wide range of velocity gradients, turbulence levels, and mixing regimes that characterize hydrogen development inside the combustion chamber.
   To investigate these effects, the author introduced a spatially varying turbulent Schmidt number, designed to assess how mixing is influenced when Sct varies near the wall rather than in the jet core. This methodology enables isolating the specific influence of Sct on the final mixing outcome and clearly demonstrates that the dominant contribution to mixing and scalar transport is affected, despite not dramatically, by the interaction of the hydrogen at high velocity to the near-wall region, but also the jet core, where velocity gradients and turbulence intensities are significantly higher**. This concludes that the turbulent Schmidt number does not have a unique value when modelling ICE**, according to the results and detailed literature, although not present in ICE and reported in this study. **The LES analysis confirms that Sct still influences mixing predictions and that a variable formulation can be**

effectively adopted within an engineering-LES framework. In URANS, where wall-guided effects are less dominant and flow motion is comparable among cases, a constant Sct remains a practical choice, although future studies will extend variable Sct formulations based on turbulence-related physical parameters also to URANS.

7. **The time-to-solution metrics were assessed to ensure computational efficiency throughout the modelling process**. The time-to-solution achieved by the LES with the proposed setup based on CFD. It should be noted that the **LES requires averaging over multiple simulation cycles**; in this study, simulations were conducted cycle-by-cycle, excluding the first two cycles used for initialization purposes. The total time-to-solution for executing **12 LES cycles** is approximately 467 hours (or about 20 days). Conversely, for **URANS simulations**, the time required for a single cycle is around 90 hours (approximately 4 days). It is important to observe that the simulation runtime for URANS tends to increase as the hydrogen mass in the system rises from the first to the second cycle. Overall, URANS simulations are more sensitive to numerical factors, as the convergence challenges associated with high gradients during hydrogen injection lead to extended CPU time for solution attainment. In fact, as evidenced by the corresponding plot, the PISO correctors enhance runtime significantly, even within a narrow CAD window. In contrast, while the LES demonstrated a faster runtime for each cycle, it is considerably influenced by the requirement for averaging across multiple cycles to achieve the final solution.

5 Chemistry-based Calculations of E-Fuels

5.1 From Chemical Kinetics to ICEs

It is well established in literature that flame propagation in spark-ignited engines can be reliably assessed, once chemistry-derived LFS is provided as an input to well-established flamelet combustion models such as ECFM-3Z or G-Equation [42,170,171]. Then, the new frontiers of engine modelling together with continuous development of high-performance clusters, led to more perspective in ICEs modelling in both RANS and LES frameworks. Furthermore, the new modelling frameworks, such as the chemistry models that can resolve the chemistry online, further widen the perspective for new frontiers of ICE CFD modelling. Of course, specific applications require more and more CPU resources, so this leads the author to consider other ways to resolve chemical kinetics outside of ICE frameworks, establishing inputs for ICEs with the previously cited flamelet models. The same can be stated regarding the occurrence of knock, which can be assessed by adopting synthetic approaches based on tabulated IDT tables instead of solving online chemical reactions, effectively reducing the computational effort of the simulations [172,173]. Both LFS and IDT rely firstly on the definition of a surrogate for the actual fuel, which, in most cases, is composed of hundreds (or even thousands) of species (partially unknown), and secondly on the identification of a suitable validated chemical mechanism. Here, since sometimes fuel suppliers struggle to divulge their own/proprietary fuel mixtures, the simplification or reduction of chemical species or limiting to the most important from ICEs impact makes this process more useful and standardized, as well as deeper when possible.

Several works in the literature provide methods for the definition of a fuel surrogate based on available information such as H/C and O/C ratios, Research Octane Number (RON) and Motored Octane Number (MON), Lower Heating Value (LHV) and more. Historically, simplified 2-component Primary Reference Fuels (PRFs) based on N-heptane and Iso-octane, as well as 3-component Toluene Reference Fuels (TRFs) based on n-heptane, iso-octane and toluene are deemed to match the burning properties of a specific fuel. Nevertheless, more recent studies have considered more than 4 species to better reproduce the fuel chemical-physical characteristics [176-179]. Generally, increasing the complexity of the surrogate increases the accuracy as well as the computational cost of both chemical kinetics and CFD simulations [180]. Starting from the methodology defined by Del Pecchia et al. [176], a six-component fuel surrogate is used to mimic the eFuels and premium gasoline compositions following an OxPIONA (Oxygenates, Paraffins, Iso-Paraffins, Olefins, Napthenes, Aromatics) approach and methodology here developed and published by the author and its collegues [32]. The prefix “E”, in previous works, standing for Ethanol, is here replaced by “Ox” to state the generality of the Oxygenate component, recognizing the importance not only of the oxygenate fraction but also of its chemical composition (Ethanol, Butanol, MTBE, ETBE, etc.) in defining the surrogate. In the current section, the detailed composition of the analyzed fuels is well known, strongly simplifying the procedure for the fuel surrogate definition. When defining the simplified composition of the actual fuels, suitable chemical kinetics mechanisms are selected from the literature and the characteristics of the fuels are assessed and compared. So, the aim of the author here is that numerical analyses based on detailed chemistry and Computational Fluid Dynamics (CFD) can play a significant role in reducing tests and costs related to performance, emissions and reliability assessment of the e-fuel technology. To increase the reliability of numerical predictions, a cost-effective modelling approach, based on 0D/1D chemical kinetics, is proposed,

laying the foundation for the development of e-fuels-based engines via 0D, 1D and 3D-CFD simulations. In particular, a methodology able to predict the laminar flame speed (LFS) and the ignition delay time (IDT) of eFuels is developed and applied to assess the characteristics of two different *POSYN (POrsche SYNthetic)* eFuels, which are compared to a Standard *SUPER PLUS RON98* European Gasoline. Both LFS and IDT are fundamental inputs to characterize the sensitivity of flame propagation and knock tendency of ICEs through 1D and 3D-CFD simulations on the eFuel composition. All the results reported in the following chapter relate to the published work on the *International Journal of Engine Research* by Dalseno et al [32].

5.2 Methodology and Workflow

The current section aims to describe the methodology developed for a detailed calculation of the LFS and IDT of real fuels moving from the experimental chemical bulletin to the fuel surrogate definition, chemical mechanism selection and 0D-1D calculations. So, the first part will be related to a detailed analysis of the available actual fuel composition, hydrocarbons and oxygenates and their major properties. The experimental full composition is firstly simplified by grouping the overall species spectra in six hydrocarbon families, i.e. Paraffins, Iso-Paraffins, Naphthenes, Olefins, Aromatics and Oxygenates. Then, three different fuel surrogates are defined, varying not only the species fractions but also the oxygenate component. This is a major update in the methodology proposed in [176], since it now accounts for the specific anti-knock properties of different oxygenate additives such as ETBE, MTBE or Ethanol. This step forward in the method is required considering that two of the three fuels considered (*SP98* and *POSYN2*) have similar composition, but different oxygenate compounds whose effect, using the original EPIONA fuel surrogate, could not be accounted for. The second step of the procedure regards the selection of a suitable chemical mechanism for IDT and LFS calculations. Considering that the final aim is the comparison of different fuels and the generation of a wide database of fuel chemical properties, the choice of the proper mechanism is driven by the availability of all the chemical pathways for the oxidation of the selected species in the surrogate, including the oxygenate component, and by the feasibility of the mechanism in terms of computational requirements. The CPU effort is a major issue concerning LFS calculation while it is much less critical for IDT. Therefore, if needed, the adoption of two different mechanisms, searching for the best trade-off between accuracy and CPU cost, is possible for the two different outputs.

It is worth highlighting that experimental measurements of IDT and LFS with the considered fuels are unavailable, which does not allow direct validation of the numerical results. Absence of fuel-specific measurements is added to the well-known lack of information under engine-relevant conditions, as the experimental characterization of fuels at high pressure and temperature levels presents significant challenges [181-183]. Mechanisms are therefore validated for the individual components and at lower pressure and temperature conditions, as referenced in the following sections. Surrogate-defined and kinetic mechanisms selected are employed to calculate IDT (using a 0D constant volume reactor) and LFS (using a 1D freely propagating reactor). Finally, the results are analyzed to assess the behavior of the considered *POSYN* fuels compared to conventional *SP98* in terms of flame speed and autoignition tendency at engine-relevant conditions.

5.3 Fuel Characteristics and Surrogates Definition

5.3.1 Chromatography Bulletin & Fuel Data Analysis

A laboratory analysis of the raw composition of the investigated fuels is provided by the fuel supplier and it is reported in figure 53, based on the OxPIONA hydrocarbon grouping. Other available fuel properties are summarized in table 16.

The following bulletin reports some specifics that one can obtain from a fuel supplier and represents the full chromatography bulletin that describes the full composition of a real fuel, in this case, gasoline. As previously mentioned, it is clear that gasoline is a complex hydrocarbon mixture that contains several byproducts from the fuel refinery and distillation process. It is also clear that, inside the fuel/gasoline mixture, there are major and minor components that have different weights on the influence of fuel properties.

Components Listed in Chromatographic Order

Minutes	Index	Group	Component	Mass %	Volume %	Mol %
7.288	305.510	--	unknown	0.0041	0.0042	0.0186
8.328	368.050	I4	i-butane	0.0089	0.0115	0.0141
9.315	400.000	P4	n-butane	0.0571	0.0709	0.0904
9.708	411.840	O4	t-butene-2	0.0017	0.0020	0.0027
9.813	414.750	I5	2,2-dimethylpropane	0.0066	0.0081	0.0085
10.312	427.500	O4	c-butene-2	0.0018	0.0021	0.0029
13.121	477.510	I5	i-pentane	5.7268	6.6404	7.3055
14.688	496.730	O5	2-methylbutene-1	0.0030	0.0033	0.0039
14.989	500.000	P5	n-pentane	0.4976	0.5709	0.6348
15.628	510.780	O5	t-pentene-2	0.0029	0.0032	0.0038
16.199	519.770	O5	c-pentene-2	0.0017	0.0019	0.0022
16.559	525.180	O5	2-methylbutene-2	0.0060	0.0065	0.0079
17.657	540.540	I6	2,2-dimethylbutane	0.4174	0.4620	0.4458
19.003	557.440	O5	cyclopentene	0.0061	0.0057	0.0082
19.846	567.120	N5	cyclopentane	22.7219	21.9002	29.8190
20.051	569.370	I6	2,3-dimethylbutane	0.0889	0.0965	0.0949
20.140	570.350	X5	methyl-t-butylether	14.1761	13.7539	14.8019
20.447	573.650	I6	2-methylpentane	0.1264	0.1391	0.1350
21.609	585.510	I6	3-methylpentane	0.0056	0.0061	0.0060
22.291	592.060	O6	hexene-1	0.0049	0.0052	0.0054
23.159	600.000	P6	n-hexane	0.0034	0.0038	0.0037
25.124	621.730	X4	2-butanol	0.0153	0.0136	0.0190
25.529	625.930	N6	methylcyclopentane	0.0045	0.0043	0.0049
25.985	630.540	I7	2,4-dimethylpentane	0.0062	0.0066	0.0057
28.933	658.000	N6	cyclohexane	7.4567	6.8814	8.1548
30.050	667.470	I7	2-methylhexane	0.0031	0.0033	0.0028
30.214	668.830	I7	2,3-dimethylpentane	0.0070	0.0072	0.0064
31.090	675.900	I7	3-methylhexane	0.0038	0.0039	0.0034
32.788	688.910	I8	2,2,4-trimethylpentane	20.9223	21.7250	16.8580
34.326	700.000	P7	n-heptane	0.0037	0.0039	0.0034
37.692	720.450	I8	2,2-dimethylhexane	0.1030	0.1064	0.0830
39.432	730.170	I8	2,5-dimethylhexane	0.7204	0.7463	0.5804
39.607	731.120	I8	2,2,3-trimethylpentane	0.5196	0.5213	0.4186

Figure 53 Chromatography bulletin from fuel supplier/laboratory

The reported bulletin represents a view of the hydrocarbons and oxygenated components inside a gasoline, as in the specific case of the POSYN2, which counts 334 peaks (single components) achieved through the Gas Chromatography (GC) System. The process consists of the preparation of a sample, diluted or not, depending on the test's specifics and methods adopted internally by the company. In any case, the guideline for tests follows the EN ISO 22854 (European Standard), starting with the introduction of a small amount of fuel into the systems, immediately vaporized. An inert gas is present (N_2 or He) that transports the sample through the system (column/long tube). The compounds separate, and at the interval of times (minutes as reported in figure 53), the substances are recorded, detected by a Flame Ionization Detector, in the software that compares with the

database, selecting each component and storing them in the analysis data storage. The chromatogram is produced using the inputs obtained during the process, and the data output can be obtained, such as mass%, volume% and mole%. The oxygenated compounds are treated separately, this due to the fact that there is the presence of oxygen, which makes the components polar. The latter has characteristics that can interfere with the stationary phase inside the column during the hydrocarbon analysis, so this is the reason why a multidimensional GC is adopted (one for hydrocarbons and one for oxygenates). Also, an important characteristic is related to the boiling point and the major evaporation properties, which can overlap with light hydrocarbons, leading to inaccurate results. The following considerations are representative of the potential of electrofuels and innovative fuels in reaching targeted properties for specific usage, as well as targeting new standards for reducing CO_2 emissions. From an experimental standpoint, it is essential to have sufficient time, specialized knowledge, and skilled operators who can first process and then post-process data. This involves conducting analyses on a large number of samples, which must subsequently be tested in ICEs to verify the final outcomes. Or, it can be performed with a pre-evaluation from the CFD modelling, which can strongly help during these steps, enabling targeting in fuel properties, specific percentage of major hydrocarbons and oxygenates and allowing pre-testing in 3D-CFD simulations at specific real operating conditions. This way also allows targeting power outputs, CO_2 emissions, CO, NOx and soot formation (in diesel or eDiesel usage). Hence, to make it possible, of course, detailed chemistry-based inputs and reliable methodology must be assessed, as will be reported later in the specific section.

Going deeper into the fuel compositions, the similarities between the *SP98* and *POSYN2* fuels are quite evident, with almost the same levels of Aromatics and Iso-Paraffins, while *POSYN1* composition shows marked differences with no Aromatics and higher levels of Naphthenes and Iso-Paraffins. The oxygenate fraction is similar when comparing the three fuels, but the composition of the oxygenate additive changes through the fuels.

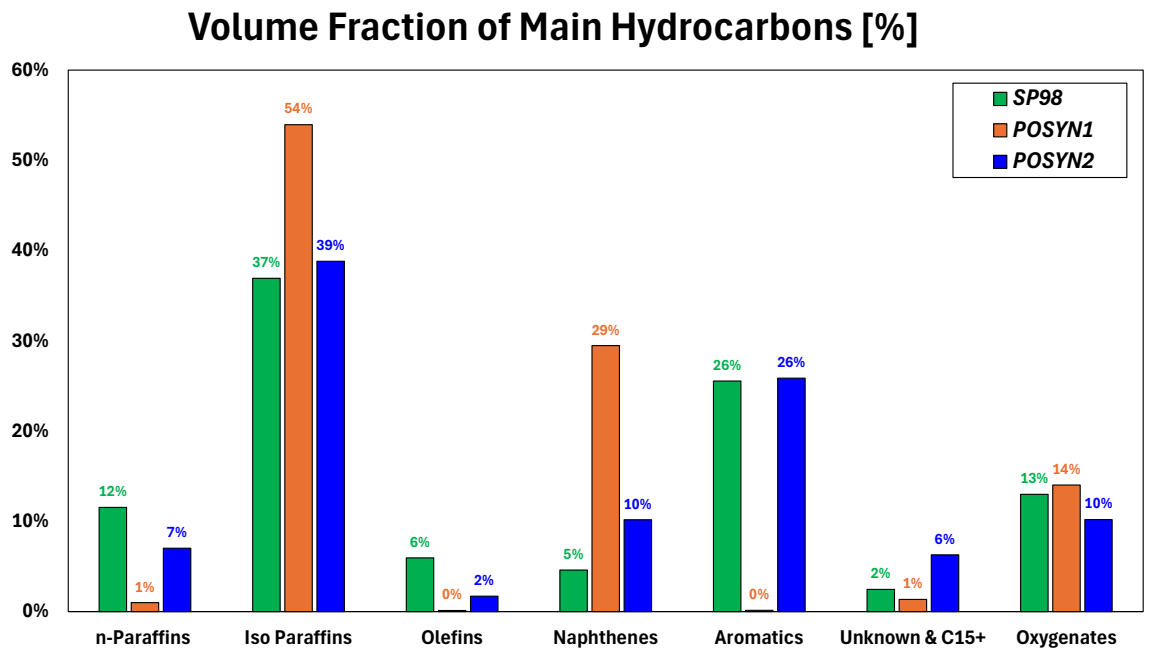

Figure 54: Percentage composition of hydrocarbons/Oxygenates/Unknown species per fuel

While a wide range of octane enhancers can be used in gasoline fuels, such as propanol and butanol isomers [184], pentanol isomers and cyclic aromatics [185,186] or oxygenates, the additives considered in this work are MTBE, ETBE, and Ethanol, with the latter being widely used worldwide. ETBE and Ethanol are used in different proportions, moving from the US (E10, fuel blend with 10 vol% of Ethanol) to Europe (E5, fuel blend with 5 vol% of Ethanol). MTBE is instead prohibited in North America and regulated in Europe for soil contamination reasons, but it is largely adopted in Asia. Interestingly, the three selected fuels present different oxygenate compounds: ETBE in *SP98*, MTBE in *POSYN1* and Ethanol in *POSYN2*.

Table 16: Chemical and physical properties of fuels

	SP98	**POSYN1**	**POSYN2**
Oxygenate Compound	ETBE	MTBE	Ethanol
Carbon Mass Fraction	84.7%	82.3%	84.2%
Hydrogen Mass Fraction	13.3%	15.1%	12.1%
Oxygen Mass Fraction	2.0%	2.6%	3.7%
Molecular Weight [g/mol]	98.5	78.7	89.8
Single Component Surrogate	$C_{6.95}H_{13.11}O_{0.12}$	$C_{5.4}H_{11.9}O_{0.13}$	$C_{6.3}H_{10.88}O_{0.21}$
H/C	1.89	2.20	1.73
O/C	0.017	0.024	0.033
$A/F_{stoichiometric}$	14.24	14.56	13.70
LHV [MJ/kg]	42.16	42.89	41.35
RON	98.4	100	97.6
MON	88	91	86.3
S (sensitivity)	10.4	9	11.3
AKI	93.2	95.5	92.0
Dynamic Viscosity@25 °C [N*s/m^2]	4.94E-04	4.81E-04	5.30E-04
RVP [kPa]	-	46.6	51.8
Density (exp) [kg/l]	0.750	0.723	0.764

The similarities between *SP98* and *POSYN2* are reflected in some macroscopic fuel characteristics, such as the lower H/C compared to *POSYN1*, due to the higher carbon content; the higher H/C of *POSYN1* results in the highest lower heating value (LHV), which is strictly linked to the highest hydrogen percentage in table 16. On the contrary, and for the same reason, the lowest LHV is achieved by *POSYN2*. A similar comparison can be made with respect to the A/F stoichiometric ratio, with *POSYN1* requiring the highest amount of air to meet stoichiometry. Also, in this case, *SP98* lies between the two eFuels.

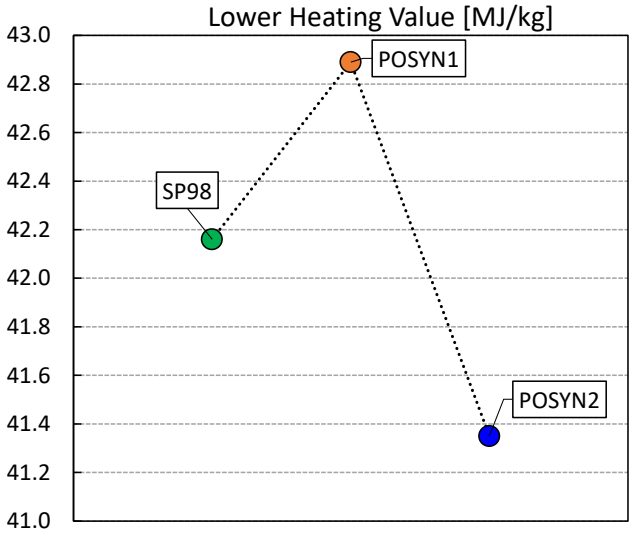

Figure 55 Lower Heating Value of e-fuels and Premium Fuel SP98

Combining the above observations, some engine-related considerations can be performed: assuming the same amount of engine air flow and targeting stoichiometric combustion, a 2.2% reduction and a 3.9% increase in fuel consumption are expected with *POSYN1* and *POSYN2,* respectively, compared to conventional Gasoline. Considering the higher LHV of *POSYN1*, the reduction of fuel consumption can potentially result in an almost negligible loss of engine performance (-0.5%) if the same combustion efficiency is met; conversely, the 3.9% increase in fuel consumption with *POSYN2* can lead to a small increase in engine performance (+1.9%) under the same previous assumption. These raw considerations based on fuel properties can help in identifying how the variation in fuel characteristics can potentially affect the engine output; however, differences in fuel vaporization mixing, combustion and knock tendency among the different fuels could turn the tables. This is the main reason why a reliable assessment of the expected combustion and knock tendency characteristics through chemical kinetics is important when trying to predict the real performance of non-conventional fuels.

Focusing on RON/MON data, a globally similar knock tendency is expected when comparing the fuels despite the differences in the oxygenate fuel composition. *POSYN1* has a higher Anti Knock Index (AKI) while *POSYN2* is characterized by the lowest value. The analysis of the IDTs is important to deepen the effect of the different fuel compositions on knock tendency.

The different fuel composition also affects the density of the fuel. Comparing the oxygenate compounds, ethanol is characterized by the highest density (0.789 kg/l) compared to MTBE (0.736 kg/l) and ETBE (0.746 kg/l). The higher Ethanol density is responsible for the increased weight of

POSYN2 compared to *SP98*, while the lowest density of *POSYN1* is mainly related to the absence of aromatics.

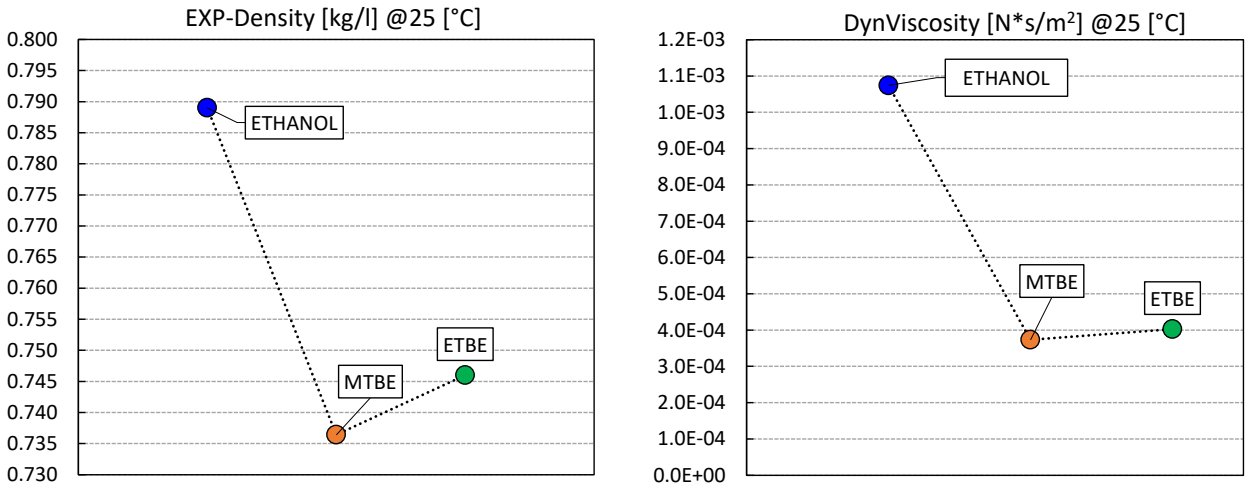

Figure 56 Liquid density and dynamic viscosity of oxygenates (Ethanol, MTBE, and ETBE)

The distillation curves for the three fuels are presented in figure 57. This characteristic, along with the Reid Vapor Pressure (RVP), is essential for accurately describing volatility. The RVP for the commercial SP98 is not included due to significant variability arising from seasonal blends. The higher RVP value of *POSYN2* compared to *POSYN1* well aligns with the front end of the distillation curves, confirming the increased volatility of certain hydrocarbons present in *POSYN2*. But not only, in fact, the early part of the distillation, and especially its specific slope, such affected by more volatile compounds, confirming the presence of highly volatile compounds, such as the presence of different oxygenates. It can be observed that MTBE is present in *POSYN1* compared to ETBE in the SP98, which gives the gasoline a faster evaporation rate due to the higher volatility that concern to MTBE with respect to ETBE. For the sake of clarity, the lower initial point of the SP98 can be attributed to other compounds, which are out of knowledge in this case and correlated to the seasonality of the fuel itself (butane can be present, affecting the starting point of the distillation curve against oxygenates behavior).

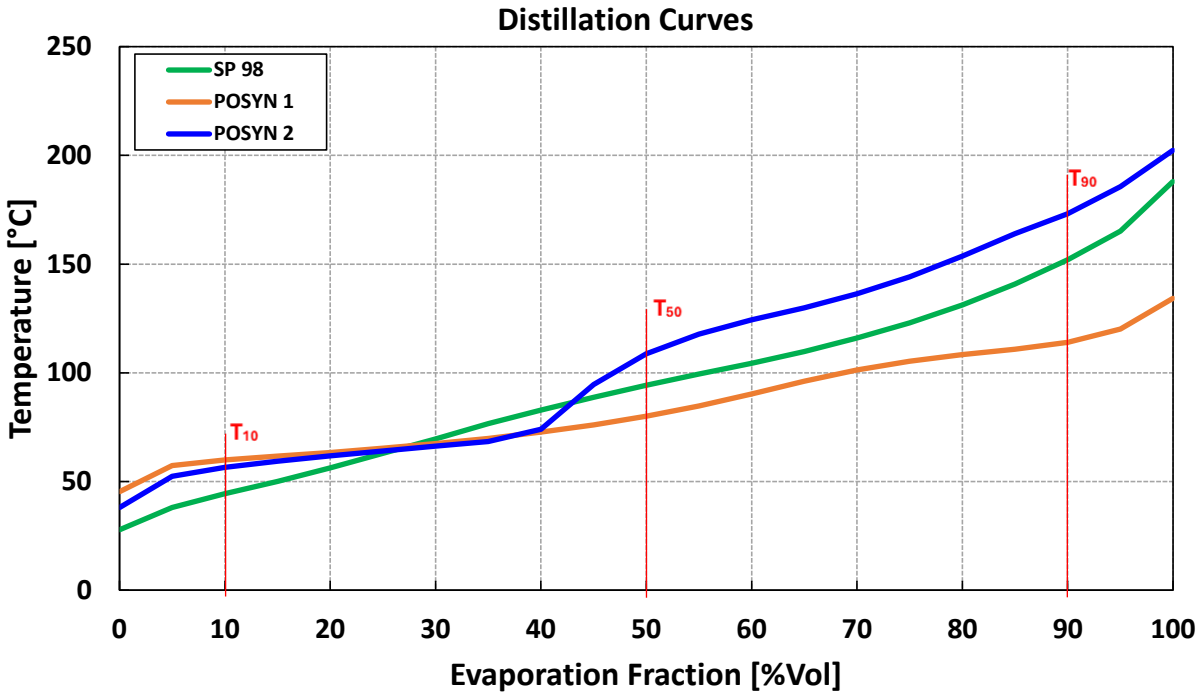

Figure 57: Distillation curves from experiments

It is well known that the fuel evaporation rate is one of the main physical factors impacting mixture preparation and fuel deposit formation in GDI units, and thus strongly affecting combustion, emission formation and knock tendency [187-189]. Focusing on the first part of the curves, up to 25% evaporation fraction, the two eFuels show similar evaporation behavior despite the different composition and a lower evaporation rate compared to SP98 is observed, as suggested by the higher temperatures at the recovered volume (T10). Between the T50-T90 portion of the distillation curve, the one that most influences the air-fuel mixing in the combustion chamber, *POSYN1* turns into the most volatile fuel while *POSYN2* remains the least volatile one. A peculiar behavior is found in *POSYN2* with a strong discontinuity on the distillation curve around T50. Considering the very similar composition between *SP98* and *POSYN2* this peculiar behavior can be attributed to the presence of Ethanol, due to its non-ideal mixing behavior, which is not observed for ETBE.

5.3.2 Fuel chemistry notes on specific Surrogate (OxPIONA)

In light of the mentioned components, the following description of a proper fuel surrogate for each of the fuels is critically reported hereafter. The concept will be to find a set of major hydrocarbons (and oxygenates) able to mimic the real characteristics of real fuels, that here is considered strictly for the flame propagation and anti-knock targets, but conceptually it is extended to be carefully predictable for potential future details related to the multiphase simulations and emission modelling outputs. In this work, the idea of detailing the fuel surrogate with at least a senary fuel surrogate structure, in which the PRF- or TPRF-based fuel surrogate structures [190-192] evolved toward more specific applications and a new generation of ICEs. Of course, as discussed, this work focuses on the context of a new generation of fuels, such as innovative gasoline/eGasoline. Here, as one can easily understand, one can face several peculiar species, following the concept of chemically designing fuels and pushing toward as high as possible degree of detail on mimic a new generation of fuels. Furthermore, another important consideration that leads to non-practical PRF or TPRF fuels on describing in well fidelity the full behavior of a fuel is represented by their quantity. As a full behavior,

the author intends the matching of several properties of the fuels, and referring to the combustion only, the presence of the aforementioned species is generally limited [193], leading to not fair modelling of the fuel surrogate compared to the real one. In fact, to meet the targeted RON of premium fuels, for example, leads to the increment of aromatics species to reach specific RON/MON targets. Of course, this leads directly to an overestimation of the carbon mass, as first, changing the LHV and the balance in the H/C ratio. Nonetheless, the higher soot tendency of the fuel can potentially misalign the comparison to the real one. In the work of Ahmed et al [193], in fact, it has been demonstrated the relation between aromatic content and soot/emissions, and pointed out also the importance of the heat capacity (or specific heat, Cp) in affecting the end-gas temperatures, making the mixture more prone to auto-ignite. The latter behavior is reachable by targeting the same octane rating but changing the property of the fuel with a lower heat capacity. Finally, an increment of aromatics can, of course, increase the knock resistance of the surrogate to align with the real fuel, but dramatically influence the laminar flame speed negatively. To bear in mind that the high presence of aromatics in the fuel mixture represents the major reduction in LFS as aromatics, in the hydrocarbon family, the species with the lowest laminar flame speed [194,195]. Then, a crucial point is also that the methodology that is reported in this work follows an experimental input from a chromatography bulletin, which can then specifically be changed, targeting percentages/properties of a fuel to tabulate the results and then adopt those as an input in ICE simulations. As will be detailed later in the following chapter, the fuel surrogate will be defined starting from 5 major hydrocarbons and 1 oxygenated compound, which will be specifically selected following the real composition of the fuel. Following the proposed order, the hydrocarbon content is predominant in the real fuel that can be reproduced by 5 major hydrocarbons. In our fuels surrogates definition, it is important to reach a high degree of detail for any kind of application, despite the major focus being on flame propagation and knock resistance. Deepening the previously introduced fuel volatility properties, as figure 57 reports, the droplet evaporation during spray injection affects the conversion of the liquid to the gas phase under certain conditions. The plot is representative of this property, as well as the RVP values. Then, further details are related to the specifics of the gasoline supplier, and affected by the weather conditions of the application of the fuel in the engine, according to fuel seasonality. The European Standards EN 13016 is the guideline for the DVPE-Dry Vapor Pressure Equivalent, or the ASTM D5191 for the U.S. Referring again to the distillation curve, it is confirmed that the use of more than two components helps reach a close to experimental output. In fact, the first evaporation occurs by the more volatile compounds, which impacts the ignition at cold start conditions. Usually, to enhance these characteristics, butane is added to the fuel composition in variable percentages. The species that evaporates first meet the lower boiling point, leaving the last to evaporate the ones with a higher boiling point. Of course, from a combustion standpoint, having low boiling point fuels as well as fast evaporative rates can consistently prevent the risks related to the hotspots in ICEs due to oil-fuel droplets deposition [196]. The mid-range, with T50 more or less pronounced, plays a role in determining the AIR/FUEL Ration becomes rich and results in rich mixture according to consequently HC emissions. On the other hand, less volatile fuels with higher T50 can easily inhibit the fuel/air mixing process by increasing soot and NO_x [197]. Then, T50-T90 of the distillation curves is more affecting on the acceleration, power output, fuel economy and unburned emissions. Of course, going deepening on the reason behind the distillation and chromatography, all relate to the components that characterize the fuel. The fuel composition falls into its own strictly defined OxPIONA, such as Oxygenated/Paraffins/Iso-Paraffins/Olefins/Naphthenes/Aromatics. Following the European standards, but focusing on Premium ones as in this work, the components that can be found inside a

gasoline such a Super Plus RON 98 are basically made by a PIONA structure with the oxygenates that can easily meet the ETBE, not ethanol only. In fact, premium fuels such as RON 98 gasoline that can be found in fuel stations Germany, and European countries fit the composition described in this work, where the oxygenate compounds can be wide, but are mainly identified by ethers or, also, alcohols. Leaving more details about oxygenates later on, the PIONA first component is the paraffinic content.

Paraffins are represented in a chromatography bulletin by several substances, such as the major in content n-Pentane and n-Heptane. To try to "simplify" the composition, and according to the major literature in this field over the years, here is a focus on European standards [173,176,191,198]. n-Heptane, specifically, is a linear paraffin, an aliphatic hydrocarbon (alkanes) characterized as a widely adopted hydrocarbon to reach cold-start ignition, which affects the first part of the previously described distillation curve, and with a nominal RON equal to 0. Despite a strongly negative anti-knock quality, they behave well in the stability of the gasoline, with no issues from soot or other harmful emissions by producing mainly H_2O and CO_2. Their composition, as saturated hydrocarbons, due to the reached maximum number of hydrogen atoms added without any double or triple C-bonds, led to high energy content and stability during combustion. As previously discussed, the composition of these substances are represented by C_nH_{2n+2}.

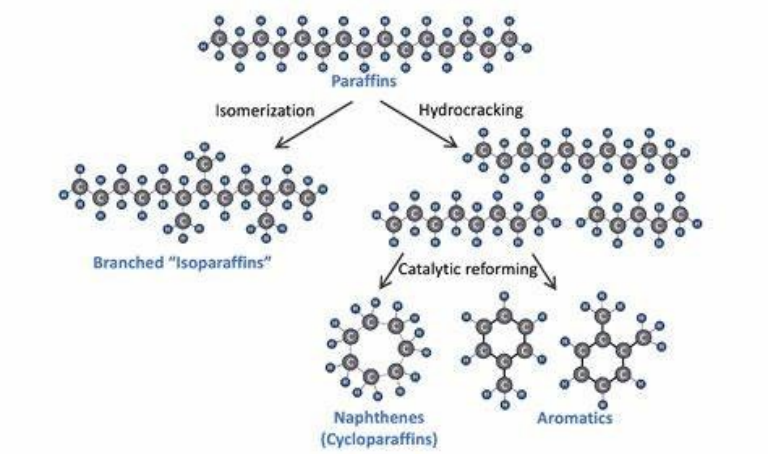

Figure 58 Chemical pathways of hydrocarbon transformation from Paraffins to iso-paraffins, cyclic paraffins and aromatics

Then, following the refinery process, the same family of hydrocarbons can be subjected to isomerization, which is the process through which the linear paraffins become branched hydrocarbons, such as isoparaffins. This process produces isomers, which is a conversion of the straight-chain structure of hydrocarbons into a branched-chain structure with enhanced properties in knock resistance. Details from chemical standpoints are also reported in the MtG explanation equations (Eq. 1,2,3) where the chemical reaction is reported leading to the iso-octane with the base formulation: C_nH_{2n}. Generally speaking, the iso-octane was used in the past as a representative surrogate itself of gasoline. This was true if the major outcome was the representative and qualitative, but of course also quantitative, in first approximation, for combustion calculations targeting a general LFS. Nevertheless, the progression and evolution of fuels currently lead to necessity to push toward a detailed degree of fuel surrogates, according to the more restrictions, and so, more details are needed to match a representative fuel to be carefully modelled in ICE simulations. Furthermore, the LHV of this component is also a gauge for the energy content, as well representative, which is relatively

aligned with a gasoline one, measured by ASTM D240, through a bomb calorimeter and reaching usually values in the range of 44-46 [MJ/kg] for C_5-C_{16} (Iso-octane=44.3 [MJ/kg], NIST database, representative as previously said). This led us to maintain, of course, the iso-octane as representative of the iso-paraffin content in the gasoline surrogate.

The next hydrocarbon present in gasoline composition is the Olefins, such as aliphatic hydrocarbons (alkenes), which are generally limited in gasoline composition due to their life storage negative affection. The composition of Olefins follows the C_5-C_8 with the double bond molecular structure according to the higher octane rating. Following the previously mentioned LFS of iso-octane, the LFS comparison of the alkanes compared to alkenes is in this order: Alkenes < Alkanes.

Finally, through the catalytic reforming, alkynes and aromatics are produced. The first ones, alkynes, unsaturated hydrocarbons as the previously alkenes, meet the formulation C_nH_n with a carbon triple bond and characterized by very high anti-knock behavior, but rarely used in fuels due to toxicity and low stability in the mixture. The aromatics, instead, show a very good behavior in gasoline, as will be discussed. Cyclopentane and cyclohexane are the most commonly adopted as representatives of cyclic paraffins. In this work, the cyclohexane is the one selected following Håkansson et at. [198], but can be assumed with discretion since their presence varies in different winter or summer seasons in the fuels. Especially, going deeper, the cyclopentane has a lower boiling point compared to cyclohexane, enhancing the winter composition of gasoline. On the contrary, cyclohexane is preferred in mild conditions (summer composition), and is characterized by a higher boiling point compared to cyclopentane, but has better knock resistance. Since this work focuses on high-performance fuels, the selection falls on cyclohexane as a representative of naphthene species.

Last but not least, the aromatics are a crucial hydrocarbon in the composition of gasoline. The content of aromatics is regulated by the EN 228 specification, and limits the content of Benzene to <1%. The aromatics, which are the second family of hydrocarbons present in gasoline, according to the European standard, after the paraffinic, are represented by Toluene. Toluene is an excellent high-weighted, soot formation, knock enhancer, most widely used in gasoline for its latter important positive property. Nevertheless, due to the characteristically high propensity of soot formation during the combustion process, its quantity is usually limited to a maximum of 30-35%. Nevertheless, in this work, as will be reported later on, its quantity can also be absent, but replaced by higher content in paraffinic and oxygenates, such as ethers with high octane rating. So, the better enhancers for the RON and MON values are represented by oxygenated compounds and this work focuses on their usage and relevance in surrogate definition.

The oxygenation of fuels plays a fundamental role as gasoline additives, and has been introduced after the phase out of the leaded gasoline in 1980s. Of course, the additives added in the gasoline limit other hydrocarbons, which led to the reduction of the carbon compounds/byproducts. In the present work, the role of the oxygenates reveals the way through which the modelling has been assessed for the fuel surrogate. Ethanol, MTBE and ETBE are found as major percentages among the full chromatography analyses, and are representative as the oxygenates in the fuel surrogates. The ethanol, which is the oxygenated content in the *POSYN2*, is the current most adopted oxygenated compound in the regulated market of fuel in Europe. It is found with a maximum percentage of 10%vol (E10). Ethanol is obtained from biomass, which usually includes corn, wheat or cassava but also sugarcane or sugar beet as well as some more agricultural residuals. Then, reporting the example of the corn as a first raw material for producing ethanol. In late 2004, the grain surplus in the U.S. was one of the

major promoters of the use of grain for ethanol production [199], now also India pushes toward the use of rise as the first product as per ethanol production [200]. Related to grain, it follows a milling process, and enzymes are added to the mash to convert it into starch, which then becomes sugar. It follows a cooking process of the mash, liquefaction and then cooling and the compound is then transferred to fermenters. Here, the process faces different byproducts such as CO_2 after adding yeast and bacteria. The process follows a distillation and dehydration and then the distilled product can be used for the next ethanol-blended gasoline for the automotive sector. As mentioned, this process also allows producing corn oil for animal feed, but also for bio-diesel/renewable diesel. On the other side, CO_2 is then adopted for beverages and many more applications. Generally speaking, here the term renewable ethanol comes from the fact that the CO_2 is used by the plants for growing and after the combustion of this ethanol in the gasoline, the CO_2 is reemitted in the environment with a net zero CO_2 emission at the lifecycle.

Then, from ethanol, another, more knock-inhibition compound, can be obtained, which is the ETBE. This is produced by mixing ethanol and isobutylene in the presence of heat and a catalyst [201], of course, improved along the years as the direct adoption of the azeotrope (mix of two or more liquids that do not change also during the change of phase, as well as the evaporation and condensation) for gasoline blends [202]. Thanks to its great properties related to low vapor pressure and high boiling point, it is well compatible to be blended into gasoline without any issue on its own transportation via pipelines. Then, a great characteristic that has been widely studied in the last decades is its low water solubility and higher affinity to the soil. Then, it has a high Henry's law constant, making this oxygenate low-risky for the groundwater compared to other ethers such as MTBE. Lastly, from a combustion standpoint, when talking about ETBE, advantages in terms of reduced formaldehyde, SOx, hydrocarbons and methane emissions can also be considered. This leads to the conclusion that, besides being environmentally "friendly" compounds, it is very suitable for ICEs issues and plays a role in improving next generation ICEs.

The latter, MTBE, is a substance that has similarities to ETBE, especially related to the RON value, which is almost the same as ETBE but higher compared to ethanol. Then, both are ethers and are adopted in gasolines, despite MTBE having recently been reduced in several countries due to its

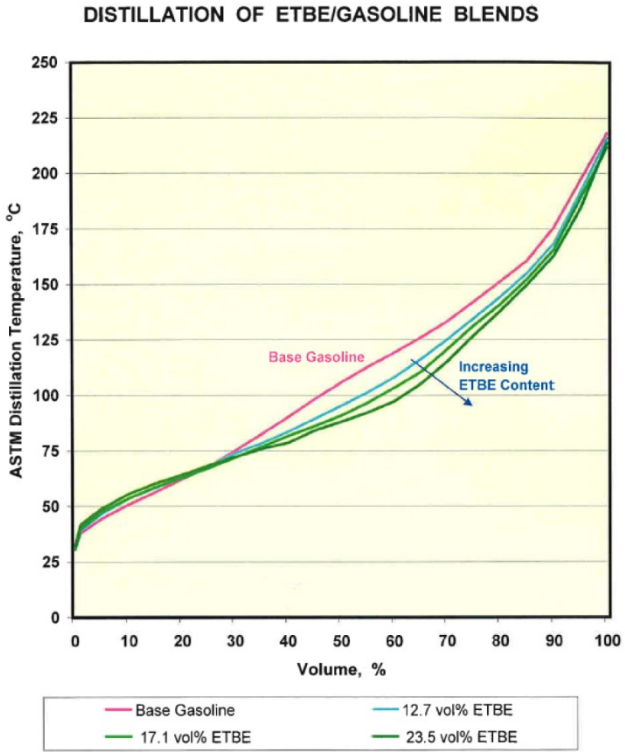

Figure 59 – Impact of ETBE on the distillation curve of a gasoline [203]

impact on the groundwater. Nevertheless, the high knock resistance and the high content of oxygen, per the previous ethanol and ETBE guarantees a better combustion, reduction of CO and HC emissions and, especially, MTBE is able to reduce NOx, acetaldehydes and ammonia emissions compared to ETBE. Of course, MTBE presents a higher volatility compared to the ETBE, which makes it as a good replacement for hydrocarbons such as Butane for the warm-up of the engines at cold temperatures, but can lead to more issues related to the toxic gases and highly flammable gasolines.

Finally, some major considerations can be resumed from the table 17, with a final consideration that relates, of course, to the RON/MON and sensitivity of the fuels that are considered in this work. Of course, these fuels are not currently adopted for automotive transportation, since ongoing developed and adopted for high-performance engines in racing competitions. Hence, according to history, what is adopted in racing competitions is then molded to be used and readapted for the passenger cars scenario as innovation and future technologies. Talking about fuels, it is important to reach the standards that Europe and the World regulations place, also related to the costs. The costs, in fuel refinery and specifically, in fuels and gasoline production, is strongly related to the previously mentioned oxygenates, which can be produced through several processes targeting oxygenates and additives acting in enhancing the knock resistance, pushing engines toward more and more efficient engines. On the other side, the targeting of high RON/MON depends strictly on the composition of the gasoline, and of course, on the oxygenates. Ethers have advantages and disadvantages depending on the specific one. MTBE is more expensive than ETBE, since the production chain of ethanol is the cheaper one. Unfortunately, when talking about gasoline, it must be considered another important

value, which is the sensitivity of the fuels (S). This value represents the difference between RON and MON and has an impact on the gasoline performance. Generally speaking, in Europe, it is regulated the minimum values of RON and MON are respectively 95 and 85. Although it is not considered a direct regulation of the sensitivity, the minimum values of both RON/MON define limits on that value. It can be simplified that a high sensitivity means that the fuel can be exposed to risks of autoignition phenomena under severe working conditions. In FACT, the MON is a test performed under more severe conditions compared to the RON one. Both are regulated respectively by ASTM D2699 and ASTM D2777 for RON and MON. So, as RON and MON are directly affected by aromatics and oxygenates content as major knock resistance enhancers, their presence significantly affects the sensitivity of the fuels. Focusing on the conventional/premium fuels and electrofuels of the present work, the one with the highest sensitivity is the one with ethanol as oxygenate, the *POSYN2*. This is something that was under expectations, and reported also by Wallace et al [204], where ethanol shows almost doubled sensitivity values compared to ETBE/MTBE and Toluene. On the other hand, the sensitivity of the *POSYN1*, is the lowest one, according to the free-aromatics composition and the presence of MTBE as an oxygenate. So, this is the link that the economic standpoint meets the regulatory market as well as the composition of the gasoline. Lastly, in [204] the impact of using ETBE or ethanol in fuels and the related impact on CO_2 emissions was also analyzed, highlighting a strong reduction when adopting ETBE by replacing ethanol. This is something that, according to the chemically designable fuels capability, and the value of the present work in computing before some specific compositions, the target of CO_2 reduction or the target of net-zero CO_2 emissions is something that can be pursued right now.

Table 17 Comparison of the major properties of oxygenates

	ETBE	**MTBE**	**ETHANOL**
Formula	$C_6H_{14}O$	$C_5H_{12}O$	C_2H_5OH
% of oxygen			
Molecular weight [g/mol]	102.2	88.2	46.1
Self-ignition [°C], [205]	304	435	363
Boiling point [°C], [205]	73	55	78.37
LHV [MJ/kg], [204,205]	36.5	35.1	26.9
RON [205,206,207]	117-120	117-119	109
MON [205,206,207]	101-102	101	90
S (sensitivity)	16-18	16-18	19
AKI	110	109	99.5
Dynamic Viscosity@25 °C [N*s/m^2]	4.02	3.73	1.07
RVP [kPa]	27.6	55.2	15.9
Density (exp) [kg/l]	0.746	0.736	0.789

5.3.3 Computational chemical analysis

As stated earlier, starting from the actual fuel compositions, a surrogate is defined for each fuel using a 6-component formulation, and lumping each of the hydrocarbon groups in one single species i.e, N-Paraffins in n-Heptane, Iso-Paraffins in Iso-octane, Olefins in 1-Pentene, Naphthenes in Cyclohexane and Aromatics in Toluene. Unidentified and C15+ species are neglected and spread

across the other ones by maintaining the same balance between relevant species. As for the other components, the oxygenate fraction in the surrogate is fuel-specific: i.e. ETBE in SP98, MTBE in *POSYN1* and ethanol in *POSYN2*. Also, traces of minor oxygenates present in the real fuel chromatography data (negligible quantities <1%) are lumped into a single oxygenate compound. The composition of the three defined fuel surrogates is reported in Table 2.

Table 18: Composition of fuel surrogates expressed as percentages based by mass

Surrogate Components		***SP98***	***POSYN1***	***POSYN2***
N-Paraffins	N-Heptane (C_7H_{16})	11.0%	1.1%	7.2%
Iso-Paraffins	Iso-octane (C_8H1_8)	34.7%	52.4%	36.6%
Olefins	1-Pentene (C_5H_{10})	5.5%	0.4%	2.8%
Naphthenes	Cyclohexane (C_6H_{12})	5.3%	31.2%	11.4%
Aromatics	Toluene (C_7H_8)	30.3%	0.4%	31.2%
Oxygenates	ETBE ($C_6H_{14}O$)	13.2%	-	-
	MTBE ($C_5H_{12}O$)	-	14.4%	-
	Ethanol (C_2H_5OH or C_2H_6O)	-	-	10.8%

The consistency in the selection of the species representative of each hydrocarbon group can be verified by comparing the density of the fuel surrogate to one of the actual fuels. This comparison, reported in Table 3, shows a negligible delta (<1%).

Table 19: Checks on fuel density by comparing surrogates to real fuel density

Fuel	Actual Fuel Density	Surrogate Fuel Density	Delta
SP 98	*0.750 [kg/l]*	*0.752 [kg/l]*	0.26 %
POSYN 1	*0.723 [kg/l]*	*0.725 [kg/l]*	0.27 %
POSYN 2	*0.765 [kg/l]*	*0.764 [kg/l]*	0.13 %

Such a definition of the surrogates can account in detail for the effect of different oxygenate compounds on the autoignition tendency of the fuels, thus enabling a detailed prediction of engine knock tendency through IDT calculations. Nevertheless, the complexity of the chemical mechanisms to be applied increases due to the need to include oxidation pathways for ETBE, MTBE and ethanol beyond those of other hydrocarbons in the surrogate. To simplify the approach, the surrogate complexity can be reduced using one oxygenate species for all the oxygenate compounds moving from a more general OxPIONA definition to an EPIONA one. This can relevantly simplify the mechanism selection process, while reducing the accuracy of the method, especially when assessing IDT. More details regarding this aspect will be provided in the next section, which will be dedicated to the selection of the chemical mechanism.

5.4 Mechanism Selection for IDT and LFS Calculations

Selecting an appropriate chemical mechanism from the literature is crucial for characterizing the autoignition quality and flame properties of real-world fuels, which are composed of hundreds of different hydrocarbons. Theoretically, if the fuel's detailed composition is well known, there would be no need to define a fuel surrogate for chemical kinetics studies. However, accurately modelling the oxidation pathways of all species involved requires, in most cases, a mechanism of extremely high complexity, making it computationally impractical. Since the computational cost increases with the number of reactions and species, a direct approach is often unfeasible. To optimize computational efficiency and enable simulations across a wide range of physical conditions, it is necessary to reduce the number of species while maintaining an accurate representation of the fuel. This is achieved by using a surrogate fuel, allowing for the adoption of smaller mechanisms with fewer species and reactions.

The fuel surrogates defined in the previous section using the OxPIONA approach require the mechanism to cover the chemical pathways of the identified five hydrocarbons and of an oxygenate. Additionally, the mechanism must account for the three oxygenate species under consideration: ethanol, MTBE, and ETBE. Another important aspect to consider is the range of validation of the selected mechanism, which should be as wide as possible, especially when targeting engine conditions.

The mechanism from Yasunaga et al. [208] is one of the most promising for ETBE and MTBE, which are important species to consider in the current study, despite the limited range of validation due to a lack of experimental measurements. Nevertheless, this chemical kinetics model cannot be adopted for gasoline surrogates since no pathways for hydrocarbons are contained.

To the extent of our knowledge, the only mechanism available in literature covering all the 8 different species composing our surrogates is the one provided by the “Creck Modelling Group” in the versions (v1412 and v2003), accounting for 225/356 species and 7645/10171 reactions [178,209,210]. Referring to the more recent v2003, the mechanism is validated for gasoline surrogates and includes oxidation pathways for all three considered oxygenate compounds, including ETBE and MTBE [212,213]; furthermore, despite the quite high number of species and reactions, the application of that mechanism is feasible when running 0D constant pressure reactor simulations of IDTs.

Since no experimental measurements of IDT are available for the three considered fuels, direct validation of the calculated ones is not possible. However, the reliability of the mechanism is assessed by comparing its IDT prediction for the main surrogate components (i.e., n-heptane, iso-octane, toluene, ethanol, MTBE, and ETBE) against published experimental data, selecting the highest available pressure and temperature ranges. The results of this validation study are provided in figures 65-66. Overall, the mechanism demonstrates reliable IDT prediction for the primary hydrocarbons, supporting the assumption that reasonable results can be achieved using a multi-component surrogate fuel composed of the same species. Considering the above, this is the mechanism selected for calculating IDT of the three considered fuels.

The primary role played by the composition of the oxygenate portion of the fuel on the autoignition tendency is noticeable from the sensitivity analysis summarized in figure 60, confirming the need for the choice of a surrogate composition and a detailed chemical scheme accounting also for the

peculiarities of the oxygenate component. The calculated IDT of the three fuels at 70 bar and an equivalence ratio equal to 1 is reported in figure 60 as a function of temperature. The calculations are performed adopting as a surrogate the previously defined OxPIONA one, accounting for the different oxygenate composition, and the EPIONA one, obtained substituting ethanol for ETBE and MTBE in *SP98* and *POSYN1* surrogates, respectively. The change in the oxygenate compound from MTBE to ethanol in *POSYN1* leads to a strong variation of the IDT at mid-to-low temperatures, able to reverse the trend comparing the three fuels, while a more similar behavior can be noticed replacing ETBE with ethanol in *SP98*. According to further analyses provided in the next section, an increase of *SP98* IDT is visible with the OxPIONA surrogate with a similar shape of the NTC region, while the peculiar NTC behavior of MTBE cannot be captured through an EPIONA surrogate, leading to non-negligible overestimation of IDT at mid-to-low temperatures and underestimation at high temperatures.

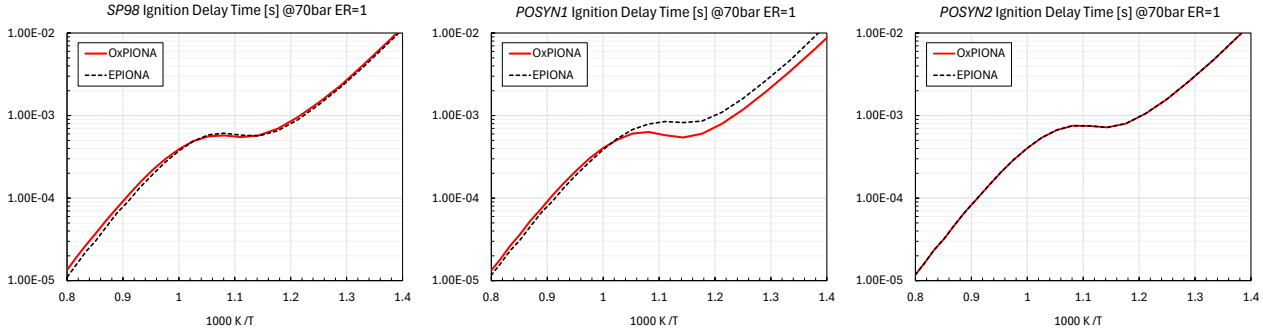

Figure 60: Ignition delay time results by comparing fuel surrogate compositions with EPIONA Vs OxPIONA structure

For LFS calculations, the most straightforward approach would be to adopt the same mechanism used for IDT. However, unlike IDT, calculating LFS requires 1D freely propagating reactors, which are at least an order of magnitude more computationally expensive than 0D reactors. This makes the use of a complex mechanism like the CRECK Mech. impractical for LFS calculations across a wide range of operating conditions. Over the years, extensive research has been conducted on laminar flame speed calculations, leading to the development of several reduced chemical mechanisms, as reported by Sarathy et al [11]. However, to the best of the author's knowledge, no existing mechanisms include both the hydrocarbon species and the three oxygenates adopted to define the surrogates. Therefore, a different strategy is needed to address this limitation.

The reduction of the CRECK Mech. to fit both species and computational requirements is possible, but it is out of the scope of the present work, considering the author’s expertise; furthermore, an effective reduction of the mechanism would be critical because of the need to include oxidation pathways for a quite high number of hydrocarbons. Therefore, the possibility of simplifying the definition of the three surrogates is investigated.

Ethers, alcohols and more in general oxygenate compounds play a fundamental role in the definition of the autoignition characteristics of actual fuels, where they are added mainly as octane enhancers. However, it is well documented in literature that there is a poor strict correlation between laminar burning velocity and the chemical formulation of the specific oxygenate compound but mostly related to hydrocarbon composition and parameters such as stoichiometric A/F, specific heat, sensitivity, and more [214-219]. According to Hu et al. [206], LFS of ETBE and MTBE are very similar, making it possible to replace ETBE with MTBE or vice versa in surrogates for LFS calculations. Furthermore, the work from Dirrenberger et al. [220] demonstrates that adding ethanol up to 15% to gasoline has

a negligible effect on LFS. The available literature on the topic suggests the scarce relevance of oxygenate composition on the LFS of the fuel, especially when the oxygenate fraction is low (<15%). This is the case of all three fuels considered, in which the maximum amount of oxygenate content is 14.5% in *POSYN1*.

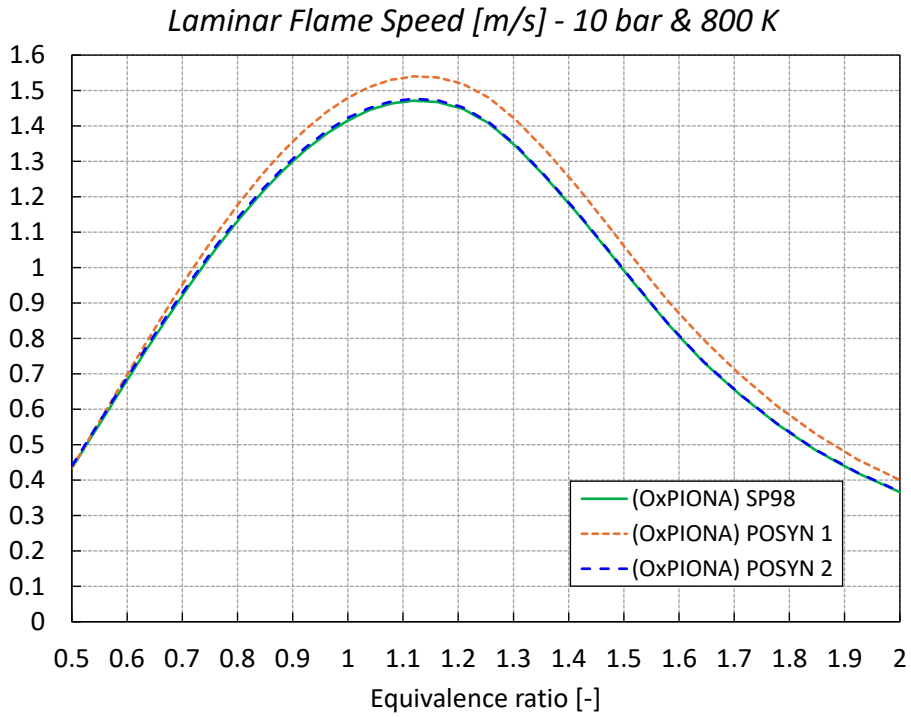

Figure 61: Laminar flame speed of fuels with the OxPIONA fuel surrogate approach

A sensitivity study is performed to verify the validity of this assumption and to understand if and how the surrogate definition can be simplified when targeting LFS. First, the detailed CRECK Mech. is adopted to calculate the LFS of *SP98*, *POSYN1*, and *POSYN2* using the previously defined OxPIONA surrogates, varying the mixture composition at 10 bar and 800 K. The results of those calculations are reported in figure 61.

As expected, the LFS of *SP98* and *POSYN2*, which mainly differ for the oxygenate compound (ETBE and ethanol, respectively), are almost superimposed, while a higher flame speed is inferred for *POSYN1*. To isolate the impact of the oxygenates, the LFS calculation of *SP98* and *POSYN1* is repeated, substituting ethanol for ETBE and MTBE and retaining the same oxygenate fraction. The results of those calculations, reported in figure 62, confirm the very low sensitivity of LFS results to the oxygenate chemical formula.

Combining literature with the performed sensitivity, it is possible to conclude that, from an engine perspective, the detailed nature of the oxygenate compound can be neglected when targeting the LFS of actual fuels, simplifying the OxPIONA surrogate definition into an EPIONA one. This greatly simplifies the selection of a suitable mechanism, considering that most of the available reduced mechanisms in the literature include ethanol.

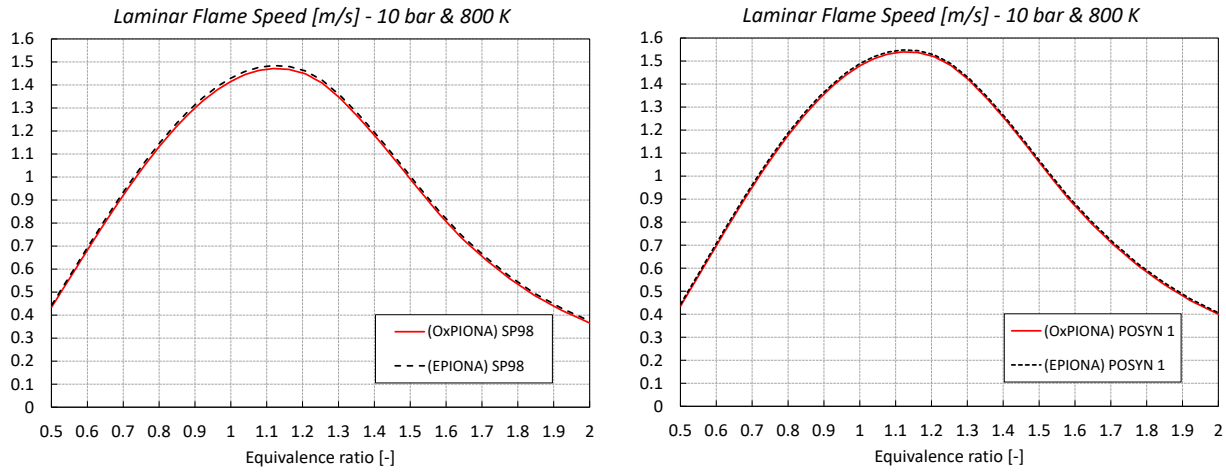

Figure 62: Laminar flame speed of SP98 compared to POSYN1 by considering OxPIONA Vs EPIONA fuel surrogate definition

Two reduced mechanisms, compatible in terms of computational requirements and including only ethanol as an oxygenate compound, are considered. The first is the one from Lawrence Livermore National Laboratory (named LLNL-Reduced 2) [132], accounting for 312 species and 1488 reactions, while the second one is the further reduced one from Ren et al. [131], accounting for 178 species and 758 reactions. This last particularly fits with our scope due to the affordable CPU requirements and because it is purposely developed for gasoline surrogates and ICE applications. The mechanism is derived from the more widespread LLNL [221-223], AramcoMech [224], Gri-Mech [225], Metcalfe [226], and Slavinskaya [227]. The validity of both the selected reduced mechanisms is assessed by performing the same validation study as for the CRECK Mech., and these results are presented in a figure 64. The comparable results obtained with LLNL and Ren chemical kinetic mechanisms orient

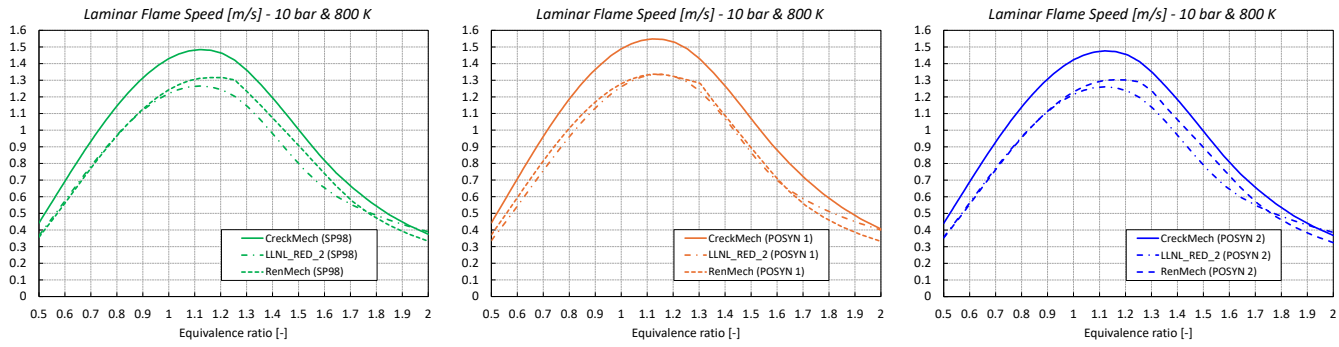

Figure 63: Laminar flame speed of EPIONA fuel surrogates by considering three different chemical mechanisms (Creck Mech., LLNL-RED 2, and Ren Mech.)

the mechanism selection for a relative comparison between the fuels towards the Ren Mech. one, due to the reduced computational effort required. More information related to the entity of the differences between the CRECK Mech, where the comparison aims at evaluating the previously cited mechanism with a proper scaling factor. Calculating the LFS for each of the fuel surrogates a proper scaling factor

allows the Creck Mechanism, enabling a reasonable matching and placement of results from both the LLNL-Reduced 2 and the Ren Mech.

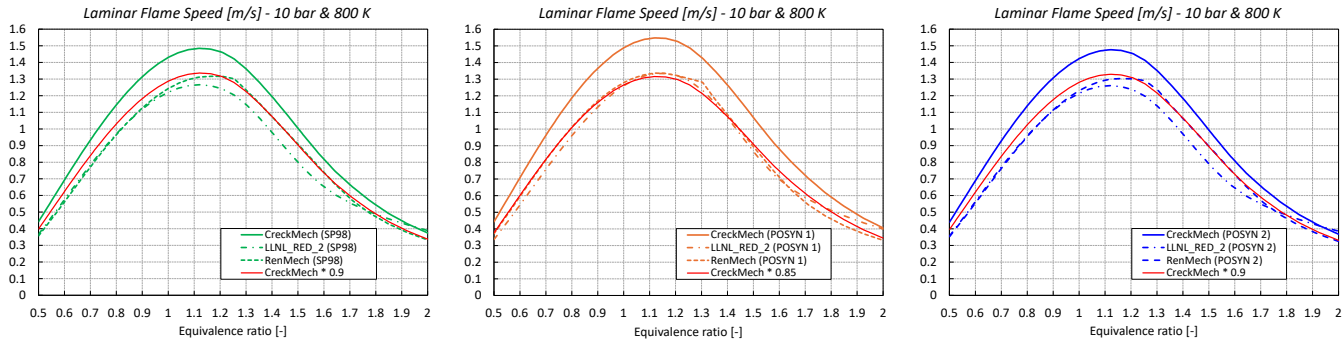

Figure 64 : A scaling factor applied to the CreckMech allowing the match to the RenMech for the three fuels. Differences are noticed between free-aromatic fuels Vs majorly paraffinic and iso-paraffinic ones (EPIONA compositions)

To complete the mechanism selection, the LLNL-Reduced 2 and the Ren Mech. ones are applied to calculate the LFS of the three fuels at the same previously considered condition (10 [bar] and 800 [K]); results are reported in figure 63. Non-negligible differences are detected comparing the full mechanism with the reduced ones, with a lower LFS estimated by the reduced mechanisms for all the considered fuels. This result is in line with the one from Hu et al. [206], showing a slight overestimation of the flame speed by the CRECK mechanism compared to others, including the LLNL one. Talking about trends, the lightest mechanism (Ren Mech.) is slightly closer to CRECK Mech., with results that appear downshifted. The LLNL mechanism underestimates the LFS reduction moving towards rich mixtures, as reported by Mehl et al [132], showing a slightly different shape of the bell.

5.5 Results: Ignition Delay Time (IDT)

Before analyzing the results in terms of IDT for the three considered fuels, some preliminary analyses aimed at characterizing the autoignition properties of the oxygenate compounds are reported. It is well known that both ethers and alcohols act as octane enhancers; however, different outcomes are found in the literature when comparing the RON/MON values of ethanol, ETBE and MTBE. A literature survey is then performed and the main results are summarized in Table 20 [22,205,206, 207].

All the studies agree with the conclusion that MTBE and ETBE have similar octane ratings; Ethanol, despite lower RON results, provides similar levels of octane improvement compared to ethers. Following experimental evidence, the expectation is that, from the simulation side, the most knock-resistant (higher IDT) compounds should be the ethers. In fact, according to Badra et al. [228], the higher the octane number (ON), the higher the IDT.

Table 20: References for RON/MON values of oxygenate compounds following literature survey

	RON	MON
MTBE	119 – 117	101 - 101
ETBE	120 - 117	102 - 101
ETHANOL	109	90

Selecting an engine with reasonably high-pressure conditions (70 [bar]) and a stoichiometric mixture, IDTs of pure oxygenate compounds are calculated at different temperatures and compared in figure 65. Increasing temperature, the higher IDTs of both ethers compared to ethanol confirm the RON/MON expectations. While ETBE exhibits higher IDTs with respect to ethanol on the overall temperature range, a high NTC region is noticed for MTBE, which results in a higher tendency to auto-ignite at lower temperatures with respect to Ethanol. Such an unexpected trend comparing MTBE and Ethanol can also be partially attributed to the overestimation of Ethanol IDTs at low temperature, which is well visible from the validation study reported in hereafter in figure 65. The prominent NTC behavior of MTBE is also assessed by a recent study of Jin-Tao Chen et al. [215], confirming the validity of the results obtained with the selected mechanism.

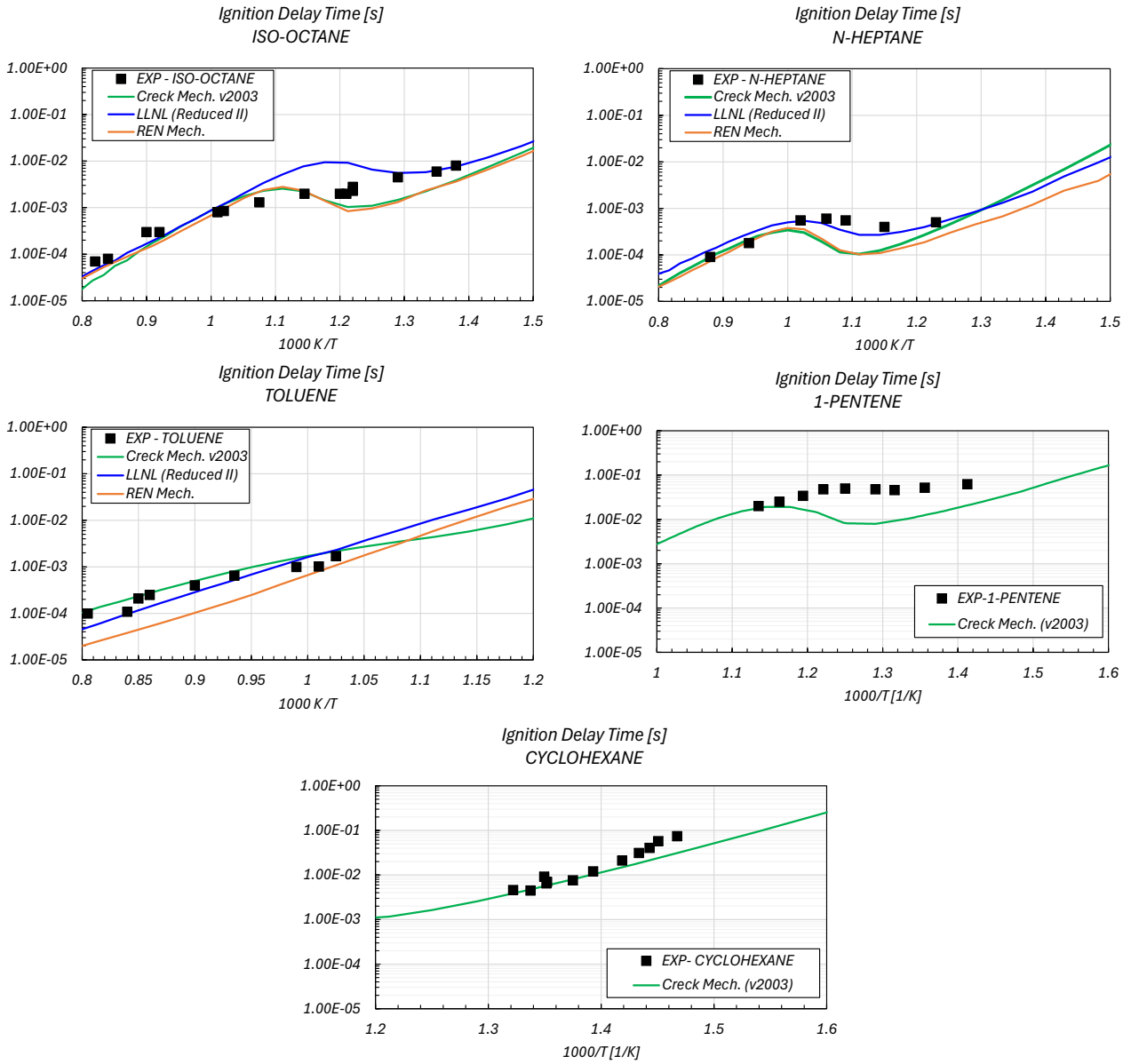

Figure 65: CFD/EXP calculation and comparison of three mechanisms for hydrocarbons of fuel surrogates at a specific pressure from literature-reported experiments (Isooctane - 36 [bar] [229], N-Heptane - 42 [bar] [177], for Toluene 47 [bar] [177], 1-Pentene at 6 [bar] [230], and Cyclohexane at 40 [bar] [231]

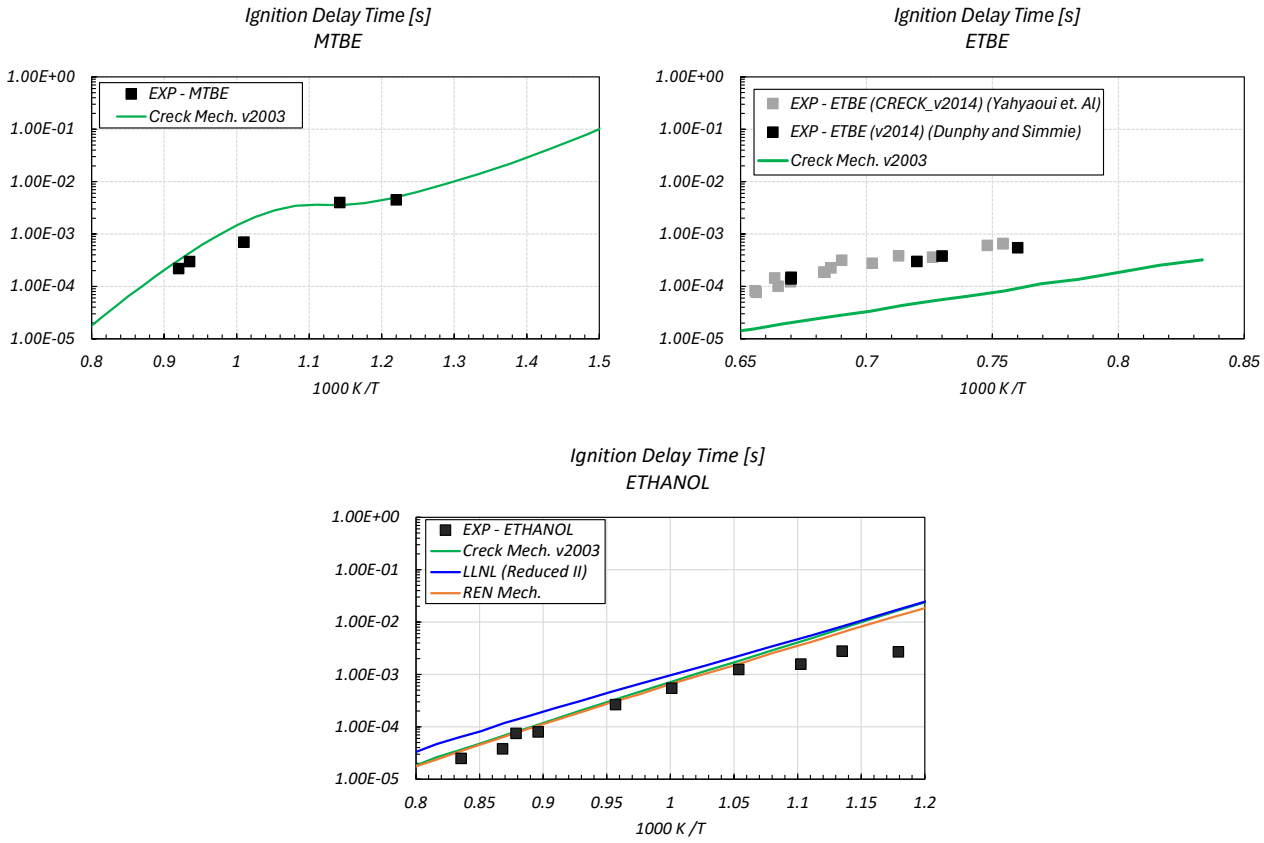

Figure 66: CFD/EXP validation of three mechanisms of oxygenate compounds of fuel surrogates at a specific pressure from literature-reported experiments (Ethanol 30 [bar] [178] and MTBE and ETBE, respectively, at 34 [bar] [231] and 3.5 [bar] [232,190])

The comparison between the autoignition tendencies of pure oxygenates compound allows us to draw some preliminary conclusions: ETBE and MTBE are characterized by similar IDTs especially at high temperature confirming literature results [205,206,233]; thanks to the prominent NTC behavior, the reactivity of MTBE at high temperatures reduces, despite the lower IDTs at low temperatures compared to ETBE; ethanol is highly reactive compared to ethers confirming experimental evidence on RON/MON tests [205,228]. A similar study is extended to pure hydrocarbons at the same pressure conditions, considering that oxygenate compounds are not the only factors driving the autoignition tendency of a real fuel. The main results are reported in figure 67. Among the hydrocarbon families, the more relevant one as RON enhancer is the aromatics i.e., toluene in this case, with a RON at the same level as ethers (toluene RON=120). This is well confirmed by the simulations, showing significantly higher IDTs for toluene. Regarding the other hydrocarbons, extreme positions are covered by iso-octane, on the high octane number side, and n-heptane on the low one. The remaining compounds lie between iso-octane and n-heptane.

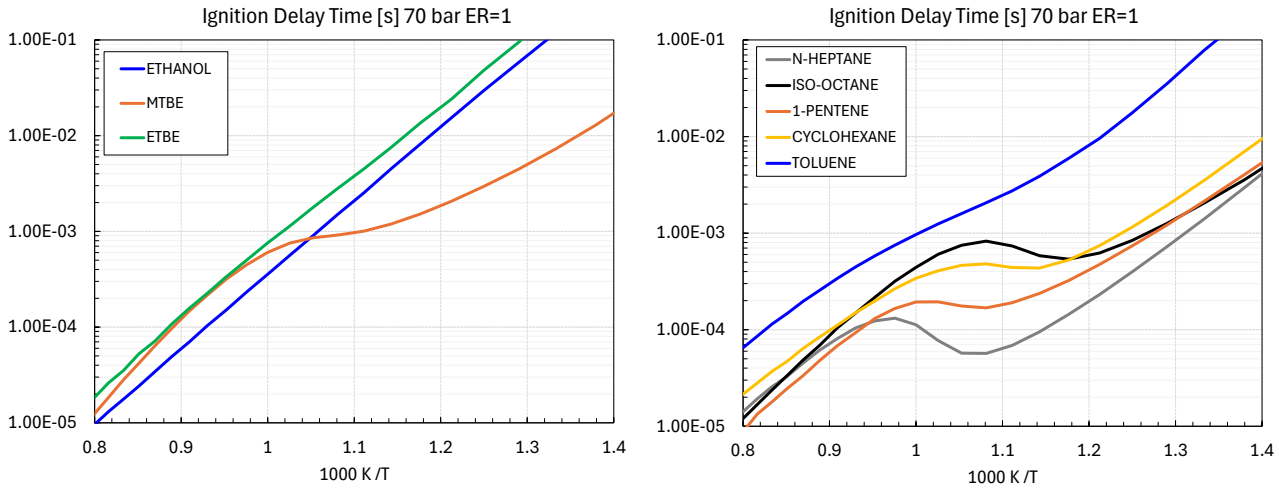

Figure 67: Ignition delay time calculations performed at the same pressure/equivalence ratio to compare each hydrocarbon and oxygenate compound

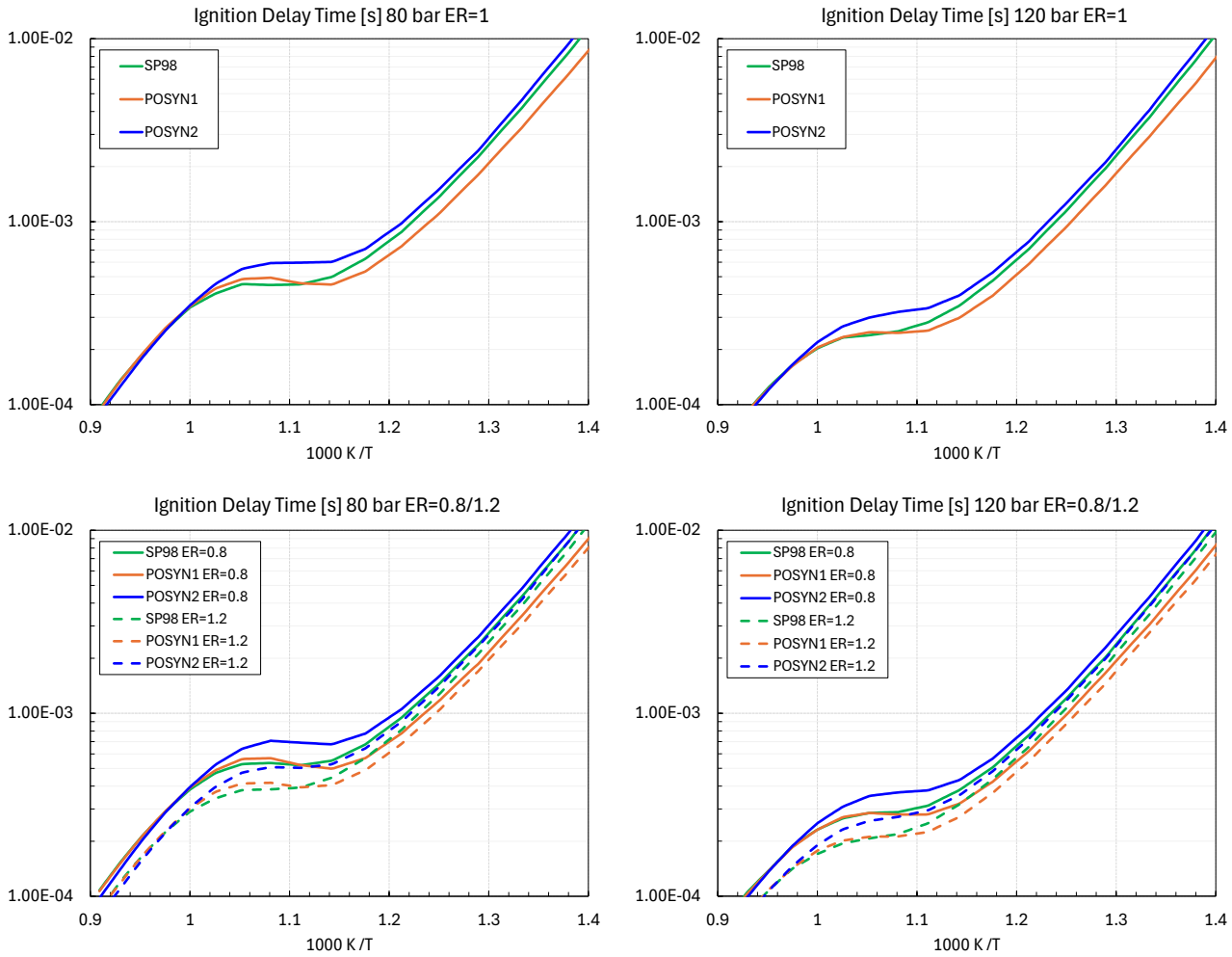

Figure 68: Ignition delay time calculations with the CRECK Mech. v2003 at different operative conditions of pressure and equivalence ratio for each fuel

IDTs at engine-relevant conditions are calculated to assess the autoignition propensity of the two synthetic fuels, which is then compared to *SP98*. The main results are summarized in figure 68 at two different pressure levels (80 bar and 120 bar) at stoichiometry and slightly lean/rich mixtures (ER=0.8 and 1.2). At first look, the three considered fuels show quite similar behaviors, confirming the similar measured AKI and RON/MON indices. Due to the peculiar MTBE behavior (figure 60) and the absence of aromatics in the mixture, *POSYN1* results in the highest reactivity at low temperatures; this is valid at all the considered pressure levels and mixture qualities. Nevertheless, the high-paraffinic content coupled with the almost null aromatics and the presence of MTBE are responsible for the more pronounced NTC behavior of *POSYN1* (confirmed and characteristic of low-sensitivity fuels), which leads to an increase of IDTs at high temperatures, resulting in higher RON. On the contrary, similar and less pronounced NTC behavior is observed for *SP98* and *POSYN2* due to their similar compositions, aromatic behavior and higher sensitivity. Comparing the two *POSYN* fuels, the higher IDT of *POSYN2* at low-to-mid temperature is in good agreement with the different behavior of MTBE compared to ethanol up to 950 K; the opposite trend (lower IDT) at high temperatures is also in good agreement with both the characteristics of the oxygenate compound and the lower NTC behavior of *POSYN2.* As mentioned, this is in agreement with the highest sensitivity due to the high aromatic content. A less intuitive behavior is noticed comparing IDTs of *POSYN2* and *SP98,* in which the difference in oxygenate compound would suggest higher IDTs for *SP98* compared to *POSYN2*. This can be partially attributed to the higher cyclohexane and lower n-heptane content of *POSYN2*, together with a possible overestimation of the reactivity of ethanol at low temperatures, as visible in the validation study reported in figure 66.

Although some differences are observed, the overall behavior of the three fuels in terms of IDTs at engine-relevant conditions appears quite similar. This similarity makes it challenging to rank the fuels based on their expected knock tendency. In this context, the importance of accounting for the real chemical characteristics of the oxygenate compounds becomes evident, as further simplifications in the fuel surrogate could lead to misleading conclusions when the actual differences between the fuels are minimal.

The most significant variations, highlighted by the logarithmic scale in the graphs, are observed at low temperatures, where IDTs are longer and have less impact on engine knock tendency. At high temperatures, the lower reactivity of *POSYN2* is confirmed by the results. This preliminary analysis lays the groundwork for more detailed CFD studies, using both 1D and 3D-CFD, aimed at characterizing the knock tendency based on actual engine conditions and actual physical fuel properties such as the volatility. Nevertheless, the proposed methodology to identify a fuel surrogate and a chemical mechanism enables the calculation of a wide IDT database, which in turn can serve as input for more refined assessments of engine-specific knock tendency across different fuels.

5.6 Results: Laminar Flame Speed (LFS)

This section presents an analysis of the LFS results obtained using the Ren mechanism for the three considered fuels. The LFS is calculated across a wide range of physical conditions to encompass various engine operating scenarios, including high-pressure and high-temperature conditions. Additionally, different mixture compositions are considered, covering both very lean and rich conditions, which may occur in GDI engines subject to high charge stratification. Results for selected significant pressure-temperature pairs are shown in figure 69.

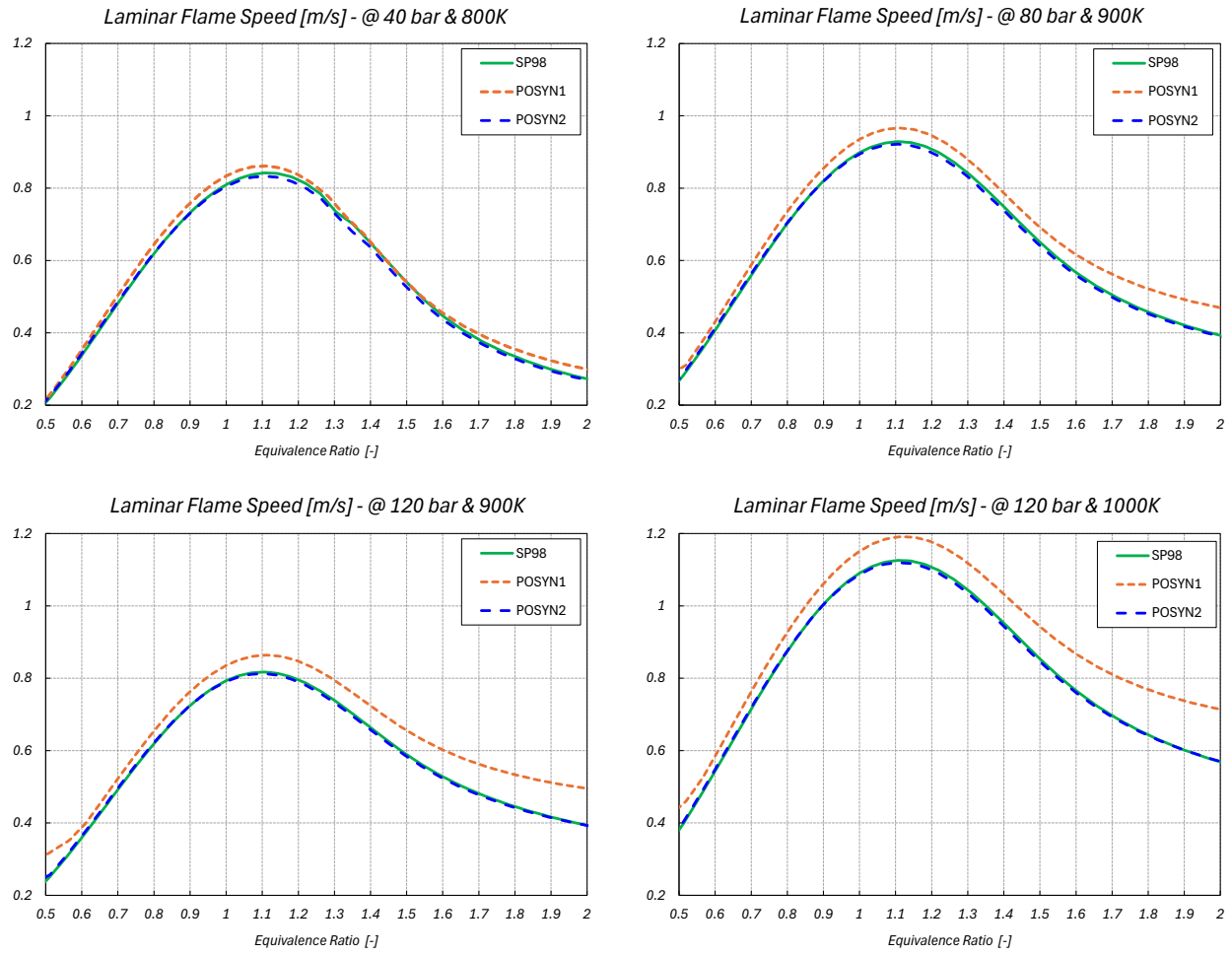

Figure 69: Laminar flame speed calculations at different pressure and temperature conditions for the three fuels

As for IDTs, differences and similarities can be noticed for the different surrogates comparing the fuels across varying pressures, temperatures and equivalence ratios. Considering that an EPIONA formulation is applied to describe the actual fuels, the differences are now driven by the different compositions, rather than by the chemical characteristics of the oxygenate compound.

Due to their quite similar composition, *SP98* and *POSYN2* are characterized by very similar LFSs across a wide range of physical conditions. Larger differences are found for *POSYN1,* which presents a higher flame speed. Differences in the aromatics content of the fuels explain the results. *POSYN1* is aromatics-free, while *SP98* and *POSYN2* contain a significant quantity (over 25%). Aromatics react differently from aliphatics, especially during combustion/oxidation [234]. Specifically, toluene turns

into a benzyl radical, which greatly reduces the flame speed (LFS), placing toluene as the lowest LFS performer in gasoline, compared to alkanes (n-heptane + iso-octane), alkenes (1-pentene) and cyclic hydrocarbons (cyclohexane). According to the hydrocarbon percentages (table 18), *POSYN 1* is confirmed to be the best LFS performer among the three fuels.

To further analyze the higher laminar flame speed of *POSYN1*, the relative difference between the laminar burning characteristics of *SP98* and those of the *POSYN* fuels is evaluated under varying pressure and temperature conditions. The results of this analysis are presented in figure 70.

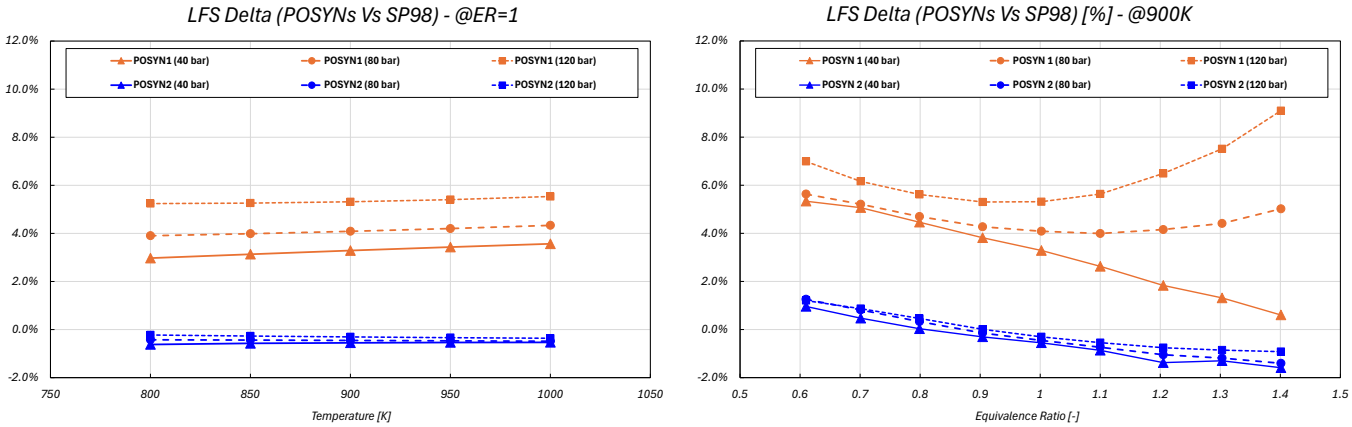

Figure 70: Laminar flame speed delta between POSYN fuels and the reference Super Plus RON 98. The delta% is reported based on temperature and equivalence ratio variation

At stoichiometry, *POSYN1* LFS is from 3% to 5.5% higher than *SP98*. Varying the temperature, the delta is almost constant, while it increases moving towards high pressure levels, which means that the LFS reduction due to pressure rise is lower in *POSYN1* compared to *SP98*. The similarity between *SP98* and *POSYN2* in terms of flame speed is further confirmed by the maximum delta of 0.6% between the two in the overall range of considered conditions at stoichiometry.

The analysis also shows a non-negligible sensitivity to mixture composition, i.e. to the equivalence ratio. Comparing *POSYN1* and *SP98,* higher differences are found moving towards rich mixtures with a strong sensitivity to pressure. At high pressure (120 bar), the delta between the fuels is higher for rich mixtures compared to stoichiometric ones, peaking around 10%. On the contrary, at lower pressure (40 bar), the delta between *POSYN1* and *SP98* reduces moving from lean to rich mixture compositions. Albeit reduced, a similar trend is also visible comparing *SP98* and *POSYN2*. These results highlight the advantage of a chemistry-based characterization of the fuel behavior across different conditions in comparison with rigid scaling factors typical of analytical correlations to provide a reliable prediction over a wide range of engine operations (pressures, temperatures and mixture stratifications).

The impact of EGR dilution on LFS varying the fuel composition is also considered, repeating the calculations at 10%, 15%, up to 20% EGR level. Starting from the LFS at zero EGR, it is possible to calculate an EGR scaling factor named K_{EGR} following the definition reported in Equation 1, representing the LFS downgrade for each percentage point of EGR dilution.

$$K_{EGR} = \left(1 - \frac{LFS_{EGR\%}}{LFS_{REF(EGR=0)}}\right) * \left(\frac{1}{EGR\%}\right) \qquad \textit{Eq. 99}$$

Where $LFS_{EGR\%}$ and $LFS_{REF(EGR=0)}$ are respectively the laminar flame speed at specific EGR and at the stoichiometry as well as the $EGR\%$ responds to the exhaust gas recirculation fraction.

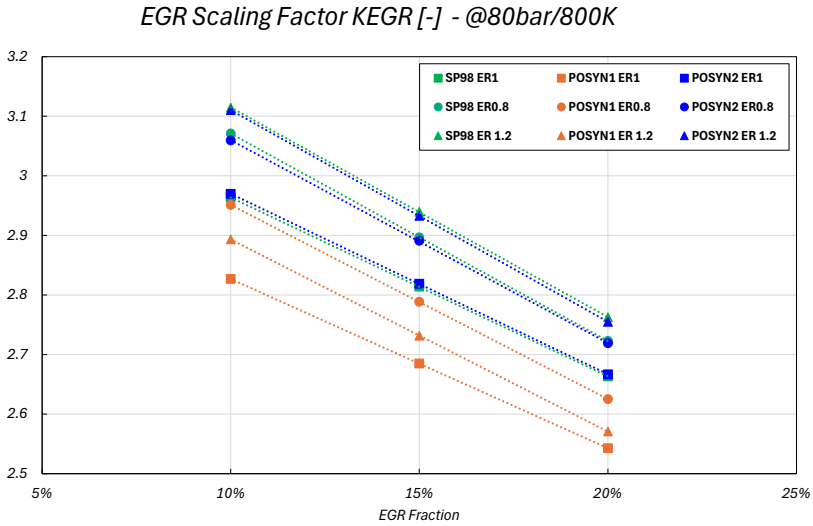

Figure 71: EGR scaling factor for LFS at different conditions of equivalence ratio and EGR

The linear reduction of LFS increasing the EGR level is confirmed for all the fuels, as reported in figure 71. K_{EGR} is not constant, as it decreases for increasing levels of dilution. This means that the reduction of LFS is relatively higher for low dilutions rather than for higher ones. Comparing the fuels, in non-diluted conditions, a very similar EGR effect on LFS is found comparing *SP98* and *POSYN2,* while a different behavior is noticed for *POSYN1*, with lower K_{EGR} values at the three different conditions considered. The results suggest a higher tolerance of *POSYN1* to EGR dilution.

5.7 Application on an Internal Combustion Engine – 4 Stroke

The work performed and described in the previous paragraphs of this block strictly responds to real applications in the automotive sector, especially, linked to the automotive industry. The e-fuels considered, as well as the SP98 gasoline, have also been tested in a high-performance TJI engine, which, for confidentiality reasons, cannot be described in detail. Nevertheless, for the sake of completeness, the previously considered fuels, calculated with the methodology proposed, were adopted for computational evaluation against experimental evidence from the test bench. Before providing some of the details pertaining to the application on the real TJI architecture engine, the previously mentioned calculations are reported in a wide range of applicability related to the conditions of the engine's operative conditions. An example, representative of the vastness of the combination of the relevant properties (P, T, Equivalence Ratio, EGR) that characterize an ICE and the fuel's combustion characteristics, is reported in figure 72.

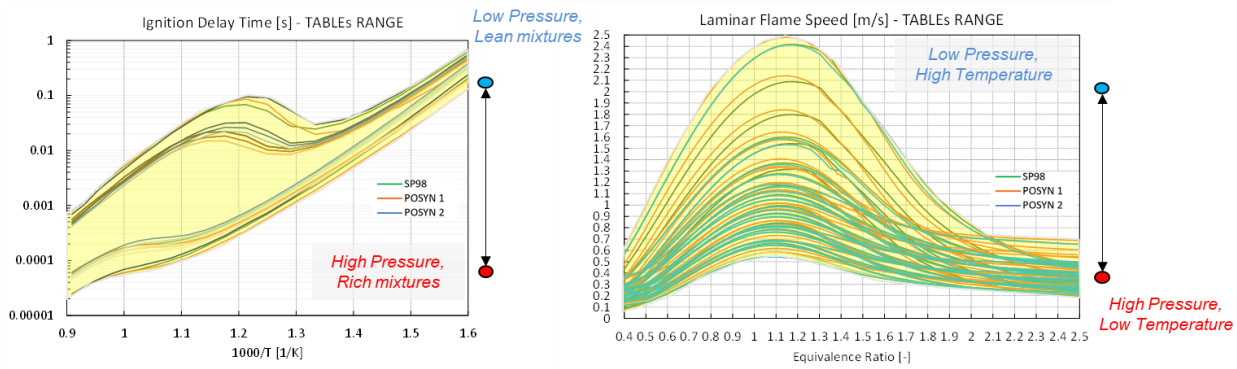

Figure 72 Example of the range extension of the IDTs and LFS with the different fuels and varying the operative points of P, T, equivalence ratio and EGR.

The engine at the bench, single cylinder derived from the real engine, is tested and reported in this block in terms of the in-cylinder pressure plot. The engine at the test bench was fed with only gasoline

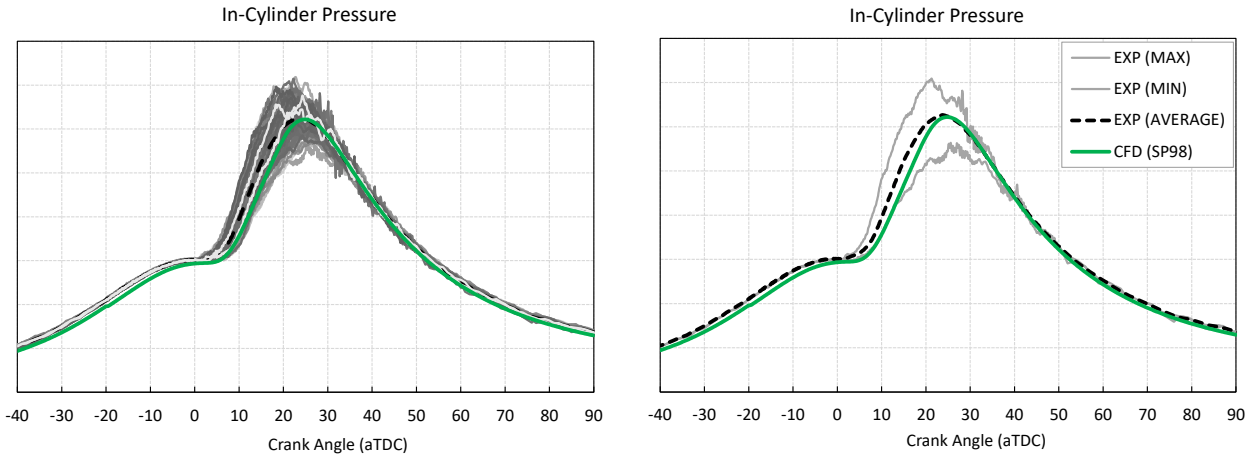

Figure 73 Pressure development of the high-performance engine comparison between 3D-CFD and EXP.

SP98, in the first campaign of the experimental analysis, with the target to enrich the experimental evaluations to e-fuels in the near future, adopting the predictive models and, currently, adopting for the SP98 the currently calculated and tabulated LFS from this work from a modelling standpoint. Across the results, due to the restrictions from the Porsche AG company, the values of the in-cylinder pressure are removed from the plot, but for the sake of the comparison, a qualitative and consistent analysis of the reliability and predictiveness of the methodology previously described in achieving the target of averaged in-cylinder pressure development is clearly achieved and reported in figure 73.

Furthermore, in the next figure 74, a detail of the instantaneous and cumulative heat released during combustion reinforces the combustion predictivity of such a peculiar engine architecture, the TJI engine, for high-efficiency applications and high-performance power output. This further emphasizes the reliability and consistency of the LFS modelling, combustion predictivity and modelling approach in real applications, compared to CFD and EXP. Lastly, the comparison in terms of pressure development is reported for the three different fuels reported in the previous study. Note that the pressure experimental benchmark is reported for only SP98 fuel according to the confidentiality of the data. Nevertheless, it can be widely noted that the pressure increases the peak only with the free-aromatic fuel, according to the faster flame development characteristic of the E-fuel (POSYN1).

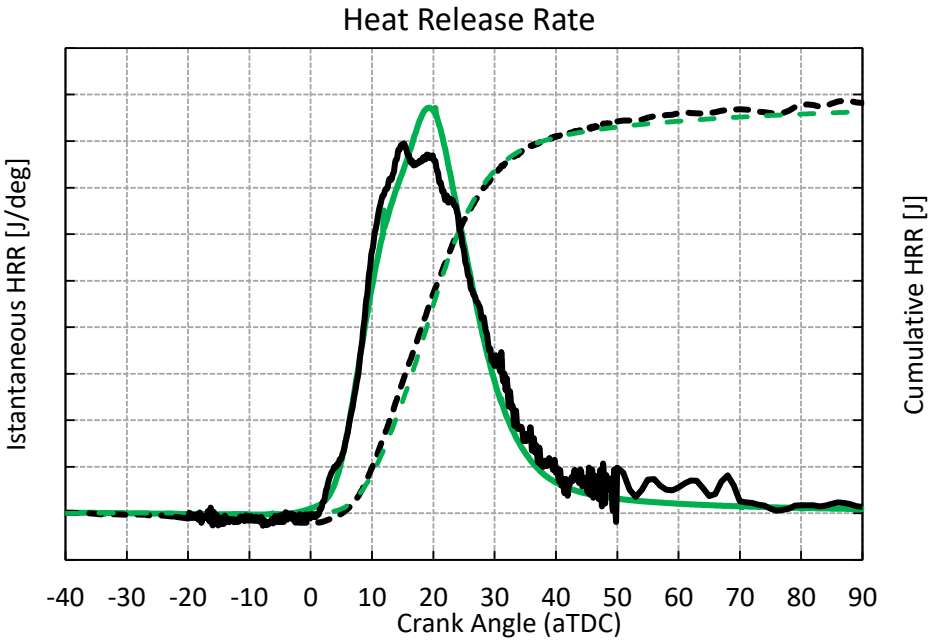

Figure 74 Correlation of the instantaneous and cumulative heat release rate.

Finally, focusing on the single fuel here considered consistent with the experiments, the MFB is also reported to further analyze the benefit of calculating the realistic LFS of the current SP98.

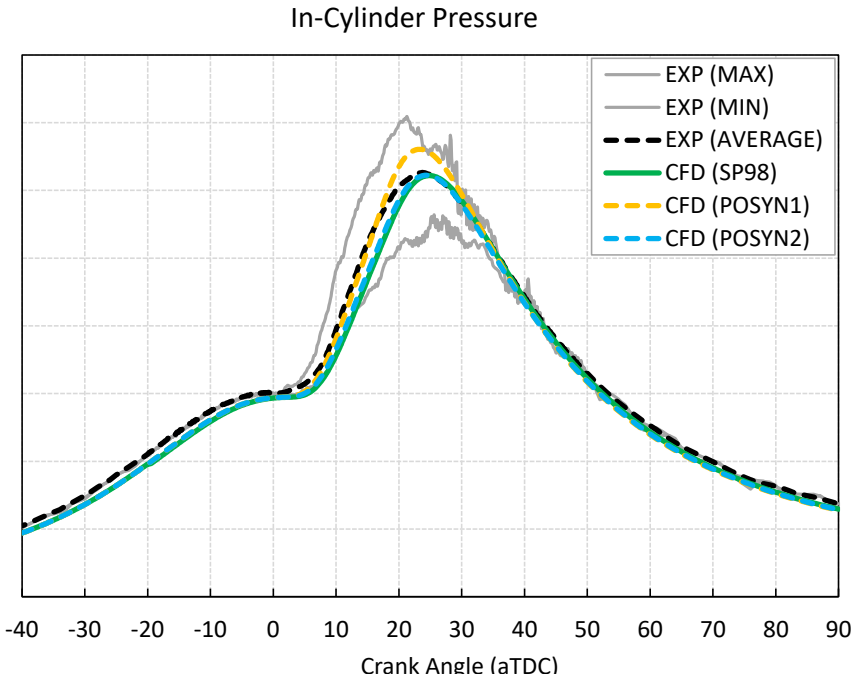

Figure 75 Comparison of the three different fuels based on the same operative conditions. For the sake of confidentiality, the test bench results are reported only for SP98.

5.8 Application on an Internal Combustion Engine – 2 Stroke

The new frontiers of ICE technology, of course, are large and wide, represented by all kinds of endothermic engines that we can find in the market. Specific applications can also be of great importance, although they are not under everyone's eyes. Let’s think about specific applications from shipping, flights, raw material transportation, but also gardening applications in most remote areas of the World. So, electrification is a promising way for those applications that involve, generally, small engines. Nevertheless, electrification is quite difficult to implement in such places where low weights are fundamental, as well as a low possibility to take with the operator a lot of equipment. Hence, talking mainly about small engines for gardening applications, some restrictions will be imposed more and more to guarantee low emissions in areas where it is fundamental to affect as little as possible. Here, low carbon fuels as well as the previously described e-fuels take a fundamental role in reducing fuel emissions, pollutants while maintaining the performance of fuelled engines. The following study focuses on a real application of e-fuels on a production engine (two engines in the specific case, despite being reported in detail for one of the most significant ones). This application is based its fundamental on the fundamental calculations from a 3D-CFD standpoint from the specific chemical calculations of the real gasoline. Next, the outputs from the chemical kinetic results will be adopted as the input in the 3D-CFD environment. The aim of this study, reported in detail in the related publication by the author of this PhD and co-authors in [31], is to demonstrate that e-fuels achieve comparable performance and emissions profiles to gasoline, indicating their potential as a drop-in replacement for conventional fuels in existing engine technology. The results are extensively validated on a test bench database, resulting in a well-aligned output.

5.8.1 Synthetic fuels – Fossil Fuels E10 / E-FUEL

This activity embraces the direct application of the methodology developed by the author and colleagues in [32] and aims to give a response to the application of the methodology in a real two-stroke ICE. To carry on this target, real fuels as well as e-fuels from CAC Engineering GmbH have been considered. Particularly, low-carbon fuels with ethanol-blended gasoline will be explored, targeting the reduction of greenhouse gas emissions together with the improvement of the combustion efficiency. The technology is based on the CAC METHAFUEL® process, developed by CAC Engineering GmbH and through which the synthetic gasoline is produced from renewable methanol in accordance with the standard following the DIN EN 228. The process through which renewable fuels, and specifically e-fuels, are reported in the previous part of this work, although it could be slightly different or the process could follow slightly different processing to reach the same or better output. Here, the essential feature of the process is the adoption of a tube bundle reactor cooled with molten salt.

A brief schematic description is reported in figure 76:

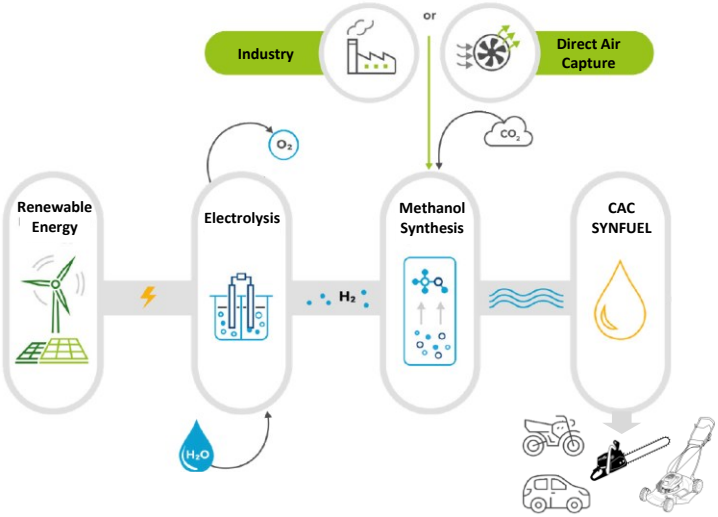

Figure 76 The simplified process for producing synthetic fuels (synfuels) at CAC Engineering GmbH.

Referring to the main stage of the process and referring to the final output, which is, for us, a performing gasoline to adopt in ICEs, the improved control over the process and greater flexibility are the first of the pros. Secondly, and most important from ICEs standpoint, the direct cooling of the highly exothermic reaction is a key point to enhance the properties of the fuel from resistance to knock (high RON). Then, the entire process as mentioned, is flexible and allows for reducing the heat dispersion, reusing the heat to generate steam for the internal process and exporting the generated excess steam to be adopted again in the production line.

The e-fuel obtained has some peculiar characteristics which are reported briefly hereafter:

- *Benzene content is < 0.5 vol. %*
- *Durene content is < 1 vol. %*
- *Total aromatics content is between 25-35 vol. %*
- *Olefins content is between 4 – 12 vol. % despite the preferred from production is < 10 vol. %*
- *With e-Methanol adoption, the gasoline is sulphur-free*
- *RON is at least 95, considering the addition of not more than 10 vol. % of bio-ethanol*

These major considerations are alongside the possible reduction in terms of greenhouse gas emission by up to 90% compared to the reference value for fossil gasoline according to the reference from REDII (94 g_{CO_2}/MJ). To bring to mind that the current specifics for reduction in greenhouse gas emissions for renewable bio-fuels is at least 65% (REDII), for renewable fuels of non-biogenic origin the value is set to at least 70% (REDIII).

The two fuels adopted for the following test are reported as surrogate compositions in table 21:

Table 21 Composition of synthetic surrogate fuels

Hydrocarbons	***Fuel A***	***Fuel B***
Paraffins	*4.5%*	*5.5%*
Iso-Paraffins	*51.9%*	*42.5%*
Olefins	*3.2%*	*2.8%*
Naphthenes	*11.4%*	*9.1%*
Aromatics	*26.4%*	*27.4%*
Unknown & C15+	*2.0%*	*2.9%*
Oxygenates	*0.6%*	*9.8%*

Despite the interest in aromatics reduction as visible in Fuel A, fuel B is preferred due to the oxygenate percentage being higher compared to the counterpart A. Briefly, fuel A is characterized of being a synthesized fuel from fossil-based methanol and has a RON of 88. The second and selected one to be adopted in ICEs is derived from bio-methanol reaching at least the RON 95. Furthermore, the presence of oxygenates compounds is in line with most of the current standards for gasoline, nd in order to a fair comparison with the counterpart from fossil fuels, it has been preferred as well as respecting the DIN EN 228 [11,235].

5.8.2 CFD approach and chemical kinetic assessment/calculations

The definition of the most appropriate fuel surrogate is fundamental when referring to CFD calculations, especially targeting promising and well-aligned results related to the experiments. The previous section has already described our methodology for fuel surrogate definition. Nonetheless, the evaluation of the major properties from combustion and knock point of view is widely treated and will be recalled here since the combustion process is considered between fossil fuels and e-fuels. More specifically, for combustion simulation in this section, we will refer to fuel surrogate chemical kinetic simulation and composition, as reported in table 22:

Table 22 Fuel surrogate definition. A comparison between the adopted Fuel B and commercial gasoline

Surrogate Specie	***Fossil High Premium Gasoline***	***Fossil ULG95 Gasoline [176]***	***Fuel B***
Paraffins: N-Heptane	*11.0%*	*10.70%*	*5.66%*
Iso-Paraffins: Iso-octane	*34.7%*	*35.10%*	*43.77%*
Olefines: 1-Pentene	*5.5%*	*5.70%*	*2.88%*
Naphthenes: Cyclohexane	*5.3%*	*10.90%*	*9.37%*
Aromatics: Toluene	*30.3%*	*31.70%*	*28.22%*
Oxygenates: Ethanol	*13.2%*	*5.90%*	*10.09%*

Some further information about the selected fuels is reported in the table below:

Table 23 Properties of the synthetic gasoline compared to the commercial one

	Fossil RON 98	***Synthetic Fuel B***
Equivalent Molecule	$C_{6.95}H_{13.11}O_{0.12}$	$C_{6.3}H_{10.9}O_{0.21}$
Molecular Weight [g/mol]	*98.5*	*89.8*
H/C	*1.89*	*1.73*
O/C	*0.017*	*0.033*
LHV [MJ/kg]	*42.2*	*41.35*
A/F (st)	*14.24*	*13.7*

The six-component surrogates are reported for three of the two considered fuels for this section. This consideration is due to the fact that the fossil fuel adopted in the experiments is not available from composition. For this reason, we reported three available compositions of gasoline from testing and literature to assess the comparison from CFD to experiments according to the similar composition of the real fuels adopted in experiments (RON 95, European standard). Some chemical calculations are reported between Fossil Fuel RON 98 and Synthetic Fuel B at different pressure conditions in line with the real engine operations and reported in figure 77:

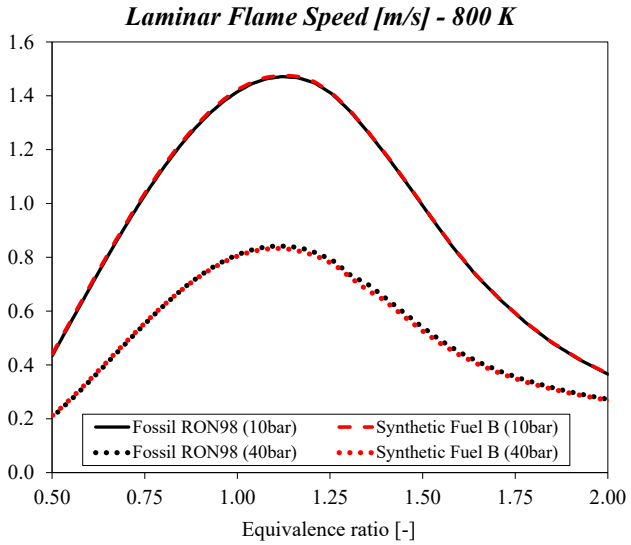

Figure 77 Detailed chemistry derived LFS and comparison between gasoline fossil RON 98 and synthetic fuel B

The chemical kinetic simulation carried out following the methodology in [32], shows very similar results from laminar flame speed at engine-like conditions, confirming the feasibility and reasonably aligned results according to the similarity in the gasoline composition. Hence, from this first outcome, the results from a combustion standpoint should be reasonably similar when using fossil fuels or e-fuels. Of course, it will also be interesting and of fundamental importance to evaluate the performance between the CFD-EXP comparison and the impact of the fuel adopted on the CO/CO_2 emissions (in this case, only from experiments).

5.8.3 From the test bench to CFD

The experimental layout and testing activity have been conducted with two engines, despite the fact that only one engine, engine B, is currently in production in EMAK S.p.A. (EMAK company). The engine B is a two-stroke engine with stratified scavenging characterized by higher displacement, compression and target performance compared to the engine A. The test facility consist majorly of an air exchange system, a cooling system that allows maintaining the temperature around the specifics of the engine test and the exhaust extractor.

The core of the test bench consists of a dynamometer MAGTROL ED-815 (hysteresis dynamometers) with a maximum capacity of breaking power of 7 [kW] and 1200 [rpm] of maximum revving speed. The post-processing is performed through many piezoelectric pressure sensors installed one inside the combustion chamber to detect the data of combustion and the other one in the crankcase. A dedicated amplifier is then considered coupled with the sensors. Then, the signals are acquired in this case by using a customized data acquisition system of proprietary and developed in-house by EMAK S.p.A., based on LabVIEW software and National Instruments Hardware.

The pressure sensors adopted for this scope are the following ones:

- Kistler 6052C (combustion chamber/high pressure sensor);
- Kistler 4007D (carters/low-pressure sensor);

The fuel consumption is evaluated through a dedicated measuring system from AVL 733 gravimetric fuel flow meter, with the fuel tank placed above the flow meter. The accuracy of this instrument is guaranteed at 0.12% under real test bench conditions.

Pollutant emissions analysis, which is measured from the test bench, despite not being simulated in this work, is a key aspect related to the combustion efficiency and impact on greenhouse gas and pollutant emissions. The Horiba Mexa 7170D gas analyser coupled with the Raw Gas Method (RGM) describes the approach of the testing nd results. The output concerns both the CO, CO_2 and NO_x, plus the total hydrocarbons (T-HC).

The experimental campaign as well as the accordance through the CFD simulations are considered at the 9000 [rpm], despite the full experimental campaign falls into a range of revving speed between 6000 and 10000 [rpm] with an incremental step of 500 [rpm].

5.8.4 3D-CFD Assessment

Starting from considering the mesh and overall setup of the CFD simulations, it can be noted that the simulation assessment comes primarily from the fidelity of the CAD of the real engine B. Furthermore, the nature of the scavenging and carter pump framework of this engine, the simulation takes place with a detailed CFD numerical assessment to consider all the parts and the real flow from the carter to the combustion chamber. In fact, in figure 78, the engine from the testbed on the left-hand side and the entire CAD with its major parts from a computational standpoint.

Follows a brief description of the engine in its main parts:

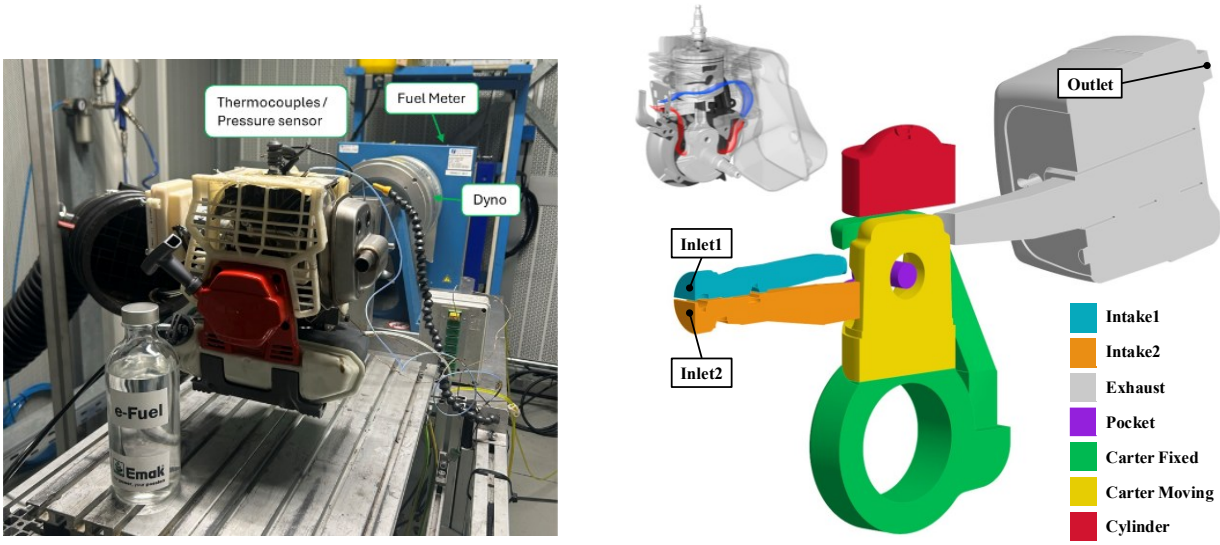

Figure 78 Test bench equipped with the engine tested (left) and CFD assessment of the specific related parts for 3D-CFD simulations (right).

- Inlet boundaries are placed downstream of the air filter and carburettor (Intake1, Intake2). The reason for the presence of two separate intakes comes from the fact that one pertaining to the Inlet1 is fed by fresh air only. The other one, pertaining to the Inlet2 boundary, is fed by a predetermined lambda over imposed value. Together, the intakes fed the combustion chamber, providing the lambda target for the best combustion process.
- Crankcase or Carter: the carter can be divided into fixed and moving parts. The volume is simplified in an equivalent volume that takes into account the real encumbrance of the carter pump from the real geometry engine. Hence, the piston motion thus allows to mimic crankcase volume variation during the engine cycle and achieving the pumping effect.
- Cylinder: the cylinder part consists of the chamber inside which the combustion takes place in accordance with the movement of the piston crown.
- Pocket: classic approach and framework for a two-stroke engine, the pocket makes in communication between the intake1 to the scavenging port. The pocket is obtained on the piston skirt.

- Exhaust: this region takes its place and functions during the phase at which the piston reaches the BDC, allowing the exhaust gas to exit the combustion chamber.

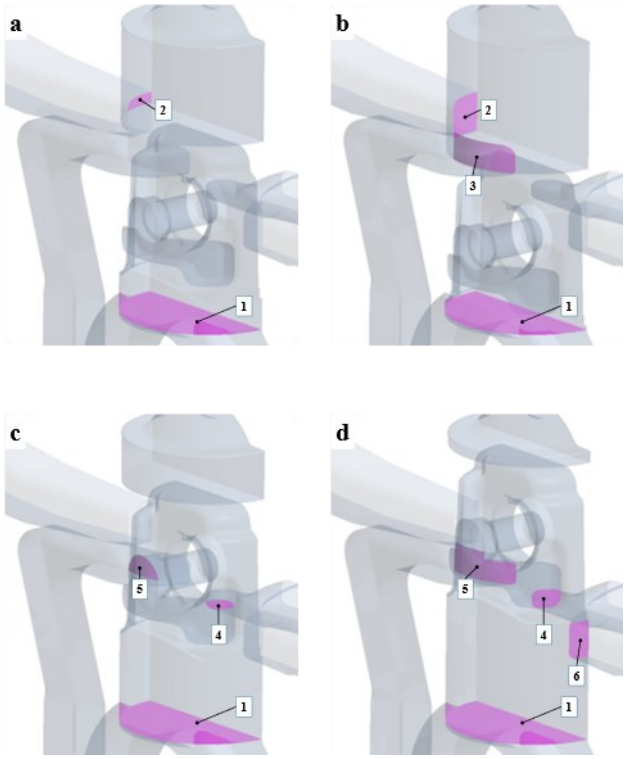

Figure 79 Schemes of the interfaces during the engine cycle

The function of the engine is briefly described, as not the aim of this section, but it is relevant to complete the process before the combustion. In figure 79, a complete overview of the workflow is reported by steps, to clearly describe the activation of each of the boundaries present in the previous description. In figure 79a, the interface 1 represents the area in between the Carter Fixed and Carter Moving, at 116.5 [CAD aTDC], exhaust starts showing the boundary that connects the combustion chamber to the ambient. Next, figure 79b, shows the connection between the combustion chamber with both the exit and interface 3, scavenge port, that introduce in the same time mass inside the cylinder at the imposed lambda. In figure 79c, the piston starts running up toward the TDC, and the connection between Intake1 and the scavenge port occurs. Here, due to the intake pressure being higher than carter pressure, the fresh air moves from 4 to 5 and dilutes the charge in the final part of the scavenge port. Finally, as reported in figure 79d, reaching the final part of the compression stroke, interface 6 finds its connection with the crankcase, allowing the latter to be filled with the fresh mixture of air and fuel.

The mesh can be observed in the figure 80, with a discretization domain made by hexahedral cells in the core region, while near the wall mesh is characterized by a two-layer approach with prismatic layers to guarantee a high-quality evaluation of the boundary layer. The calculations are made through the commercial licensed software Simcenter STAR-CCM+ In-Cylinder from SIEMENS DISW. The overall mesh resulting in almost a constant number of cells equal to 880’000 with a maximum grid size of 1 [mm] and a minimum of 0.25 [mm], though a middle o.5 [mm] related to the discretization reference of the exhaust plenum.

The setup from a physical standpoint can be summarized with ECFM-3Z with regard to the combustion modelling [236], along with the GruMo-UniMORE thermal law of the wall [237] to account for the heat rejected. The ISSIM ignition model [238] is used to predict the energy released at the spark location before flame development by the direct coupling from the ignition mode and combustion. The turbulence modelling is applied to the RNG k-ε turbulence model with its All-y+ formulation implemented in the software.

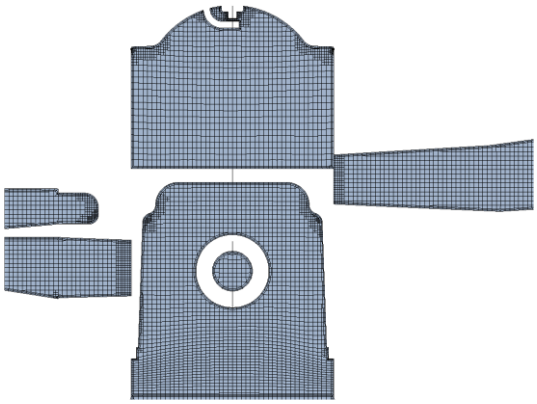

Figure 80 Detail of the computational mesh adopted for 3D-CFD simulations

5.8.5 Combustion and Performance - Results

The pressure development is one of the first and most important results that we report to compare CFD to EXP outputs. The experimental results are reported in their range from the minimum and maximum pressure peaks, according to the fact that only the lowest and maximum pressure development are reported along with the 200 consecutive cycles from the test bench. Thus, the average pressure curve comes from the average from all the realizations from the experiments. The wide range of variability is due to the characteristics of the engine tested, which is carburettor feed and is expected to be particularly high cycle-to-cycle variability. So, the results are reported in figure

81, where a good alignment in terms of pressure development from CFD is reached according to the EXP evidence.

Of the same importance is the mass fraction burned plot, reported in figure 82, which refers to the combustion efficiency and velocity of combustion between experiments and CFD led to the same

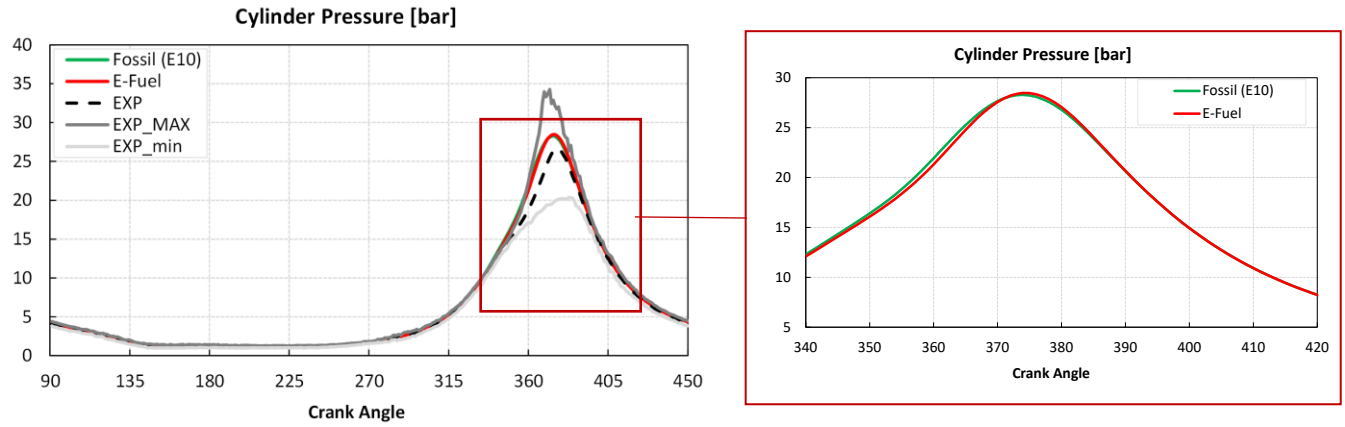

Figure 81 A comparison of in-cylinder pressure development using both fossil and synthetic fuels, including experimental data (left). A detailed analysis shows the similarity in pressure development between fossil and synthetic fuels from a CFD-only perspective (right).

outcome. Despite the early combustion phase, which seems a bit advanced compared to the average data but well inside the range of validity, great results characterize the overall combustion results.

Further imaging related to the flame development between the two cases, one with fossil fuel and the other with the synthetic one, leads to almost identical flame development, as also confirmed by the pressure development and MFB. Some Images are reported from CFD post-processing of the flame development. These results and processing can be observed in figure 84.

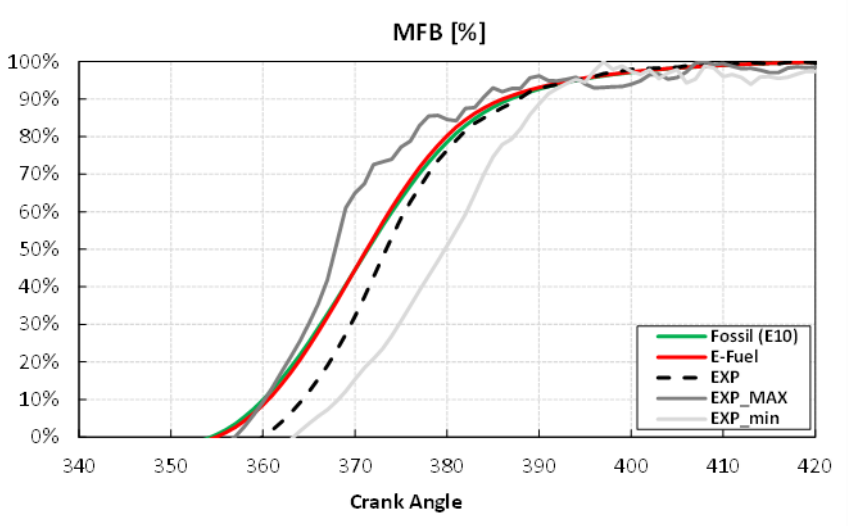

Figure 82 Combustion development is reported as the mass fraction burning shape over the crank angle. The results are reported for both experiments and CFD involving fossil and synthetic fuels.

Figure 83 Comparison of flame development from a 3D-CFD perspective between fossil fuels and e-fuels.

Finally, by comparing the CFD to the EXP and the relative behavior, visible in figure 84, it is clear that from a computational standpoint, the adoption of a synthetic/e-fuel in replacement of gasoline leads to the same power output along with the same performance and flame development in the combustion chamber.

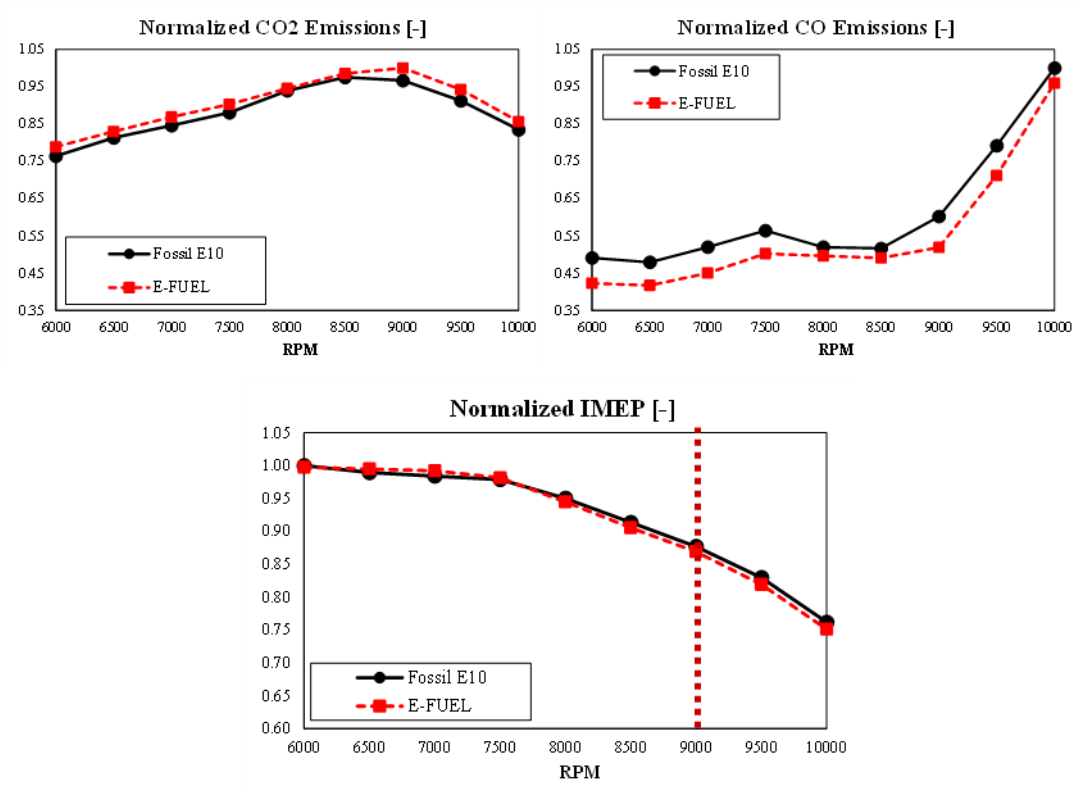

Figure 84 Experimental results related to the CO, CO_2 emissions and IMEP related to the operative conditions (dotted is the one simulated through the CFD)

These results are also supported by the experimental output from an emission standpoint, through which it is demonstrated that the overall CO emission reduces when using synthetic fuels. Moreover, it is also shown that the combustion efficiency increases due to the formation of higher CO_2 as a product of more efficient combustion compared to the fossil counterpart. In any case, the slightly relative increment of the carbon dioxide, which comes from the e-fuel supply chain, means that CO_2 emitted leads to net zero greenhouse gas emissions since the same byproduct is used to produce the synthetic gasoline.

5.9 Sum up: LFS/IDT Methodology of E-Fuels in ICEs

A 0D-1D chemical kinetics-based study is performed to calculate the LFS and IDT of e-fuels and to compare results to a commercial premium gasoline (SP98). To this aim, an OxPIONA six-component surrogate is defined together with the identification of a proper chemical kinetics mechanism. The evaluations start from IDTs, which are computed by adopting a large chemical kinetics mechanism using a detailed composition for both the hydrocarbons and the oxygenate species building up the surrogates. Such a choice proves to be mandatory to accurately forecast the impact of oxygenates on the knock resistance. Since large chemical mechanisms would be excessively CPU-expensive for the calculation of 1D freely propagating flames, the calculations of LFS are performed with reduced chemical mechanisms and using a simpler EPIONA surrogate composition. This approach is shown to be sufficiently accurate for the estimation of LFSs since the impact of oxygenate compounds below 15% in mass is negligible. The tabulated database is then adopted to simulate combustion in a 3D-CFD framework with both two- and four-stroke engines for different applications. A great correlation to the experimental database available confirmed the wide applicability of the methodology, reliability of results and feasibility with respect to the surrogate composition.

In light of the considerations that guided this work and from the evidence that is described, the major outcomes of the proposed work are summarized:

1. **The OxPIONA surrogate formulation is viable and robust** to accurately reflect the real fuel composition.
2. **For IDT calculations, it is imperative to include the real oxygenate species**; conversely, for **LFS calculations, EPIONA is suitable for the calculations** despite the different oxygenates in the analyzed fuels.
3. **Creck Mech. v2003 is selected for the simulation of IDTs**, given the presence of both ethanol and ethers; **on the LFS side, the Ren Mech. is selected** as a trade-off between the number of species/reactions, robustness, range of validation and suitability for 1D freely propagating flame calculations.
4. **The IDTs calculated for each fuel across the ranges of pressure/temperature/equivalence ratio/EGR** typical of engine conditions enable the ranking of the tested fuels in terms of knock tendency.
5. **The LFS simulations highlight that aromatics-free *POSYN1* has a faster laminar burning velocity** compared to *SP98* and *POSYN2,* which are penalized by the presence of aromatics in the composition.
6. The **tolerance to dilution with EGR is analyzed** for the three fuels across different operating conditions. A **K_{EGR} factor is defined** and calculated to simplify the comparison of the fuels at different values of temperature and equivalence ratio. The results highlight a higher tolerance to charge dilution for *POSYN1* compared to *SP98* and *POSYN2*.
7. **Tabulated data adopted in a four-stroke high-performance TJI engine.** Faster combustion velocity is achieved with the free-aromatic e-fuel (POSYN 1) and a **great correlation for the SP98 is also experienced (experimental data referred to SP98).**
8. **The same tabulated data were also applied to a two-stroke engine.** The results, again, **demonstrated a high level of correlation** and highlighted the significant advantages of e-fuels in a completely different application compared to point 7.

Publications and Congress

Publications (2022-2026):

Fontanesi, S., Dalseno, L., and Magnani, M., *"Numerical Characterization of Hydrogen Combustion in a High-Performance Engine: Potentials, Limitations, Modelling Uncertainties," SAE Int. J. Adv. & Curr. Prac. in Mobility 5(3):1322-1333, 2023, https://doi.org/10.4271/2022-24-0016*

Madia, M., Vaccari, M., Dalseno, L., Cicalese, G., Corrigan, D., Villa, D., Fontanesi, S., Breda, S., *"Assessment of Knock Tendency in a Hydrogen-Fuelled High-Performance Internal Combustion Engine: A Chemistry-Based Numerical Study," SAE Technical Paper 2025-01-8429, 2025, doi:10.4271/2025-01-8429.*

Breda, S., Fontanesi, S., Merolla, S., Gagliardi, M., Cicalese, G., V., Pati M., Dalseno, L., Kuschel, M.*, "Assessment of E-Fuels Applicability as Gasoline Replacement in a Small Two-Stroke Engine," SAE Technical Paper 2025-32-0058, 2025, https://doi.org/10.4271/2025-32-0058*

Dalseno, L., Breda, S., Cicalese, G., Berton, A., Tommolini, L., Villforth, J., Fontanesi, F., *Computational study of ignition delay times and laminar flame speed of POrsche SYNthetic fuels: Comparison with conventional gasoline. International Journal of Engine Research. 2026;0(0). doi:10.1177/14680874261418142*

Congress/Events:

AIMSEA 4th Winter School for PhD Students – *Fluid Machinery and Energy System Engineering, Renewable Energies, Energy Storage and Energy Transition* – March 27–31, 2023 – Pisa, Italy

Hydrogen for Sustainable Mobility Forum – Energy Center, Politecnico di Torino – October 17–18, 2023 – Turin, Italy

SAE International World Congress Experience (WCX 2024) – April 16–18, 2024 – Huntington Place, Detroit, Michigan, USA

The 29th Small Powertrains and Energy Systems Technology Conference – November 10-13, 2025 – Florence, Italy

SAE International World Congress Experience (WCX 2025) – April 8–10, 2025 – Huntington Place, Detroit, Michigan, USA

Realize LIVE Europe (Siemens) – RAI Congress Centre – June 30 – July 2, 2025 – Amsterdam, Netherlands

International Siemens Virtual ICE Conference – October 7, 2025 – Virtual International Event

Conclusions

This PhD thesis has provided an opportunity to develop insights linking modelling to real-engine behavior for next-generation internal combustion engines. With emissions reduction, particularly CO_2 and harmful pollutants, at the center of the automotive sector's environmental challenges, the insights presented here demonstrate how computational approaches can support this transition. Robust modelling strategies can reduce development costs, shorten the time required to meet governmental targets, and offer replicable methodologies capable of enhancing technical perspectives in future ICE development.

Several insights, topics, and comprehensive numerical–experimental validations are addressed throughout this work. Each "sum-up" paragraph presents the detailed outcomes of the corresponding application and modelling approach. For completeness and clarity, each major topic is summarized at the end of its respective section. Nevertheless, an overall summary is provided here to close the manuscript and introduce future perspectives.

When retrofitting ICEs, from gasoline to hydrogen, several major considerations must be accounted for. Specifically, this thesis has shown that operating with hydrogen requires a dedicated injection strategy and lambda review to reasonably achieve laminar burning velocity and feasible pressure development and peak compatible with thermo-structural resistance. Then, proper valve control, combustion phasing and a carefully evaluated spark time and compression ratio to achieve operating conditions avoiding knock but maintaining consistency with performance and power output. The temperature reached in the combustion chamber, as well as that of the surrounding surfaces during and after combustion, is directly correlated with abnormal-combustion risk. NO_x emissions, directly influenced by temperature, can be mitigated through correct EGR or PWI management, which increases resistance to NO_x formation and reduces the propensity to detonation. Hotspot surfaces play a critical role in this context: limiting maximum temperatures at the exhaust valve and spark plug, ideally using cold-type spark plugs, proves beneficial. Modelling supports these evaluations when combustion is coupled with chemistry-based simulations using appropriate models and well-structured chemical-kinetics methodologies.

Furthermore, accurate prediction of mixing and fuel distribution at TDC is fundamental, as deviations in mixture stratification can significantly affect agreement between simulations and experimental references. In this context, the thesis provides both URANS and LES perspectives, enabling engineers to evaluate, meticulously and effectively, mixing behavior, injector targeting, and expected in-cylinder distribution before fTDC within a development workflow for next-generation ICEs.

As emphasized throughout this work, relying on a single "silver-bullet" solution is increasingly risky in a technological landscape that demands diversification. For this reason, the methodologies proposed for e-fuel modelling play a key role. The predictive framework based on IDT and LFS, major operational combustion characteristics, provides essential inputs for CFD simulations. These methods, workflows, and chemistry-based modelling strategies have been developed and applied to engines against experimental reference data. The ability of these models to achieve very strong alignment with experiments highlights the robustness of the approach and sets the direction for future high-fidelity URANS/LES and DNS studies. Ultimately, this thesis outlines the path for increasingly advanced developments in combustion chemistry modelling and in the detailed methodologies needed to support the future of ICE technology.

References

[1] Hedges Company, "How Many Cars Are There In The World? Statistics by Country," hedgescompany.com.
[2] Kalghatgi, G., "Is it really the end of internal combustion engines and petroleum in transport?", Applied Energy, 225:965–974, 2018.
[3] Our World in Data, "Tracking global data on electric vehicles," ourworldindata.org.
[4] Fuel Freedom Foundation, "What cars will we be driving in 2050?", https://www.fuelfreedom.org/cars-in-2050 (Accessed 13 October 2019).
[5] UNFCCC, "Glasgow Climate Change Conference – October-November 2021," unfccc.int.
[6] European Environment Agency, "The European Green Deal," europa.eu.
[7] Consilium, "Fit for 55 - The EU's plan for a green transition," europa.eu.
[8] Visnic, B., "Europe steps back from 2035 ICE ban," 2023-03-28.
[9] Kalghatgi, G., "Is it the end of combustion and engine combustion research? Should it be?", Transportation Engineering, 10:100142, 2022. https://doi.org/10.1016/j.treng.2022.100142.
[10] Senecal, P.K., Leach, F., "Diversity in transportation: Why a mix of propulsion technologies is the way forward for the future fleet," Results in Engineering, 4:100060, 2019. https://doi.org/10.1016/j.rineng.2019.100060.
[11] Sarathy, S., Farooq, A., Kalghatgi, G.T., "Recent progress in gasoline surrogate fuels," Progress in Energy and Combustion Science, 65:67–108, 2018. https://doi.org/10.1016/j.pecs.2017.09.004.
[12] Peak oil demand is still a decade away | Goldman Sachs
[13] Russia's War on Ukraine – Topics - IEA
[14] Global Energy Review 2025 – IEA
[15] IEA (2025), *Global electric car sales, 2014-2024*, IEA, Paris https://www.iea.org/data-and-statistics/charts/global-electric-car-sales-2014-2024, Licence: CC BY 4.0
[16] IEA (2024), *Battery electric car price premium compared to internal combustion engine cars, 2018-2023*, IEA, Paris https://www.iea.org/data-and-statistics/charts/battery-electric-car-price-premium-compared-to-internal-combustion-engine-cars-2018-2023, Licence: CC BY 4.0
[17] IEA (2022), By 2030 EVs represent more than 60% of vehicles sold globally, and require an adequate surge in chargers installed in buildings, IEA, Paris https://www.iea.org/reports/by-2030-evs-represent-more-than-60-of-vehicles-sold-globally-and-require-an-adequate-surge-in-chargers-installed-in-buildings, Licence: CC BY 4.0
[18] European Union, "Directive 2009/30/EC," http://data.europa.eu/eli/dir/2009/30/oj.
[19] U.S. Energy Information Administration, "U.S. Oxygenate Production," eia.gov.
[20] API, "Alcohols and Ethers – A Technical Assessment of Their Application as Fuels and Fuel Components," API Publication 4261, 3rd Edition, June 2001.
[21] Arteconi, A., Mazzarini, A., Di Nicola, G., "Emissions from ethers and organic carbonate fuel additives: Review," Water, Air & Soil Pollution, 2011:1–19.
[22] lyondellbasell.com, "Cleaner Fuels for Latin America with MTBE and ETBE," https://www.lyondellbasell.com/48f335/globalassets/documents/chemicals-technical-literature/Cleaner-Fuels-for-Latin-America-with-MTBE-and-ETBE-English/
[23] U.S. Energy Information Administration, "Monthly Biodiesel Production Report," eia.gov.
[24] EFOA, "The European Fuel Oxygenates Association," August 2011. https://www.sustainablefuels.eu.
[25] EIA, "Eliminating MTBE in gasoline," Release 02/22/2006, eia.gov.
[26] Wallace, G., Blondy, J., Mirabella, W., Schulte-Körne, E., Viljanen, J., "Ethyl Tertiary Butyl Ether – A review of the technical literature," SAE Technical Paper 2009-01-1951.
[27] HIF GLOBAL, "OUR SUSTAINABLE JOURNEY 2023", https://hifglobal.com/our-sustainability-journey-2023#haruoni
[28] Premiere for the Porsche Mobil 1 Supercup with eFuels - Porsche Newsroom
[29] F1 - How sustainable fuels can benefit the world – and are more than just the future of F1 | Formula 1®
[30] LeMans - All 24 Hours of Le Mans Race Cars to Use 100% Renewable Fuel Produced by TotalEnergies | TotalEnergies.com
[31] Breda, S., Fontanesi, S., Merolla, S., Gagliardi, M., Cicalese, G., V., Pati M., Dalseno, L., Kuschel, M., "Assessment of E-Fuels Applicability as Gasoline Replacement in a Small Two-Stroke Engine," SAE Technical Paper 2025-32-0058, 2025, https://doi.org/10.4271/2025-32-0058
[32] Dalseno L, Breda S, Cicalese G, et al. Computational study of ignition delay times and laminar flame speed of POrsche SYNthetic fuels: Comparison with conventional gasoline. International Journal of Engine Research. 2026;0(0). doi:10.1177/14680874261418142
[33] Toyota developing hydrogen engine technologies through motorsports. (2021). https://global.toyota/en/newsroom/corporate/35209996.html
[34] Toyota develops a prototype hydrogen combustion road car (toyota-europe.com)
[35] https://www.yamaha-motor.eu/cy/en/news/tapping-the-potential-within-100--hydrogen-powered-engines/#/
[36] 410 Hp from 2-Liter Displacement – Prototype of the H_2-ICE Race Engine from AVL RACETECH Proves Itself on the Testbed | AVL
[37] Fontanesi, S., Dalseno, L., and Magnani, M., "Numerical Characterization of Hydrogen Combustion in a High-Performance Engine: Potentials, Limitations, Modelling Uncertainties," *SAE Int. J. Adv. & Curr. Prac. in Mobility* 5(3):1322-1333, 2023, https://doi.org/10.4271/2022-24-0016
[38] Port injection of water into a DI hydrogen engine[R] SAE Paper (2015) 2015-01-0861

[39] A. Nande, T. Wallner, J. Naber Influence of water injection on performance and emissions of a direct-injection hydrogen research engine SAE Paper (2008) 2008-2011-2377
[40] Younkins, M., Wooldridge, M., and Boyer, B., "Port Injection of Water into a DI Hydrogen Engine," SAE Technical Paper 2015-01-0861, 2015, https://doi.org/10.4271/2015-01-0861.
[41] Puyan Xu, Changwei Ji, Shuofeng Wang, Xiaoyu Cong, Zedong Ma, Chuanqi Tang, Hao Meng, Cheng Shi, Effects of direct water injection on engine performance in a hydrogen (H2)-fueled engine at varied amounts of injected water and water injection timing, International Journal of Hydrogen Energy, Volume 45, Issue 24, 2020, Pages 13523-13534, ISSN 0360-3199, https://doi.org/10.1016/j.ijhydene.2020.03.011.
[42] Sfriso, S., Berni, F., Breda, S., Fontanesi, S. et al., "Proposal and Validation of 3D-CFD Framework for Ultra-Lean Hydrogen Combustion in ICEs," SAE Technical Paper 2024-01-2685, 2024, https://doi.org/10.4271/2024-01-2685.
[43] Sfriso, S., Berni, F., Fontanesi, S., D'Adamo, A. et al., "A 3D-CFD Numerical Approach for Combustion Simulations of Spark Ignition Engines Fuelled with Hydrogen: A Preliminary Analysis," SAE Technical Paper 2023-01-0207, 2023, https://doi.org/10.4271/2023-01-0207.
[44] Madia, M., Vaccari, M., Dalseno, L., Cicalese, G., Corrigan, D., Villa, D., Fontanesi, S., Breda, S., "Assessment of Knock Tendency in a Hydrogen-Fuelled High-Performance Internal Combustion Engine: A Chemistry-Based Numerical Study," SAE Technical Paper 2025-01-8429, 2025, doi:10.4271/2025-01-8429.
[45] Baudone, A.D., Madia, M., Pavan, N., Cordisco, I. et al., "Chemical Kinetics Calculation of H2 Laminar Flame Speed: Assessment of the Performance of Public Available Mechanisms at Engine Relevant Conditions," J. Phys.: Conf. Ser., 2893, 2024, doi:10.1088/1742-6596/2893/1/012094.
[46] Herold, R.E., Ghandhi, J.B., "Data Normalization Schemes for Assessing Mixture Stratification from PLIF Data," SAE Int. J. Fuels Lubr., 1(1):559-569, 2008.
[47] Salazar, V.M., Kaiser, S.A., Halter, F., "Optimizing precision and accuracy of quantitative PLIF of acetone as a tracer for hydrogen fuel," SAE Int. J. Fuels Lubr., 2(1):737–761, 2009.
[48] Salazar VM, Kaiser SA. An optical study of mixture preparation in a hydrogen-fueled engine with direct injection using different nozzle designs. SAE Int J Engines 2009;2(2):119–31.
[49] Salazar, V.M., Kaiser, S.A., *Influence of the In-Cylinder Flow Field (Tumble) on the Fuel Distribution in a DI Hydrogen Engine Using a Single-Hole Injector*, SAE Int. J. Engines, 3(1):309–325, 2010. https://doi.org/10.4271/2010-01-0579
[50] Messner, D., Wimmer, A., Gerke, U., and Gerbig, F., "Application and Validation of the 3D CFD Method for a Hydrogen Fueled IC Engine with Internal Mixture Formation," SAE Technical Paper 2006-01-0448, 2006, https://doi.org/10.4271/2006-01-0448.
[51] Scarcelli, R., Wallner, T., Salazar, V., and Kaiser, S., "Modelling and Experiments on Mixture Formation in a Hydrogen Direct-Injection Research Engine," *SAE Int. J. Engines* 2(2):530-541, 2010, https://doi.org/10.4271/2009-24-0083.
[52] Scarcelli R, Wallner T, Matthias N, Salazar V, Kaiser S. Numerical and optical evolution of gaseous jets in direct injection hydrogen engines. SAE 2011 World Congr Exhib. 2011.
[53] Lucchini T, Errico GD, Fiocco M, Milano P. Multi-dimensional modelling of gas exchange and fuel-air mixing processes in a direct-injection, gas fueled engine. SAE Int J Engines 2011;24.
[54] Le Moine, J., Senecal, P.K., Kaiser, S.A., Salazar, V.M., Anders, J.W., Svensson, K.I., Gehrke, C.R., *A Computational Study of the Mixture Preparation in a Direct–Injection Hydrogen Engine*, ASME J. Eng. Gas Turbines Power, 137(11):111508, 2015. https://doi.org/10.1115/1.4030397
[55] Yong Li, Wenzhi Gao, Pan Zhang, Yixiang Ye, Zhaoyi Wei, *Effects study of injection strategies on hydrogen-air formation and performance of hydrogen direct injection internal combustion engine*, International Journal of Hydrogen Energy, Vol. 44, Issue 24, 2019, pp. 13523–13534. https://doi.org/10.1016/j.ijhydene.2019.08.055
[56] Barbato, A. and Cantore, G., "3D CFD Simulation of a Gaseous Fuel Injection in a Hydrogen-Fueled Internal Combustion Engine," E3S Web Conf. 312 (2021): 07001
[57] Addepalli SK, Pei Y, Zhang Yu, Scarcelli R. Multi-dimensional modelling of mixture preparation in a direct injection engine fueled with gaseous hydrogen. Int J Hydrogen Energy 2022;47(67):29085–101.
[58] Potenza, M.E.C., Gaballo, M.R., Arvizzigno, A., Anaclerio, G. et al., "3D CFD Analysis of Mixture Formation in Direct Injection Hydrogen-Fueled Internal Combustion Engines," 2385, no. 1 (2022): 012080
[59] Anaclerio, G., Capurso, T., Torresi, M., Camporeale, S., *Influence of the Injection Timing on the Mixture Formation Process in a Spark-Ignition Hydrogen Fuelled ICE*, SAE Technical Paper 2023-24-0079, 2023. https://doi.org/10.4271/2023-24-0079
[60] Ramognino, F., Sforza, L., D'Errico, G., Gomez-Soriano, J., Onorati, A., Novella, R., *CFD Modelling of Hydrogen-Fueled SI Engines for Light-Duty Applications*, SAE Technical Paper 2023-24-0017, 2023. https://doi.org/10.4271/2023-24-0017
[61] Bifen Wu, Roberto Torelli, Yuanjiang Pei, Numerical modelling of hydrogen mixing in a direct-injection engine fueled with gaseous hydrogen, Fuel, Volume 341, 2023, 127725, ISSN 0016-2361, https://doi.org/10.1016/j.fuel.2023.127725
[62] Torelli, R., Wu, B., Park, J.-W., Pei, Y., *Multicycle Large-Eddy Simulations of a Direct-Injection Hydrogen-Fueled Optical Engine*, SAE Technical Paper 2024-01-4295, 2024. https://doi.org/10.4271/2024-01-4295
[63] Akar, F., Özener, O., *Numerical investigation of in-cylinder gas motion dynamics in a heavy-duty direct injection hydrogen internal combustion engine*, SAE Technical Paper 2025-01-0301, 2025. https://doi.org/10.4271/2025-01-0301
[64] Kaczmarczyk, K.O., Liu, X., Im, H.G., Turner, J.W. et al., "Investigation of URANS CFD Methods for Supersonic Hydrogen Jets," SAE Technical Paper 2024-01-2687, 2024, doi:10.4271/2024-01-2687.
[65] Capecci, M., Sforza, L., Lucchini, T., D'Errico, G., Pezza, V., Tosi, S., *Numerical Analysis of Direct-Injection and Combustion Inside a H_2 Engine*, SAE Technical Paper 2025-01-0301, 2025. https://doi.org/10.4271/2025-01-0301
[66] Zhao, L., Zhang, A., Lago Sari, R., Popuri, S.S., Bowen, N., Matuszak, G., *Simulated-Based Combustion System Development in a Direct-Injection Spark-Ignited Hydrogen Engine*, SAE Technical Paper 2025-01-8360, 2025. https://doi.org/10.4271/2025-01-8360

[67] Pavan, N., Cicalese, G., Gestri, L., Fontanesi, S. et al., “Effects of Jet Caps on Hydrogen Piezoelectric Injectors for DI Applications: Experiments and 3D-CFD Simulations,” SAE Technical Paper 2025-01-8454, 2025, doi:10.4271/2025-01-8454.
[68] Fontanesi, S., Postrioti, L., Magnani, M., Martino, M. et al., “Preliminary Assessment of Hydrogen Direct Injection Potentials and Challenges through a Joint Experimental and Numerical Characterization of High-Pressure Gas Jets,” SAE Technical Paper 2022-24-0014, 2022, doi:10.4271/2022-24-0014.
[69] S. Verhelst, C. T'Joen, J. Vancoillie, J. Demuynck, A correlation for the laminar burning velocity for use in hydrogen spark ignition engine simulation, International Journal of Hydrogen Energy, Volume 36, Issue 1, 2011, Pages 957-974, ISSN 0360-3199, https://doi.org/10.1016/j.ijhydene.2010.10.020.
[70] Rouleau, L., Duffour, F., Walter, B., Kumar, R. et al., “Experimental and Numerical Investigation on Hydrogen Internal Combustion Engine,” SAE Technical Paper 2021-24-0060, 2021, doi:10.4271/2021-24-0060.
[71] Ramalho Leite, C., Laignel, M., Brequigny, P., Borée, J. et al., "Experimental Combustion Analysis in a Gasoline Baseline Hydrogen-Fueled Internal Combustion Engine at Ultra-Lean Conditions," SAE Technical Paper 2023-24-0073, 2023, https://doi.org/10.4271/2023-24-0073.
[72] Yip, H.L., et al., (2019), ‘A Review of Hydrogen Direct Injection for Internal Combustion Engines: Towards Carbon-Free Combustion’, Applied Sciences, 9(22), p. 4842. doi: 10.3390/app9224842.
[73] S.T.P. Purayil, Mohammad O. Hamdan, S.A.B. Al-Omari, M.Y.E. Selim, E. Elnajjar, Review of hydrogen–gasoline SI dual fuel engines: Engine performance and emission, Energy Reports, Volume 9, 2023, Pages 4547-4573, ISSN 2352-4847, https://doi.org/10.1016/j.egyr.2023.03.054.
[74] Electrifying road transport with less mining : A global and regional battery material outlook - International Council on Clean Transportation - https://theicct.org/publication/ev-battery-materials-demand-supply-dec24/
[75] Nevada Electricity Generation Mix 2025 | Low-Carbon Power Data - https://lowcarbonpower.org/region/Nevada
[76] New York State Energy Research and Development Authority. 2006. Hydrogen Production – Steam Methane Reforming (SMR). Hydrogen Fact Sheet, pp. 1-2.
[77] Eberle, U., Mueller, B., Helmolt, V., Rittmar. 2012. Fuel cell electric vehicles and hydrogen infrastructure: status 2012" Energy & Environmental Science, pp. 10.
[78] Flynn, T. 2004. Cryogenic Engineering, Second Edition, Revised and Expanded. CRC Press, pp. 401.
[79] Ahluwalia, R.K., Peng, J.K., Hua, T.O. 2016. Hydrogen Storage, Transportation and Infrastructure. Woodhead Publishing, pp. 119-145.
[80] Park C, et al. Effect of the operation strategy and spark plug conditions on the torque output of a hydrogen port fuel injection engine. Int J Hydrogen Energy 2021;46(74):37063e70.
[81] Pandey JK, Kumar GN. Effect of variable compression ratio and equivalence ratio on performance, combustion and emission of hydrogen port injection SI engine. Energy 2022;239.
[82] Gao J, et al. Review of the backfire occurrences and control strategies for port hydrogen injection internal combustion engines. Fuel 2022;307.
[83] Salvi BL, Subramanian KA.A novel approach to experimental study and numerical modelling of combustion characteristics of a hydrogen-fuelled spark-ignition engine. Sustain Energy Technol Assessments 2022;51.
[84] Shi C, et al. Potential improvement in combustion and pollutant emissions of a hydrogen-enriched rotary engineby using novel recess configuration. Chemosphere2022:134491
[85] Zehao Sun, Jichao Hong, Tiezhu Zhang, Binbin Sun, Binbin Yang, Liqun Lu, Lin Li, Kaiwei Wu, Hydrogen engine operation strategies: Recent progress, industrialization challenges, and perspectives, International Journal of Hydrogen Energy, Volume 48, Issue 1, 2023, Pages 366-392, ISSN 0360-3199, https://doi.org/10.1016/j.ijhydene.2022.09.256.
[86] Qian, L., Wan, J., Qian, Y., Sun, Y., Zhuang, Y., 2022. Experimental investigationof water injection and spark timing effects on combustion and emissions ofa hybrid hydrogen-gasoline engine. Fuel 322, 124051
[87] Salek, F., Babaie, M., Hosseini, S.V., Bég, O.A., 2021. Multi-objective optimizationof the engine performance and emissions for a hydrogen/gasoline dual-fuelengine equipped with the port water injection system. Int. J. Hydrog. Energy.46 (17), 10535–10547.
[88] Dhyani, V., Subramanian, K.A., 2019. Control of backfire and NOx emission reduction in a hydrogen fueled multi-cylinder spark ignition engine usingcooled EGR and water injection strategies. Int. J. Hydrog. Energy. 44 (12),6287–6298
[89] Stępień, Z., 2021. A comprehensive overview of hydrogen-fueled internal combustion engines: Achievements and future challenges. Energies 14 (20), 6504.
[90] Beyer, M., Markus, D., (2011), ‘Ignition of explosive atmospheres by small hot particles: Comparison of experiments and simulations’, Science and Technology of Energetic Materials, 73(1).
[91] Roth, D., et al., (2014), ‘Ignition by Mechanical Sparks: Ignition of Hydrogen/Air Mixtures by Submillimeter-Sized Hot Particles’, Combustion Science and Technology, 186(10-11), pp. 1606-1617. doi: 10.1080/00102202.2014.935606.
[92] Roth, D., Thomas, H., Henning, B., (2017), ‘Experimental and numerical study on the ignition of fuel/air mixtures at laser heated silicon nitride particles’, Proceedings of the Combustion Institute, 36(1), pp. 1475-1484. doi: 10.1016/j.proci.2016.05.054.
[93] R. 1937. The ignition of gaseous mixtures by hot particles. Philosophical Magazine Series 7, 23(156), 633–657.
[94] Ungut, A., & James, H. (2001). Autoignition of gaseous fuel–air mixtures near a hot surface. IChemE Symposium Series. [accessed, august 2024]: https://www.icheme.org/media/10183/xvi-paper-38.pdf
[95] Xing, F., Holzberger, S., Kettner, M. et al. Numerical and experimental investigation of the surface ignition temperature for hydrogen-air mixture in catalytic combustion on platinum surface. J Therm Anal Calorim (2026). https://doi.org/10.1007/s10973-026-15309-6

[96] Chi, C., Abdelsamie, A., Thévenin, D., (2018), 'Direct Numerical Simulations of Hotspot-induced Ignition in Homogeneous Hydrogen-air Pre-mixtures and Ignition Spot Tracking', Flow Turbulence and Combustion, 101, pp. 103–121. doi: 10.1007/s10494-
017-9883-1.
[97] Xing, F., Holzberger, S., Kettner, M. et al. Numerical and experimental investigation of the surface ignition temperature for hydrogen-air mixture in catalytic combustion on platinum surface. J Thermal Analysis and Calorimetry (2026). https://doi.org/10.1007/s10973-026-15309-6
[98] Rao A, Liu Y, Ma F. Study of NOx emission for hydrogen enriched compressed natural along with exhaust gas recirculation in spark ignition engine by Zeldovich' mechanism, support vector machine and regression correlation. Fuel 2022;318.
[99] Wei H, et al. Gasoline engine exhaust gas recirculation e a review. Appl Energy 2012;99:534e44.
[100] Salvi BL, Subramanian KA. Experimental investigation on effects of compression ratio and exhaust gas recirculation on backfire, performance and emission characteristics in a hydrogen fuelled spark ignition engine. Int J Hydrogen Energy 2016;41(13):5842e55.
[101] Boretti, A. Water injection strategies to control gas temperatures in hydrogen–air internal combustion engines. *J Braz. Soc. Mech. Sci. Eng.* 46, 54 (2024). https://doi.org/10.1007/s40430-023-04623-x
[102] Sipos, G.; Bukovácz, K.; Istvánkó, K.; Sebestyén, L.Á. Hydrogen Engine Conversion Aspects. *Eng. Proc.* 2024, *79*, 6. https://doi.org/10.3390/engproc2024079006
[103] Mohamed M, Biswal A, Wang X, et al. Exploring the benefits of hydrogen-water injection technology in internal combustion engines: A rigorous experimental study. *International Journal of Engine Research*. 2024;26(5):724-740. doi:10.1177/14680874241288624
[104] Kim, J., Chun, K.M., Song, S., Baek, H.-K., Lee, S.W., 2017. The effects of hydrogen on the combustion, performance and emissions of a turbo gasoline direct- injection engine with exhaust gas recirculation. Int. J. Hydrog. Energy. 42 (39), 25074–25087.
[105] Gaikwad, R., Bansode, A. & Urakawa, A., 2016. High-pressure advantages in stoichiometric hydrogenation of carbon dioxide to methanol. Journal of Catalysis, Volume 343, pp. 127-132.
[106] Atsonios, K., Panopoulos, K. D. & Kakaras, E., 2016. Investigation of technical and economic aspects for methanol production through CO2 hydrogenation. International Journal of Hydrogen Energy, 4 January, 41(4), pp. 2202-2214.
[107] Lim, H.-W.et al., 2009. Modelling of the Kinetics for Methanol Synthesis using Cu/ZnO/Al2O3/ZrO2 Catalyst: Influence of Carbon Dioxide during Hydrogenation. Industrial & Engineering Chemistry Research, 48(23), pp. 10448-10455
[108] K. Shi, B. Guan, Z. Zhuang, J. Chen, Y. Chen, Z. Ma, Z. Huang, Perspectives and
Outlook of E-fuels: production, Cost Effectiveness, and Applications, Energy &
Fuels 38 (9) (2024) 7665 – 7692
[109]] K. Atsonios, J. Li, V.J. Inglezakis, Process analysis and comparative assessment ofadvanced thermochemical pathways for e-kerosene production, Energy 278
(2023) 127868.
[110] Juan Gabriel Segovia-Hernández, Advancing E-fuels production through process intensification: overcoming challenges and seizing opportunities for a sustainable energy future - A critical review, Chemical Engineering and Processing - Process Intensification, Volume 208, 2025, 110107, ISSN 0255-2701, https://doi.org/10.1016/j.cep.2024.110107.
[111] Honeywell UOP eFining™ Technology – Methanol to Jet - https://uop.honeywell.com/en/industry-solutions/renewable-fuels/efining
[112] CO_2 to methanol | Johnson Matthey - https://matthey.com/products-and-markets/chemicals/methanol/co2-to-methanol
[113] ExxonMobil and Porsche test lower-carbon fuel in race conditions - https://corporate.exxonmobil.com/news/news-releases/2021/0330_exxonmobil-and-porsche-test-lower-carbon-fuel-in-race-conditions
[114] ExxonMobil licenses fluid bed Methanol-to-Gasoline (MTG) technology to Aramco for synthetic fuel demonstration plant in NEOM, Saudi Arabia - https://www.exxonmobilchemical.com/en/resources/library/library-detail/109708/exxonmobil_aramco_neom_methanol_to_gasoline_technology_en?utm_source=othermedia&utm_medium=banner&utm_campaign=cl_downstream&utm_content=exxonmobil_aramco_neom_press_release_oct24
[115] Bratsky D, Stacho D. Impact of motor gasoline chemical composition and additive treatment on inlet valve and combustion chamber deposits. SAE Technical Paper 2000-01-2022 2000.
[116] Aradi AA, Imoehl B, Avery NL, Wells PP, Grosser RW. The effect of fuel composition and engine operating parameters on injector deposits in a high-pressure direct injection gasoline (DIG) research engine. SAE Technical Paper 1999-01-3690 1999.
[117] Carlisle HW, Frew RW, Mills JR, Aradi AA, Avery NL. The effect of fuel composition and additive content on injector deposits and performance of an air-assisted direct injection spark ignition (DISI) research engine. SAE Technical Paper 2001-01-2030 2001.
[118] Di Iorio S, Catapano F, Sementa P, Vaglieco BM, Florio S, Rebesco E, et al. Effect of octane number obtained with different oxygenated components on the engine performance and emissions of a small GDI engine. SAE Technical Paper 2014-32-0038 2014.
[119] G.T. Kalghatgi, Developments in internal combustion engines and implications for combustion science and future transport fuels, Proceedings of the Combustion Institute, Volume 35, Issue 1, 2015, Pages 101-115, ISSN 1540-7489, https://doi.org/10.1016/j.proci.2014.10.002. (https://www.sciencedirect.com/science/article/pii/S1540748914004283
[120] Joel H. Ferziger, Milovan Perić, Robert L. Street, Computational Methods for Fluid Dynamics, Springer Nature Switzerland AG 2020, https://doi.org/10.1007/978-3-319-99693-6
[121] Rutland, C.J., *Large-Eddy Simulations for Internal Combustion Engines — A Review*, *International Journal of Engine Research*, 12(1):1–15, 2011. https://doi.org/10.1177/1468087411407248

[122] Yakhot, V. and Orszag, S.A., "Renormalization Group Analysis of Turbulence. I. Basic Theory," Journal of Scientific Computing 1, no. 1 (1986): 3-51, doi:10.1007/BF01061452.
[123] Kolmogorov, A. N. (1941). *The local structure of turbulence in an incompressible viscous fluid for very large Reynolds numbers*. Doklady Akademii Nauk SSSR, 30, 301–305.
[124] Smagorinsky, J. (1963). *General circulation experiments with the primitive equations: I. The basic experiment*. Monthly Weather Review, 91, 99–164.
[125] Schlichting, H., & Gersten, K. (2017). *Boundary-layer theory* (9th ed.). Springer.
[126] Nicoud, F., & Ducros, F. (1999). Subgrid-scale stress modelling based on the square of the velocity gradient tensor. *Flow, Turbulence and Combustion, 62*(3), 183–200. https://doi.org/10.1023/A:1009995426001
[127] Van Driest, E. R. (1956). *On turbulent flow near a wall.* Journal of Aeronautical Sciences, 23, 1007–1011.
[128] Reichardt, H. 1951. "Vollstaendige Darstellung der turbulenten Geschwindigkeitsverteilung in glatten Leitungen", Z. Angew. Math. Mech, 31(7), pp. 208-219.
[129] Vervisch, P.E., Colin, O., Michel, J., and Darabiha, N., "NO Relaxation Approach (NORA) to predict thermal NO in combustion chambers," Combustion and Flame 158, no. 8 (2011): 1480-1490, doi:https://doi.org/10.1016/j.combustflame.2010.12.014 .
[130] Knop, V., Nicolle, A., and Colin, O., "Modelling and Speciation of Nitrogen Oxides in Engines," Proceedings of the Combustion Institute 34, no. 1 (2013): 667-675, doi: https://doi.org/10.1016/j.proci.2012.06.082.
[131] Ren, S., et al., (2017), 'A multi-component wide distillation fuel (covering gasoline, jet fueland diesel fuel) mechanism for combustion and PAH prediction', Fuel, 208, pp. 447-468. doi: 10.1016/j.fuel.2017.07.009.
[132] Mehl, M., et al., (2011), 'An Approach for Formulating Surrogates for Gasoline with Application Toward a Reduced Surrogate Mechanism for CFD Engine Modelling', Energy and Fuels, 25, pp. 5215-5223. doi:10.1021/ef201099y.
[133] O'Connaire, M., et al., (2004), 'A Comprehensive Modelling Study of Hydrogen Oxidation', International Journal of Chemical Kinetics, 36, pp. 603-622. doi:10.1002/kin.20036. [134] Ranzi, E., Frassoldati, A., Stagni, A., Pelucchi, M. et al., "Reduced Kinetic Schemes of Complex Reaction Systems: Fossil and Biomass-Derived Transportation Fuels," Int. J. Chem. Kin. 46, no. 9 (2014): 512-542, doi:10.1002/kin.20867.
[135] Ranzi, E., Cavallotti, C., Cuoci, A., Frassoldati, A. et al., "New Reaction Classes in the Kinetic Modelling of Low Temperature Oxidation of N-Alkanes," Combustion and Flame 162, no. 5 (2015): 1679-1691, doi:10.1016/j.combustflame.2014.11.030 .
[136]. Ranzi, E., Frassoldati, A., Grana, R., Cuoci, A. et al., "Hierarchical and Comparative Kinetic Modelling of Laminar Flame Speeds of Hydrocarbon and Oxygenated Fuels," Progress in Energy and Combustion Science 38, no. 4 (2012): 468-501, doi:10.1016/j.pecs.2012.03.004.
[137] Konnov, A.A., "Yet another Kinetic Mechanism for Hydrogen Combustion," Combustion and Flame 203 (2019): 14-22, doi:10.1016/j.combustflame.2019.01.032 .
[138] Cancino, L.R., da, A., De Toni, A.R., Fikri, M. et al., "A Six-Compound, High Performance Gasoline Surrogate for Internal Combustion Engines: Experimental and Numerical Study of Autoignition Using High-Pressure Shock Tubes," Fuel 261, no. 1 (2020): 116439, doi:10.1016/j.fuel.2019.116439.
[139] Fieweger, K., Blumenthal, R., and Adomeit, G., "Shock-Tube Investigations on the Self-Ignition of Hydrocarbon-Air Mixtures at High Pressures," Symposium (International) on Combustion 25, no. 1: 1579-1585, doi:10.1016/S0082-0784(06)80803-9.
[140] Fieweger, K., Blumenthal, R., and Adomeit, G., "Self-Ignition of SI Engine Model Fuels: A Shock Tube Investigation at High Pressure," Combustion and Flame 109, no. 4 (1997): 599-619, doi:10.1016/S0010-2180(97)00049-7.
[141] Davidson, D.F., Gauthier, B.M., and Hanson, R.K., "Shock Tube Ignition Measurements of Iso-Octane/Air and Toluene/Air at High Pressures," Proceedings of the Combustion Institute 30, no. 1: 1175-1182, doi:10.1016/j.proci.2004.08.004.
[142] Hartmann, M., Gushterova, I., Fikri, M., Schulz, C. et al.,
"Auto-Ignition of Toluene-Doped N-Heptane and Iso-Octane/Air Mixtures: High-Pressure Shock-Tube Experiments and Kinetics Modelling," Combustion and Flame 158, no. 1: 172-178, doi:10.1016/j.combustflame.2010.08.005 .
[143] Laster, W.R. and Sojka, P.E., "Autoignition of H2-Air: The Effect of NOx Addition," Journal of Propulsion and Power 5, no. 4 (1989): 385-390, doi:10.2514/3.23166.
[144] Petersen, E.L., Davidson, D.F., Rohrig, M., and Hanson, R.K., "Shock-Induced Ignition of High-Pressure H2-O2-Ar and CH4-O2-Ar Mixtures," in AIAA 95-3113, 31st AIAA/ASME/SAE/ASEE Joint Propulsion Conference and Exhibit, 1995, doi:10.2514/6.1995-3113.
[145] Leachman, J.W., Jacobsen, R.T., Penoncello, S.G., and Lemmon, E.W., "Fundamental Equations of State for Parahydrogen, Normal Hydrogen, and Orthohydrogen," J. Phys. Chem. Ref. Data 38, no. 3 (2009): 721-748, doi:10.1063/1.3160306.
[146] Livengood, J.C. and Wu, P.C., "Correlation of Autoignition Phenomena in Internal Combustion Engines and Rapid Compression Machines," Symp (Int) Combust 5, no. 1 (1955): 347-356, doi:10.1016/S0082-0784(55)80047-1.
[147] DENSO Corporation, 'Spark Plug Basic: Heat Range', accessed June 26, 2024. Available at: https://www.denso.com/global/en/products-and-services/automotive-service-parts-andaccessories/plug/basic/heatrange/#:~:text=There%20are%20restrictions%20on%20the,C%20and%20950%C2%B0C.
[148] Chi, C., Abdelsamie, A., and Thévenin, D., "Direct Numerical Simulations of Hotspot-Induced Ignition in Homogeneous Hydrogen-Air Pre-Mixtures and Ignition Spot Tracking," Flow Turbulence and Combustion 101 (2018): 103-121, doi:10.1007/s10494-017-9883-1.
[149] Hasse, C. (2015). Scale-resolving simulations in engine combustion process design based on a systematic approach for model development. International Journal of Engine Research, 17(1), 44–62. https://doi.org/10.1177/1468087415597842

[150] Soave, G., “Equilibrium Constants from a Modified Redlich-Kwong Equation of State,” Chemical Engineering Science 27, no. 6 (June 1972): 1197-1203, doi:10.1016/0009-2509(72)80096-4.
[151] Rodi, W., *Experience with Two-Layer Models Combining the k-ε Model with a One-Equation Model Near the Wall*, 29th Aerospace Sciences Meeting, AIAA Paper 91-0216, Reno, NV, January 7–10, 1991. https://doi.org/10.2514/6.1991-216
[152] Reynolds, A. The prediction of turbulent Prandtl and Schmidt numbers. Int. J. Heat Mass Transf. 1975, 18, 1055–1069
[153] Gualtieri C., Angeloudis A., Bombardelli F., et al., “On the Values for the Turbulent Schmidt Number in Environmental Flows” Fluids 2017, 2(2), 17; https://doi.org/10.3390/fluids2020017
[154] Donzis, D. A.; Aditya, K.; Sreenivasan, K. R.; Yeung, P. K. (2014). "The Turbulent Schmidt Number". Journal of Fluids Engineering. 136 (6): https://doi.org/10.1115/1.4026619
[155] Li D, Luo K, Fan J (2016) Direct numerical simulation of heat transfer in a spatially developing turbulent boundary layer. Phys Fluids 28(10):105104. https://doi.org/10.1063/1.4964686
[156] Marquardt, P., Klaas, M. & Schröder, W. Experimental investigation of the turbulent Schmidt number in supersonic film cooling with shock interaction. Exp Fluids 61, 160 (2020). https://doi.org/10.1007/s00348-020-02983-x
[157] Ivan Di Venuta, Andrea Boghi, Ivano Petracci, Carlo Bartoli, Fabio Gori, Flow evolution and mass transfer in a turbulent rectangular free jet of air with small laminar Schmidt number, International Communications in Heat and Mass Transfer, Volume 107, 2019, Pages 44-54, ISSN 0735-1933, https://doi.org/10.1016/j.icheatmasstransfer.2019.06.001.
[158] Sutherland, W., "The viscosity of gases and molecular force," Philosophical Magazine, S. 5, 36, pp. 507-531, 1893.
[159] White, F.M., "Viscous Fluid Flow," 3rd ed., McGraw-Hill, 2006.
[160] Hirschfelder, J.O., Curtiss, C.F., Bird, R.B., "The Molecular Theory of Gases and Liquids," John Wiley, New York, Chapman & Hall, London, 1954.
[161] Chapman, S., Cowling, T.G., Park, D., "The mathematical theory of non-uniform gases," 1939.
[162] Poling, B.E., Prausnitz, J.M., O'Connell, J.P., "The Properties of Gases and Liquids," 5th edition, McGraw-Hill, New York, 2001. DOI: 10.1036/0070116822.
[163] Pope SB. Turbulent flows. Cambridge University Press; 2000
[164] Celik, I., Cehreli, Z., Yavuz, I., "Index of resolution quality for large eddy simulations," J. Fluid Eng., 127(5):949-958, 2005.
[165] Celik, I., Klein, M., Janicka, J., "Assessment measures for engineering LES applications," J. Fluids Eng., 131, 2009. http://dx.doi.org/10.1115/1.3059703.
[166] Kravchenko AG, Moin P. On the effect of numerical errors in large eddy simulation of turbulent flows. J Comput Phys 1997;131:310–22.
[166] Geurts BJ, Frohlich J. A framework for predicting accuracy limitations in large- eddy simulations. Phys Fluids 2002;14:L41–4.
[167] Francesca di Mare, Robert Knappstein, Michael Baumann, Application of LES-quality criteria to internal combustion engine flows, Computers & Fluids, Volume 89, 2014, Pages 200-213, ISSN 0045-7930, https://doi.org/10.1016/j.compfluid.2013.11.003
[168] M. Baumann, F. di Mare, J. Janicka, “On the Validation of Large Eddy Simulation Applied to Internal Combustion Engine Flows –Part II: Numerical Analysis”, Flow, Turbulence and Combustion, Springer, DOI: 10.1007/s10494-013-9472-x
[169] Hydrogen Engine – Engine Combustion Network - https://ecn.sandia.gov/engines/hydrogen-engine/ [accessed: February 2026]
[170] Breda, S., D'Adamo, A., Fontanesi, S., D'Orrico, F. et al., "Numerical Simulation of Gasoline and n-Butanol Combustion in an Optically Accessible Research Engine", SAE Int. J. Fuels Lubr. 10(1):32-55, 2017, https://doi.org/10.4271/2017-01-0546
[171] Breda, S., D'Adamo, A., Fontanesi, S., Giovannoni, N. et al., "CFD Analysis of Combustion and Knock in an Optically Accessible GDI Engine", SAE Int. J. Engines 9(1):641-656, 2016, https://doi.org/10.4271/2016-01-0601
[172] D'Adamo, A., Breda, S., Iaccarino, S., Berni, F. et al., "Development of a RANS-Based Knock Model to Infer the Knock Probability in a Research Spark-Ignition Engine", SAE Int. J. Engines 10(3):722-739, 2017, https://doi.org/10.4271/2017-01-0551
[173] Pera C, Knop V., "Methodology to define gasoline surrogates dedicated to auto-ignition in engines", Fuel 2012;96:59–69. (http://refhub.elsevier.com/S0360-1285(15)30019-8/sbref0078)
[174] Pomraning, E., & Rutland, C. J. (2002). *A dynamic one-equation non-viscosity LES model*. AIAA Journal, 40(4), 689–701.
[175] Kalghatgi G, Babiker H, Badra J., "A simple method to predict knock using toluene, n-heptane and iso-octane blends (TPRF) as gasoline surrogates", SAE Int J Engines 2015;8:505–19
[176] Del Pecchia M, Fontanesi F., "A methodology to formulate multicomponent fuel surrogates to model flame propagation and ignition delay", Fuel, Volume 279, 2020, 118337, ISSN 0016-236, https://doi.org/10.1016/j.fuel.2020.118337
[177] L.R. Cancino, M. Fikri, A.A.M. Oliveira, C. Schulz, "Ignition delay times of ethanol containing multi-component gasoline surrogates: Shock-tube experiments and detailed modelling", Fuel 90 (2011) 1238–1244
[178] A. Frassoldati, A. Cuoci, T. Faravelli, E. Ranzi, "Kinetic modelling of the oxidation of ethanol and gasoline surrogate mixtures", Combustion Science and Technology, 182, pp. 653-667 (2010), doi:10.1080/00102200903466368
[179] Corinna Netzer, Lars Seidel, Frédéric Ravet, Fabian Mauß, "Impact of the surrogate formulation on 3D CFD engine knock prediction using detailed chemistry", Fuel, Volume 254, 2019, 115678, ISSN 0016-2361, https://doi.org/10.1016/j.fuel.2019.115678
[180] D. Bradley, R. A. Hicks, M. Lawes, C. G. W. Sheppard, R. Woolley, "The Measurement of Laminar Burning Velocities and Markstein Numbers for Iso-octane–Air and Iso-octane–n-Heptane–Air Mixtures at Elevated Temperatures and Pressures in an Explosion Bomb"

[181] D'Adamo, A., Del Pecchia, M., Breda, S., Berni, F. et al., "Chemistry-Based Laminar Flame Speed Correlations for a Wide Range of Engine Conditions for Iso-Octane, n-Heptane, Toluene and Gasoline Surrogate Fuels", SAE Technical Paper 2017-01-2190, 2017, https://doi.org/10.4271/2017-01-2190
[182] D'Adamo, A., Del Pecchia, M., Breda, S., Berni, F. et al., "Chemistry-Based Laminar Flame Speed Correlations for a Wide Range of Engine Conditions for Iso-Octane, n-Heptane, Toluene and Gasoline Surrogate Fuels," SAE Technical Paper 2017-01-2190, 2017, https://doi.org/10.4271/2017-01-2190
[183] Del Pecchia, M., Breda, S., D'Adamo, A., Fontanesi, S. et al., "Development of Chemistry-Based Laminar Flame Speed Correlation for Part-Load SI Conditions and Validation in a GDI Research Engine," SAE Int. J. Engines 11(6):715-741, 2018, https://doi.org/10.4271/2018-01-0174
[184] Sarathy SM, Vranckx S, Yasunaga K, Mehl M, Oßwald P, Metcalfe WK, et al., "A comprehensive chemical kinetic combustion model for the four butanol isomers," Combust Flame 2012;159:2028–55
[185] Yang Y, Dec JE, Dronniou N, Simmons B., "Characteristics of isopentanol as a fuel for HCCI engines," SAE Int J Fuels Lubr 2010;3:725–41
[186] Sarathy SM, Park S, Weber BW, Wang W, Veloo PS, Davis AC, et al., "A comprehensive experimental and modelling study of iso-pentanol combustion," Combust Flame 2013;160:2712–28
[187] Li T, Xu M, Hung D, Wu S, Cheng S., "Understanding the effects of fuel type and injection conditions on spray evaporation using optical diagnostics," SAE Technical Paper 2015-01-0926, 2015
[188] VanDerWege BA, Hochgreb S., "Effects of fuel volatility and operating conditions on fuel sprays in DISI engines: (1) Imaging investigation," SAE Technical Paper 2000-01-0535, 2000
[189] Giovannoni, N., Breda, S., Paltrinieri, S., D'Adamo, A. et al., "CFD Analysis of the Effects of Fuel Composition and Injection Strategy on Mixture Preparation and Fuel Deposit Formation in a GDI Engine," SAE Technical Paper 2015-24-2408, 2015, https://doi.org/10.4271/2015-24-2408
[190] Yahyaoui, N. Djebaili-Chaumeix, P. Dagaut, C.-E. Paillard, "Ethyl Tertiary Butyl Ether Ignition and Combustion Using a Shock Tube and Spherical Bomb," Energy & Fuels 2008, 22, 3701–3708
[191] Gauthier BM, Davidson DF, Hanson RK. Shock tube determination of ignition delay times in full blend and surrogate fuel mixtures. Combust Flame 2004;139:300-11.
[192] Andrae JCG, Bjornbom P, Cracknell RF, Kalghatgi GT. Autoignition of toluene reference fuels modelled by a semidetailed chemical kinetic model. Combust Flame 2007;149:2-24.
[193] Ahmed A, Waqas M, Naser N, Singh E, Roberts W, Chung S, et al., "Compositional effects of gasoline fuels on combustion, performance and emissions in engine," SAE Int J Fuels Lubr 2016;9(3):460–8
[194] Ranzi E, Frassoldati A, Grana R, et al. Hierarchical and comparative kinetic modelling of laminar flame speeds of hydrocarbon and oxygenated fuels. Prog Energy Combust Sci 2012; 38(4): 468–501.
[195] Frassoldati, A., Grana, R., Cuoci, A., Faravelli, T., & Ranzi, E. (2010). *A wide range kinetic modelling study of laminar flame speeds of reference fuels and their mixtures*. Italian Section of the Combustion Institute.
[196] Mayer M, Hofmann P, Geringer B, Williams J, Moss J. Influence of different fuel properties and gasoline - ethanol blends on low-speed pre-ignition in turbo-charged direct injection spark ignition engines. SAE Int J Engines 2016;9:841–8.
[197] Ryan TW, Matheaus AC. Fuel requirements for HCCI engine operation. SAE Technical Paper 2003011813 2003.
[198] Håkansson A, Stromberg K, Pedersen J, Olsson JO. Combustion of gasolines in premixed laminar flames european certified and California phase 2 reformulated gasoline. Chemosphere 2001;44:1243-52.
[199] Renewable Fuels Association. (2004). *Industry Outlook 2004: Synergy in Energy*. Renewable Fuels Association
[200] Reuters. (2025, June 26). *From shortage to surplus: India pours record rice crop into ethanol*. ET EnergyWorld.
[201] Brockwell, H. L., Sarathy, P. R., & Trotta, R. (1991). Synthesize ethers. *Hydrocarbon Processing*, 70(9), 133–141.
[202] Eliana Weber de Menezes, Renato Cataluña, Optimization of the ETBE (ethyl tert-butyl ether) production process, Fuel Processing Technology, Volume 89, Issue 11, 2008, Pages 1148-1152, ISSN 0378-3820, https://doi.org/10.1016/j.fuproc.2008.05.006.
[203] Shiblom, C.M., Schoonveld, G.A., Riley, R.K., and Pahl, R.H. Use of Ethyl-t-Butyl Ether (ETBE) as a Gasoline Blending Component, SAE Technical Paper 902132, October 1990
[204] Wallace, J. et al. (2009). *Review of material compatibility, drivability, and fuel behavior for oxygenated gasoline blends (ETBE, MTBE, Ethanol).* IEA-AMF.
[205] Owen, K., Coley, T., & Weaver, C. S. (1995). Automotive Fuels Reference Book (2nd ed.). Society of Automotive Engineers.
[206] Erjiang Hu, Jinfeng Ku, Geyuan Yin, Chanchan Li, Xin Lu, Zuohua Huang, "Laminar Flame Characteristics and Kinetic Modelling Study of Ethyl Tertiary Butyl Ether Compared with Methyl Tertiary Butyl Ether, Ethanol, iso-Octane, and Gasoline," Energy & Fuels 2018 32 (3), 3935-3949 DOI: 10.1021/acs.energyfuels.7b03636
[207] Fayolle, A., François, L., Garnier, D., Godefroy, H., Mathis, P., Piveteau, F., Monot, F., "Limitations in MTBE Biodegradation"
[208] Yasunaga, K., Simmie, J. M., Curran, H. J., Koike, T., Takahashi, O., Kuraguchi, Y., Hidaka, Y., "Detailed chemical kinetic mechanisms of ethyl methyl, methyl tert-butyl and ethyl tert-butyl ethers: The importance of uni-molecular elimination reactions," Combust. Flame 2011, 158 (6), 1032 – 1036
[209] https://www.creckmodeling.polimi.it1/menu-kinetics/menu-kinetics-detailed-mechanisms/ [accessed: April 2024]
[210] Frassoldati, A., Cuoci, T., Faravelli, U., Niemann, E., Ranzi, R., Seiser, K., Seshadri, An experimental and kinetic modelling study of n-propanol and iso-propanol combustion, Combustion and Flame 157 (1), pp. 2-16 (2010), doi:10.1016/j.combustflame.2009.09.002

[211] Frassoldati, R., Grana, T., Faravelli, E., Ranzi, P., Oßwald, K., Kohse-Höinghaus, Detailed kinetic modelling of the combustion of the four butanol isomers in premixed low-pressure flames, Combustion and Flame 159 (2012) 2295–2311, doi:10.1016/j.combustflame.2012.03.002
[212] Goldaniga, T., Faravelli, E., Ranzi, P., Dagaut, M., Cathonnet, Oxidation of oxygenated octane improvers: MTBE, ETBE, DIPE, and TAME, Twenty-Seventh Symposium (International) on Combustion, Volume 27, Issue 1, 1998, Pages 353–360
[213] Zhao Z, Conley JP, Kazakov A, Dryer FL., "Burning velocities of real gasoline fuel at 353 K and 500 K," SAE Technical Paper 2003-01-3265, 2003
[214] Tian G, Daniel R, Li H, Xu H, Shuai S, Richards P., "Laminar burning velocities of 2,5-dimethylfuran compared with ethanol and gasoline," Energy Fuels 2010;24:3898–905
[215] Jin-Tao Chen, A. Abd El-Sabor Mohamed, Pengzhi Wang, Yitong Zhai, Shashank S. Nagaraja, Chong-Wen Zhou, Henry J. Curran, "A comprehensive experimental and kinetic modelling study of methyl tert-butyl ether combustion"
[216] Ahmed A, Waqas M, Naser N, Singh E, Roberts W, Chung S, et al., "Compositional effects of gasoline fuels on combustion, performance and emissions in engine," SAE Int J Fuels Lubr 2016;9(3):460–8
[217] Mannaa OA, Mansour MS, Roberts WL, Chung SH., "Laminar burning velocities at elevated pressures for gasoline and gasoline surrogates associated with RON," Combust Flame 2015;162:2311–21
[218] Mannaa OA, Mansour MS, Roberts WL, Chung SH., "Laminar burning velocities of fuels for advanced combustion engines (FACE) gasoline and gasoline surrogates with and without ethanol blending associated with octane rating," Combust Sci Technol 2016;188:692–706
[219] Sileghem L, Alekseev VA, Vancoillie J, Van Geem KM NEJK, Verhelst S, et al., "Laminar burning velocity of gasoline and the gasoline surrogate components iso-octane, n-heptane and toluene," Fuel 2013;112:355–65
[220] Dirrenberger P, Glaude PA, Bounaceur R, Le Gall H, da Cruz AP, Konnov AA, et al., "Laminar burning velocity of gasolines with addition of ethanol," Fuel 2014;115:162–9
[221] Mehl M, Pitz WJ, Westbrook CK, Curran HJ., "Kinetic modelling of gasoline surrogate components and mixtures under engine conditions," Proc Combust Inst, 2011;33:193–200
[222] Silke EJ, Pitz WJ, Westbrook CK, Ribaucour M., "Detailed chemical kinetic modelling of cyclohexane oxidation," J Phys Chem A, 2007;111:3761–75
[223] Pitz WJ, Naik CV, Mhaoldúin TN, et al., "Modelling and experimental investigation of methylcyclohexane ignition in a rapid compression machine," Proc Combust Inst, 2007;31:267–75
[224] Metcalfe WK, Burke SM, Ahmed SS, Curran HJ., "A hierarchical and comparative kinetic modelling study of C1–C2 hydrocarbon and oxygenated fuels," Int J Chem Kinet, 2013;45:638–75
[225] Smith GP, Golden DM, Frenklach M, Moriarty NW, Eiteneer B, Goldenberg M, Bowman CT, Hanson RK, Song S, Gardiner WC Jr, Lissianski VV, Qin Z., "GRI-Mech 3.0," http://www.me.berkeley.edu/gri_mech/, 2000
[226] Metcalfe WK, Pitz WJ, Curran HJ, Simmie JM, Westbrook CK., "The development of a detailed chemical kinetic mechanism for diisobutylene and comparison to shock tube ignition times," Proc Combust Inst, 2007;31:377–84
[227] Slavinskaya NA, Riedel U, Dworkin SB, Thomson MJ., "Detailed numerical modelling of PAH formation and growth in non-premixed ethylene and ethane flames," Combust Flame, 2012;159:979–95
[228] Jihad A. Badra, Nehal Bokhumseen, Najood Mulla, S. Mani Sarathy, Aamir Farooq, Gautam Kalghatgi, Patrick Gaillard, "A methodology to relate octane numbers of binary and ternary n-heptane, iso-octane and toluene mixtures with simulated ignition delay times," Fuel, Volume 160, 2015, Pages 458-469, ISSN 0016-2361, https://doi.org/10.1016/j.fuel.2015.08.007
[229] K. Fieweger, R. Blumenthal, G. Adomeit, "Shock-tube investigations on the self-ignition of hydrocarbon-air mixtures at high pressures," Twenty-Fifth Symposium (International) on Combustion/The Combustion Institute, 1994/pp. 1579-1585
[230] Ribaucour, M., Minetti, R., & Sochet, L. R. (1998). Autoignition of n-pentane and 1-pentene: Experimental data and kinetic modelling. Symposium (International) on Combustion, 27(1), 345–351. https://doi.org/10.1016/S0082-0784(98)80422-0
[231] Vranckx, S., Lee, C., Chakravarty, H. K., & Fernandes, R. X. (2013). A rapid compression machine study of the low temperature combustion of cyclohexane at elevated pressures. *Proceedings of the Combustion Institute*, 34(1), 377–384. https://doi.org/10.1016/j.proci.2012.06.071
[232] Dunphy MP and Simmie JM. Preliminary observationson the high temperature oxidation of ethyl tert-butyl ether. Int J Chem Kinet 1991; 23: 553–558.
[233] Renato Cataluna, Dimitrios Samios, Rosangela da Silva, Eliana Weber de Menezes, "Addition of an azeotropic ETBE/ethanol mixture in eurosuper-type gasolines," Fuel 85 (2006) 2567-2577
[234] Brezinsky K., "The high-temperature oxidation of aromatic-hydrocarbons," Progress in Energy and Combustion Science 1986;12:I-24
[235] Badra J., AlRamadan A. S., Sarathy S. M., "Optimization of the octane response of gasoline/ethanol blends", Applied Energy, Volume 203, 1 October 2017, Pages 778-793, https://doi.org/10.1016/j.apenergy.2017.06.084
[236] O. Colin, A. Benkenida, C. Angelberger, "3d Modelling of Mixing, Ignition and Combustion Phenomena in Highly Stratified Gasoline Engines", Oil & Gas Science and Technology - Rev. IFP 58 (1) 47-62 (2003), DOI: 10.2516/ogst:2003004
[237] Berni, F., Cicalese, G., & Fontanesi, S. (2017). A modified thermal wall function for the estimation of gas-to-wall heat fluxes in CFD in-cylinder simulations of high performance spark-ignition engines. *Applied Thermal Engineering, 115*, 1045–1062. https://doi.org/10.1016/j.applthermaleng.2017.01.055
[238] Colin, O. and Truffin, K., "A Spark Ignition Model for Large Eddy Simulation based on an FSD Transport Equation (ISSIM-LES)," Proceedings of the Combustion Institute 33 (2011): 3097-3104.

Acknowledgements

It was the end of 2021 when I decided to take this pathway, a long and not easy, I would say, pathway. I made this decision because of the reflections coming from my daily work, always focused on providing innovation, solutions for companies and essentially offering know-how on the progress and giving a unique vision to push customers forward. As daily study shaped my routine, I decided and communicated to my parents my idea: a contribution to the research field, to the scientific community, to the world of science and progress, built upon a lot of study and sacrifice. A life characterized by sharing thoughts with the people I love, my parents and my girlfriend. That day in 2021, I told my parents about my idea, and my dad said, ironically and lovingly "he will never finish studying". Long studies, technical studies before university, a Bachelor's degree, then a Master's Degree, and now the PhD, to which I dedicated four years in parallel to my daily work as an engineer. It is true, maybe, we never stop studying, maybe because of our technical extraction and background, or mentality, or because we take satisfaction in achieving all the goals we reach and share with the people who made sacrifices to allow these successes and growth in life. It has always been my pleasure to share and smile at success, as in a family, as in a team, because it is never achieved alone. In my case, I had mentors such as my parents, the only reason for my sacrifices and dedication.

Over the last few years, after starting work as a CFD engineer at R&D CFD Srl, and even before that, I have had the opportunity to meet wonderful people. Here, I wish to thank all of them, starting with Giuseppe Cicalese and Stefano Fontanesi. I would say two awesome people, professionals, and mentors. I want to thank them by expressing my gratitude for all the opportunities, daily work and challenges, congress and conferences all around the world, and for giving me the possibility to undertake this PhD as an Industrial PhD Student, continuously working both on my daily work and engineering activities and on the research topics with direct industrial focus and application. Thank you for these amazing years together, and for the upcoming challenges as well.

I want to gratefully thank my colleagues, tutor, and co-authors for many publications and extensive work. Thank you to Fabio Berni and Alessandro d'Adamo, whom I met as a student, and always supporting in challenges in GruMo UniMORE and R&D CFD Srl. Thank you to Sebastiano Breda, my tutor during my Master's degree, later a colleague after graduation, and a mentor as I started working as an engineer at R&D CFD Srl, who always supported me personally whenever I needed help. Thank you to Paolo Filippini for his valuable support in corporate and professional coaching, and for his motivation throughout my continuous personal and professional development. Thank you to my uncles, to all my sincere friends and thank you to Alessandro Mangano for the best friendship. It was a long pathway, I had the pleasure of finding a strong and amazing group with whom every activity always turned into remarkable experiences and excellent results, congress and conferences, meetings, trips, publications and now I can finally gather all these works in a single document, which is my PhD Thesis. This represents a contribution, my contribution to the field of research and progress, in an area to which I dedicated my studies, my professional competencies, skills, and time, embracing the idea of contributing to all related fields.

So, it is true that we never finish studying, exactly as my dad said, and we never stop remembering the people who leave an unforgettable education, a life example, a human example, a mentorship, a pillar in our lives. I want to remember my Dad in the middle of these words, on this manuscript, just as I remember him every day. I miss him every day. During this journey, during these years of study, he passed away, leaving me with a legacy to carry on. I completed this work while struggling many times, every day, losing the strength and motivation on several occasions, but I completed it, perhaps even proving wrong the idea I would "never finish studying", as he lovingly joked.

I dedicate this work to my family, to my beloved Dad, to my Mom, my second pillar in life, to whom I dedicate every day, moving forward together through smiles and tears, living days bound by a link that will never end. Together with my girlfriend, a wonderful person whom I had the privilege to meet, our puppy, our lovely dogs, and my girlfriend's family, we continue each day sharing thoughts, life and support.

Luca

Ringraziamenti (versione italiana)

Era la fine del 2021 quando decisi di intraprendere questo percorso, conscio delle difficoltà che si sarebbero celate dietro un importante obiettivo come questo. Procedetti con questa, ponderata, decisione a causa del continuo riflesso che le attività seguite nella sfera professionale quotidiana, volte alla costante innovazione, al fornire alle aziende cui prestiamo consulenza soluzioni innovative, e conoscenze che fanno la differenza nel mondo odierno, fatto di nuove sfide ed incessante progresso. Pertanto, visto lo studio costante che caratterizzava le mie giornate, decisi di procedere con questo percorso, comunicando in primis, ai miei genitori l'idea di contribuire nel campo della ricerca, collaborare con la comunità scientifica, farne parte, conscio dei futuri studi e relativi sacrifici. Una vita, d'altra parte, costellata di idee verso il "mettersi in gioco", portare avanti i propri obiettivi, una vita caratterizzata sempre dal "condividere", con i miei genitori e con la mia fidanzata. Quel giorno, nel 2021, dissi ai miei genitori della mia idea di intraprendere il dottorato di ricerca, e a tavola, quel giorno, mio padre disse quella frase, ironicamente e amorevolmente: "non finirà più di studiare". Lo studio ha caratterizzato anni della mia vita, dall'Istituto Tecnico con indirizzo Meccanica, alla Laurea Triennale in Ingegneria Meccanica, e la Laurea Magistrale in Ingegneria del Veicolo, ora il Dottorato di Ricerca, o Industriale in questo caso, visto il mantenimento in parallelo del mio lavoro come ingegnere calcolista nel settore "automotive". Era vero, dunque, non si smette mai di studiare, probabilmente per estrazione tecnica ed esperienze, oppure per mentalità, o perché si ha il piacere di condividere i propri risultati mossi dalla volontà di raggiungere i propri obiettivi e di valorizzare il sacrificio che i propri genitori fanno per permetterci di realizzare il proprio percorso. Non da meno, averne poi la possibilità di condividere, e avere ancora quella forza e volontà di fare per l'orgoglio e la felicità negli occhi di chi ci vuole bene. Nel mio caso, ho avuto mentori, quali una famiglia alle spalle che mi ha sempre supportato, e ha permesso di realizzare la persona che sono oggi, nei risultati professionali e nella vita di tutti i giorni, con sacrificio e dedizione che rappresentano ancora oggi due capi saldi di me stesso.

In questi anni, dopo aver intrapreso il mio percorso come professionista in R&D CFD Srl, azienda presso la quale lavoro, e così, come anche negli anni che hanno preceduto questo evento, ho avuto la possibilità di conoscere persone stupende. Qui, voglio ringraziare tutti loro, partendo da Giuseppe Cicalese e Stefano Fontanesi. Voglio esprimere la mia gratitudine a queste incredibili persone, professionisti, e mentori. Voglio ringraziarli per tutte le opportunità, di lavoro quotidiano e di obiettivi aziendali, di congressi e conferenze in giro per il mondo, e per avermi dato la possibilità di intraprendere questo dottorato industriale, tra le attività aziendali e le attività di ricerca con una attenzione alla continua fattibilità e applicabilità diretta dei risultati nella sfera industriale. Grazie per questi anni condivisi insieme, ed un in bocca al lupo a noi ai prossimi anni e alle nuove avventure. Voglio ringraziare i miei colleghi, tutor, e co-autori per le pubblicazioni frutto di collaborazione e condivisione di lavoro. Voglio ringraziare Fabio Berni e Alessandro d'Adamo, conosciuti quando ancora ero studente, cui sempre hanno prestato il loro supporto in GruMo UniMORE e R&D CFD Srl. Grazie a Sebastiano Breda, mio tutor durante la Tesi di Laurea Magistrale prima e collega dopo il mio ingresso in R&D CFD Srl, sempre disponibile a farsi carico di pensieri e supporto sia professionale che personale. Grazie a Paolo Filippini per il prezioso supporto in ambito di coaching aziendale e professionale, e per il costante contributo motivazionale nella progressione personale. Grazie ai miei zii, ai miei amici sinceri, e grazie al mio caro amico Alessandro Mangano per la nostra sincera e pura amicizia.

È stato un lungo percorso, ho avuto la possibilità e il privilegio di trovare un gruppo forte ed incredibile, con il quale condividere avventure che hanno portato un inestimabile bagaglio di esperienze, conoscenze e risultati. Congressi, conferenze, riunioni, viaggi lavorativi e per la ricerca, pubblicazioni internazionali e finalmente la possibilità di raccogliere tutto questo in un singolo documento quale la mia Tesi di Dottorato. Quest'ultima, vuole essere un contributo, il mio contributo nel campo della ricerca e del progresso, nell'area cui ho avuto la possibilità di sviluppare negli anni,

di studiare, e mettere a disposizione il mio bagaglio di esperienze professionali, di abilità personali, di tempo e che tutte permettono di abbracciare l'idea di contributo e condivisione.
Quindi, posso dire che è vero, non si finisce mai di studiare, come disse il mio papà, ed è vero che non si deve mai smettere di ricordare le persone che ci hanno donato l'educazione, un indimenticabile insegnamento di vita, insegnamento umano, di mentore, un pilastro nella propria vita. Voglio ricordarti così, papà, tra queste righe, su questo manoscritto, per continuare a ricordarti ogni giorno. Mi manchi ogni giorno. Durante questi anni, durante questo percorso di studi, sei mancato alle persone che ti volevano bene, ora vegli su di noi da lassù, nel cielo che ogni tanto guardo nei momenti di riflessione, con un lascito importante nella mia vita. Ho completato questo lavoro con difficoltà, così come con difficoltà affronto ogni sfida della vita senza di te fisicamente presente, ed in molte occasioni, ho perso la motivazione di ogni cosa, di questo impegno preso, di ogni sfida della vita. Alla fine, ho trovato la forza di completare questa Tesi, completare questi studi, presentare i lavori ai congressi in giro per il mondo e completare le pubblicazioni con soddisfazione, e forse, potrei anche dire che oggi ho finito di studiare, contrariamente a quanto mi dicesti, caro papà. Ma sappiamo, che proprio sulle tue parole, non si completeranno quest'oggi i miei studi, così come continuerò nello studio quotidiano, continuerò a crescere con il tuo ricordo vivo con me.
Dedico questo lavoro alla mia famiglia, al mio papà, alla mia mamma, mio secondo pilastro in questa vita, alla quale dedico ogni giorno, cercando insieme di proseguire questa vita nel migliore dei modi, dai sorrisi alle lacrime, col nostro legame che durerà per sempre. Una vita condivisa con la mia amata compagna Chiara, alla nostra cucciola a casa nostra, ai nostri cani, a casa con mamma, e all'amata famiglia della mia compagna, persone speciali, continuando ogni giorno a condividere sorrisi, pensieri, vita e supporto reciproco.
Luca